FACULTÉ
DES SCIENCES

UNIVERSITÉ LIBRE DE BRUXELLES

Modelling mixoplankton functional types – examples from the cryptophyte-*Mesodinium-Dinophysis* complex

Thesis submitted by Anna-Adriana ANSCHÜTZ
in fulfilment of the requirements of the PhD Degree in agronomics and bioengineering
Academic year 2020-2021

Supervisor: Professor Nathalie GYPENS

Co-supervisor: Dr Aditee MITRA

Thesis jury:

Christian HERMANS (Université libre de Bruxelles, Chair)
Nathalie GYPENS (Université libre de Bruxelles, Supervisor, Secretary)
Bruno DANIS (Université libre de Bruxelles)
Aditee MITRA (Co-supervisor, Cardiff University)
Kevin J FLYNN (Plymouth Marine Laboratory)
Paolo LAZZARI (Istituto Nazionale di Oceanografia e di Geofisica Sperimentale)
Matthew JOHNSON (Woods Hole Oceanographic Institution)

ECOLE
INTERFACULTAIRE DE
BIOINGENIEURS

MIXOTROPH.ORG
MIXITIN

Acknowledgements

This thesis was done within the EU-funded H2020 Marie Skłodowska-Curie Actions ITN MixITiN (766327). The project gave me many great opportunities in the form of secondments abroad and in different institutions, the attendance of conferences and seminars and training in a variety of different skills. I am grateful for all the support I received, the scientific exchange and the friends that I have made over the past three years. I would like to thank Aditee Mitra for creating these opportunities, putting together a wonderful early stage researcher team and pushing me to learn invaluable skills that I did not dream that I would learn when I applied for this PhD. I am grateful to Kevin Flynn for bringing me into the modelling world, for teaching me a great new tool and that in science not everything is gold that glistens.

I would further like to thank Per Juel Hansen for his guidance in culturing *Teleaulax amphioxeia*, his advice and providing his lab. Willem Stolte for teaching me about coastal and marine management in the EU. Nathalie Gypens for teaching me as much Fortran as possible on a secondment that was cut short by the onset of a pandemic. Also, for helping me with doing a PhD at the ULB remotely and all the associated paperwork. I thank my examiners Christian Hermans, Bruno Danis, Paolo Lazzari and Matthew D. Johnson for giving me a fresh perspective with their critical comments and exciting questions that helped improve the final version of this thesis.

I am grateful to the ESRs Kostas, Lisa, Gui, Maira, Mena, Claudia, Joost, Andreas, Jon and Nikola for keeping in touch for three years against all odds and the fantastic support and exchange this group has provided. To Maria and Claudia for the great and enriching team work. To Steve for helping over the last hurdles.

I am thankful to all my friends I made in these three years with whom I shared so much pain and laughter and the unforgettable time: Suzana, Frances, Jordi, Kasper, Dania, Sergio, Tiffany and Cam. I would also like to specially thank Andreas Norlin, who was the best office mate I could have hoped for, his friendship and patience. Last but not least, I am grateful to my mother for her unwavering support and belief in me.

UNIVERSITÉ LIBRE DE BRUXELLES

Abstract

Mixoplankton are protist plankton that are capable of phototrophy and phagotrophy. These organisms are increasingly recognised not just as freaks of nature, but as a substantial part of marine plankton. Most existing plankton models still assume a strict dichotomy between phototrophs and heterotrophs. Few models consider mixoplanktonic activity as a synergism of the two trophic modes. Many different mixoplankton functional types exist on a gradient between heterotrophy and phototrophy. The cryptophyte (*Teleaulax)-Mesodinium-Dinophysis* (TMD) complex is a specific predator-prey interaction of different types of mixoplankton and a good example of the complexity of mixoplankton interaction and trophodynamics. The specialist non-constitutive mixoplankton (SNCM) *Mesodinium* acquires its chloroplasts strictly from a specific constitutive mixoplankton (CM) cryptophyte, while the harmful algal bloom (HAB) species *Dinophysis* acquires its third-hand chloroplasts exclusively from *Mesodinium*.

The generic NPZ-style protist model developed here shows that mixoplankton displays dynamics that are distinctly different from strict heterotrophs and autotrophs in terms of growth and the way they shape their environment. In addition, there is a clear niche separation between different mixoplankton types (general non-constitutive mixoplankton (GNCM), SNCM and CM) according to nutrient, prey and light resource availabilities indicating a niche separation of each type. Thus, considering the different mixoplankton functional types in specialised multi-organism relationships as they are found in the TMD-complex may be important for their understanding and accurate prediction of growth and biomass development. Currently, none of the many models of *Dinophysis* capture the biological dependencies. Results from a nitrogen-based TMD model suggest that the timing and quantity of prey availability is crucial for the bloom dynamics of *Mesodinium* and *Dinophysis*. Some CMs may only feed when phosphate is the limiting nutrient. The results of the variable stoichiometric “Perfect Beast” model that was configured as *Teleaulax amphioxeia* in combination with experimental data strongly suggest that the cryptophyte feeds on bacteria to compensate for phosphate limitation.

This work shows the importance of considering mixoplankton in ecosystem models alongside strict heterotrophs and autotrophs and that distinction between different mixoplankton functional types matters. Mixoplankton distinctly differ in their nutrient utilisation and growth dynamics. Predator-prey interactions have different implications for mixoplankton than for heterotrophs and their inclusion in models could improve our understanding of the formation of harmful mixoplankton blooms. The unique physiology of mixoplankton and their nutrient utilisation and trophic levels need consideration in species specific models.

UNIVERSITÉ LIBRE DE BRUXELLES

Résumé

Le mixoplancton inclut les protistes planctoniques capables de phototrophie et de phagotrophie. Ces organismes sont de plus en plus reconnus comme une partie importante du plancton marin. Toutefois, la plupart des modèles mathématiques planctoniques existants supposent encore une stricte dichotomie entre les organismes phototrophes et hétérotrophes et peu de modèles considèrent l'activité mixoplanctonique comme une synergie entre les deux modes trophiques. De nombreux types fonctionnels mixoplanctoniques différents existent dans un gradient entre l'hétérotrophie et la phototrophie. Le complexe cryptophyte (*Teleaulax*)-*Mesodinium*-*Dinophysis* (TMD) est une interaction prédateur-proie spécifique entre différents types de mixoplancton et un bon exemple de la complexité des interactions et des relations trophodynamiques du mixoplancton. *Mesodinium*, mixoplancton spécialiste non constitutif (SNCM), ne peut acquérir ses chloroplastes que de cryptophytes (mixoplancton constitutif (CM)) spécifiques (tel que *Teleaulax*), tandis que l'espèce *Dinophysis*, responsable d'efflorescences algales nuisibles, acquiert ses chloroplastes exclusivement de *Mesodinium*. Le modèle générique de protistes, de type NPZ, développé dans ce travail montre que le mixoplancton présente une dynamique nettement différente de celle des hétérotrophes et autotrophes strictes en termes de croissance et de la façon dont ils façonnent leur environnement. En outre, il existe une séparation de niches claire entre les différents types de mixoplancton (mixoplancton généraliste non-constitutif (GNCM), SNCM et CM) en fonction de la disponibilité en lumière, en nutriments et en proies. En conséquence, la prise en compte des différents types fonctionnels du mixoplancton dans des relations multi-organismes spécialisées, telles qu'on les trouve dans le complexe TMD, peut être importante pour leur compréhension et la prédiction précise de leur croissance et biomasse. Actuellement, aucun des modèles existants de *Dinophysis* ne rend compte de ces dépendances biologiques. Les résultats d'un modèle TMD basé sur l'azote suggèrent que le moment et la quantité de proies disponibles sont des facteurs cruciaux pour la dynamique de *Mesodinium* et de *Dinophysis*. Certains CM peuvent se nourrir uniquement lorsque le phosphate est le nutriment limitant. Les résultats du modèle à stœchiométrie variable "Perfect Beast", qui a été configuré pour représenter *Teleaulax amphioxeia* sur base de données expérimentales, suggèrent fortement que le cryptophyte se nourrit de bactéries pour compenser la limitation en phosphate. Ce travail montre l'importance de prendre en compte le mixoplancton dans les modèles d'écosystème en plus des hétérotrophes et des autotrophes stricts et que la distinction entre les différents types fonctionnels de mixoplancton est importante. Le mixoplancton se distingue par son utilisation des nutriments et sa dynamique de croissance. Les interactions prédateur-proie n'ont pas les mêmes implications pour le mixoplancton que pour les hétérotrophes et leur prise en compte dans les modèles pourrait améliorer notre compréhension de la formation des efflorescences nuisibles de mixoplancton. La physiologie unique du mixoplancton, son utilisation des nutriments et ses niveaux trophiques doivent être pris en compte dans les modèles spécifiques aux espèces.

Contents

List of Figures

List of Tables

List of Abbreviations and Definitions

ABM	**A**gent **B**ased **M**odel
CM	**C**onstitutive **M**ixoplankton
DSA	**D**ynamic **S**ensitivity **A**nalysis
DVM	**D**ial **V**ertical **M**igration
eSNCM	**e**ndosymbiontic **S**pecialist **N**on-**C**onstitutive **M**ixoplankton
GNCM	**G**eneral **N**on-**C**onstitutive **M**ixoplankton
HAB	**H**armful **A**lgae **B**loom
IBM	**I**ndividual **B**ased **M**odel
LD	**L**ight **D**ark cycle
NCM	**N**on-**C**onstitutive **M**ixoplankton
PAR	**P**hotosynthetically **A**ctive **R**adiation
PFD	**P**hoton **F**lux **D**ensity
pSNCM	**p**lastidic **S**pecialist **N**on-**C**onstitutive **M**ixoplankton
SNCM	**S**pecialist **N**on-**C**onstitutive **M**ixoplankton
SSSA	**S**teady **S**tate **S**ensitivity **A**nalysis
in-silico	computer-based (e.g. experiments with models)
mixoplankton	protist plankton capable of phototrophy and phagotrophy

Scope of this thesis

Marine plankton have commonly been divided based on their mode of nutrition into the strict categories of “plant”-like phytoplankton and “animal”-like zooplankton. However, there is the additional category of mixoplankton which are capable of both means of nutrition. In addition, there are many different mixoplankton types covering a spectrum between phototrophy and phagotrophy. This tropic mode does not commonly find representation in existing plankton models, plankton research and our general conceptual model of plankton interaction. However, a growing body of research over the last decade shows that mixoplankton make up a large proportion of plankton communities. In addition, there is great variety in their functionality and degree of phototrophy and phagotrophy suggesting that they should no longer be omitted from plankton research. **The aim of this study** are the possible implications of mixoplankton and their different types on marine ecosystems and their environmental pressures using a modelling approach and providing ways in which to integrate mixoplankton and their different types into plankton models.

Chapter 1 gives an introduction to marine plankton and specifically mixoplankton, their different functional types and physiological and ecological characteristics. Here, possible implications of mixoplankton characteristics for marine ecosystems will be reviewed. This chapter introduces cryptophytes from the *Teleaulax-Plagioselmis-Geminigera*-clade, the ciliate *Mesodinium* and the dinoflagellate *Dinophysis* and their relevance from an ecological and anthropocentric perspective. The specific relationships within the cryptophyte-*Mesodinium-Dinophysis*-complex will be explained as well as the reasoning for using it as a model complex in a modelling study. Lastly, an introduction to modelling biological processes and the applied methods is followed by the research aim of this thesis along with the hypotheses.

Chapter 2 gives an overview of the material and methods used to answer the hypotheses and research aim outlined in chapter 1. The system dynamics modelling approach used in this work is introduced along with the employed modelling software and general modelling techniques. In addition, the experimental setup and methods applied in chapter 5 are described.

Chapter 3 addresses the first hypothesis of this thesis "The hypothesis addressed in this chapter is: Distinguishing between different mixoplankton types in nitrogen-based plankton models makes a difference to the outcome of the biomass predictions". This

was approached with the development of a mechanistic generic nitrogen-based protist model describing mixoplankton as a synergism of photo- and phagotrophy. The model comprises phytoplankton, protozooplankton and the mixoplankton types GNCM, SNCM and CM. The results of this chapter revealed a niche separation between mixoplankton types and differences in biomass prediction depending on the employed protist functional type.

Chapter 4 explores the possible implications of considering different mixoplankton types within a mixoplankton complex. The hypothesis of this chapter is "Prey and nutrient availability influence the bloom dynamics and the HAB potential of *Dinophysis*. Specialised mixotrophic relationships significantly influence the bloom dynamics of multi-organism mixoplankton complexes like the TMD complex". Here, a nitrogen-based mixoplankton model was developed from chapter 3 and configured with literature data. The results suggest that prey availability and timing of blooms are key factors for the bloom potential of *Mesodinium* and especially *Dinophysis*.

Chapter 5 targets the third hypothesis "*T. amphioxeia* feeds on bacteria in conditions of low inorganic phosphorous to compensate for the missing nutrient". For this purpose, the existing variable stoichiometric model "Perfect Beast" (Flynn and Mitra, 2009) was configured as the CM *T. amphioxeia*. In addition, the model was tuned to data on *T. amphioxeia* from an experiment that was designed for the purpose of generating suitable data to model tuning. The question on the triggers for bactivory in *T. amphioxeia* could not be answered. However, this chapter resulted in a successfully tuned variable stoichiometric model ready for deployment in larger variable stoichiometric models such as a variable stoichiometric TMD-model.

Chapter 6 provides a summary of all results and a description of how they relate to the research aim outlined in chapter 1. Possible further developments and uses of these results are discussed in addition to how they contribute to the existing body of knowledge on mixoplankton. The general modelling process will be reviewed in a broader context as well as the limitations of this study and the challenges future research on mixoplankton will face. Options for future research based on the results of this work going forward will be reviewed in addition to potential ways to implement the findings of mixoplankton research into coastal and marine management. Lastly, the remaining key questions in mixoplankton research and ecosystem modelling are highlighted.

Chapter 1

Introduction

1.1 Marine plankton

The term plankton describes organisms in the water column that are not able to swim against the current, either because they are too small or lack the necessary motility. These organisms get transported with the current, while many have some ability for vertical movement within the water mass. This differentiates plankton from nekton like fish, large squid and marine mammals that can swim against currents and are thus independent from them. Plankton comprises many different organism types of a large size range. Most of these organisms are microscopic including viruses, bacteria, protists and crustaceans like krill. However, plankton also includes much larger organisms like jellyfish that can stretch several meters in diameter (Fig. 1.1).

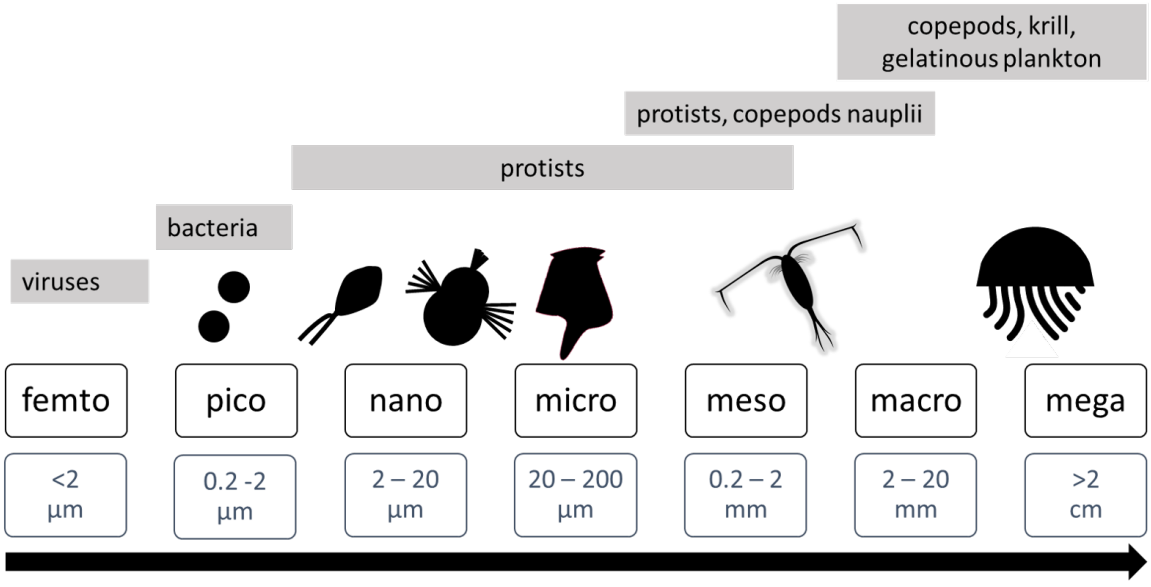

FIGURE 1.1: Schematic of the plankton size spectrum. Plankton is defined as organisms that are unable to swim against the current. The schematic gives the size spectrum (grey lined boxes) of each size category (black lined boxes), the type of organisms that fall into the categories (grey boxes) and icon of an example organism.

Marine protist plankton are at the base of marine food webs. Despite their microscopic size, they drive not only marine but to some extent terrestrial ecosystems, too. The

phototrophically active part of plankton produces around 50 % of all atmospheric oxygen, and thus greatly contributes to binding atmospheric carbon and exporting it to the deep sea (Sekerci and Ozarslan, 2020) with the carbon bound in dead organisms, fecal pellets and detritus for instance. This process is known as the biological carbon pump (Raven and Falkowski, 1999). The microbial loop describes the process of bacteria using organic matter and dissolved organic carbon that is too small to utilize for larger microzooplankton. The material thus does not get "lost" and reenters the foodweb making energy transfer up the food web more efficient (Azam et al., 1983).

Grazing on bacteria and protists by microzooplankton transport energy and nutrients up the trophic food web to higher trophic levels supporting, for example, large pelagic fish and whales (Fig. 1.2). The drivers of these processes are protists, which are single-cell eukaryotes. Protists are a paraphyletic group that comprises many phyla like foraminifera, radiolarians, cryptophytes, ciliates, dinoflagellates.

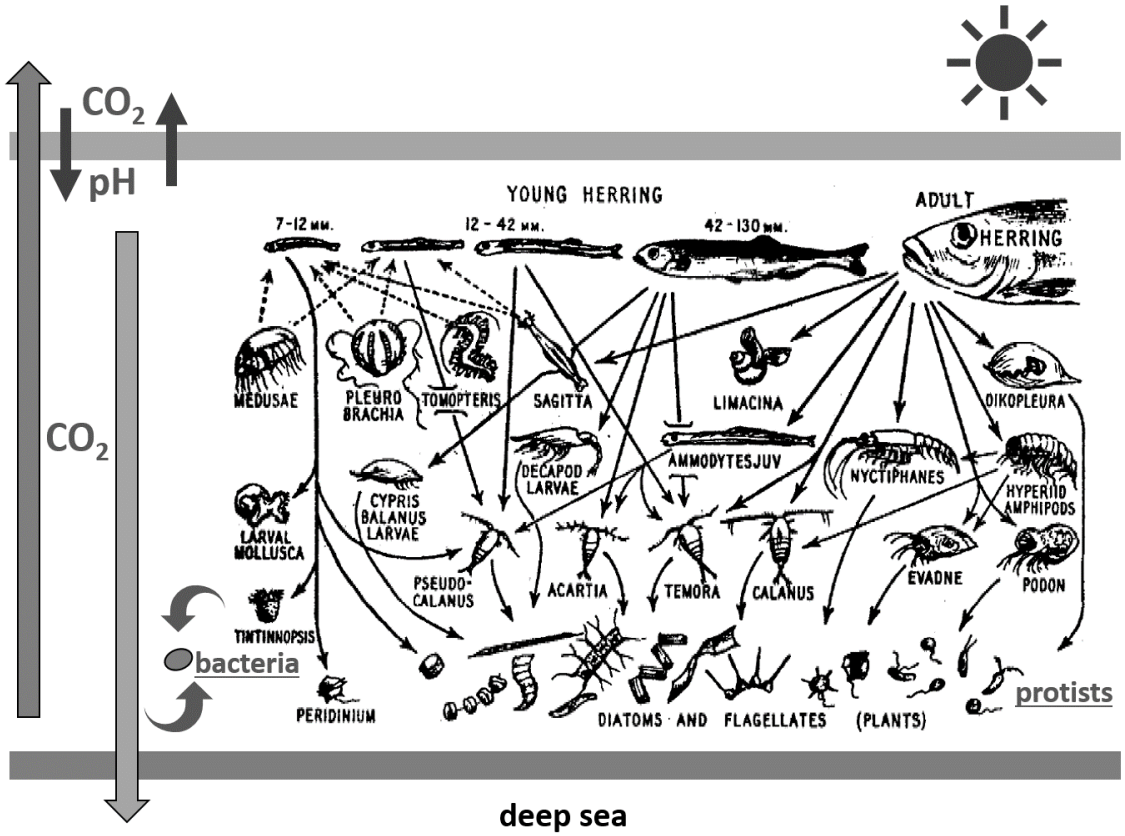

FIGURE 1.2: Schematic of a general foodweb. In the bottom row are protists, where the part capable of photosynthesis use irradiance to fix the CO_2 dissolved in the water. The concentration of dissolved CO_2 in the water depends on the concentration of CO_2 in the atmosphere and the temperature of the water. Photosynthetically fixed atmospheric carbon is exported to the deep sea by sinking organic debri unless it is integrated into the microbial loop (Azam et al., 1983). Heterotrophic activity releases CO_2 back into the water and atmosphere. The food web schematic was taken from Landry (2002) with the additions made here coloured in grey.

As plankton cannot escape the water layer they are in, plankton is limited by the resources and pressures within that water layer: abiotic and biotic. Photosynthetically active plankton is confined to the surface water layer, where sufficient light is available. Different spectra of light reach different water depths (Lalli and Parsons, 2006). Light with a lower wavelength and higher energy like violet and blue light reaches into deeper layers than light with higher wavelengths and less energy like red light. Only a part of the light spectrum can be used for photosynthesis which is known as the photosynthetically active radiation (PAR, 400 – 700 nm). In order to absorb light energy, organisms capable of photosynthesis produce different types of photopigments, not all of which are found in all photosynthetically active organisms. The most commonly known pigment is chlorophyll which is absorbes blue and red light with around 450 and 680 nm, respectively. There are also phycobillins and xanthophylls that can use wavelengths of other parts of the spectrum. At a very low level, light gets absorbed by the water itself (Lalli and Parsons, 2006). Most light however, is lost by absorption via in the water suspended material, especially if that material contains chlorophyll and other photoabsorbent pigments (Lalli and Parsons, 2006).

High irradiances can cause photodamage due to free radicals. Low irradiance limits the organisms in their energy resource. Strategies to compensate for both are photoacclimation and photoregulation. Photoacclimation describes the ability to change slope of the response curve of the photosynthesis rate to irradiance with the level of irradiance. The ciliate *Mesodinium* spp. is an example for an organism capable of photoacclimation and photoregulation (Johnson et al., 2006; Moeller et al., 2011). Photoregulation involves the ability to change the concentration of photoactive and photoprotective pigments. The dinoflagellate *Dinophysis acuta* is capable of photoregulation but not photoacclimation, for example (Hansen et al., 2016).

Apart from sufficient light, photosynthetically active plankton also need access to nutrients for growth. Limiting nutrients in the marine environment are typically nitrogen, phosphorous, iron and in the case of diatoms, silica (Lalli and Parsons, 2006; Bristow et al., 2017). The average atomic ratio of carbon, nitrogen and phosphorous in marine plankton is 106:16:1 and is referred to as the Redfield ratio (Redfield et al., 1963). This ratio is regarded as an indicator for non-limiting conditions of any of these nutrients.

Marine regions differ greatly in the amount of available nutrients. Oligotrophic regions such as the open oceans and tropical regions, have very low nutrient concentrations that support little primary production. Eutrophic regions contain high nutrient concentrations that support a lot of biological production such as coastal regions and estuaries. Mesotrophic regions have intermediate nutrient concentrations (Lalli and Parsons, 2006). Reduced nitrogen forms are preferred, meaning that ammonium is taken up rather than nitrate. All nitrate needs to be actively reduced before it can be used meaning an additional cost. The use of nitrate requires the organism to be able to produce nitrate and nitrite reductase (Syrett, 1981; Solomonson and Barber, 1990; Flynn et al., 1997). However, the ability to use nitrate comes with biochemical costs and may not necessarily

be an advantage where other more readily available forms of nitrogen are abundant (**faure_co-_1991**; Syrett, 1981; Solomonson and Barber, 1990). Iron is necessary for nitrate usage, because it is used in the reduction to ammonium. Therefore, there are high nutrient low chloroplyll regions as in the Southern ocean, where the concentrations of nitrate are high, but primary production is still low, due to the limitation in the necessary micronutrient iron (Lalli and Parsons, 2006).

1.2 What are mixoplankton?

Scientists have historically divided plankton strictly into phototrophs and heterotrophs (Fig. 1.3). This dichotomic perception has started to change over the past two decades as an increasing number of protists are now being recognized as capable of both phototrophy and phago-heterotrophy (Thingstad et al., 1996; Stickney et al., 2000; Stoecker et al., 2009; Flynn et al., 2013; Mitra et al., 2016). Protists with the capability of both trophic modes (phototrophy and phagotrophy) are now collectively termed "mixoplankton" (Flynn et al., 2019). Examples for phytoplankton according to this definition are diatoms and cyanobacteria that have no phagotrophic capabilities. Mixotrophy is not a simple addition of two trophic modes, but rather a synergism of the two (Flynn et al., 2019). In contrast to "traditional" phytoplankton, inorganic nutrients are not the only nutrient source driving growth in mixoplankton harmful algae bloom (HAB) species.

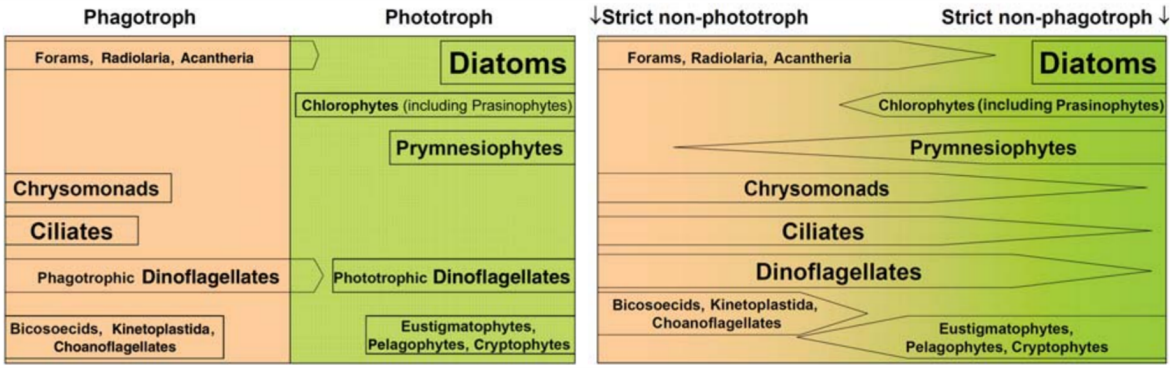

FIGURE 1.3: Schematic of the traditional categorization of plankton under the dichotomic paradigm of functional types (left) vs the mixoplankton paradigm that assumes a gradient (right) between strict phytoplankton and zooplankton (taken from Flynn et al. (2013)).

1.2.1 Mixoplankton functional types and role in marine ecosystems

Not all mixoplankton are created equal. Mixoplankton can differ greatly in how the synergism of their trophic modes function. The functional types of mixoplankton can be divided into two major groups: "constitutive" and "non-constitutive". Constitutive mixoplankton (CM) have an innate ability for phototrophy as they produce their own (constitutive) chloroplasts (Fig. 1.4). Their feeding triggers are not linked to the acquisition of chloroplasts

and grazing rates and the trigger for feeding can differ greatly among species (Jones et al., 1993; Stoecker, 1998; Mitra et al., 2016). As they are not dependent on prey for chloroplasts, in summer they often outcompete strict autotrophs in stratified water, when they become depleted in dissolved inorganic nutrients (Stoecker, 1998; Burkholder et al., 2008). Non-constitutive mixoplankton (Fig. 1.4) acquire their ability for phototrophy by the chloroplasts of their prey (kleptochloroplasts). Generalist non-constitutive mixoplankton (GNCM) require a continuous supply of prey as they cannot maintain their chloroplasts (Fig. 1.4), while specialist non-constitutive mixoplankton (SNCM) such as *Mesodinium* and *Dinophysis* are specialised on a few species of prey, and can last weeks or months without prey as they have adopted genetic material to maintain the prey chloroplasts (Park et al., 2008; Nielsen et al., 2012; Hansen et al., 2013; Hansen et al., 2013). SNCMs can be mistaken for strict autotrophs due to their lower feeding rates, but rely on a sufficient supply of their specialist prey as well as light and inorganic nutrients. *Mesodinium* and *Dinophysis* are specifically plastidic SNCM (pSNCM) as they capture prey and asset strip them for their plastids. This makes them distinct from endosymbiotic SNCM (eSNCM) like green *Noctiluca scintillans* which harbour fully functioning endosymbionts that provide photosynthetic products (Hansen et al., 2004). Mixoplankton functional types are not another conceptual box next to phytoplankton and zooplankton but rather a mixotrophic gradient (Fig. 1.3) between the two with more heterotrophic and more phototrophic types (Sanders et al., 1990; Flynn et al., 2019).

Nutrient acquisition in mixoplankton differs in a few ways from strict autotrophs as by incorporating a prey cell mixoplankton can take up a high concentration of nutrients at once compared to the uptake of dissolved nutrients via the cell membrane they can take up a lot of nutrients by consumption of just one prey item at once (Tang, 1995). Mixoplankton often dominate in mature ecosystems (Mitra et al., 2014) with complex and diverse ecology where most nutrients are bound in organics. Such conditions appear in temperate regions in summer following immature ecosystem conditions with plenty of inorganic nutrients during a spring bloom.

Mixoplankton likely also have a different relationship with light. There is an indication that light stimulates or inhibits feeding in some mixoplankton species (Brutemark and Granéli, 2011). Light attenuation (e.g., due to high sediment perturbation) may affect mixoplankton less than pure autotrophs as they can resort to predation as a source of energy (Skovgaard, 1996; Stoecker, 1998). It appears that mixoplankton must often supply its carbon budget with a minimum amount from phototrophy to ensure survival. For example, the pSNCM *M. rubrum* died in completely dark conditions in experiments (Smith and Hansen, 2007). The reason for this could be a demand for certain metabolites from photosynthesis for specific parts of biosynthesis pathways. Stratification and turbulence may have different implications for mixoplankton than for pure autotrophs, as vertical migration is found in mixoplankton like *Mesodinium* spp. to optimise growth by balancing their needs for light, dissolved nutrients and prey (Sjöqvist and Lindholm, 2011).

Mixoplankton influence energy transfer, competition and selection in plankton food

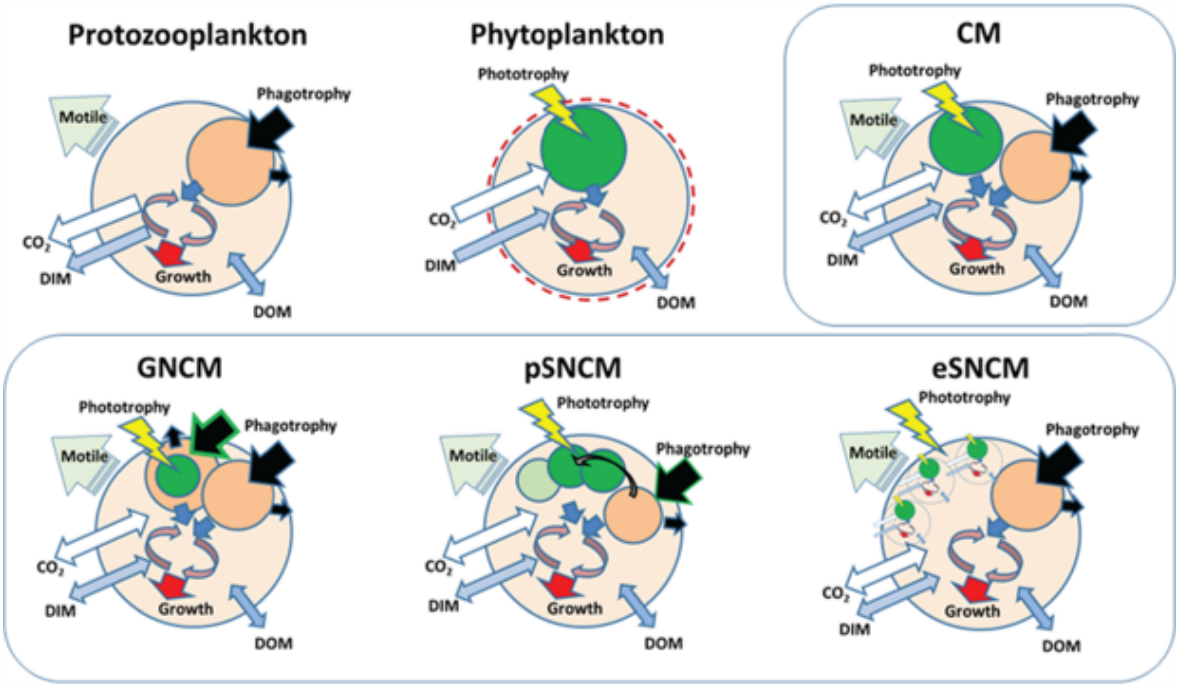

FIGURE 1.4: Schematics showing the distinct differences between different protist plankton physiologies. The protozooplankton are osmo–phagotrophic; they are incapable of phototrophy. The phytoplankton are photo-osmo mixotrophic; they are incapable of phagotrophy. The constitutive mixoplankton (CM) and non-constitutive mixoplankton (NCMs) are all photo-, osmo- and phago-mixotrophic. The generalist GNCMs acquire phototrophy from many phototroph prey types; pSNCMs are plastidic specialists acquiring phototrophy from specialist prey type(s); eSNCMs are endosymbiotic acquiring phototrophy by harbouring specific phototrophic prey.Note: illustrations are not to scale; in particular, eSNCMs are in relative terms ca. 10 to 100 times larger than the others. Taken from Flynn et al. (2019) with shortened original figure legend.

webs (Jones et al., 1993; Stoecker, 1998; Flynn et al., 2013; Flynn et al., 2019; Mitra et al., 2016) differently than it is currently considered in conceptual and simulation models. In addition, even under fluctuating inorganic nutrient ratios, mixoplankton are stoichiometrically more stable than autotrophs, which decreases the variability in seston stoichiometry in food webs (Moorthi et al., 2017). Zooplankton growth and reproduction increases in the presence of mixoplankton as observed in marine calanoid copepods and freshwater daphnids (Ptacnik et al., 2004; Katechakis et al., 2005) and mixotrophy may enhance biomass transfer up the food chain thereby increasing sinking carbon flux (Mitra et al., 2014; Ward and Follows, 2016), maybe even up to $\sim$35 % (Ward and Follows, 2016). Mixoplankton impacts nutrient fluxes and the food web status. Due to its unique ecology mixoplankton should not be grouped with phytoplankton or zooplankton in research, modelling and management policies. The complexity of the synergism in different types of mixoplankton call for a more holistic representation than just a simple addition of two trophic modes in one organism.

Many HAB species are in fact mixoplankton (Smayda, 1997; Heisler et al., 2008; Anderson et al., 2012) such as *Karlodinium veneficum*, *Alexandrium* and *Prymnesium*

(Blauw et al., 2006; Adolf et al., 2009). Early detection and better measures for managing mixoplankton HAB species may improve by gaining a better understanding of their prey specific needs. This may be especially true as mixoplankton predation is often triggered by different factors than in zooplankton such as plastid acquisition or compensation for a specific nutrient and some mixoplankton species have highly complex relations with their prey (Pitta et al., 2001; McManus et al., 2004; Park et al., 2006; Calbet et al., 2012; Schoener and McManus, 2012). In addition, the traditionally assumed predator-prey allometry of prey being smaller by a 10-fold does often not apply to mixoplankton. Many mixoplankton feed on very large prey in comparison to their own body size (Hansen et al., 1994; Calbet, 2008). Specialised feeding strategies such as feeding via a peduncle (*Dinophysis*) may allow straying from a certain size bracket as they do not engulf the entire cell and might only use certain organelles. The role of phagotrophy in mixoplankton can vary among functional types. Thus, prey availability may be a limiting factor for some and thereby could influence population size and their toxicity in HAB species (Gao et al., 2017; Hernández-Urcera et al., 2018).

Considering mixoplankton in the context of marine ecosystems is also relevant from a management perspective, as mixoplankton may react differently to anthropogenic drivers and climate change. Eutrophication as a result of high nutrient inputs leading to light attenuation decreased water quality and anoxia due to high respiration is still widespread in many coastal ecosystems (European Parliament et al., 2008). While higher nutrient concentrations benefit autotrophs and mixoplankton alike, mixoplankton have an advantage as they can tolerate low light conditions (Anderson et al., 2002; Reynolds, 2006; Reynolds, 2006; Glibert and Burkholder, 2011; Mitra et al., 2016) such as in estuaries where mixoplankton is known to outcompete autotrophs (Gobler et al., 2011). Additionally, they can fulfill nutrient imbalances in stoichiometry of dissolved inorganic nutrients (e.g hight N:P) (Burkholder et al., 2008).

Mixoplankton interact with their environment both as primary producers and grazers. Standards in measuring inorganic and organic nutrients and chlorophyll concentrations as a proxy for primary production mirror our diatom-centric analysis. They may wrongly estimate primary and secondary production in plankton communities with a high proportion of mixoplankton. *In-silico* experiments indicate that mixoplankton distinctly differ from pure autotrophs and heterotrophs in the way they grow and change their environment (Hammer and Pitchford, 2005; Mitra et al., 2014; Ghyoot et al., 2017b; Leles et al., 2018; Anschütz and Flynn, 2020; Leles et al., 2021).

Therefore, we need to consider plankton functional types beyond the dichotomy of heterotrophy and autotrophy in models. This may change how we predict species composition and more importantly energy transfer to higher trophic levels, maximum biomasses, consecutive plankton blooms and the overall ecosystem signature.

We need to include mixoplankton in its many forms in our conceptual models of marine ecosystem functioning Fig. 1.5. We need to build models that include this concept beyond the traditional dichotomic view. In the least to assess whether existing models

featuring the dichotomy are indeed reliable in the light of emerging evidence of the ubiquity of mixoplankton in marine ecosystems. But also, to improve our understanding of how mixoplankton links into our existing concepts, removing potential falsehoods and a potential to improve monitoring and forecasting in marine ecosystem management.

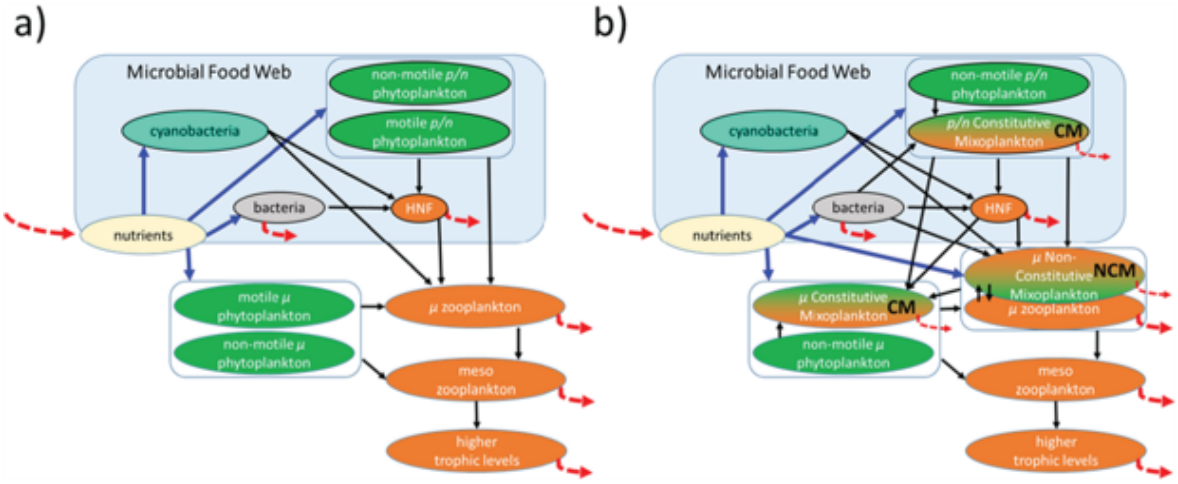

FIGURE 1.5: Differences between the pre-2010 paradigm for plankton trophic dynamics, (a), and the post-2010 paradigm, (b), that acknowledges the significance and roles of mixoplankton. The microbial food web components are within the blue boxes; viruses impact all organism groups though (because of higher numeric host abundances) may impact smaller organisms more. Red dashed arrows indicate input and outputs of dissolved inorganic and organic nutrients, blue arrows are nutrient uptakes and black arrows indicate grazing routes. Non-motile phytoplankton include diatoms, and also non-motile life stages of others (notably organisms such as the nanoplanktonic coccolithorphorid *Emiliania*, and the microplanktonic colonial *Phaeocystis*). In configuring (b), motile phytoplankton in (a) are considered to be potentially mixoplankton, as are ca. half of the protozooplankton indicated in (a). CM: constitutive mixoplankton. NCM: non-constitutive mixoplankton. HNF: heterotrophic nanoflagellates. p/n: pico/nano-sized organisms (i.e. 0.2–2.0 and 2.0–20 µm diameter, respectively). µ: micro-sized organisms (i.e. 20–200 µm diameter). Taken from Flynn et al. (2019) with original figure legend.

1.3 Cryptophytes: the *Teleaulax*/*Plagioselmis*/*Geminigera* clade

Cryptophytes are ubiquitous in phytoplankton communities in coastal and oceanic waters alike from the polar to tropical regions (Yih et al., 2004; Jeong et al., 2013; Johnson et al., 2013; Johnson et al., 2016; Šupraha et al., 2014). Cryptophyte abundance has been suggested as a trigger for HABs caused by the mixotroph *Karlodinium veneficum* (Adolf et al., 2008). Some species of this clade have been identified as the origin of the kleptochloroplasts in the pSNCM *Mesodinium* and *Dinophysis* (Gustafson et al., 2000; Reguera et al., 2012; Rial et al., 2013). The cryptophyte genus *Teleaulax* is

sometimes the most abundant phytoplankton species (Cerino and Zingone, 2006; Balrow and Krugens, 2002). So far, this genus comprises the species *Teleaulax amphioxeia*, *T. acuta*, *T. gracilis* and *T. minuta* (Fig. 1.6). The species *Plagioselmis prolonga* has recently been identified as the haploid form of *T. amphioxeia* (Altenburger et al., 2020a). External nutrient conditions drive the life cycle of *T. amphioxeia* as the diploid *T. amphioxeia* is found in conditions of high dissolved inorganic nitrogen (DIN) concentrations whereas its haploid form *Plagioselmis prolonga* is predominant in periods of low DIN (Altenburger et al., 2020a).

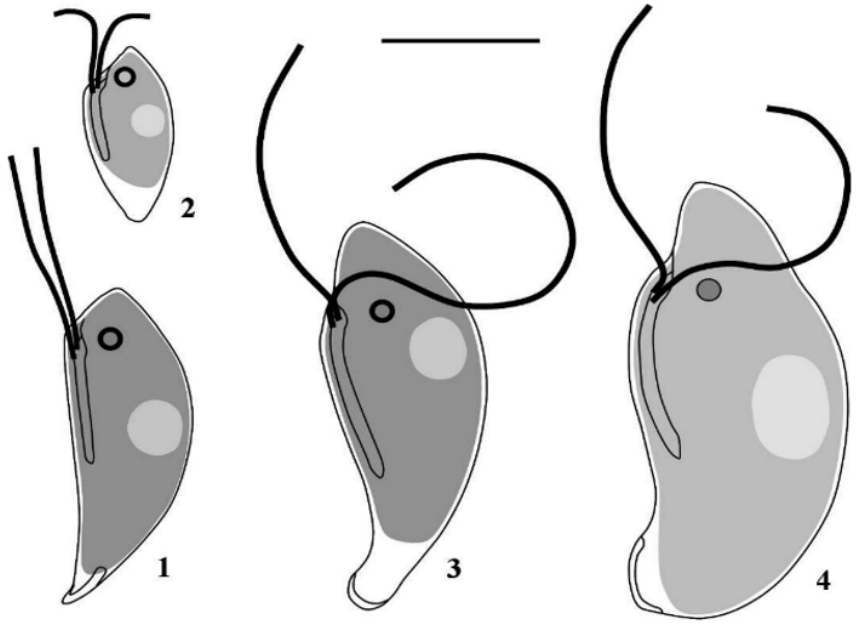

FIGURE 1.6: Illustrations of species of *Teleaulax* in lateral view. 1: *T. gracilis*, 2: *T. minuta*, 3: *T. amphioxeia*, 4 : *T. acuta*. Scale bar = 5 µm. The figure was taken from Laza-Martínez et al. (2012).

The species in the *Teleaulax* genus are small cone-shaped solitary cells with two flagella and an equivalent spherical diameter (ESD) 4 to 8 µm and swimming speeds up to 143 µm s^{-1} (Meunier et al., 2013). The genus has a single chloroplast with thylakoids stacked in three and produces the pigments chlorophyll and phycoerythrin (Laza-Martínez et al., 2012; Rial et al., 2013). *Teleaulax* has a unique secondary plastid and four genomes comprising the nuclear, mitochondrial, plastid and nucleomorph genomes (Kim et al., 2015a). Plastid evolution through secondary endosymbiosis between phagotrophic and photoautotrophic eukaryotes can be studied in cryptophytes that contain plastids (Douglas et al., 1991; McFadden, 1993; Kim et al., 2015a). The nucleomorphs originally stem from red algae nuclei and reside in the cytosol of the engulfed algal cells between inner and outer plastid membranes (Archibald, 2007; Curtis et al., 2012; Kim et al., 2015a). The highly conserved plastidic gene psbA (Morden and Sherwood, 2002) may be a tracer for the origin of the plastid in the cryptophyte-*Mesodinium*-*Dinophysis* food chain (Rial et al., 2015). *T. amphioxeia* is a confirmed CM as it was documented grazing on

Synechococcus sp. and heterotrophic bacteria with maximum ingestion rates of 0.3 and 0.7 cells predator^{-1} h^{-1} (Yoo et al., 2017).

Meunier et al. (2013) found that phosphate limitation had a strong negative effect on the escape response of *Teleaulax* from the predator *Oxyrrhis marina*. The authors argue that this is mainly owed to smaller flagella or deformed cell shapes as described in Donk et al. (1997) rather than a lack of ATP as its phosphate content (0.05 %) is negligible in comparison to the overall organismal phosphate (Elser and Hassett, 1994). Furthermore, the authors suggest that motility may stem from an overall slower metabolism as a result of the deficient phosphate pool including nucleic acids. In conclusion, cell shape, missing flagella and a slower metabolism may need to be considered as potential sinks for motility in *Teleaulax* under the influence of phosphate limitation when describing their physiology in models.

In the field, cryptophytes were found to respond to differences in nutrient loadings as for example in the case of the life cycle of *T. amphioxeia* (Altenburger et al., 2020a). Plankton communities shifted from diatoms to cryptophytes as the dominant group under increased loadings of nutrients in European estuaries (Cloern, 2001). Cryptophytes were already earlier found to outcompete diatoms in riverine areas with high nitrogen loadings (Margalef, 1978). Lastly, the species *T. amphioxeia* is the prey of many mixotroph and heterotroph dinoflagellate species (Fig. 1.7), some of which are known HAB species (Yoo et al., 2017).

1.4 The ciliate *Mesodinium*

Mesodinium is a common globally occurring ciliate genus. The species *M. rubrum* formerly called *Myrionectra rubra* is known to form blooms of very large cell abundances that are described as red tides. These tides are often associated with nutrient-rich estuaries and upwelling systems (Packard et al., 1978; Jimenez and Intriago, 1987; Crawford et al., 1997). Earliest observations of such red tides were made by Charles Darwin of the coast of Chile (Taylor et al., 1971). In Korea, massive algal blooms caused by *M. rubrum* are recorded to cause hypoxia in the ecosystem (Yoo et al., 1991; Yih et al., 2013).

The genus *Mesodinium* currently comprises the mixoplankton pelagic species *M. major* and *M. rubrum*, the benthic species *M. chamaeleon*, *M. coatsi* and the heterotrophic species *M. pulex* and *M. pupula* (Kim and Park, 2019). *Mesodinium* cf. *major* is larger than *Mesodinium rubrum*, has medusa-like forms and bright red coloured cells (Rial et al., 2015). Gustafson et al. (2000) isolated a strain of *Mesodinium rubrum* from McMurdo Sound, Antarctica, and were the first to successfully culture the ciliate by feeding it the cryptophyte *Geminigera cryophila* (identified by Johnson et al. (2006)). Since then, prey of the genera *Teleaulax* and *Geminigera* were found to be suitable for growing *Mesodinium* sp. in Korean waters (Park et al., 2007). The cryptophyte species *T. amphioxeia*, *T. minuta*, *T. gracilis*, and *Plagioselmis prolonga* all proved suitable prey to sustain the growth of *Mesodinium rubrum* (Rial et al., 2015). Other studies showed that while *M.*

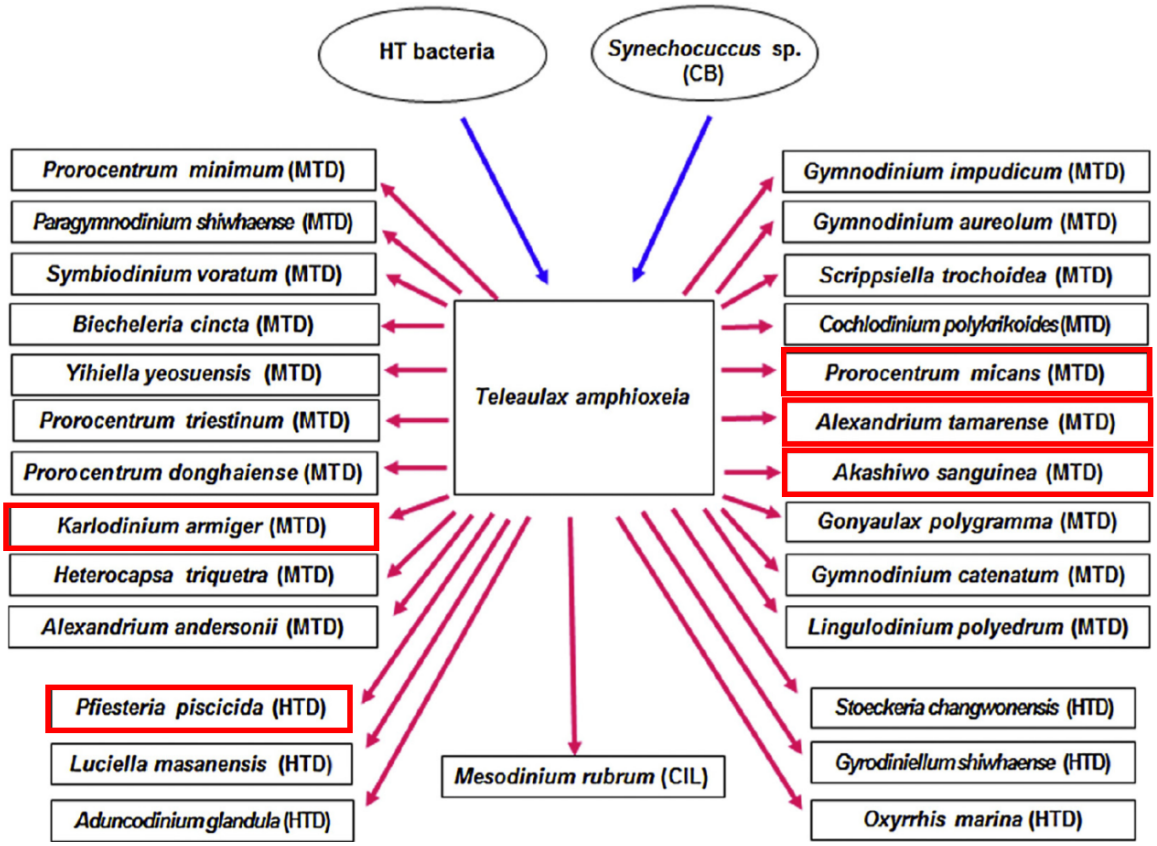

FIGURE 1.7: Species that prey on *T. amphioxeia*. Blue arrows are the prey of *T. amphioxeia* and the red arrows point towards its predators. HT: heterotroph, CB: cyanobacteria, HTD: heterotrophic dinoflagellate, MTD: mixotrophic dinoflagellate, CIL: ciliate. The red boxes indicate HAB species. Reproduced after Yoo et al. (2017).

rubrum could be grown with different species of *Teleaulax* and *Plagioselmis*, the best growth yields were achieved with strains of *T. amphioxeia* from the same area as the ciliate (Hernández-Urcera et al., 2018). The authors suggest that local adaptation may allow the predator to recognize prey for plastid acquisition from the same geographical area by possibly the same plastid sequences. While *M. rubrum* can grow on several species of the *Teleaulax*/*Plagioselmis*/*Geminigera* clade, the length of adaptation to the new plastids is species specific (Hernández-Urcera et al., 2018). *Mesodinium rubrum* also feeds on the cyanobacterium *Synecchococcus* sp. with maximum ingestion rates that are equivalent to 1.2 % of the predator's carbon (Yoo et al., 2017).

The solitary genus *Mesodinium* covers a large size range from 10 to 70 µm diameter (Gustafson et al., 2000; Rial et al., 2013). *Mesodinium* spp. range in size between 10 – 50 µm and have a strawberry-like spherical shape (Olenina et al., 2006). The ciliate does not move continuously, but rather remains motionless for certain periods followed by fast and large jumps (Tamar, 1979; Yih et al., 2004). These jumps can cover a distance of 0.16 mm and with a velocity of up to 1.2 cm s^{-1}, *Mesodinium* is one of the fastest ciliates (Fenchel and Hansen, 2006). Lindholm (1985) estimated swimming velocities up to 8 mm s^{-1}. *Mesodinium* has two types of cilia (Fig. 1.8): long cirri serve

as mechanoreceptors that are sensitive to shear and orientate the cell before jumps and ciliary rows on the posterior part of the cell that serves propulsion (Fenchel and Hansen, 2006). *Mesodinium* controls its vertical movement with the frequency of sinking and vertical jumps (Fenchel and Hansen, 2006).

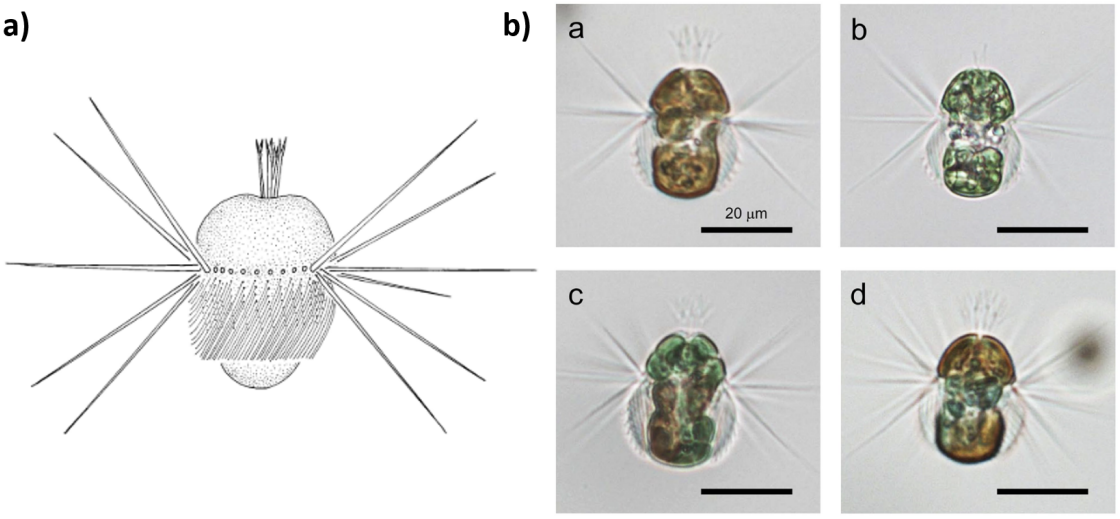

FIGURE 1.8: a) Schematic drawing of *M. rubrum* at rest (taken from Fenchel and Hansen (2006). b) *Mesodinium* spp. with red (a), green (b), or red and green (c, d) kleptochloroplasts derived from cryptophyte prey. All scale bars = 20 µm (taken from Nishitani and Yamaguchi (2018)).

The vertical movement of *Mesodinium* is furthermore dependent on light intensity. Its strong swimming abilities allow it to exploit dissolved mineral nutrient reserves beyond the limitations of molecular diffusion (Jiang and Johnson, 2017). *Mesodinium* has an effective escape response to predators like *Dinophysis*, which therefore need to have developed a very effective capture mechanism.

The ciliate instantly seizes prey with its oral tentacles on the encounter (Yih et al., 2004). In search of prey, *Mesodinium* swam in a zigzag pattern of 20 to 60 µm long linear paths instead of the usual long jumps. The prey cell is moved to the oral surface and ingested via a cytostome-like structure which takes around 15 seconds. The ciliate remained motionless for this process after capture.

M. rubrum needs to feed periodically on its specific prey like *T. amphioxeia* to continue photosynthesis, despite a certain ability to synthesise chlorophyll for about 16 days without any new acquisitions of prey (Gustafson et al., 2000). *Mesodinium* spp. has been shown to retain ingested cryptophyte nuclei for up to 100 days and keep them transcriptionally active (Hansen et al., 2016). In order to maintain its maximum growth rate, *Mesodinium* spp. only needs to ingest as little as a single cryptophyte cell, which is the equivalent of around 1 % of its daily carbon needs (Smith and Hansen, 2007). In experiments, maximum ingestion rates of 4 to 8.9 cryptophytic cells ciliate^{-1} day^{-1} were determined (Yih et al., 2004; Hansen et al., 2013).

M. rubrum partly digests the incorporated prey leaving the chloroplast and nucleomorph (Hansen et al., 2012). Only 1-2 % of *Mesodiniums* carbon demands (the equivalent of 1 prey cell d^{-1}) must come from prey to achieve its maximum growth rate (Hansen et al., 2013).

In lab conditions, *Mesodinium* sp. was found to contain between 6–36 plastids (Fenchel and Hansen, 2006). In field samples, plastid numbers up to 50 were counted (Lindholm et al., 1988). *M. rubrum* will replace old plastids when new suitable prey becomes available. When food is available in excess, *M. rubrum* may alter its strategy and down-regulate its photosynthetic apparatus (Smith and Hansen, 2007). As an SNCM, *Mesodinium* displays close control of its chloroplasts and is capable of photoacclimation (Moeller et al., 2011). It is thereby able to tolerate very low light conditions which may be attributed to the Antarctic origin of the isolated strain used in the study (Moeller et al., 2011).

The availability of suitable cryptophyte prey is crucial for the bloom formation of *Mesodinium* species (Nishitani and Yamaguchi, 2018). In a field study, the ratio of coloured plastids in *Mesodinium* depended on the season (Fig. 1.8, Nishitani and Yamaguchi, 2018). In the same study, the analysed *Mesodinium* sp. used both red and green plastid cryptophytes as prey. *M. rubrum* in particular preferentially ingested red plastid cryptophytes (especially *T. amphioxeia*). In addition to the suitable prey species, the quality of the prey's plastids is also an important factor for bloom formation (Kim et al., 2015a; Hernández-Urcera et al., 2018). A full plastid replacement from *T. amphioxeia* to *T. acuta* takes approximately two weeks in *M. rubrum* (Hansen et al., 2012). In a low light treatment (70 µmol photons m^2 s^{-1}) *M. rubrum* had around 60 times more Chl *a* than *Teleaulax amphioxeia* in the same treatment (Rial et al., 2013), which implies an ability of *Mesodinium* to "drive" the acquired chloroplast.

Blooms of *M. rubrum* often start at low water depths and appear to be promoted by stable water conditions (Hamilton et al., 2017). In the Columbia River Estuary, the increase in cells of *M. rubrum* reportedly coincides with the decline of *Teleaulax*-like cryptophytes (Peterson et al., 2013), as the ciliate needs to ingest these cryptophytes to acquire the plastids necessary for photosynthesis. Annual blooms of *M. rubrum* appear to be initiated in summer neap tides (Herfort et al., 2011), and have been linked to an extended summer saltwater intrusion as a result of tidal forcing and the seasonality of freshwater discharge (Chawla et al., 2008). Blooms of the ciliate have been observed to begin as a surface accumulation in spring to be later distributed uniformly over the water column from the surface to 30 m depth (Olli, 1999). The ability to use deep nutrient resources is likely an advantage of the highly motile species over non-motile ones like diatoms in late-season nutrient deplete and stratified conditions. This advantage might prolong the bloom in summer. An important trigger of blooms caused by this ciliate is the appearance of its specific prey from which it can obtain its chloroplasts (Nishitani and Yamaguchi, 2018). The potential for a bloom may be influenced by water temperature and dissolved inorganic nutrients (Nishitani and Yamaguchi, 2018).

1.5 The dinoflagellate *Dinophysis*

Dinophysis is a large dinoflagellate genus that comprises over a hundred species of which at least ten are known to be toxic and responsible for the causation of HABs that cause diarrheic shellfish poisoning and thus economic harm to local shellfisheries (Reguera et al., 2012; Reguera et al., 2014). Mixoplankton activity was first described in the species *D. acuminata* and *D. norvegica* (Jacobson and Andersen, 1994). Since then many more species have been discovered to be mixoplankton and specialised in their prey on certain species of *Mesodinium* (Reguera et al., 2012).

Like all dinoflagellates, *Dinophysis* has two dissimilar flagella (Fig. 1.9), a longitudinal, smooth flagellum and a transverse, "hairy" one (Nielsen and Kiørboe, 2015). The longitudinal, smooth flagellum trails the cell, while the hairy, transverse flagellum encircles the apical and anterior end of the cell. *Dinophysis* uses the longitudinal flagellum for propulsion, but also turning and reorientation by exerting a stirring motion (Jiang et al., 2018). The species of *Dinophysis* differ greatly in morphology and size (Fig. 1.9, Reguera et al., 2014).

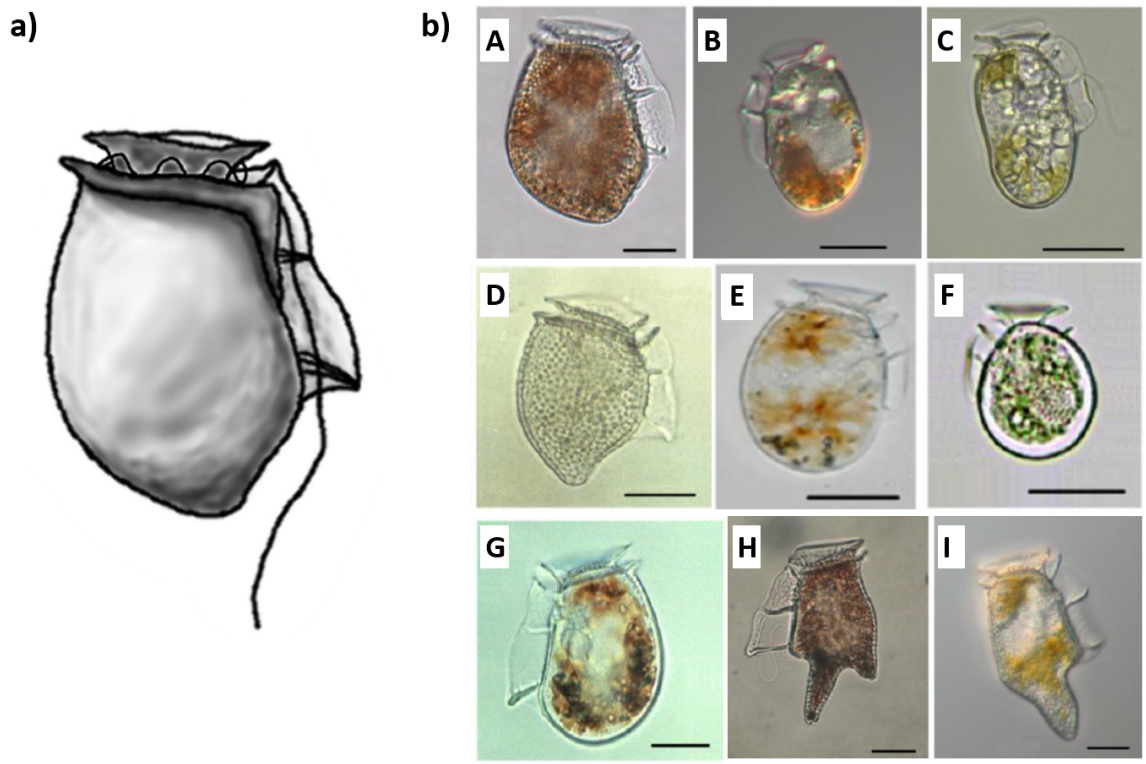

FIGURE 1.9: a) Schematic of *D. acuta* (section of a figure by Nielsen and Kiørboe, 2015). *Dinophysis* has a longitudinal and a transverse flagellum; b) Different species of *Dinophysis* (rearranged figure by Reguera et al., 2014 and Riobó et al., 2013). A: *D. acuta*, B: *D. acuminata*, C: *D. sacculus*, D: *D. norvegica*, E: *D. ovum*, F: *D. infundibula*, G: *D. fortii*, H: *D. tripos*, I: *D. caudata*. Scale bar = 20 µm.

Dinophysis has a complex life cycle with vegetative, sexual and intermediate stages that result in many different shapes and sizes of each species which makes species

identification in the field a challenge (Taylor, 1976; Hallegraeff and Lucas, 1988; Larsen and Moestrup, 1992; Berland et al., 1995; Reguera and González-Gil, 2001; Park et al., 2019). Many species of *Dinophysis* have later been discovered to be a different life stage of another species as for example in the cases of *D. acuminata* and *D. ovum* (Reguera and González-Gil, 2001; Reguera and González-Gil, 2007; Park et al., 2019). Cysts for sexual reproduction appear to form at the end of a *Dinophysis* bloom (Reguera and González-Gil, 2001).

While *Dinophysis* receives its chloroplasts from the ciliate genus *Mesodinium* they originally stem from cryptophytes (Nishitani et al., 2003; Kim et al., 2012a; Hansen et al., 2016; Hernández-Urcera et al., 2018) of the *Plagioselmis*/*Teleaulax*/*Geminigera* clade. Even though the plastids most commonly originate from *T. amphioxeia* (Takishita et al., 2002; Janson, 2004; Kim et al., 2015b), plastids of other origins are also frequently found. Plastids originating from the cryptophytes *T. acuta*, *Geminigera cryophila* (Minnhagen and Janson, 2006; Nishitani et al., 2010) and *Rhodomonas*/*Storeatula* (Stern et al., 2014; Díaz et al., 2020) were found in *Dinophysis*. *Dinophysis* spp. is able to simultaneously retain plastids from multiple algal origins (Kim et al., 2012a), but they seem to have a preference toward plastids from a certain species (Park et al., 2010). In addition, sequences of the raphidophyte *Heterosigma akashiwo* and the prasinophyte *Pyramimonas* sp. were found (Kim et al., 2012a). Rial et al. (2013) suggest that these findings may indicate *Dinophysis* can resort to an alternative prey genus than the cryptophyte-*Mesodinium* chain.

While *M. rubrum* and *M.* cf. *major* seem the preferred prey (Rial et al., 2015), *M. chamaeleon* (Moestrup et al., 2012) and *M. coatsi* (Nam et al., 2015) have been described as two potential intermediate prey species. *Mesodinium* is faster swimmer than *Dinophysis* (Mafra et al., 2016), and the predator has therefore developed a couple of hunting strategies that focus on stealth. The dinoflagellate can chemically detect its prey better than *Mesodinium* detects its predator which allows the predator to get closer to its prey (Jiang et al., 2018). *M. rubrum* detects its predator via mechanoreceptors (Jiang et al., 2018) allowing the predator to “sneak up” on its prey and capture it. Once *Dinophysis* detected its prey it approaches it with reduced speed as *M. rubrum* responds to the detection of a predator with long jumps to detach the chemical trail of its surface. *Dinophysis* captures *Mesodinium* by immobilization once it is close enough.

The weapon arsenal for prey capture involves toxins, peduncles that serve like spears and mucus traps (Hansen et al., 2016; Mafra et al., 2016). *Dinophysis* releases mucus traps for prey capture and toxic compounds to immobilise their prey (Mafra et al., 2016). Species of *Dinophysis* may also produce toxins or bioactive chemicals that aid to immobilize their prey (Giménez Papiol et al., 2016; Mafra et al., 2016; Ojamäe et al., 2016; Jiang et al., 2018). If the production of toxins solely serves the capture of food or even at all is not entirely clear. Alternative reasons could be allelopathy and grazer defense (Nielsen et al., 2013).

Dinophysis ejects a poisoned peduncle like a spear, which can adhere to several *M. rubrum* at the same time and reduce their ability to jump (Jiang et al., 2018). The

predator is then towed by its prey until it remains motionless and proceeds to extract the contents of its prey via a peduncle (Park et al., 2006). *D. acuminata* may target specifically weakened *M. rubrum* cells while their motility (*Mesodinium*) may be compromised by exposure to previously released toxins or injuries from earlier attacks by *Dinophysis* (Jiang et al., 2018). The authors argue that the predator-prey encounter-rate model by Gerritsen and Strickler (1977) of a cruising predator and a slow-moving or stationary prey applies to *Dinophysis* and *Mesodinium* as the ciliate displays phases of stationary behaviour between its characteristic fast and long jumps.

A few good feedings in a season seem to suffice to sustain population of *Dinophysis* for months (Velo-Suárez et al., 2014). Better growth conditions for *Mesodinium* eventually lead to higher growth for *Dinophysis* (Hernández-Urcera et al., 2018). Intensive feeding at a time and the addition of photosynthesis enable the survival of the organism for long periods without feeding. *Dinophysis* seems to be able to accumulate chloroplasts as *D. caudata* was found to contain up to 30 prey plastids of cryptophyte origin (Kim et al., 2012b). In addition, the dinoflagellate displays some level of control over the acquired chloroplasts.

Despite its dependency on chloroplasts from the prey, *Dinophysis* can survive in the light for about two months without prey (Park et al., 2008; Hansen et al., 2016; García-Portela et al., 2018) by resorting to their carbon storage built up while the chloroplasts were intact (Park et al., 2008; Nielsen et al., 2012; Hansen et al., 2016). After a while, *Dinophysis* begins to lose control over their kleptochloroplasts and they have to acquire new ones. Some species of *Dinophysis* can hold on to their plastids longer than others (*D. caudata* vs *D. acuta*) before starting to lose their photosynthetic capabilities and reserves (Park et al., 2008; Hansen et al., 2016). *Dinophysis* spp. (*D. acuta*) seems capable of photoregulation by increasing Chl *a* and other photosynthetic pigments (photoregulation), but not photoacclimation, which involves a change in the photosynthetic light response curve (Kim et al., 2012b; Rial et al., 2013; Hansen et al., 2016). *Dinophysis* may compensate for that by ingesting photoacclimitized prey cells and maintaining a higher number of chloroplasts. *Dinophysis* also seems unable to repair photodamage to the chloroplasts (Kim et al., 2012a; Rial et al., 2013).

Dinophysis gradually modifies the acquired plastids after ingestion (Kim et al., 2012b) to the point where the ultrastructure of the plastids between *Mesodinium* and *Dinophysis* differs (Garcia-Cuetos et al., 2010). However, it does not retain the prey nuclei, which contain the genes involved in the regulation of RuBisCo (Hansen et al., 2016). *Dinophysis* is, therefore, unable to increase its carbon uptake at higher irradiances and loses carbon fixing ability after a month in the experiments. In addition, *Dinophysis* seems to be able to divide and therefore replicates its chloroplasts (Minnhagen et al., 2008; Hansen et al., 2016).

Like *Mesodinium*, *Dinophysis* will only divide 3 to 4 times upon sudden starvation of specific prey (Hansen et al., 2013). This tactic prevents a dilution of chloroplasts under division. There may however be variation in prey dependency versus obligational

phototrophy in the *Dinophysis* genus. For example, *D. acuta* may have higher heterotrophic needs than *D. acuminata* but a lower dependency on phototrophy (García-Portela et al., 2018; Hernández-Urcera et al., 2018). *Dinophysis* needs to supply half their carbon demand from prey (Hansen et al., 2013) while a minimum of 25 % of the carbon demand comes from photosynthesis (Nielsen et al., 2012).

On the one hand, due to their ability to maintain their kleptochloroplasts for some time, *Dinophysis* is independent of a continuous supply of prey. In fact, field populations of *Dinophysis* often mismatched with their ciliate prey (González-Gil et al., 2010; Sjöqvist and Lindholm, 2011; Díaz et al., 2016). On the other hand, their heterotrophic abilities may allow *Dinophysis* to survive at very low light intensities. Active cells of *Dinophysis* have been found as deep as 81 m in the Celtic Sea (Fux et al., 2010). In addition, light tolerance may depend on nutrient availability as dinoflagellates were found to tolerate light levels of up to 1000 µmol m^{-2} s^{-1} in nutrient replete conditions, but only 150 µmol m^{-2} s^{-1} in nutrient depletion (Heaney and Eppley, 1981). Thin water layers for the capture of fast *Mesodinium* prey may be more important to *Dinophysis* than irradiance. *Dinophysis* often forms high density thin layers of up to 10^5 cells L^{-1} in the surface layer or close to the pycnocline (Gentien et al., 1995; Moita et al., 2006; Velo-Suárez et al., 2008; Sjöqvist and Lindholm, 2011; Farrell et al., 2012). Such high population densities could increase the capture rate of its prey *Mesodinium*.

Even though blooms of some species of *Dinophysis* can cause major damage to local fisheries (Reguera et al., 2012; Hernández-Urcera et al., 2018), the proportion of *Dinophysis* of the total microplankton is small (Reguera et al., 2012). Cell concentrations are usually lower than 100 cells L^{-1}, but can reach 10^6 cells L^{-1} in seasonal blooms (Reguera et al., 2012; Reguera et al., 2014; Hattenrath-Lehmann et al., 2015; Jiang et al., 2018).

Blooms of *Dinophysis* often follow blooms of their prey *Mesodinium* (Velo-Suárez et al., 2014; Ajani et al., 2016). As both genera need to receive their chloroplasts from cryptophytic prey, they are also dependent on the bloom of their specific cryptophyte. Areas known to produce blooms of *Mesodinium* and *Dinophysis* are often reported to also foster blooms of cryptophytes (Souza et al., 2014; Velo-Suárez et al., 2014; Brito et al., 2015). However, there are conflicting reports of blooms of *Mesodinium* and *Dinophysis* to covary with blooms of cryptophytes (Souza et al., 2014) and reports where they do not (Velo-Suárez et al., 2014).

Blooms can form within a week and are triggered by various events like the change in weather or the previous bloom of its specific prey *Mesodinium* (Reguera et al., 2012; Velo-Suárez et al., 2014). Most harmful algae blooms caused by *Dinophysis* are linked to meteorological conditions, which might stop upwelling and lead to stratification and the thin stable water layers that *Dinophysis* uses to catch their prey (Reguera et al., 2012). Thermohaline stratification is suspected as a trigger of *Dinophysis* blooms (Souza et al., 2014; Velo-Suárez et al., 2014; Moita et al., 2016) with the worst HABs observed in thin subsurface layers within the pycnocline (Moita et al., 2016). A statistical model revealed

season and thermal stratification as significant (60%) predictors to blooms of *D. acuminata* and salinity and dissolved oxygen to blooms of *D. caudata* (Ajani et al., 2016). Another factor in the formation of *Dinophysis* blooms lateral currents caused by upwellings forcing winds and the consequent displacement of populations (Moita et al., 2016).

Both *Mesodinium* and *Dinophysis* regularly form blooms in coastal areas and estuaries (Hattenrath-Lehmann et al., 2013; Brito et al., 2015; Moita et al., 2016). Estuaries are some of the most productive ecosystems in the world and are dominated by light limitation (sediment and primary production), the tidal regime and a large input of organic matter and nutrients from rivers, land runoff and sewage discharges (Brito et al., 2015). High or excessive nutrient loadings in estuaries have long been associated with harmful algal blooms (Hattenrath-Lehmann et al., 2015; Ajani et al., 2016), which could drive DSP events as they promote the growth of *Mesodinium* (Cloern et al., 1994; Herfort et al., 2011; Peterson et al., 2013). Increased nitrogen in the form of ammonia and glutamine promotes growth (Hattenrath-Lehmann et al., 2015; Ajani et al., 2016) and toxicity in *Dinophysis* (Hattenrath-Lehmann et al., 2015). Nutrients were predictors for both species (Ajani et al., 2016). The ability to use nitrate is very limited to not existent in *Dinophysis* (García-Portela et al., 2020).

Apart from external factors, the seasonality of the bloom may depend on the species of *Dinophysis*. In a ten-year weekly time series on the northwest Iberian coast, the species *D. acuminata* and *D. acuta* were found to bloom yearly in distinct seasons with different conditions with a few exceptions (Moita et al., 2016). *D. acuminata* reached peaks in March with around three weeks difference in the two observed stations (Moita et al., 2016). The decline in *Dinophysis* blooms is brought on by various factors like physical dispersion (Velo-Suárez et al., 2010), positive temperature anomalies (Escalera et al., 2006), biological grazing from micro- (Nézan and Chomérat, 2009) and mesozooplankton (Kozlowsky-Suzuki et al., 2006) and infections by *Parvilucifera* (Norén et al., 1999) or the parasite dinoflagellate *Amoebophrya* spp. (Velo-Suárez et al., 2014).

Several species cause a major threat to shellfish aquaculture in Europe, Chile, Japan, and New Zealand (Reguera et al., 2012). However, there are differences in the toxicity of the species causing the outbreaks as well as regional differences in toxicity of the same species (Reguera et al., 2012; Reguera et al., 2014). While *D. miles* is only found in the tropics and *D. norvegica* is exclusive to the boreal regions, other species like *D. acuta*, *D. acuminata* and *D. caudata* occur in different climates (Reguera et al., 2012). Consumption of shellfish that are contaminated with okadiac acids and dinophysitoxins produced by *Dinophysis* can cause diarrhetic shellfish poisoning (DSP) in humans with diarrhoea, nausea, vomiting and abdominal pain (Reguera et al., 2014). HABs formed by *Dinophysis* have repeatedly forced the closure of shellfish aquacultures in various regions around the world (Reguera et al., 2012; Blanco et al., 2013; Hernández-Urcera et al., 2018). Shellfish aquacultures that were contaminated with *Dinophysis* toxins can remain closed for up to nine months (Vale et al., 2008; Blanco et al., 2013; Reguera et al., 2014).

The potential threat of HABs by *Dinophysis* is difficult to determine. It can commonly

be found in the surface mixed layer in low numbers without causing any harm (Reguera et al., 2012). It is challenging to predict when they reach high numbers and form blooms because it depends on various partly unknown factors including its mixoplankton nature (Reguera et al., 2012; Souza et al., 2014). When and whether they produce toxins when they form blooms is also not always certain (Hattenrath-Lehmann and Gobler, 2015).

1.6 The cryptophyte-*Mesodinium*-*Dinophysis* complex

Many harmful algae species that were long assumed to be autotrophic, are now known to be in fact mixoplankton (Flynn et al., 2019). Predicting harmful algae blooms is often a challenge because the mechanisms behind their formation were shrouded in mystery as their mixotrophic nature and their complex relationships were often poorly understood (Reguera et al., 2012; Reguera et al., 2014; Moita et al., 2016). The TMD complex is exemplary for this problem, in which the toxigenic genus *Dinophysis* frequently draws attention by causing the shutdown of shellfish aquacultures (Reguera et al., 2012; Reguera et al., 2014; Moita et al., 2016) while it is dependent on plastid acquisition from specific prey (Fig. 1.10). It is also a mixoplankton complex that comprises not one but two different mixoplankton functional types.

Marine mixoplankton species long failed to be cultured, because their mixotrophic needs were unknown. Therefore, an essential requirement for their long-term survival was missing from early experiments where they were assumed to be purely autotroph. The first successful culturing of *Mesodinium* in 2000 was a breakthrough for the research of its physiology and relation to its prey (Gustafson et al., 2000). However, culturing *Dinophysis* was unsuccessful until the discovery of its prey dependency (Takishita et al., 2002; Hackett et al., 2003; Janson, 2004) and that they need to be fed their specific prey. Park et al. (2006) were then the first to culture *Dinophysis* and prove its mixotrophic nature in the laboratory. Since then, both *Mesodinium* and *Dinophysis* were the subject of many culturing experiments and several studies focused on experiments with a combination of both including *Teleaulax* (Rial et al., 2013; Hernández-Urcera et al., 2018).

Even though prey availability is essential to the ability of *Dinophysis* to form blooms and produce toxins (Tong et al., 2010; Hattenrath-Lehmann and Gobler, 2015), *Mesodinium* and *Teleaulax* are rarely considered in monitoring (Reguera et al., 2012; Ajani et al., 2016). Since neither *Mesodinium* nor *Teleaulax* are toxic (Kim et al., 2008), that may be due to their harmlessness from an anthropocentric perspective in comparison with *Dinophysis*. The study of the TMD complex is a source of new revelations on the functioning of different mixoplankton types, their multilevel relations with other species, their ecophysiology and the impact of mixoplankton on higher trophic levels and ecosystems. This knowledge should prove useful to improve coastal management with better monitoring and the design of predictive models for the blooms of mixotrophic harmful algae species.

Due to the impact on public health and economy in coastal regions, there are many initiatives for forecasting and monitoring bloom events of *Dinophysis* (Velo-Suárez and

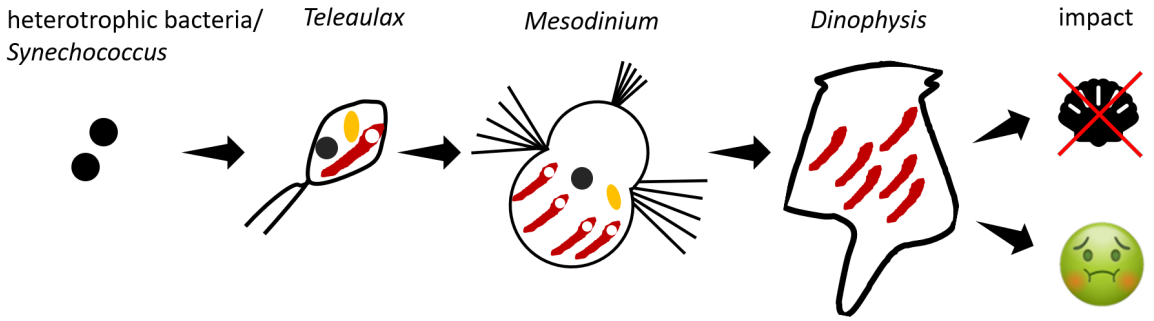

FIGURE 1.10: Schematic of the mixoplankton food chain of the *Teleaulax-Mesodinum-Dinophysis* complex. The constitutive mixoplankton *Teleaulax* feeds on bacteria. *Mesodinium* captures *Teleaulax* and retains its chloroplasts and nucleus. *Dinophysis* captures *Mesodinium* and takes over its third-hand kleptochloroplasts, but does not retain the nucleus. Various species of *Dinophysis* are notorious for causing diarrheic shellfish poisoning outbreaks and consequent aquaculture closures around the world.

Gutiérrez-Estrada, 2007; Velo-Suárez et al., 2010; Moita et al., 2016; Ajani et al., 2016; Hernández-Urcera et al., 2018). Aquacultures may be particularly vulnerable to HABs by mixoplankton as they are both sites of inorganic and organic eutrophication and light limitation while also harbouring organisms (e.g. shellfish) that are particularly susceptible to toxic HABs. Increasing stratification due to climate change (Sallée et al., 2021) may promote the growth of HAB species like *Dinophysis* that need stable water columns to form large abundances.

Forecasts can be used to improve shellfish harvesting schedules and decrease the economic impact of blooms. Monitoring and toxin analyses for seafood safety controls are expensive and laborious (Vale et al., 2008; Blanco et al., 2013). Models can help improve our understanding of bloom formation and can be used in forecasting and thereby greatly reduce cost and economic loss due to contamination (Flynn and McGillicuddy, 2018).

Models designed for the prediction of *Dinophysis* blooms (Reguera et al., 2012; Moita et al., 2016) currently do not include biotic factors for bloom formation of *Dinophysis* such as eutrophication by nutrients or availability of *Mesodinium* and *Teleaulax*. Existing models for forecasting are often statistical or hydrodynamic models that focus on weather events or current input that were linked to previous blooms. While some of these models are very reliable in predicting blooms, others still have room for improvement. Models that take into account the trophodynamics of the TMD-complex can help improve our understanding of the functioning of these organisms and the triggers for DSP events. Current hydrodynamic models have the potential to be improved in their forecasting abilities by being joined with a biological model that takes into account prey availability.

A closer look at the organisms of the TMD-complex shows the functional and ecological diversity of mixoplankton types and that even organisms that are classified as the same mixoplankton type like the SNCMs *Mesodinium* and *Dinophysis* can differ greatly in how their mixoplanctonic activity is expressed. The study of the TMD-complex with numerical

models that simulate the organisms physiology provides the unique opportunity to better understand how different mixoplankton functional types shape their environment and what implications their physiology have in interaction with other mixoplankton functional types. Results from a first modelling attempt of multi-organism mixoplankton complex featuring different mixoplankton functional types as the TMD-complex can indicate caveats in considering their trophodynamics that may have previously been overlooked.

1.7 Modelling biological processes

Models are, in their simplest sense, an imitation of a selected part of reality. Features of that reality are either selected or omitted as simplifications based on the purpose and type of the model. Such purposes can be a visualisation of large or small-scale aspects of nature like a visual model of a protein or the solar system.

Conceptual models have the purpose to illustrate functional relationships between different components and focus on a concept. An example of this are food web models that describe predator to prey interactions in an ecosystem (Flynn and Mitra, 2009). Mathematical models describe the quantitative relationship between components. These can either be statistical models that are based on relationships between parameters derived from real data. Statistical models are for example linear regressions (Flynn and McGillicuddy, 2018). Or they can be deterministic models that translate relationships and functional dependencies between the agents of a model into mathematical equations.

Nutrient uptake rates by phytoplankton are often described with Michaelis-Menten-kinetics and prey:predator interactions as following the Lotka-Volterra rule (Soetaert and Herman, 2009; Crane and Grover, 2010; Flynn, 2018). Both types of mathematical models can be used for fore- and hind casting of the described events. Statistical models such as linear regressions (Flynn and McGillicuddy, 2018) however are limited to the parameters set by the original data set to a certain level of feasible extrapolation.

Deterministic models can be used to theoretically explore the relationship of components and their functioning. These models rarely consider random variability of environmental parameters, unless they include for example weather. In that way, they are similar to controlled laboratory experiments. Such models can be used for testing hypotheses, visualisation, understanding (statistics), pattern finding, analysis and prediction. Models can describe different numbers of dimensions depending on the number of space variables contained in the model. In addition, models can be in a steady state and dynamic state.

Steady-state models show no change over time, while dynamic models describe change over time. Zero dimension (0D) models only change over time and have no reference to space. This can be done to describe evenly mixed system such as culture flasks where it is expected that each point in in the given space is equal. 1D models contain one space variable. This space variable could be water depth in a plankton model to account for light attenuation by biomass over depth or simply a river where change

happens on a linear trajectory. 2D models describe the process on a plane or surface and could find application in the dispersions of a species in a certain area or migration patterns of birds. 3D models describe dynamics in volumes and would find application in plankton models that take into account water bodies and currents. Models describing fewer than 3 dimensions basically assume homogeneity over the omitted dimensions to justify the simplification.

An example of a simple classical deterministic plankton model are nitrogen-phytoplankton-zooplankton-models (NPZ-models) that describe the dynamics of the transfer of nitrogen from a dissolved nutrient to phytoplankton to zooplankton by nutrient uptake and predation (Fasham et al., 1990). These models are built with the purpose of describing simple plankton dynamics. The most notable simplification of this model is the reduction of the relevant driving nutrients to simply nitrogen and omitting other elements like carbon and phosphate (and silicate, only relevant for diatoms) and micronutrients like iron. The reason this simplification is done is that nitrogen is often assumed to be the main limiting nutrient in marine ecosystems, and the common element in organic matter and dissolved nutrients. Limiting a model to one element has the advantage of reducing the number of state variables which will drive up the demand for computational power. In large marine plankton models, computational power increases run time and cost. Nitrogen-based models are suitable for answering many questions and also for making predictive models. These models assume a fixed stoichiometry. Stoichiometry is the quantitative molar ratio of chemical elements in a given volume or mass (e.g. the biomass of an organism). In reality, the stoichiometry of available nutrients and organisms are variable. The ratio of external nutrients changes with variable external input as well as uptake by organisms (Sterner and Elser, 2002). The stoichiometry of prey changes the stoichiometry of the predator, and thus also grazing rates and other physiological parameters. In food webs, variable stoichiometry affects the trophic level of the organisms (Waal et al., 2010). As many mixoplankton types mainly feed as a means to acquire limiting nutrients like phosphorous (Jones et al., 1995; Carvalho and Granéli, 2010; McKie-Krisberg et al., 2015), variable stoichiometry may substantially impact grazing rates and place on the spectrum between autotrophs and heterotrophs in an ecosystem. Nitrogen-based models are not suitable to describe these processes, which creates the demand for variable stoichiometric models.

For photosynthetically active plankton, another important limiting factor to consider is light. Apart from daily and seasonal variation in irradiance, light availability will also be affected by the organisms described in the model as their biomass itself attenuates light. In dynamic biomass models, light can thus become a limiting factor over time.

Plankton models can either describe entire plankton communities (Yool et al., 2013; Butenschön et al., 2016) or focus on single plankton species (Ghyoot et al., 2015; Moeller et al., 2016). As mixoplankton become increasingly recognised as significant agents in marine plankton dynamics a rising number of plankton models have emerged that include mixoplankton (Thingstad et al., 1996; Baretta-Bekker et al., 1998; Stickney et al., 2000;

Hammer and Pitchford, 2005; Hood et al., 2006; Flynn and Mitra, 2009; Ward et al., 2011; Mitra et al., 2014; Våge et al., 2013; Moita et al., 2016; Ghyoot et al., 2017a).

Few models consider mixoplankton and they vary greatly in the degree of complexity in which they describe mixoplanktonic activity. Some of these models describe mixoplanktonic activity as the mere sum of phagotrophy and phototrophy (Thingstad et al., 1996; Baretta-Bekker et al., 1998; Jost et al., 2004; Ward et al., 2011). Some describe different modes of mixoplanktonic activity with varying compositions of phagotrophy and phototrophy (Crane and Grover, 2010) and others describe mixoplanktonic activity as a synergism of the two trophic modes (Stickney et al., 2000; Hammer and Pitchford, 2005; Flynn and Mitra, 2009). Moeller et al. (2016) and Ghyoot et al. (2017a) describe different mixoplankton types following the definition by Mitra et al. (2016). So far, very few models explicitly describe acquired phototrophy (Flynn and Mitra, 2009; Moeller et al., 2016). The "Perfect Beast" model (Flynn and Mitra, 2009) is a complex mechanistic model that describes mixotrophy as a synergism of both trophic modes that changes with its environment and the state of the cell. The mixoplankton protist in the model can be switched to function as different mixoplankton functional types. This model has been applied in several further modelling studies on mixoplankton types (Flynn and Hansen, 2013; Mitra and Flynn, 2010; Mitra et al., 2016; Leles et al., 2018; Leles et al., 2021).

1.8 Research aim

This thesis was aimed at studying the effect of describing different mixoplankton functional types in models and the implications of this on the species level for mixoplankton organisms using the example of the TMD-complex. There are already a few variable stoichiometric models on mixoplankton and various mixoplankton functional types that show their unique interaction with their biochemical environment (Flynn and Mitra, 2009; Ghyoot et al., 2017b). This work comprises a simple nitrogen-based model that distinguishes between different mixoplankton functional types, a nitrogen-based model of the TMD-complex and a variable stoichiometric model of the CM *T. amphioxeia.* N-based models are simple and therefore low in computational power. Their simplicity can help to understand the complexity of multi-organism mixoplankton interaction as found in the TMD-complex. The implications for predation in CMs as in *T. amphioxeia* have barely been explored, yet. Application of the variable stoichiometric model of *T. amphioxeia* is expected to shine some light on the implications of mixotrophy for the interaction of CMs with the stoichiometric signature of their changing environment.

1. First, a generic nitrogen-based model is presented that simulates five different functional types (chapter 3) protist zooplankton, protist phytoplankton and the three major mixoplankton types GNCM, SNCM and CM. A key question of emerging plankton models is, if a distinction between zooplankton, phytoplankton and mixoplankton makes any difference to the outcome of these models. An additional question

is, if a distinction between different mixoplankton types will affect the outcome of these models. The TMD-complex features two distinct mixoplankton functional types. *Teleaulax* is a CM and both *Mesodinium* and *Dinophysis* are pSNCMs. The model presented here can be explored in a variety of different nitrogen loadings, irradiances and mixed layer depths. A nitrogen model is compatible with larger ecosystem models.

Hypothesis: Distinguishing between different mixoplankton types in nitrogen-based plankton models makes a difference to the outcome of the biomass predictions.

2. The results of the first model imply that the bloom dynamics predicted by the generic N-based model differ greatly, depending on which mixoplankton type was used. Therefore, it is important to distinguish between functional types when building a nitrogen-based TMD-model. The generic N-based model was further developed to comprise the SNCMs *Mesodinium* and *Dinophysis* and the physiological constants of the TMD-model were configured with literature data (chapter 4). The mechanistic model is expected to improve the comprehensive understanding of the qualitative and quantitative trophodynamics of the TMD-complex. The model allows *in-silico* experiments of the complex exploring the effect of prey availability and bloom succession as well as abiotic conditions as nutrient load and irradiance on the interaction and bloom potential of the three elements of the TMD-complex. In the presence of many existing hydrodynamic models of *Dinophysis*, the question is if the consideration of the whole TMD-complex may improve predictive models and if their mixotrophic nature makes a difference to its bloom dynamics?

   Hypothesis: Prey and nutrient availability influence the bloom dynamics and the HAB potential of *Dinophysis*. Specialised mixotrophic relationships significantly influence the bloom dynamics of multi-organism mixoplankton complexes like the TMD complex.

3. The third model is a variable stoichiometric model of the cryptophyte *Teleaulax amphioxeia* (chapter 5). The variable stoichiometric model was deployed as there are certain limitations to N-based models. A variable stoichiometric model has the capacity to simulate limitations in nutrients other than nitrogen. Certain physiological aspects and triggers for mixotrophic behaviour such as feeding to compensate for a limiting nutrient cannot be captured in an N-based model that assumes fixed stoichiometry. The CM *T. amphioxeia* displays very low feeding rates and the trigger for feeding may well be the compensation for low phosphorous concentrations in its environment. The model presented here is a development of the “Perfect Beast” model (Flynn and Mitra, 2009) that was configured as *T. amphioxeia* and tuned to growth data of *T. amphioxeia* that were acquired in an experiment where the cryptophyte was grown in three different ratios of nitrogen to phosphorous.

Hypothesis: *T. amphioxeia* feeds on bacteria in conditions of low inorganic phosphorous to compensate for the missing nutrient.

The models presented here are aimed to improve the understanding of mixoplankton and the implications of considering them in plankton models and differentiating between different functional types. The major groups of mixoplankton functional types are CMs and NCMs, but there is great variation in the species of each group regarding their degree of phototrophic abilities, their triggers for feeding and means of interaction with other plankton types. The TMD-model presented here is the first model that describes the trophic relationship of three mixoplankton genera. The TMD-model may find application in the theoretical exploration of the trophodynamics of the complex. The variable stoichiometric model of *T. amphioxeia* is the first to describe mixotrophy in a CM cryptophyte.

These models can either be integrated into existing larger N-based or variable stoichiometric ecosystem models or be coupled with hydrodynamic models that are used for forecasting purposes. The full scope of the interaction of mixoplankton with marine ecosystems and the implications for trophic level estimation, eutrophication and generally changing environments in the face of climate change is still not be grasped. Improved understanding of different kinds of mixoplankton may find implementation in coastal management and monitoring.

Chapter 2

Material and Methods

What follows is a general description of the modelling and experimental methods used in this work and that are described specifically in the chapters.

2.1 System dynamics modelling approach

System dynamic models describe change over time in a defined system (Flynn, 2018). For example, a nitrogen-based model can describe where and how the total nitrogen of the system is stored at a given time (e.g. dissolved inorganic nitrogen vs organic nitrogen). The models in this study were built in the software Powersim Studio 10 (`www.Powersim.com`). The software provides a graphic user interface in which models can be built with a system dynamic approach. Modelling platforms with graphic user interfaces usually demand more computational power than writing direct code of the programming language such as FORTRAN, MATLAB or Python. The comparatively low computational power of the models in this thesis allowed the use of the sofware Powersim Studio and a more accessible approach to modelling. The models can be built as conceptual models in the graphic user interface as Forrester diagrams (Fig. 2.1) that are later joined with equations describing rates of change. State variables that contain the value for amounts are symbolised by rectangles in a Forrester diagram. Circles indicate auxiliaries that calculate rates and diamonds symbolise constants. Flows between state variables is indicated by double lined arrows.

The models here calculate the rate of change of a quantity over time. Such calculations require ordinary differential equations (ODEs) or partial differential equations (PDEs). PDEs are used in more complex models including space, for instance. In the models described here, only ODEs were applied. There are two main approaches to solving ODEs: the Euler method and the Runge-Kutta method. The Euler method is a first order method that estimates the next value based on the rate of change of the current value. The Runge-Kutta method are ODEs of several orders. The first order Runge-Kutta method is in fact the forward Euler Method. Higher order Runge-Kutta methods are often more accurate than the Euler method as they involve multiple slope calculations between the discrete values. The additional calculations make the Runge-Kutta approach of higher orders slower than the Euler method. In comparison, the Euler method is less accurate

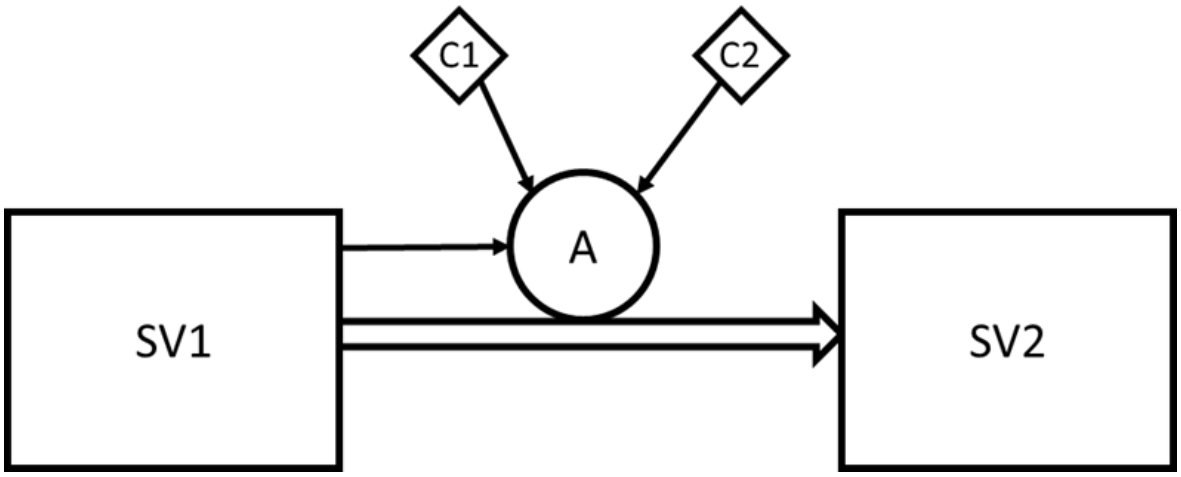

FIGURE 2.1: Forrester diagram of a conceptual model. The rectangles symbolise state variables, the circle an auxiliary and the diamond shapes constants. The hollow arrow represents the flow from state variable 1 (SV1) to state variable 2 (SV2) at the rate of the auxiliary (A). The thin arrows indicate which values the auxiliary references.

but faster due to fewer calculations. The error of the Euler method can be decreased by lowering the step size. The models described here use the Euler method. The timestep of each model was chosen as high as possible to ensure the model runs reasonably fast to facilitate the integration of the model into other models. At the same time, the timestep was chosen low enough ensure that the model runs stable and captures the daily light:dark cycle.

2.2 Sensitivity Analyses

Models are by definition a simplified version of reality. Every model excludes details that are either irrelevant for the features of reality the model is supposed to imitate, unknown or too complex to be implemented in the model and need to be reduced to the essential. Further simplifications can be setting fixed constants for parameters that are variable in nature or certain assumptions about the system. Examples for such simplifications are constants for variable parameters like assimilation efficiency of ingested nitrogen and the maximum growth rate as well as the assumption that all cells in the system are of the same size. Despite all simplifications, a model must still mimic the selected processes in reality. Only a model that does this properly is useful and can be learned from. The variation of the model output depends on two factors: The constants that the model was given and the model structure. The exact values of some constants like assimilation efficiency and maximum growth rate are often difficult to obtain, as these rates are challenging to measure. In addition, they are often not constants either. It is therefore important to validate the model to gauge the model's sensitivity to major changes of these factors by for example 50 %. Big changes in the model output with a variation of a single constant can indicate either a problem in the model structure itself or that this factor has particular

ecological influence in reality. In comparison, a risk analysis is performed to test if the model is robust and does not "crash" (e.g. divides by 0) when run in different conditions.

2.2.1 Steady State Sensitivity Analysis

Before a model's sensitivity to changes in certain physiological parameters is tested in dynamic conditions, the model is tested in steady state. In steady state the initial conditions remain the same over time and there is no accumulative change. Running a model with the exclusion of dynamic change, allows to test the impact of physiological parameters on the performance of an organism alone without distortion by a changing environment. For example, how much does the nitrogen uptake change with changes in maximum growth rate. For this purpose, all the input and output rates are set to a fix value and the model is put under stress (i.e. nutrient and light limitation). That way, potential weaknesses will show more clearly. The sensitivity of the model for each parameter was calculated with the equation 2.1 for single parameter sensitivity analysis by Haefner (1996).

$$S = \frac{\frac{Ra - Rn}{Rn}}{\frac{Pa - Pn}{Pn}} \tag{2.1}$$

Sensitivity (S) equals 1 when a doubling of the input value (Ra) doubles the output value (Pa). Negative sensitivity indicates the reverse effect. The equation determines the variation of the output from the default (*Rn* and *Pn*) versus the variation of the constant from the default value (*Ra* and *Pa*). For the analysis, the constant is both decreased and increased by 50 %.

2.2.2 Dynamic Sensitivity Analysis

Dynamic sensitivity analyses test a model's sensitivity to changes in physiological parameters in dynamic conditions where the effects can accumulate. For this analysis the model is run multiple times with the value of the constants being examined randomly varied (using a Latin Hypercube routine) assuming a standard deviation of 10 % of the original value. In addition to changing the value of physiological parameters (assumptions), the model is also run at different environmental conditions (decisions). These conditions are purposefully selected to include a range of extreme conditions, to ensure the model will still perform sensibly even in stressful conditions without breaking and returning an error.

2.3 Tuning

Often, the physiological parameters described in a model are difficult or even impossible to measure. To approximate or "guess" these parameters, the model can be tuned to existing data from experiments of field studies. For this purpose, the models external and initial parameters are set to the values of the conditions in which the real data was procured. The model output is then made to better fit the real data by changing the physiological parameters within possible limits to match the data. The Powersim software does not have a tuning tool. Therefore, tuning is done using the optimisation tool which is a genetic-algorithm of the Powersim software. The tool runs an evolutionary search for the best fit of the lowest standard deviation between the simulation and the provided data. The model is run numerous times changing the values of constants and state variables within a decided range in each generation. After each run the optimal fit is stored becoming the parent value for the next run. For this step, it is important to provide the model with evenly spaced data as missing data would cause errors in the tuning process. Such seamless continuous data is very rare for multiple reasons. Data may be missing due to sampling frequency, deleted outliers or measurement issues. It is legitimate to interpolate the missing data of a growth curve with reasonable points based on the existing data to make the data set fit for tuning purposes. Once a model is tuned to real data, it should be validated with another data set. The expectation is that the model can accurately reproduce the new data set without further adjustment of any physiological parameters. If it does, the model reliably simulates the organism it was designed to represent.

The process of tuning models requires continuous and evenly spaced data sets without missing data or outliers that divert from the rest of the data by a large margin. Such data is is hard to get for biological processes as sampling is often linked to man power, feasibility of sampling schedule and limitations in analysis. An approach to overcome this problem is to interpolate missing data in existing data sets for the tuning process. Unfortunately, it is a real challenge to find enough data sets for both tuning and validation of mixoplankton model due to the scarcity of suitable data for the purpose.

2.4 Validation

There are two main challenges in gathering suitable data for modelling. As the vast majority of biological experiments are not conducted with the idea in mind to produce data for the improvement of models, many data are not suitable for implementation in models. The data needed for the configuration of the model are often difficult to measure or quantify such as assimilation efficiency and biomass values. Measuring biomass in plankton is challenging as large cell numbers and thus high concentration cultures are necessary to achieve sample sizes that are well above the detection limit of the instrument. The bulk of physiological data references cells while biomass models need concentrations

and volume. As a result, the available data needs to be converted into the units of the model (e.g. mg N m^{-3}).

2.5 Experimental methods

For chapter 5 and the third research aim (chapter 1.8) an experiment with the cryptophyte *T. amphioxeia* was conducted specifically to generate data for tuning the variable stoichiometric model "Perfect Beast" (Flynn and Mitra, 2009). *T. amphioxeia* was grown in batch cultures under three treatments of varying nitrogen to phosphorous ratios to obtain physiological data of the organism in different conditions of external nutrient stoichiometry (Fig. 2.2).

2.5.1 Experimental set-up

T. amphioxeia was grown in Redfield ratio (control), nitrogen limiting and phosphorous limiting conditions in two replicates per treatment. All culture equipment was autoclaved or sterilised with ethanol and the cultures were assembled in a clean bench to avoid contamination with other organisms. The medium was prepared from autoclaved sea water and added nitrogen, phosphorous, vitamins and metals (Fig. 2.2). The stock culture of *T. amphioxeia* was grown at Redfield ratio. The culture volume of each batch culture was set to 5 L to ensure enough culture volume for the analysis of cellular carbon, nitrogen and phosphorous (2.5.6). Once the cultures were inoculated with *T. amphioxeia*, the culture flasks were sealed with an air tight stopper. This stopper was fitted with a tube for extracting samples, a tube for aeration to prevent the culture from running out of CO_2 and a tube to release excess air. The two latter tubes were fitted with a filter to avoid contamination from the environment. The cultures were kept in a culture room with a steady temperature and a set light:dark cycle. The cultures were regularly checked for contamination with flagellates to ensure that any biological activity was only attributed to *T. amphioxeia* and bacteria.

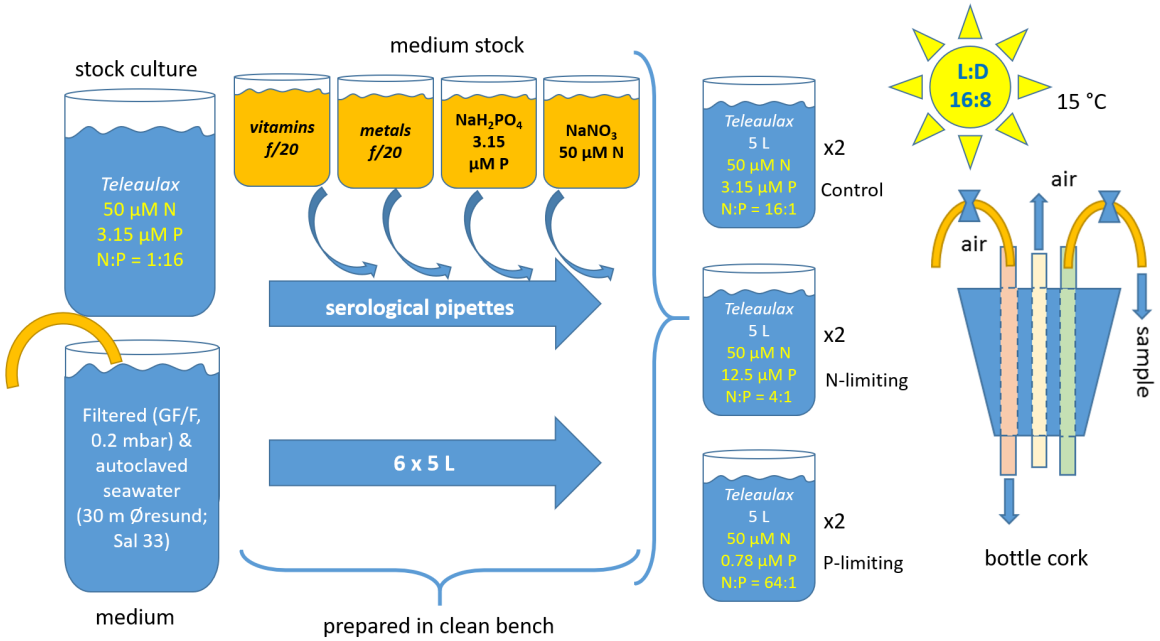

FIGURE 2.2: Experiment set-up of the *T. amphioxeia* experiment. The cryptophyte was grown at three different conditions of external nutrient ratios: Redfield, nitrogen-limiting and phosphorous limiting.

2.5.2 Cell numbers and biovolume

Cell numbers are an important parameter as they are used to calculate the per cell quota of other parameters. Therefore, cell numbers were measured with the flow cytometer (Beckmann Coulter, Cytoflex) and the Coulter counter (Beckmann Coulter Counter). The flow cytometer detects cells based on differences in cell complexity, cell size and pigment fluorescence (chlorophyll and phycoerythrin). The range for *T. amphioxeia* was set at the beginning of the experiment and used for the entirety of the experiment.

For bacteria counts glutardialdehyde was added immediately after sampling to stop any biological activity. Later, the fluorescent marker SYBR green was added to the samples to enable detection of bacteria by the flow cytometer.

Cell numbers and biovolume were measured in a Coulter counter with an aperture of 100 µm diameter (Fig. 2.3). The samples were diluted with filtered seawater (GF/F, salinity 33) by a factor 3 to avoid blockage and irregular counts by samples that are too dense. Two replicates of each experimental treatment replicate were measured. The range of *T. amphioxeia* cells to count was chosen based on the biovolume output and the size range specific to *T. amphioxeia* (4-9 µm). If a blockage occurred during measurement the sample was discarded and the value not used to take the average of two measurements.

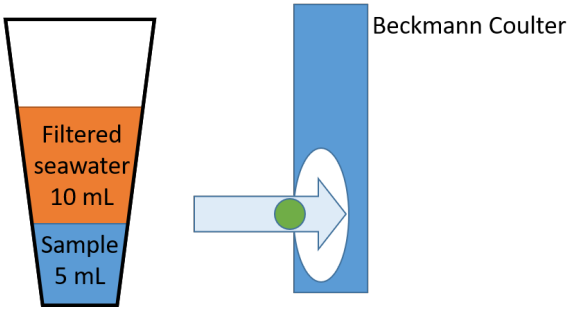

FIGURE 2.3: Schematic of Coulter counter measurements. The particles are detected in the aperture. Diluting dense samples decreases the risk of blockage of the aperture and ensures a steady stream of particles.

2.5.3 Chl *a*

For the analysis of Chl *a* the sample was filtered with a glass fibre filter (Fig. 2.4). The filter was then placed in ethanol over night to extract the Chl *a*. The filter was kept cool and shielded from light to avoid disintegration of the light sensitive pigment. For the determination of the Chl *a* concentration a sub-sample of the extract was measured spectrophotometrically.

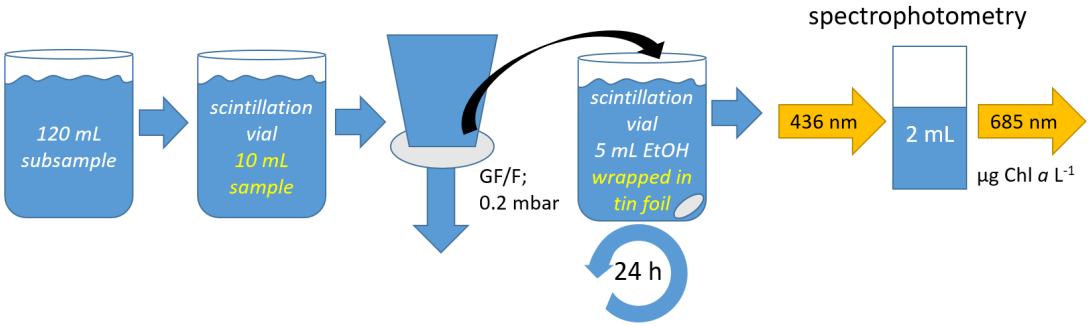

FIGURE 2.4: Schematic of Chl *a* measurement. Chl *a* was extracted with ethanol and the pigment concentration was measured spectrophotometrically.

2.5.4 Inorganic carbon uptake - ^{14}C incorporation

The uptake of inorganic carbon was determined by measuring the amount of incorporated radioactive carbon (^{14}C) for a given amount of time (Fig. 2.5). Two samples of the same volume of the culture were taken and spiked with the same amount of ^{14}C. In the culture room for the same amount of time, the one sample was kept in the light while the other was kept in the dark. After incubation, a sub-sample of the light incubation sample was transferred to a new glass vial prepared with phenylethylamine to stop biological activity and for determination of the specific activity (Skovgaard et al., 2000). For equal volume size the same volume of the sub-sample of the light treatment was also discarded of the dark treatment. The biological activity in both vials was stopped by acidification with 10 %

glacial acetic acid in methanol, which also removes the dissolved inorganic carbon. The liquid in the samples was then evaporated overnight on a heat plate at 60 °C. The residue was re-dissolved in ultra-pure water. For analysis, Packard Insta-Gel Plus scintillation cocktail was added to all vials and mixed with the sample by giving the vials a gentle shake while avoiding bubbles to form or the liquid to touch the lid. Three standards were run for each analysis prior to the samples. A Packard 1500 Tri-Carb liquid scintillation analyser with automatic quench correction was used to measure disintegrations per minute (DPM, disintegrations min^{-1} mL^{-1}) in the samples (specific activity, light, dark). Together with DIC concentrations, specific activity (total ^{14}C) and incubation time (h), DPM corrected for dark values was used to calculate photosynthetic activity (PA, pg C $cell^{-1}$ h^{-1}) per cell (Fig. 2.5).

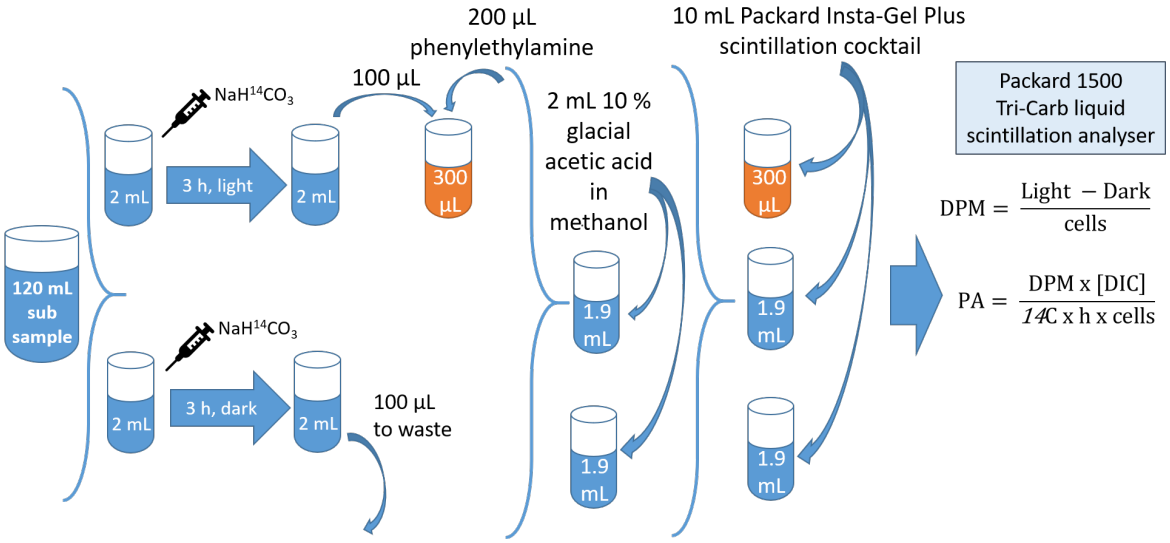

FIGURE 2.5: Schematic of inorganic carbon uptake (^{14}C incorporation). The method measures how much ^{14}C is incorporated by the organisms. For this purpose, one sample is kept in the dark while the other is exposed to the light conditions of the experiment. The ^{14}C incorporation by the cells is determined with the balance of total ^{14} (300 µL specific activity), the light incubation and the dark incubation.

2.5.5 Dissolved inorganic carbon (DIC)

Dissolved inorganic carbon (carbonate, bicarbonate and dissolved carbon dioxide) was measured with a combustion catalytic oxidation method (Fig. 2.6). The sample was filled into a glass vial, covered with aluminium foil and sealed with a screw cap allowing no air in the sample to avoid any contamination with DIC from the surrounding air. In this method, organic carbon is removed from the samples via acidification with H_2SO_4 which changes it to CO_2. Then the sample is oxidised and combusted and thus turned into gas-form. A non-reactive gas (halogen) functions as a carrier gas for the sample. In a moisture chamber the sample is cleared of any unwanted particles. Then, the halogen is removed and the inorganic carbon are measured in a detector.

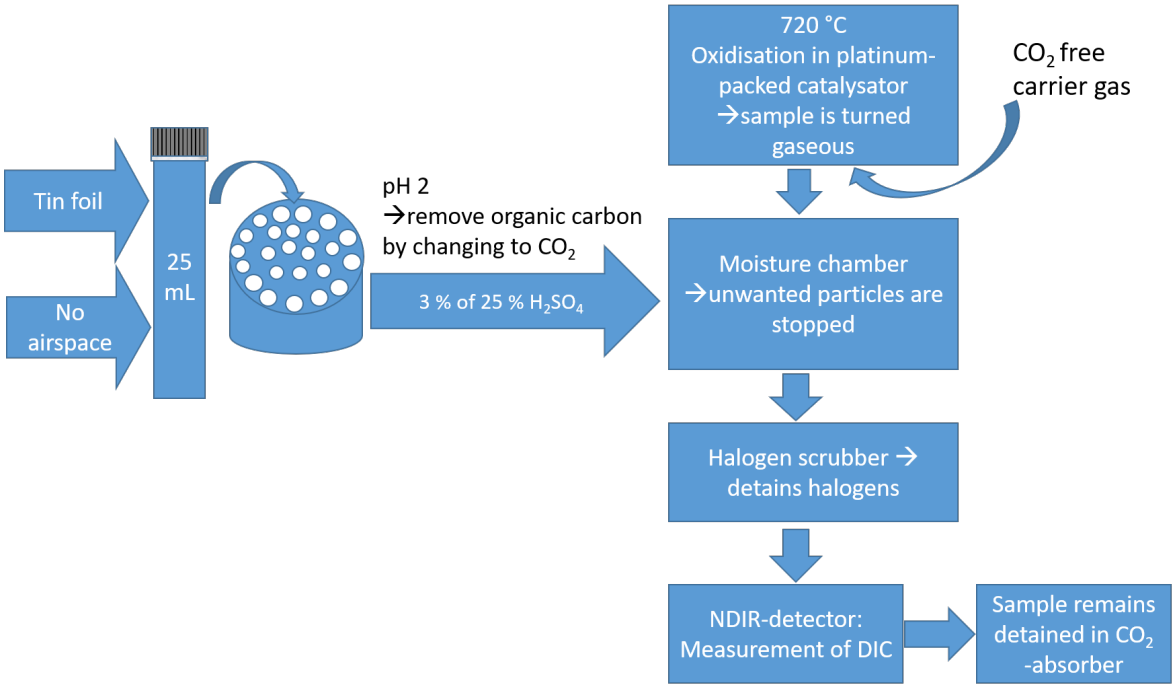

FIGURE 2.6: Schematic of analysis of dissolved inorganic carbon (DIC). DIC was measured by first removing all organic carbon. Then the sample was turned gaseous and the remaining inorganic carbon was detected.

2.5.6 Cellular organic carbon, nitrogen & phosphorous (C, N, P)

The sample for the analysis of cellular carbon, nitrogen and phosphorous is filtered with an ashed glass fibre filter to avoid contamination with carbon, nitrogen and phosphorous from the air and the filter (Fig. 2.7). The filter then needs to be dried in an ashed glass petri dish or a plastic petri dish that is lined with ashed tin foil to avoid contamination with organic carbon, nitrogen or phosphorous. Once the filter is dried it is ready for analysis. For the analysis, the filter is folded and put inside a tin cup, which is then folded shut. The tin cup is then placed into the analyser, where it is combusted and transported further via a non-reactive carrier gas (noble gas). Hydrogen and oxygen are filtered out and the elemental carbon, nitrogen and phosphorous can then be detected. As protists have a very low biomass per cell, enough sample needs to be filtered to obtain sufficient carbon, nitrogen and phosphorous on the filter to exceed the detection limit ($\sim$ 10 000 cells per filter) of the elemental analyser. As a result, low cell concentrations of the culture require large sample sizes.

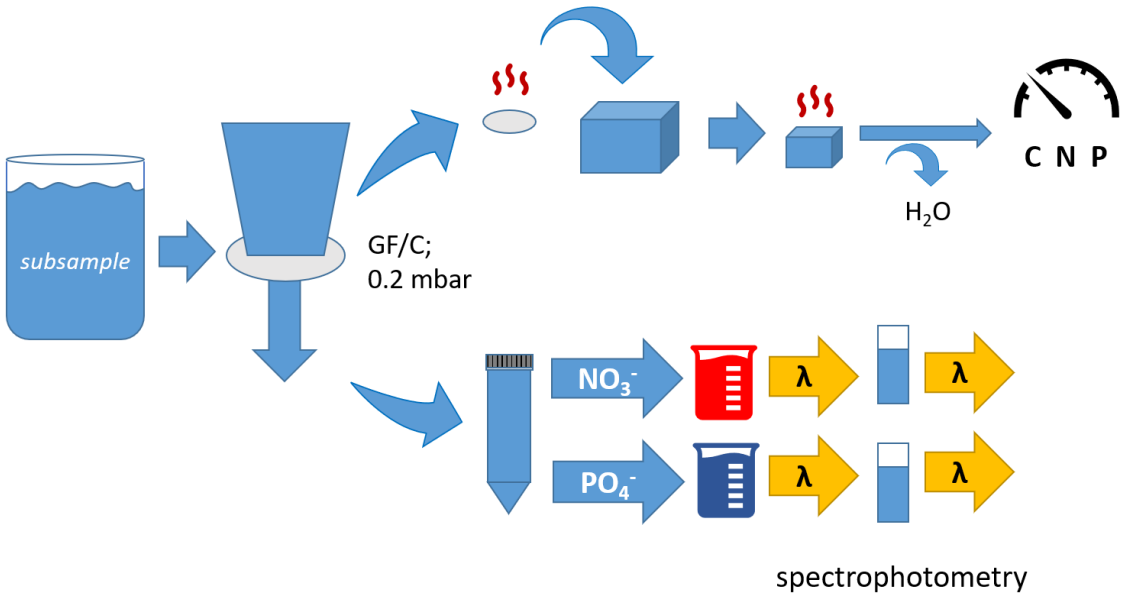

FIGURE 2.7: Schematic of of analysis of organic carbon, nitrogen and phosphorous (CNP) and dissolved inorganic nitrogen (DIN) and phosphorous (DIP). Both analyses were preceded by the same filtering step. The filter was used for the analysis of CNP while the filtrate was used for the analysis of DIN and DIP. DIN and DIP were measured spectrophotometrically after reaction with a photoactive compound. CNP was measured by removing all DIC, turning the sample gaseous and then detecting it with an element detector.

2.5.7 Dissolved inorganic nitrogen and phosphorous

Dissolved inorganic nitrogen and phosphorous were measured by light spectrometry. The filtrate from the analysis for cellular organic carbon, nitrogen and phosphorous was used for this analysis as the particular matter was filtered out in that process (Fig. 2.7). Other than Chl *a* nitrate and phosphorous can not be measured directly with light spectrometry. In preparation for this method, a coloured complex is added to the sample which binds to the parameter and absorbs light in a specific wavelength. Nitrate is made to react with such a compound to form a reddish azo dye, while phosphate is made to form a blue antimony-phospho-molybdate complex. Both are excited at different wavelength in the spectrometer and measured at different emission wavelengths.

Chapter 3

Niche separation between different functional types of mixoplankton: results from NPZ - style N - based model simulations

Marine Biology (2020) 167:3
https://doi.org/10.1007/s00227-019-3612-3

Niche separation between different functional types of mixoplankton: results from NPZ - style N - based model simulations

Anna-A Anschütz[1,2,3], Kevin J. Flynn[1]

Abstract

Protist plankton comprise phytoplankton (incapable of phagotrophy), protozooplankton (incapable of phototrophy) and mixoplankton (capable of phototrophy and phagotrophy). Of these, only phytoplankton and zooplankton are typically described in models. Over the last decade, however, the importance of mixoplankton across all marine biomes has risen to prominence. We thus need descriptions of mixoplankton within marine models. Here we present a simple yet flexible N-based model describing any one of the five basic patterns of protist plankton: phytoplankton, protozooplankton, and the three functional groups of mixoplankton: general non-constitutive mixoplankton (GNCM), specialist non-constitutive mixoplankton (SNCM), and constitutive mixoplankton (CM). By manipulation of a few input switch values, the same model can be used to describe any of these patterns, while adjustment of salient features, such as the percent of C-fixation required for mixotrophic growth, and the rate of phototrophic prey ingestion required to enable growth of GNCM and SNCM types, readily provides fine tuning. Example outputs are presented showing how the performance of these different protist configurations accords with expectations (set against empirical evidence). Simulations demonstrate clear niche separations between these protist functional groups according to nutrient, prey and light resource availabilities. This addition to classic NPZ plankton models provides for the exploration of the implications of mixoplankton activity in a simple yet robust fashion.

[1] Biosciences, Swansea University, Singleton Park, Swansea SA2 8PP, UK

[2] School of Earth and Ocean Sciences, Cardiff University, Park Place, Cardiff, Wales CF10 3AT, UK

[3] Université libre de Bruxelles, Ecologie des Systémes Aquatiques, cp-221, Boulevard du Triomphe, 1050 Brussels, Belgium

3.1 Introduction

Although often superseded by variable stoichiometric constructs, the simplicity of the classic nitrogen-based NPZ model (Fasham et al., 1990; Franks, 2002) still finds favour as a tool for exploration of conceptual ecology, and also in large-scale models where computational costs are at a premium (Yool et al., 2013). The NPZ structure originated at a time when microbial plankton were typically considered as primarily phototrophic phytoplankton or heterotrophic protozooplankton. We now better appreciate that this represents a gross simplification; it transpires that much of the protist classically labelled as "phytoplankton" and as much as 50% of the "protozooplankton" in the photic zone are actually mixoplankton, combining photo(auto)trophy and phago(hetero)trophy in the same organism (Flynn et al., 2013; Flynn et al., 2019). The "P" and "Z" in NPZ models are therefore behaving in a way that at least on occasion grossly misrepresents reality. Mixoplankton express various forms of photo–phago mixotrophy; there is not one mixoplankton functional type (mPFT), but at the minimum two (Table 3.1). These two mPFTs are those that have a constitutive ability to photosynthesise (CMs) and those that acquire that capability using photosystems taken from their prey or using symbionts (the non-constitutive mixoplankton, NCMs). The NCMs can be further divided into those that can acquire phototrophy from many phototrophic prey (generalist; GNCMs) and those that require specialist prey (SNCM) as plastidic forms (pSNCM)or with endosymbionts (eSNCM). This mPFT classification is described in full by (Mitra et al., 2016). To date, there is only one model structure that attempts to simulate the variety of mixoplankton physiology (excluding eSNCM), namely the "perfect beast" model of Flynn and Mitra (2009) which provides a single variable stoichiometric (C:N:P:Chl) construct switchable between different modes of mixotrophy. Although the perfect beast model has been used in ERSEM-like simulators (Leles et al., 2018), the inherent complexity of a variable stoichiometric model can act as a hindrance to those who are hesitant to explore the implications of the inherently complex different mixoplankton strategies. This current work developed from a desire to derive a construct that, while still describing the essence of the different mPFTs, is simple enough to operate within NPZ-style simulators.

The characteristic functions of the five protist variants portrayed in the model are shown in Table 3.2. These cover the range of functional types described in Mitra et al. (2016), with the exception of the endosymbiotic SNCM forms. The function types in Table 3.2 are arranged in the order in which phototrophy was added stepwise with increasing levels of integration of phototrophy with phagotrophy, beginning with purely phagotrophic protozooplankton (hereafter, protoZ), GNCM, SNCM, CM, and then finally (with the loss of an ability to perform phagocytosis) protist phytoplankton (hereafter protP). The protoZ align with "Z" in classic NPZ terminology and are incapable of phototrophy. The protP, "P" in classic NPZ terminology, are incapable of phagotrophy; the most ecologically important representatives of protP are the diatoms. We sought to build a model that could, by setting a few switch (parameter) values, enable a single construct to represent any

one of these five protist forms. Within those forms, further modification can be made to fine-tune salient features affecting features such as prey selection, the relative roles of phototrophy and phagotrophy, the periodicity of ingestion of phototrophic prey for GNCM and SNCM, and so on. These functional type descriptions hide a significant level of taxonomic variation. Thus, while many GNCMs are ciliates (Dolan and Pérez, 2000; Pitta et al., 2001; McManus et al., 2004; Calbet et al., 2012; Mitra et al., 2016), the model would apply equally if one wished to consider flagellate GNCM. The SNCM is largely modelled in the image of the ciliate SNCM *Mesodinium* and the dinoflagellate SNCM *Dinophysis*. They are involved in the *Teleaulax–Mesodinium–Dinophysis* complex, where *Mesodinium* acquires its kleptochloroplasts from the cryptophyte *Teleaulax* (which itself may be a CM, feeding on bacteria) via ingestion and *Dinophysis* in turn acquires these chloroplasts from *Mesodinium* (Jacobson and Andersen, 1994; Gustafson et al., 2000; Reguera et al., 2012; Yoo et al., 2017).

3.2 Methods

We provide a discursive description of the model here; the equations are provided in a linear form within an Excel file in the ESM to assist in deployment into the reader-preferred simulation software platforms. The model operates using ordinary differential equations. Figure 3.1 gives an overview of the submodels describing functionality in each of the five protist types, while Fig. 3.2 gives an overview of the entire NPZ-style model structure. In the ESM we provide additional information for the whole simulator as used here (i.e., including the abiotic submodel, and the trophic connectivity). Nutrient N is provided as ammonium and nitrate, and light is provided in a light–dark cycle. References to additional figures in the Electronic Supplementary Material are identified in what follows in the style of "Fig. Sx". Some elements of the model exist for several organisms individually and are marked with a suffix indicating their affiliation (e.g. *"_Prot)"*; suffixes are omitted here for clarity and simplicity.

Protist biomass is described as a single state variable for N-biomass (mgN m^{-3}); additional state variables are required when (as here) the model is run within a light–dark cycle, as intermediaries are required for calculating day average growth and photosynthetic rates. Depending on the value of a constant that acts as a switch (Switch_Protist; see ESM), the model conforms to the behaviour of one of five protist functional types. Switch_Protist takes the following values: 0 = protoZ, 1 = GNCM, 2 = SNCM, 3 = CM, 4 = protP. While the order of the protist functionality in evolutionary terms is likely akin to protoZ, GNCM, SNCM, CM and protP, for simplicity we will first describe protoZ, then protP, followed by CM, GNCM and SNCM. There are also two prey types described in the model, termed "microalgae" (Alg1 and Alg2) which act as feed for protoZ, or as feed and/or competitors for mixoplankton and protP. The GNCM variant can acquire phototrophy by feeding on either of Alg1 or Alg2; the SNCM can also feed on both, but specifically needs to ingest Alg1 (as its specialist prey) to acquire its phototrophic potential. Functionally, Alg1 and

TABLE 3.1: Definition of mixoplankton types, with examples of species. Definitions are after (Flynn et al., 2019). Examples for the mixoplankton types are given in Mitra et al. (2016) and Leles et al. (2017) and Leles et al. (2019).

Mixoplankton type	Definition (after Flynn et al. (2019))	Examples
CM Constitutive mixoplankton	Protist plankton with an inherent capacity for phototrophy that can also exhibit phagotrophy (cf. NCM)	*Prymnesium* *Karlodinium*
NCM Non-constitutive mixoplankton	Protist plankton that acquires its capacity for phototrophy from prey or from endosymbionts (cf. CM)	see GNCM, SNCM
GNCM Generalist non-constitutive mixoplankton	NCMs that acquire their capacity for phototrophy from general (i.e. nonspecific) phototrophic prey (cf. SNCM)	*Laboea* *Strombidium*
SNCM Specialist non-constitutive mixoplankton	NCMs that acquire their capacity for phototrophy from specific phototrophic prey (plastidic—pSNCM) or from endosymbionts (eSNCM)	*Mesodinium* *Dinophysis* Green *Noctiluca*

TABLE 3.2: Functionality of the protist model in each variant setting. The protist types are listed broadly in line with evolution. See also Table 3.1. Although nitrate usage is indicated as optional for GNCM (and was disabled in simulations shown here), it is also optional for the other phototrophic variants. Black circle = function expressed; white circle = function not expressed; black and white circle = function can be de/activated with a switch; no circle = function does not apply *protoZ* protozooplankton, *GNCM* general non-constitutive mixoplankton, *SNCM* specialist non-constitutive mixoplankton, *CM* constitutive mixoplankton, *protP* phytoplankton.

Function	protoZ	GNCM	SNCM	CM	protP
Phagotrophy	●	●	●	●	○
Phototrophy	○	●	●	●	●
Acquired phototrophy		●	●		
Daily acquired phototrophy (poor management of acquisition)		●			
Interval acquired phototrophy (management of acquisition)			●		
Use of NH_4^+ with phototrophy		●	●	●	●
Use of NO_3^- with phototrophy		◐	●	●	●

Alg2 are analogous to the protP variant, and provide classic NPZ-style descriptions of organisms that could be considered as cyanobacteria or as protist "phytoplankton". The food web could be further developed as required, but an SNCM variant must make specific reference to one of the phototrophic preys (either to a CM, a protP or perhaps another SNCM, as appropriate to the purpose at hand) as the source of its acquired phototrophy.

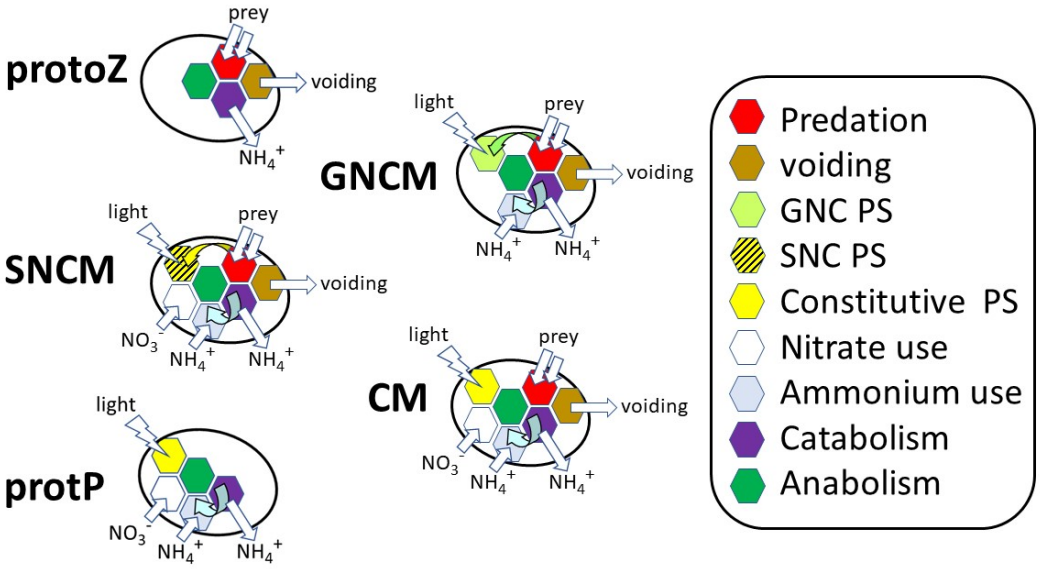

FIGURE 3.1: Schematic representations of the five protist functional type configurations. They contain the submodels for various physiological functions as indicated. *protoZ* protozooplankton, *GNCM* generalist non-constitutive mixoplankton, *SNCM* specialist non-constitutive mixoplankton, *CM* constitutive mixoplankton, *protP* protist phytoplankton. See also Tables 3.1 and 3.2. The microalgal prey, Alg1 and Alg2, have the same functions as protP.

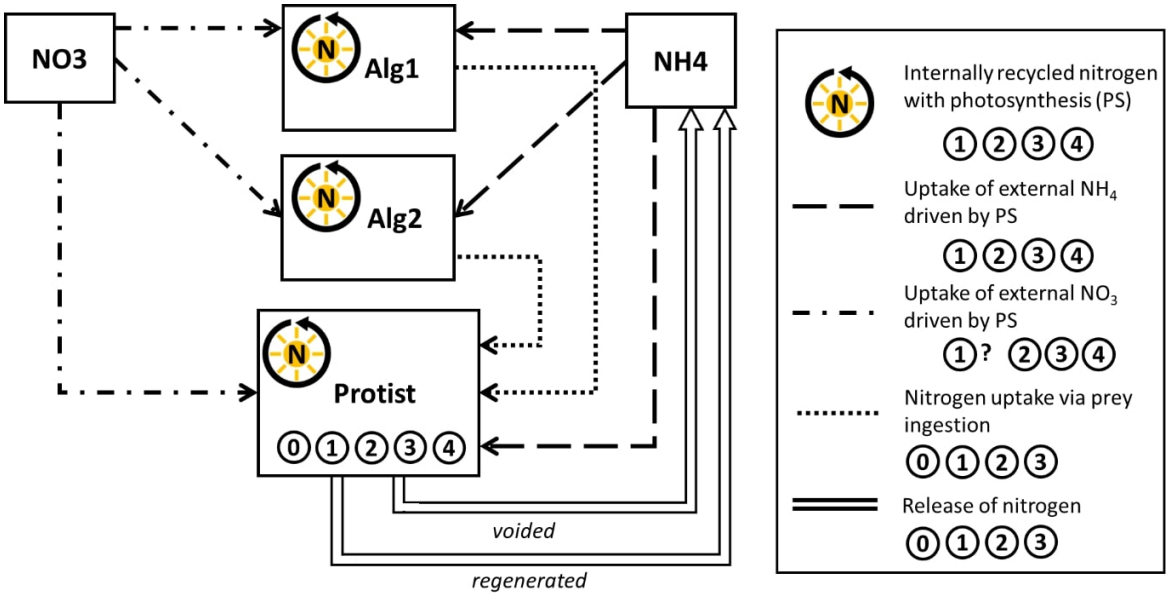

FIGURE 3.2: Schematic of the main model and its state variables. The protist submodel can function as five different protist types (see Fig. 3.1, Table 3.2) by activating the respective physiology functions with a switch specific to the protist types. As an SNCM, the protist can prey on both Alg1 and Alg2 but only acquire chloroplasts from Alg1. The priorities in the use of inorganic nitrogen types are: 1. internally recycled nitrogen, 2. NH_4^+, 3. NO_3^-. Effective use of external nitrate by GNCMs appears to be at best rare, which is why here this function was disabled (see also Table 3.2).

3.2.1 protoZ variant

Only one state variable (N-biomass) is used with one inflow of nitrogen, in the form of ingested prey (*ing*, ingestion rate). The approach used here to describe prey encounter, capture and ingestion is justified and described in detail by Flynn and Mitra (2016) as modified in Flynn (2018). Encounter considers the allometric- based cell-specific encounter rate between predator and prey, where the cell numbers are calculated from carbon biomass and converted to N-biomass assuming fixed C:N stoichiometry. The encounter rate (Enc) per day is calculated after Rothschild and Osborn (1988) and makes reference to cell radius of protoZ and of prey (e.g., *r_Alg1*, ESD/2 in meter), prey cell number (*nos_Alg1*), speed of motilities (*v*) and water turbidity (*w*). Prey optimality for handling is considered by reference to the size of both predator and prey. A prey handling index (*PR*) defines whether prey size is in the suitable range for capture, indicating the likelihood of the predator successfully capturing it. In addition to prey handling and prey encounter rate, prey capture (*CR*) is also dependent on the palatability of the prey and the proportion of prey of optimal characteristics captured by a starved protist (*Optimal_CR*). The model contains a routine to reference palatability according to its N:C ratio and its toxicity (*tox*), though this is not implemented for this present work. The resultant capture rate is then multiplied by the prey:predator cell abundance ratio in *CRC*.

If the prey biomass is above a certain threshold, actual ingestion (*ingC*) of captured cells is controlled by the maximum carbon-specific ingestion rate (*ingCmax*; see below) and a constant for satiation control of ingestion (*KI*). If more than one prey type is available, *ingC* makes reference to the sum of captured cell biomass (*SCRC*); the ingestion rates are applied individually as outflows of the prey models (*lig*). To correspond with the otherwise nitrogen- based model, *ingC* is converted to nitrogen by reference to the N:C ratio (NC_plank). The ingestion rate depends on its maximum possible assimilation of ingested material (*opmaxIAss*), which in turn depends on its demand for nitrogen to achieve maximum growth rate (*Umax*) accounting for losses and basal respiration (*BR*). The two outflows (Figs. 3.1, 3.1) are the release of regenerated nitrogen (*reg*) from catabolism and voided nonassimilated ingested material (*void*). The maximum possible ingestion rate (*opmaxIng*) satisfying *opmaxIAss* takes into account losses due to assimilation efficiency (*AEN*) and the specific dynamic action (*SDA*, anabolic cost for assimilating nitrogen). Ingested nitrogen lost by *SDA* is released as regenerated nitrogen (*regNsda*), while the non-assimilated nitrogen is voided (*voidN*). The growth rate (*u*) of the protoZ is the ingestion rate minus the rate of voiding and release of regenerated nitrogen. When *u* falls below a certain limit, biomass is further lost through a mortality rate (*mortRate*, Supplemental Material Fig. S1). Mortality increases gradually at $u < 0$ and attains a maximum value when $u <$ negative half the *BR* rate assuming that below this threshold most of the population will die. The rate of prey ingestion depends on satiation (*opmaxIng*), prey optimality (*PR*), the encounter rate (*Enc*) of suitable prey and its capture (*CRC*); see Supplemental Material Fig. S7.

3.2.2 protP, Alg1 and Alg2 variants

These model variants are structurally the same. Ammonium and nitrate assimilations are handled using a priority approach favouring ammonium, while photosynthesis uses a depth-integrated routine where the maximum rate is controlled by the N-status. (This routine can be replaced using one that makes reference to just the average at depth irradiance level). Only one state variable (N-biomass) is used. The phototrophic configuration of the protP and of Alg1 and Alg2 is described here identically with just minor differences in the photosynthesis parameterisation (slope alpha and the plateau maximum) to help differentiate them in model outputs. They could, of course, be made more or less different as required. For brevity, the following only makes reference to protP, but also applies to Alg1 and Alg2. Dissolved inorganic nitrogen (DIN) uptake is needed to support the photosynthetic growth rate up to a maximum (*maxGPS*). DIN is acquired as nitrate and/or ammonium coupled to photosynthesis. In conditions where photosynthesis is less than respiration, ammonium is regenerated (*RegN*). DIN (as ammonium and nitrate) is taken up according to Michaelis-Menten kinetics with a maximum value set by *maxGPS*, a half saturation constant for the substrate (*Knh4*, *Kno3*) and a scalar to define the transport needed to match to growth needs (*TGnh4*, *TGno3*). Through reference to the external DIN concentration, potential transport rates for ammonium (*PVnh4*) and nitrate (*PVno3*) are computed. The nutrient status (*Nu*) is contributed to by internally recycled (regenerated) ammonium (*RegN*), externally provided ammonium and externally provided nitrate, in that order of priority. The value of *Nu* down-regulates the achievable gross photosynthetic rate (*grossPS*) as described below. The actual nitrogen demand to support concurrent photosynthesis (*Ndem*) is corrected for the costs of assimilating DIN (metabolic respiration, *MR*). The difference of Ndem and RegN needs to be taken up as DIN (*uTP*). Organisms that can use both ammonium and nitrate prioritise ammonium; they take up nitrate (*Vno3*) if their nitrogen demand is not covered by the uptake of ammonium (*Vnh4*) and internal regenerated nitrogen (*RegN*).

Light and nutrient status (via *Nu*) limit photosynthesis. Photosynthetic efficiency (alpha, as the slope of the PE curve, *alphau*) depends on both quality of chlorophyll (*opAlphaChl*) and the (fixed) chlorophyll-to-carbon ratio of the organism (*opChlC*). Light is described as the photon flux density (PFD, µmol photon m^{-2} s^{-1}) and, in the implementation presented, is set within a light-dark cycle. Photosynthesis is described according to a depth-integrated variant of the Smith equation (Smith (1936); see Kenny and Flynn (2016)), which takes into account light attenuation in the water column. Both water and suspended particles attenuate light; the growing biomass thus attenuates light and causes selfshading. Attenuation by chlorophyll (*abco_Chl*; 0.02 m^2 mg Chl^{-1}) is used together with assumed fixed Chl:C and N:C stoichiometries values for each photosynthetic organism to derive the organism-specific attenuation coefficient (*abco*). Attenuation by this component then references the biomass abundance (mgN m^{-3}) to give *attco*. The total light attenuation in the water column is the sum of the light attenuation by all photosynthetic organisms and the water (*attco_W*) multiplied by the mixed layer depth (*MLD*; m). The

negative exponent of the light attenuation (*exatt*; EXP(*-att_tot*)) is used in the calculation of the depth-integrated photosynthetic rate. The maximum photosynthetic rate under nutrient stress (*PSqmax*) the organism will achieve under optimal light conditions (*pytq*) depends on its photosynthetic efficiency described by the hyperbolic PE curve where *PSqmax* is the saturation factor. Light is the photon flux density expressed in units per day. The gross photosynthetic rate of the population in the water column (*grossPS*) is determined by integrating *pytq* over depth as a proportion of the light actually available after attenuation by water and photosynthetic organisms (*att_tot*). In darkness, the growth rate is decreased to zero; no mortality rate is implemented here as within a reasonable time frame (weeks), phytoplankton typically survive in darkness consuming previously accumulated organic C (not explicitly simulated here in this N-based model). See the end of the description for SNCM (below) concerning the enabling of the use of nitrate by protP.

3.2.3 CM variant

This variant merges the functionality of the protoZ and protP variants (see above and Fig. 3.1), placing an obligatory requirement for a stated level of phototrophy while permitting enhanced growth when operating as a mixoplankton. Only one state variable (N-biomass) is used. Constitutive mixoplankton have an inherent capability for photosynthesis. In addition, they can acquire organic nitrogen through prey ingestion. Like the protP, the CM does not have a mortality rate when the growth rate becomes very small. Growth is controlled differently from the protP and protoZ variants, because phototrophy and phagotrophy are coupled. The configuration of the CM prioritises phototrophy, with any difference between the maximum growth rate and net phototrophy (*PAss*) being topped up via phagotrophy. While growth as a mixoplankton can exceed that of growing solely as a phototroph, there is the operational caveat that a critical amount of nutrient must come via phototrophy. This minimum proportion of the maximum growth rate to come from phototrophy is set by *pCritMin*; it accounts for the need to obtain certain metabolites via photosynthesis. The maximum assimilation of ingested material (*maxIAss*) can therefore not be higher than *maxGU*, defined as gross assimilation needed to support *Umax*, minus the critical amount of phototrophy (*op_pCritMin*). The operational maximum assimilation of ingested material (*opmaxIAss*) cannot exceed maxIAss or fall below BR (e.g., in darkness); the latter permits survival but not positive growth when feeding in darkness, unless *pCritMin* = 0. See the end of the description for SNCM (below) concerning the enabling of the use of nitrate by CM.

3.2.4 GNCM variant

This variant merges the functionality of the protoZ and protP variants (see above and Fig. 3.1), but here without an ability to use nitrate and also a need for phagotrophy of photosynthetic prey to provide phototrophic potential. Like the CM variant, there is an

obligatory requirement for a stated level of phototrophy. NCMs do not have an inherent capability for phototrophy and thus need to acquire their phototrophic ability (chloroplasts) from their phototrophic prey. Ingestion and phototrophy are therefore much more closely linked than they are in the CM variant. In addition to the single state variable describing N-biomass, the GNCM variant makes use of an additional state variable to track the history of the acquired phototrophic potential, which decays over time in the absence of recent photosystem acquisition. The maximum photosynthetic growth rate is maintained as long as the GNCM ingests at least a minimum number of chloroplast- containing prey items per day and decreases at lower ingestion rates. The ingestion rate of chloroplast-containing prey, relative to the minimum required to support maximum phototrophy is indexed by the prey ingestion index (*PiI*). *Strombidium capitatum* reportedly replaces its chloroplasts after 40 h (Schoener and McManus, 2012). Such minimum requirements are computed through reference to prey:GNCM cell ingestion rates. Noting that GNCMs simply asset strip their prey's photosynthetic machinery, the maximum photosynthetic growth rate of the GNCM is a combination of the maximum photosynthetic growth rates of their ingested prey species in proportion to the ratio they were ingested in. As GNCMs have very limited control over the performance of their chloroplasts, the same applies to the photosynthetic efficiency of the chlorophyll (*alphaChl*) and the chlorophyll carbon ratio (*ChlC*). We note that increasing gross growth efficiency is dependent upon the carbon from photosynthesis being sufficient to re-assimilate SDA-released ammonium (Schoener and McManus, 2017). If the rate of fixed carbon is low relative to the rate of ingestion, then this may result in an inability to recover the ammonium; it may just balance BR, for example. However, under a high-prey scenario, the need to retain nutrients is lessened. See the end of the description for SNCM (below) concerning the enabling of the use of nitrate by GNCM.

3.2.5 SNCM variant

This model variant merges the functionality of the protoZ and protP variants (see above and Fig. 3.1), placing an obligatory requirement for a stated level of phototrophy and also for phagotrophy from a specific prey source to provide phototrophic potential. This variant (like the GNCM variant) makes use of an additional state variable to track the history of the acquired phototrophic potential. The SNCM differs from the GNCM in its ability to control the ingested chloroplasts and that it can only use the chloroplasts of one prey species (set here as *Alg1*). SNCMs are known to be able to maintain maximum photosynthesis with their acquired chloroplasts up to 30 days or longer. The prey ingestion index (*PiI*) of the SNCM records the ingestion rate of the special prey over the last 30 days (or any other critical time frame) (Park et al., 2008; Hansen et al., 2016).

Mesodinium reportedly can survive up to 100 days without prey (Johnson et al., 2007; Hansen et al., 2016) and *Dinophysis* up to 30 days (Hansen et al., 2016), with *D. caudata* surviving for up to 2 months (Park et al., 2008). In the absence of continuing

chloroplast acquisition from the special prey, the operational maximum photosynthetic rate gradually declines, described here using a hyperbolic function. Due to its ability to control the performance of the chloroplasts, the SNCMs *opPSmax*, *alphaChl* and *ChlC* are all inherent to the mixoplankton protist and not to its prey, as is the case for GNCMs. However, these photosynthesis parameters are modulated by the prey ingestion index (*PiI*), applied now specifically with reference to the special prey (here, Alg1). For both the GNCM and the SNCM, the degree of similarity in the functioning of the chloroplast in the prey and the host can be changed by making alpha either dependent or independent of the host. The ability to use nitrate can be switched on or off for all mixoplankton types and also in the protP, as required to conform to the physiology of the organisms of interest. Thus, while GNCMs are typically suspected to lack an ability to use nitrate, *Strombidium rassoulzadegani* (Schoener and McManus, 2017), can use nitrate (Schoener and McManus, 2012). In the SNCM *Mesodinium*, the ability to used nitrate appears to be linked to chloroplast possession (Wilkerson and Grunseich, 1990). This switching is achieved by changing value of *TGno3_Prot* from 1.1 for nitrate use to 0 to turn nitrate use off.

3.2.6 Simulations

The model was built and run using Powersim Studio 10 (`www.Powersim.com`); the Studio 10 model is provided in the ESM. For the simulations presented here, the model was run using an Euler routine to solve ordinary differential equations, with a step size of 0.0625 day^{-1}. For illustration, growth of the protist (configured as one of the 5 variants) is simulated over a 30-day period also with microalgae Alg1 and Alg2. Steady-state and dynamic sensitivity analyses were conducted, the latter using the "risk" tool in Studio 10, using a Latin hypercube sampling routine.

3.3 Results

3.3.1 Results Sensitivity analyses

To test the model's sensitivity to the value of constants controlling protist behaviour, functional dependence and dynamic state sensitivity analyses were performed. The numeric results of both analyses can be found in the ESM. The most sensitive parameters for the protist model alone are assimilation efficiency (*AEN*), BR rates, the maximum proportion of growth that can come from phototrophy (*pCrit Max*), and the maximum growth rate (*Umax*). In the dynamic sensitivity analysis, performance of the whole model showed sensitivity to the same parameters, and additionally also to the anabolic respiration cost for assimilating DIN (*MR*). For operation as a GNCM or SNCM, the critical minimum ingestion index (which affects the dynamics of the acquisition of phototrophy) showed sensitivity. None of these levels of sensitivity were considered as being excessive

in terms of the effect changing of the value of the constant would have on the general production of the organism. All are in the direction and of the magnitude expected. A lowering of the assimilation rate for example drives up the ingestion rate pro rata, as expected.

3.3.2 Functional dependence

Figure 3.3 shows, for each of the protist functional types, the net growth rate at different combinations of light and prey abundance. The protoZ and protP plots provide references against which to judge the performance of the mixoplankton. Note that in all instances the maximum growth rate was set at the same value, and indeed as far as applicable (see Table 3.2) all constants were of the same value. It is evident that all mixoplankton configurations have emergent features of lower half saturation points for light and prey abundance than do the protP and protoZ variants. The protP does not attain growth rates near the maximum (0.693 day-1) until PFD > 500 µmol photons m^{-2} s^{-1} (not shown). The mixoplankton do much better in this regard even at low prey abundances, because they acquire additional nutrition via predation. The form of the GNCM vs SNCM plots reflect the fact that the former cannot (as configured here) use nitrate and thus grows phototrophically using ammonium regenerated by prey digestion; no external ammonium was supplied for these particular model solutions.

It is also noteworthy that there is no net growth for GNCM or SNCM with zero prey; these protist configurations acquire their phototrophic potential from ingestion of their phototrophic prey. Figure 3.4 shows how the differences in behaviour in Fig. 3.3 have potential to define niches for the different protist configurations versus protoZ. The protoZ is only superior against GNCM at very low light, and GNCM is superior mainly at low prey abundance (noting a critical prey availability is required to support acquired phototrophy); otherwise they are quite similar. A similar trend is seen for SNCM v protoZ, except SNCM is superior to GNCM at low prey, because SNCM can use nitrate while GNCM here relies solely on recovery of ammonium from prey digestion to support phototrophy. This also explains the difference between SNCM v GNCM. CM is superior to protoZ at even low prey availability, and is likewise superior to GNCM and SNCM, because CM does not depend on ingestion of phototrophic prey for acquired phototrophy. Figure 3.5 is analogous to Fig. 3.4 but now defining niches for the different protist configurations versus protP. Superiority of protP over protoZ relies on the absence of prey and the presence of sufficient light (nitrate nutrient being supplied in abundance in these simulations). In comparison, GNCM is equal to protP at zero light as GNCM is critically dependant on a minimum level of phototrophy and so cannot grow solely phagotrophically. Similarly, SNCM and also CM are also reliant on low light to grow even with abundant prey. At very low prey levels, GNCM and SNCM are disadvantaged in comparison with protP by the need to acquire phototrophy from their prey. However, CM is superior to protP over the entire prey–light

range, although it too cannot achieve net positive growth in total darkness, hence the difference between protoZ and CM at 0 PFD (i.e., darkness; Fig. 3.3).

3.3.3 Dynamic simulations

Figure 3.6 shows how each of the protist descriptions behave in dynamic scenarios under different light and nutrient regimes. The system is conservative, with system nitrogen (*sysN*) as the sum of dissolved nitrogen and biomass-N being constant. Details for different facets of these interactions are shown in Figs. 3.7, 3.8 and 3.9, and Supplemental Material Figs. S4-S8. Light is affected by the MLD and also by the self-shading that develops as the supplied inorganic N is converted to Chl-containing biomass (Supplemental Material Fig. S5). As the inoculation (initial biomass value) of the protist is half that of either of the algae, the increase in algal (Alg1 and Alg2) biomass is more obvious at the start of the simulations. Growth of the protist follows that of Alg1 and Alg2 with a delay that is greater according to the level of heterotrophy (i.e., the matching of protist growth with that of Alg1 and Alg2 was closest in the order protP $\geq$ CM > SNCM > GNCM > protoZ). This reflects the need of protists dependent on phago-heterotrophy for sufficient prey abundance to support their growth; the more dependent the protist type is on the ingestion of prey to grow, the more it requires the prey biomass to increase first to effectively support its own growth. Below, we first consider the configuration-specific results from these dynamic scenarios, and then we consider more general results.

3.3.4 protoZ

When the protist is set as protoZ, the model behaves like a typical NPZ model. Ammonium and nitrate (in that order of selection) decrease as they are consumed by Alg1 and Alg2 (Fig. 3.6). The increase in algae biomass is followed by a rapid rise in the protoZ biomass. Following the voiding of non-assimilated biomass (with its assumed instantaneous remineralisation in this model) and release of regenerated nitrogen by the protoZ, ammonium levels increase while the algal biomass is removed by predation. On near extinction of the algal prey, protoZ starve and die, further contributing to the ammonium concentration. Ammonium reaches a maximum on the effectual death of all protoZ. The pattern of rapid increase and decline in biomass is mirrored by the growth rate of the protoZ (Fig. 3.7); after a peak, the growth rate rapidly declines and becomes negative as prey consumption fails to meet respiratory demand. The predator– prey cycle is more frequently repeated in low nutrient ("oligotrophic") conditions (Fig. 3.6), as the interactions are less affected by boom-and-bust dynamics when both algal and predator growth are restrained by resource abundance. At around day 15, the protoZ's growth rate increases again at a slower rate than previously, but reaches a higher value and a plateau before it collapses again. At greater MLDs, the dynamics were slowed with decreased prey growth rates at lower light levels, contributed to also by self-shading from high algal biomass. Algal growth rates

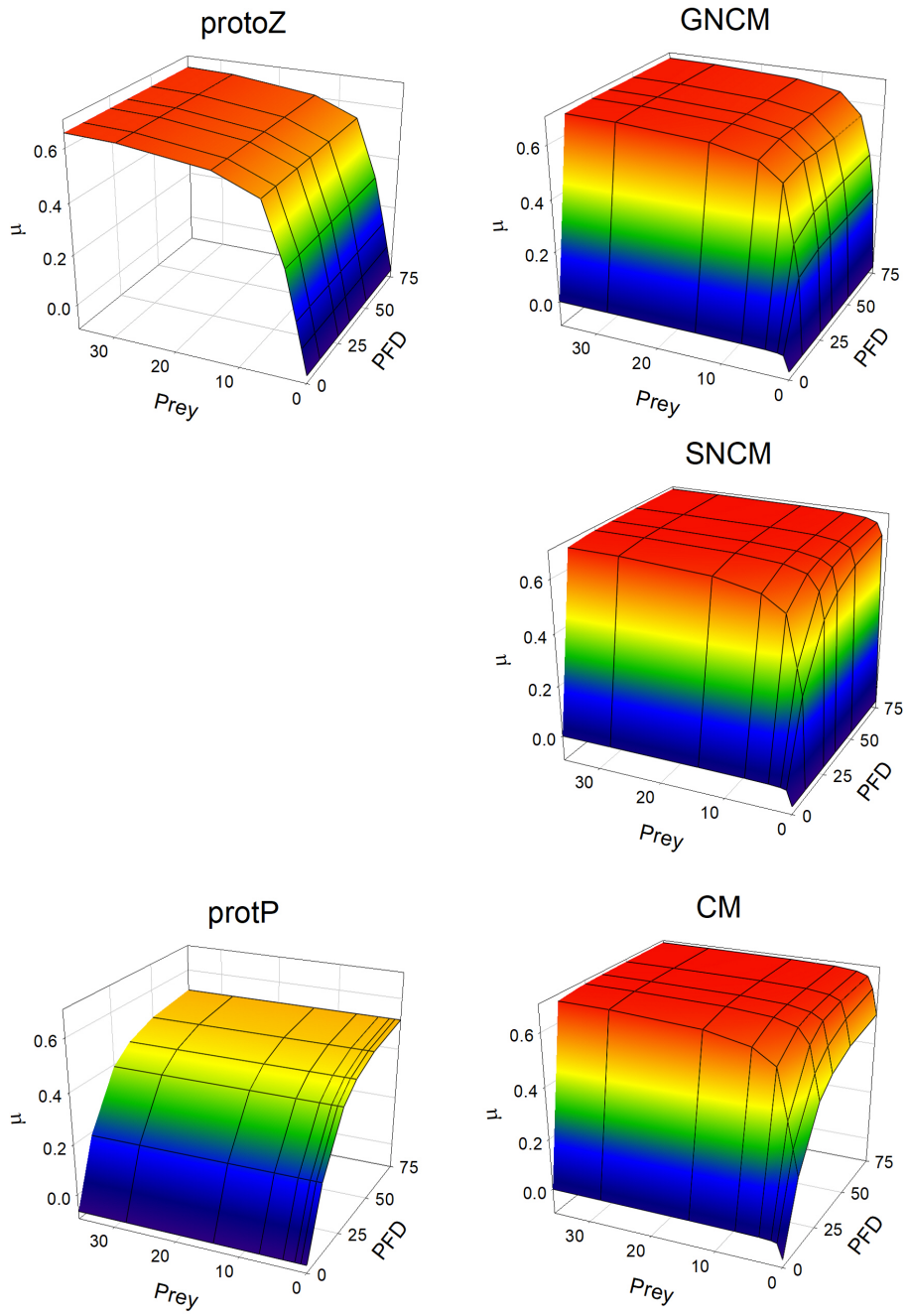

FIGURE 3.3: 3D-mesh plots showing the relationship between growth rate (μ; day^{-1}) and sources of energy supplied as light (PFD; μmol m^{-2} s^{-1}) or prey (mgN m^{-3}) for different protist configurations. Nitrate is supplied as the sole external N source, at 700 mgN m^{-3} (50 μM). The colour gradient relates to the change in growth rate μ indicated by the z-axis. Prey are phototrophic and assumed also to be the special prey species required to support acquired phototrophy by the SNCM. Protozooplankton (protoZ) and protist phytoplankton (protP) can only use prey or light, respectively. GNCM as configured here cannot use nitrate and hence are solely reliant upon inorganic N regenerated from digestion of prey. SNCM can use nitrate, explaining the differences between SNCM and GNCM configurations. However, both GNCM and SNCM must also engage in predation to acquire phototrophy. CM can engage in phototrophy in the absence of prey. Note that the relationships for growth vs PFD and prey for GNCM, SNCM and CM are all steeper than for their protoZ and protP comparators.

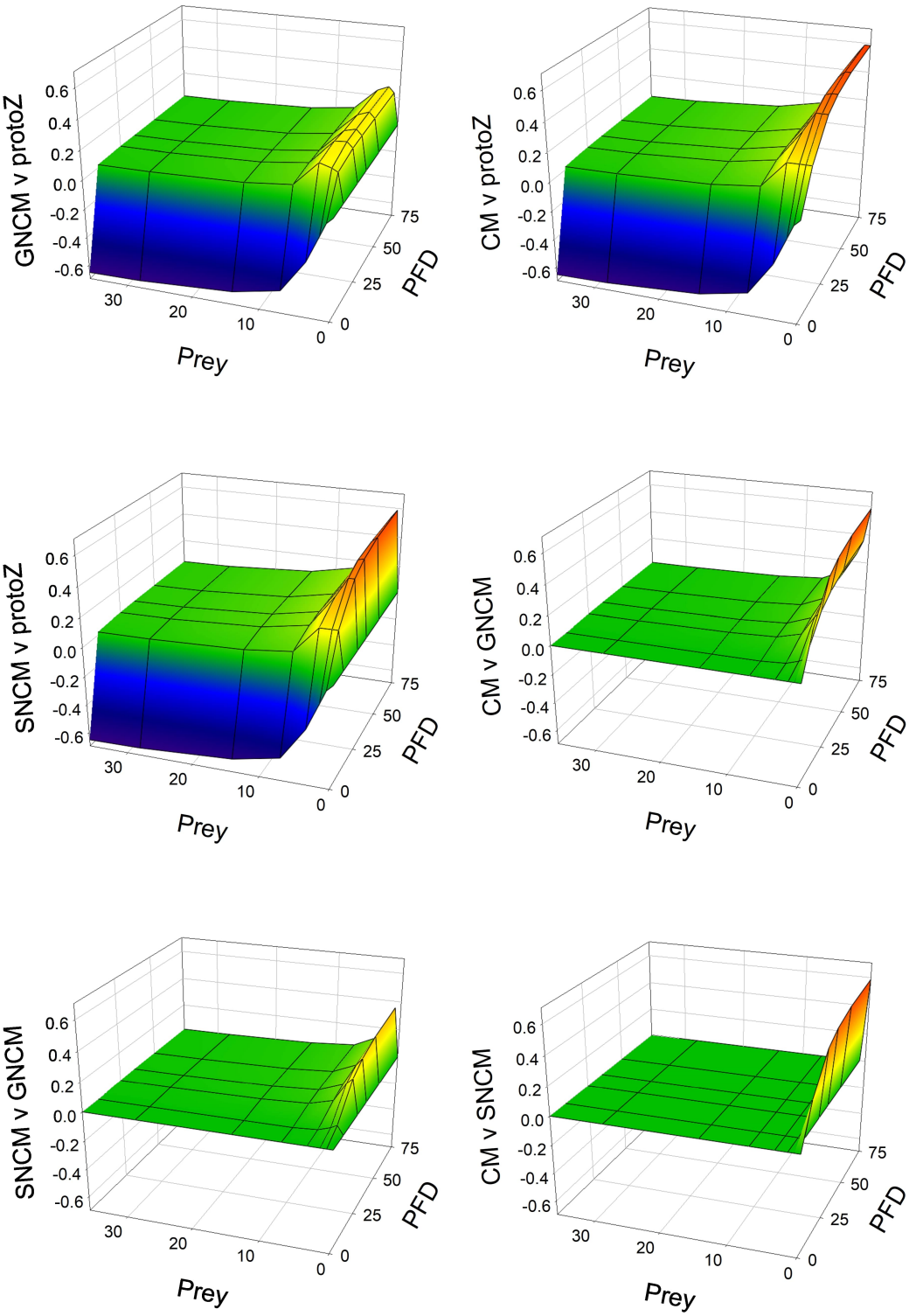

FIGURE 3.4: 3D-mesh plots providing niche comparisons between pairs of protist variants excluding protP (see Fig. 3.5). The colour gradient relates to the change in growth rate μ indicated by the z-axis. These are based on the relationship plots shown in Fig. 3.3 between growth rate and sources of energy supplied as light (PFD; μmol m^{-2} s^{-1}) or prey (mgN m^{-3}). The z-axis shows the difference between the growth rate (μ; day^{-1}) of the first named protist type and the second named; a positive value indicates a niche where the first named is superior, a negative where the second named is superior.

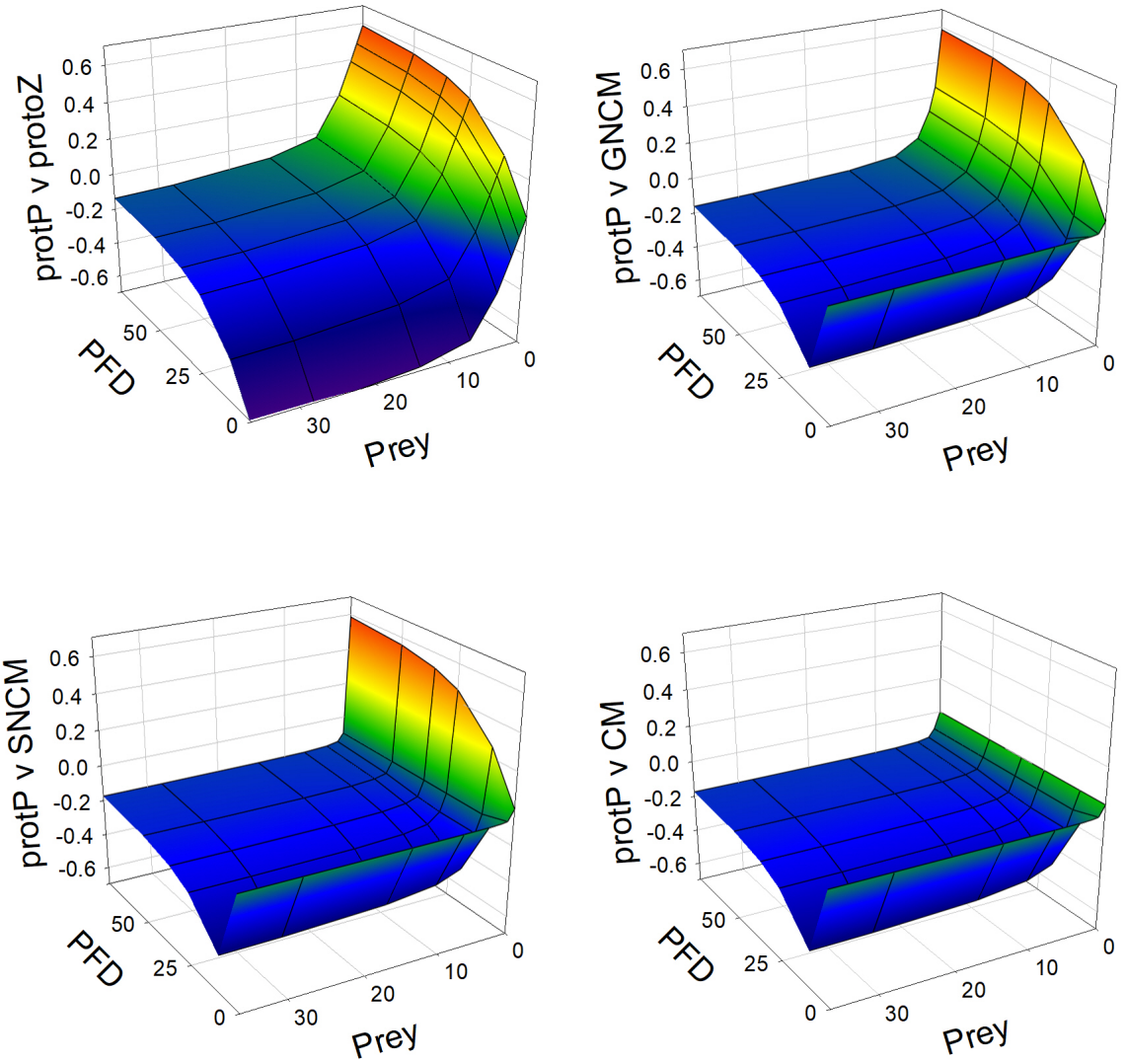

FIGURE 3.5: As Fig. 3.4 but for niche comparisons between protP and the other protist configurations. The colour gradient relates to the change in growth rate μ indicated by the z-axis. Note that for clarity the rotation of the 3D mesh is different to that used in Fig. 3.4.

increase again when light limitation (self-shading) is relieved by predation decreasing the total algal biomass. In conditions with lower nutrient loads, events are prolonged as prey availability limits the predator. At high nutrient loads, growth of the algae is prolonged due to biomass-linked self-shading causing light limitation (Supplemental Material Fig. S5).

3.3.5 GNCM

Despite their shared high level of dependency on phagotrophy, the simulations using the GNCM display certain differences to those using the protoZ. For one thing, growth commences earlier for the GNCM (Fig. 3.6). This is due to two factors: (1) once the GNCM becomes phototrophically active from consuming Alg1 and/or Alg2 it increases its growth rate, (2) as the ammonium released with SDA is recovered (rather than being released, as in protoZ), the conversion of prey capture to protist growth is greater than it would be for a protoZ for a given grazing rate. The GNCM grows by coupled photo-phago-trophy thus becoming also a competitor for ammonium and light to the algae. The GNCM growth rate exceeds that of the algae, because the protist is not so limited by light attenuation and can in addition feed on the algae. Rather than displaying a short-duration biomass peak, the growth rate of the GNCM remains higher for longer - the duration of the plateau in growth rate is affected by MLD and nutrient load (Fig. 3.9) - before the steep decline.

Ammonium did not accumulate as it did with the protoZ version, and nitrate usage by the algal prey (GNCM not being allowed to use nitrate in these simulations) became more apparent. Since the GNCM prioritises phototrophy as long as the conditions for it are opportune (Fig. 3.7, low nutrient load/self-shading and MLD), they exert a lower grazing pressure on the algae than do protoZ, thus allowing the algae to achieve a larger biomass than in the protoZ scenario. The GNCM also generated larger peak biomasses than the protoZ, particularly in shallower MLDs. Once the algae prey are consumed, the GNCM growth rate falls, as it can no longer perform acquired phototrophy. Like the protoZ, the GNCM then immediately begin to starve and die. When the protist operates as a GNCM, any second bloom cycles starts with a much greater delay than when operating as a protoZ, because the GNCM grazes down the prey more completely.

3.3.6 SNCM

The SNCM grew for longer and generated much more biomass during blooms than the GNCM variant. In addition, nitrate levels declined further and faster than when the protist was a GNCM, because the SNCM is also able to use nitrate in addition nitrate usage by the Alg1 and Alg2. The net phototrophic growth rate is also more stable as the SNCM can use nitrate in addition to ammonium. On exhaustion of resources, the growth rate of the SNCM declines at a much slower rate than does the GNCM variant, as it has a much less frequent demand of prey ingestion than does the GNCM. Just as the GNCM

outperformed the protoZ in biomass yield in shallow and oligotrophic conditions, so the SNCM outperformed the GNCM in those conditions. The explanations are that: (1) the SNCM needs to ingest prey much less frequently than does GNCM to maintain its acquired phototrophy capability, making it more independent of the biomass of its prey and (2) it can use nitrate granting it an additional source of nitrogen especially in oligotrophic conditions. The ability to photosynthesize and thence use inorganic nitrogen only gives the NCMs an edge over protoZ under good light conditions (Fig. 3.4). In deep highly eutrophic water, light attenuation is so high (Supplemental Material Fig. S6) that they have to resort almost completely to phagotrophy (noting that a critical proportion of N must nonetheless come via phototrophy). This also affects the use of ammonium vs nitrate. In the SNCM configuration, the ratio between nitrate and ammonium usage reverses (f-ratio goes low, Supplemental Material Fig. S8) at the end of the bloom with ammonium exceeding nitrate usage in oligotrophic conditions until 40 m and mesotrophic conditions until 10 m. As long as the SNCM can acquire sufficient photosynthetic capacity from their prey, they can also use nitrate, as their internally recycled ammonium is insufficient to meet their needs in primary production. Indeed, they can become net contributors to DIN and ammonium starts to accumulate.

3.3.7 CM

The CM configuration differs from the NCMs in that the former can commence growth without needing to acquire phototrophy from ingesting phototrophic prey. In addition, after depletion of prey, the CM can continue growing by phototrophy alone. The CM thus remains as an established bloom, because it does not have the starvation-associated death rate seen in the other phagotrophic forms. This configuration attained the maximum possible biomass, all as just CM (the algae having been eliminated), under any nutrient load and *MLD* (taking longer to do so with lower light attributed to a deeper *MLD* and/or self-shading at high nutrient loads). It not only competes with the algae for nutrients (actually outcompeting them, because phagotrophy contributes to CM biomass growth), but also removes its competitors for light by feeding on them in light-limiting conditions. The CM growth rate is similar to the SNCMs, but develops more smoothly and does not eventually go negative.

3.3.8 protP

The protP growth dynamics are the same as the two algal organisms as it functions identically (noting that its Chl:C is configured as being like Alg1, while Chl:C for Alg2 is lower). The growth rate of the protP is equal to the net phototrophic growth rate of the CM after the latter runs out of prey. Here, the algae accumulate biomass faster than they do in the presence of a phagotroph (protoZ or mixoplankton), because of the lack of grazing pressure. By the same token, growth of protP biomass is slightly slower than

the mixoplankton, because it does not have the added advantage of phagotrophy and is restricted by light availability in dense blooms. The protP biomass does not surpass that of either of the algae, which is a consequence of the lower inoculum (start biomass value) of the protist. Like the CM, protP continues to grow until nitrate is depleted, and then remains at that established high biomass. The overall biomass yield of all organisms in the protP scenario (i.e., Alg1 + Alg2 + protP) equals that of the CM alone in the CM variant simulations. The CM removes its competition and then uses all nutrients in the system for itself, whereas when the protist is configured as protP the three organisms (Alg1 + Alg2 + protP) have to share the DIN.

3.3.9 General results

Under any given combination of nutrient loading and *MLD*, the functional configuration of the protist greatly influences the use of external nitrogen and the development of the biomass of the different components algal and protist biomass (Fig. 3.6), and thence affects cumulative productivity (Supplemental Material Fig. S4). Not only are there clear differences between the simulations using a protP vs mixoplankton, and mixoplankton vs protoZ, but there are clear differences between the different mixoplankton types (i.e., GNCM vs SNCM vs CM). Increased nutrient loads generally lead to larger yields in the biomass for both the algal prey/competitors and protist. Configuring the protist as a protoZ generated the lowest total biomass, as this form cannot contribute directly to primary production. The protist peak biomasses were highest in the mixoplankton settings, with the SNCM and CM configurations both surpassing the GNCM version. Configured as a mixoplankton, the protist outcompeted its algal prey in all three modes (GNCM, SNCM, CM). As protP, the protist was an equal competitor to the algae resulting in the final overall biomass level of the three phototrophs combined being similar to that of the CM alone. Under all protist configurations, additional bloom cycles are seen if the simulation is played out over longer periods (not shown). The gap between cycles increased with nutrient load and degree of phototrophy in the protist; the SNCM simulation failed to repeat a cycle even after 500 days due to a failure of its Alg1 photosystem donor to regrow. The maximum instantaneous prey assimilation rate is a constant in the protoZ configuration, and there is no diel oscillation. In contrast, the mixoplankton configurations have a variable operational maximum prey assimilation rate that depends on the concurrent photosynthetic rate, and therefore varies between a maximum value and that required to just match *BR*, and also with the cycle of illumination. As the mixoplankton can only (re)assimilate the ammonium released by *SDA* during assimilation of prey N concurrently with photosynthesis, their prey ingestion only takes place during the light phase. The changing maximum ingestion rates in the mixoplankton configurations result in their food lasting longer.

3.3.10 Physiological features

All phototrophic organisms in the model prioritise the use of ammonium (Fig. 3.8). Once, ammonium levels become insufficient to support growth, the algae, SNCM, CM and protP begin to take up nitrate to achieve maximum growth rate. The NCMs only use inorganic nitrogen as long as prey are available, as they require those prey to provide their photosynthetic potential. The balance of nitrate and ammonium usage, and the specific rates of usage are affected by the degree of light limitation and the rate of ammonium regeneration (which, for mixoplankton, is affected also by internal ammonium recycling). The decrease in the use of ammonium does not stem from limitation in ammonium, but due to light limitation associated with high phototrophic biomass causing self-shading (Supplemental Material Fig. S5).

Under high nutrient load, with a high initial organism inoculum, the encounter rate of prey is greater. Phagotrophs feed at their maximum capacity, outstripping the environment of their prey faster, in conditions with high nutrient load. When prey concentrations fall below the minimum concentration, below the threshold to sustain the NCMs minimum chloroplast demand, NCM mixoplankton lose their phototrophic ability.

In Supplemental Material Fig. S5, the biomass levels of all five protist configurations are shown growing under combinations of nutrient loading and *MLD* that would yield similar depth-integrated levels of irradiance. Except for the development of biomass of the protoZ in oligotrophic conditions at 40 m, the levels of nitrate, ammonium, the two algae and the protist show similar patterns for a given protist configuration. Differences between simulation scenarios in Fig. 3.6 are thus most strongly driven by the impact of irradiance. Light limitation (Supplemental Material Fig. S6) affects energy inputs and thence the organism growth rates and system dynamics. The behaviour of the SNCM is like an intermediate between the very different GNCM and CM in this context.

3.4 Discussion

3.4.1 Model overview

We describe a low computation cost protist model that can be readily configured to represent different protist plankton types, physiology, size and growth rates. The model explicitly considers allometry for prey encounter kinetics and also the acquisition of chloroplasts into NCMs. The model as presented allows for comparing performances of these protist types in different conditions of water depth, nutrient load and irradiance. Thus, the model provides a useful tool to explore hypotheses and questions concerning plankton dynamics under different scenarios. As a nitrogen-based model with few state variables, it is simple and runs fast. It is therefore suitable for implementation in large ecosystem dynamic models that use plankton models. The subject of plankton trait trade-off has provided a rich ground for theoretical research over the last few decades, including

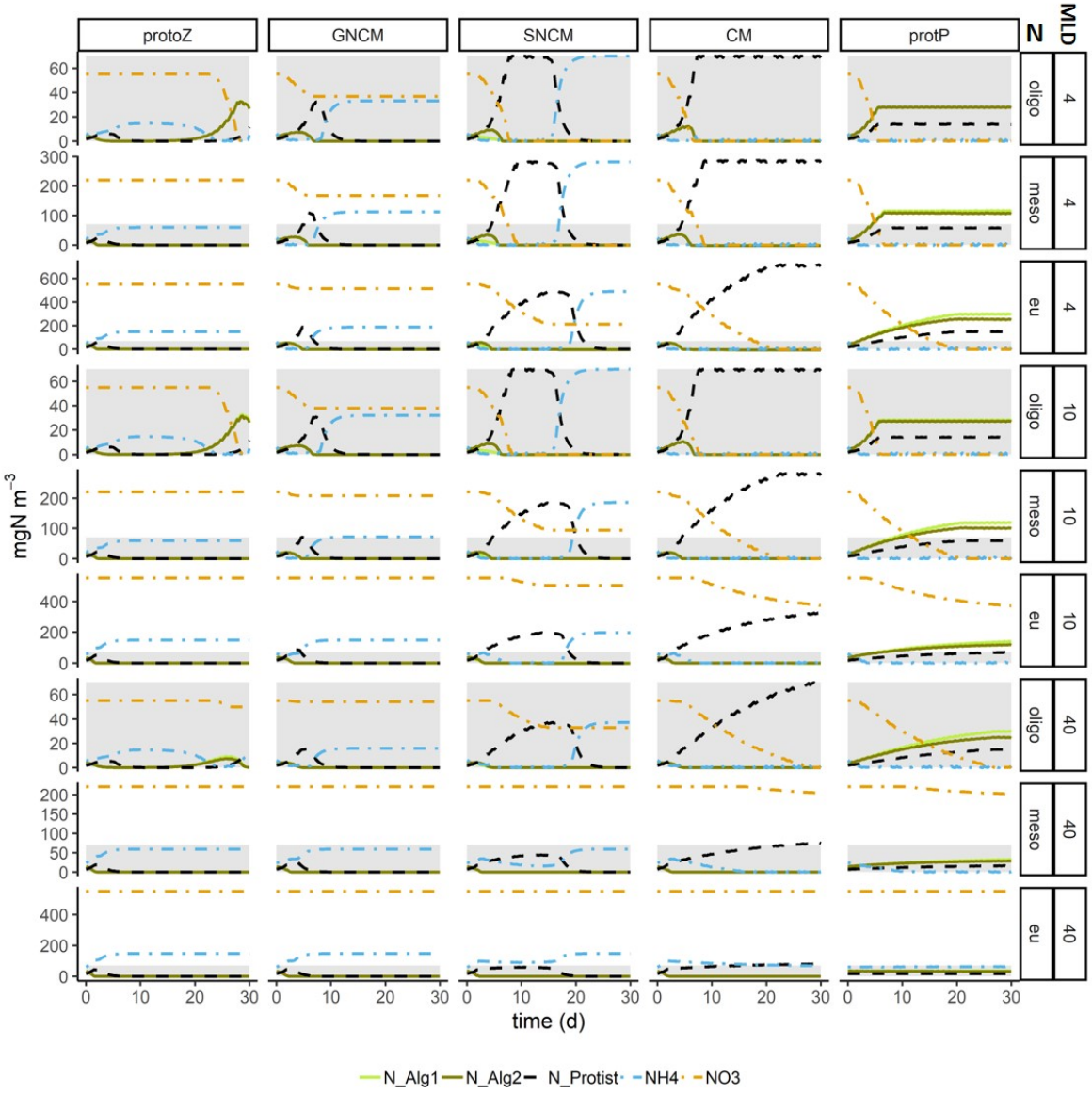

FIGURE 3.6: Changes in biomass and nutrient concentrations in simulated systems of different nutrient loadings (oligo-, meso- and eutrophic) and mixed layer depth (*MLD*; 4, 10 and 40 m). In all instances, two phototrophs (Alg1 and Alg2) are present as competitors and/or prey for the "Protist". Dissolved inorganic nitrogen (DIN) is present as nitrate (NO_3^-) and ammonium (NH_4^+). The "Protist" is configured, as indicated in columns left to right, as microzooplankton (protoZ, which can consume both Alg1 and/or Alg2), GNCM (which acquires phototrophy from consumption of Alg1 and/or Alg2), SNCM (which acquires phototrophy only from Alg1, but can graze on both Alg1 and Alg2), CM (which can consume both Alg1 and/or Alg2, but has its own phototrophic potential), and as a non-phagotrophic protist phytoplankton (protP). Alg1 and Alg2 were each inoculated at a N-biomass equal to 5% of initial DIN, while the protist was inoculated at 2.5% of initial DIN. The chlorophyll-carbon ratio of Alg2 (*ChlC_Alg2*) was 0.05, while that for Alg1 was 0.06 so to create a slight physiological difference between the two prey species. The grey box indicates the maximum nutrient load in the oligotrophic scenario to facilitate comparison between the different nutrient loads.

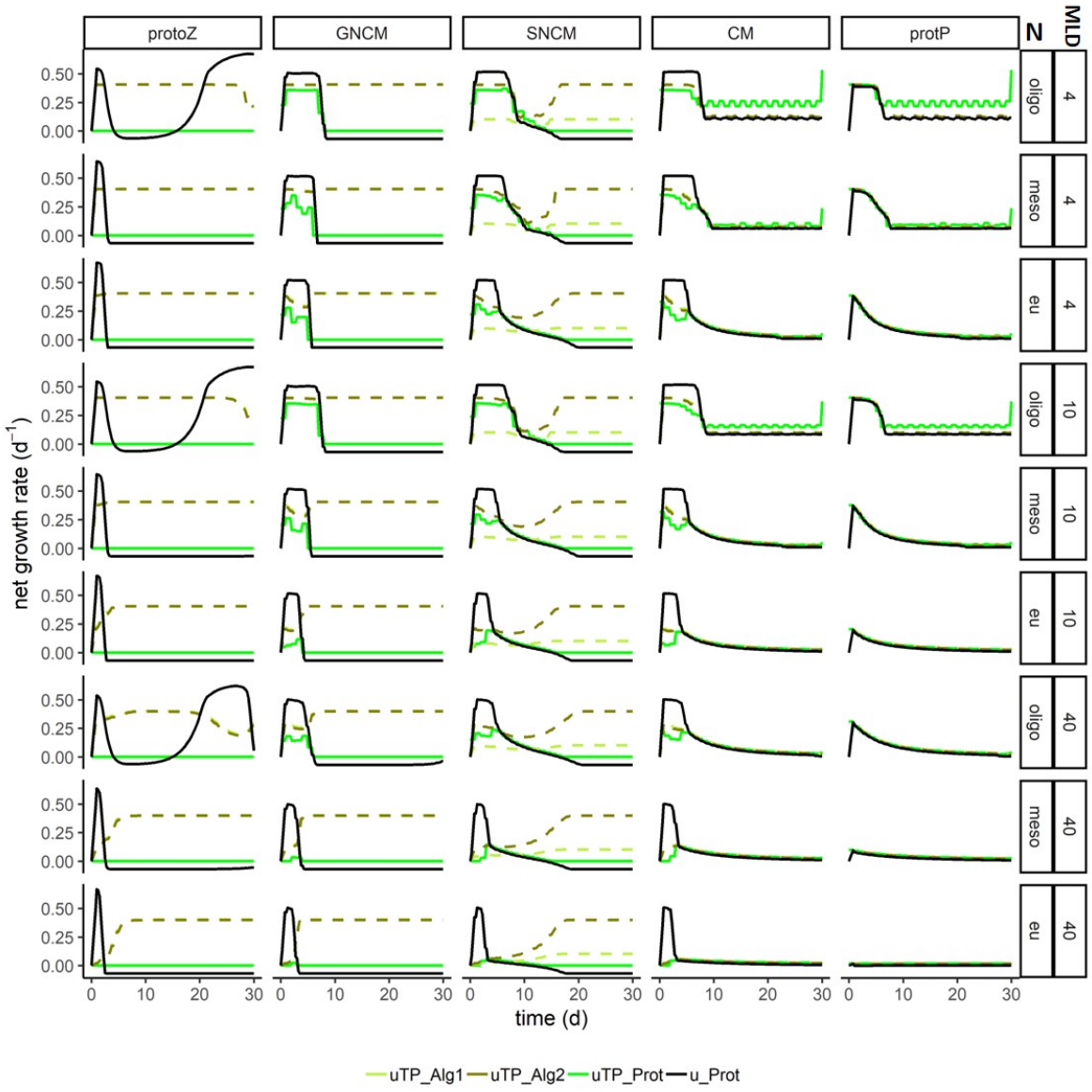

FIGURE 3.7: Daily averaged (of light and dark) growth specific growth rates. uTP values are day-averaged net photosynthesis (which for the Alg1 and Alg2, and also for protP, is the growth rate), while for the protoZ and mixotrophs, the day average is designated as *u*. For mixotrophs, *u* is the total growth rate of combined phototrophy and phagotrophy. The rows indicate *MLD* (4, 10 and 40 m) and nutrient load (oligo-, meso- and eutrophic, Electronic Supplementary Material Table S1).

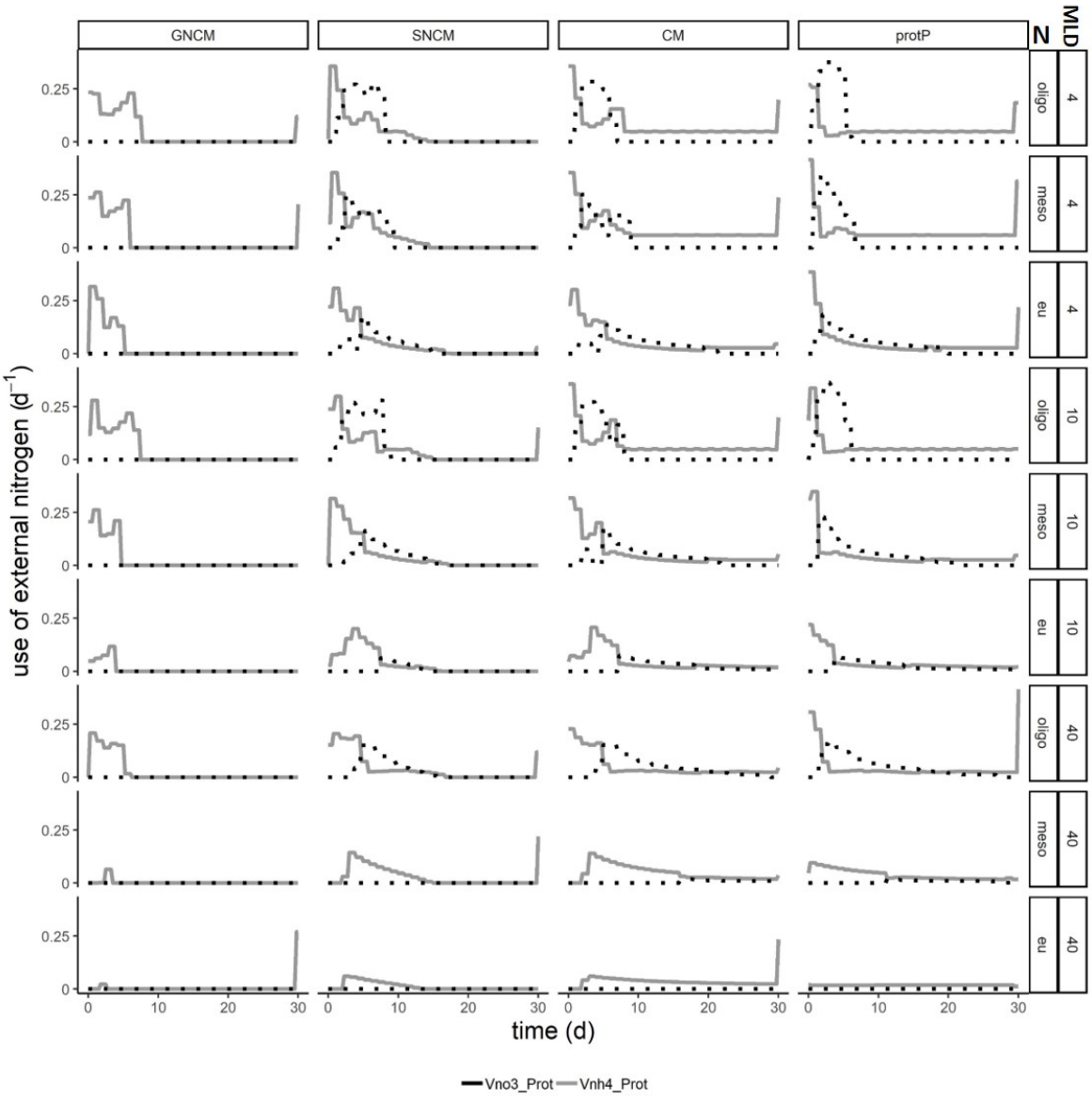

FIGURE 3.8: Daily averaged rates of inorganic nitrogen uptake by the phototrophic protist variants in oligo-, meso- and eutrophic conditions and in three different mixed layer depths (*MLD*, m). Vno3 and Vnh4 are the uptake rates for nitrate and ammonium, respectively.

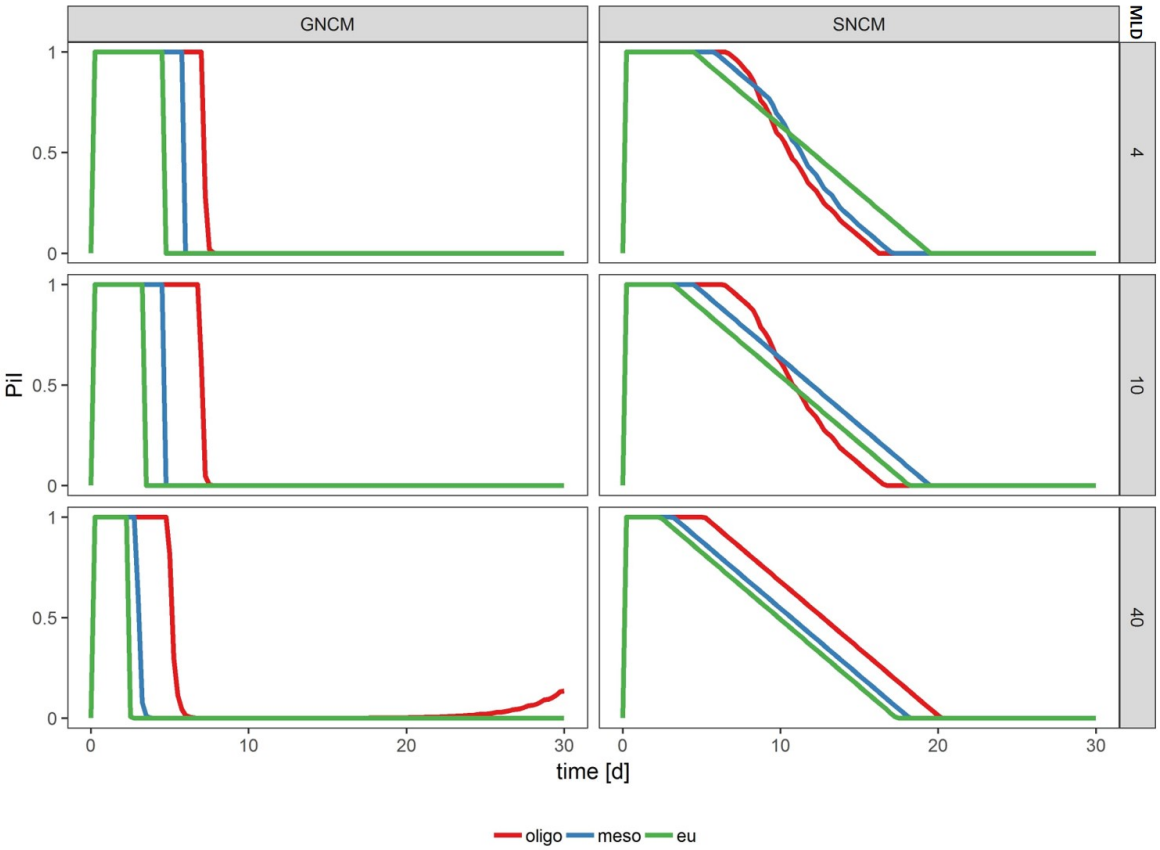

FIGURE 3.9: Variation in the NCM prey ingestion index (*PiI*) for the simulations shown in Fig. 3.6. These indicate that the availability of prey which thence limits the potential for acquired phototrophy remains greater in low nutrient-loaded systems. Although these are similar for GNCM and SNCM, the impact is much greater for the GNCM as these need to acquire plastids with greater frequency (see Fig. 3.6). Nutrient load (oligo-, meso- and eutrophic, Electronic Supplementary Material Table S1) also has an effect on the slope of the *PiI* decline in the SNCM, because nutrient availability impacts the expiration period of the acquired chloroplasts. Rows give the *MLD* (4, 10 and 40 m).

for mixoplankton (Thingstad et al., 1996; Stickney et al., 2000; Hammer and Pitchford, 2005; Ward et al., 2011; Berge et al., 2017). Much of this literature not only makes assumptions of mixoplankton physiology that are not supported by rigorous analysis, but the models lack flexibility for configuring in line with different MFTs (Flynn et al., 2019). Mixotrophy is not simply an addition of phototrophy and phagotrophy, to be described in models by employing a common simple set of additive equations (Mitra and Flynn, 2010), and neither is it so simulated here. There is a synergism that is important for mixoplankton physiology, and that differs radically between CM and NCM variants. While the CM variant prioritises phototrophy, provided that a certain proportion of nutrition comes via that route, it can be configured to grow faster under mixotrophy.

The NCMs have an essential requirement for phagotrophy and also phototrophy, but again elevated growth rates require close coupling of phototrophy and phagotrophy. The competitive functioning of these mixoplankton can also not be judged readily by reference to resource acquisition. If we consider just the rate of phagotrophy, for example, then for a given growth rate a mixoplankton may indeed appear inferior to the protoZ in terms of ingestion; however, by virtue of recovering the *SDA*-attributed loss of ammonium (ca. 30% of assimilated N) the conversion efficiency is much higher. Similar arguments can be made for comparisons of phototrophy in protP versus that in mixoplankton. The consequences of mixotrophy can be seen from our simulations where, assuming all else is equal, the effective half saturation concentration of nutrient or prey can be seen to be lower in comparison with non-mixotrophic competitors (Fig. 3.3).

Most models considering mixoplankton describe only one functional type (e.g., Faure et al., 2019). The simplicity of our model allows inclusion of a broader variety of mixoplankton functional types and thus an improved level of representation within a single simulation platform. The sensitivity analysis (Supplemental Material Fig. S2 and S3) indicates which parameters most influence growth and functioning of the organism and are thus factors upon which most emphasis should be placed in experiments. These include respiration and assimilation efficiency, as well as the expected sensitivity to the maximum growth rate. *AEN*, BR and costs of assimilating DIN (*MR*) all influence the efficiency with which the protist uses the acquired nitrogen. Thus, these parameters affect the proportion of nutrient and prey uptake to growth of the protist. The maximum proportion of growth supported by phototrophy alone (*pCritMax*) determines whether the protist is vulnerable to prey scarcity or the relative role of phototrophy. As this model assumes a fixed stoichiometry, it will not be as sensitive to parameters related to stoichiometry as a model with variable stoichiometry (C:N:P:Chl) like the perfect beast (Flynn and Mitra, 2009) as implemented by Leles et al. (2018).

3.4.2 Ecological and biogeochemical implications

An important difference between a system containing protoZ and protP, rather than one dominated by mixoplankton as the grazer, is that growth of protoZ is inevitably associated

with ammonium regeneration which supports further growth of the phototrophic prey. In contrast, mixoplankton can internalise ammonium regeneration during photosynthesis (noting that often mixoplankton predation appears to be phased to be concurrent with photosynthesis (Caron et al., 1993; Strom, 2001; Brutemark and Granéli, 2011; Izaguirre et al., 2012; Arias et al., 2017). If we consider such activity from the perspective of new vs regenerated production (Dugdale and Goering, 1967), a nitrate-supported protP bloom would see new nitrogen supporting not only their primary production but also subsequently the primary production of predatory mixoplankton further supported by incorporation of protP-N that is internally regenerated and re-assimilated within the mixoplankton. In the simulations (which had a fixed input ratio of ammonium:nitrate), high f-ratios are seen mainly with the protist configured as protP or CM, and was highest in oligotrophic conditions, where organisms have to tap into the nitrate pool (Supplemental Material Fig. S8). If the growth phase of the SNCM was longer after its prey were eliminated, then the SNCM also contributes to new production. In contrast, despite their photosynthetic activity, GNCMs as described here do not directly contribute to 'new' production, because they do not use nitrate. It is not clear how important the consumption of nitrate for GNCMs is (Schoener and McManus, 2017), ultimately measurements of nitrate reductase activity are required to prove such an ability. However, it is perhaps likely, given that GNCMs need to feed frequently and will thus be regenerating and recycling ammonium, that any ability to use nitrate would be minimal in any case. This is because sufficient internal ammonium would provide for the repression of nitrate and nitrite reductases and of nitrate transport (Syrett, 1981; Solomonson and Barber, 1990; Flynn et al., 1997). The higher the nutrient load, the higher the biomass yield. In such situations, the CM was the most successful variant in terms of biomass yield, closely followed by the SNCM (Fig. 3.6). Their success is attributed to the ability to remove their competition when resources for photosynthesis (nutrients, light) become limiting. While the protP is an equal competitor to the algae in the simulation, it cannot remove its competition. When the nutrient load is too high, light becomes more attenuated due to the presence of photo-pigment carrying organisms in the water. As a result, purely phototrophic organisms cannot make as much use of the overabundant nutrients. In this context, CMs have a clear potential for more likely forming uni-species blooms, perhaps forming HABs or EDABs (ecosystem disruptive algae bloom; Mitra and Flynn, 2006). Flynn and Hansen (2013) explored the dynamics of the end of NCM blooms, noting the potential of the NCMs to continue photosynthesising as their photosystems degraded as the community Chl concentration decreased so relieving self-shading. GNCMs and SNCMs are more limited by prey ingestion than are the CMs, as predation provides them with their photosystems. However, this same prey ingestion provides them with combined source of nutrition that also means that they are less likely to be directly limited (stressed) by inorganic nutrient availability. From the standpoint of ecological stoichiometry (Mitra and Flynn, 2005; Meunier et al., 2013; Thingstad et al., 1996) this may be expected to render the NCMs as good quality prey for other trophic levels. Indeed, NCM ciliates do appear to provide good feed for higher trophic levels

(Bils et al., 2017; Stoecker and Lavrentyev, 2018; Zingel et al., 2019) , though whether this reflects a higher visibility to predators such as fish larvae rather than a nutritional factor is not clear. Growth of both CM and protP is more likely to be limited by external nutrient availability as they can build their own chloroplasts from scratch. However, nutrient availability for protP is dissolved inorganic while for CM this is augmented by prey nutrient. Accordingly, in the simulations the protP show signs of nutrient limitation from early in the simulations, while the CM later exploits the DIN acquired initially by the Alg1 and Alg2 and then ingested by phagotrophy (Fig. 3.6). CMs are not only likely to give the largest terminal bloom sizes, but those species that are toxic when nutrient stressed can form HABs (Granéli and Turner, 2006) as they exhibit high levels of variability in their stoichiometry.

3.4.3 Niche separation between protist types

Exploring the simulation behaviour shows that mixoplankton not only behave differently from classical phytoplankton and NPZ models, but also that there is a distinctive variation among different forms of mixoplankton (Fig. 3.1). A key question revolves around niche separation between the protist types: under what conditions would one or other variant be at best advantage? Not only does the mixoplankton configuration affect steady-state niche competition (Figs. 3.3, 3.4, 3.5), but it affects the temporal dynamics (Fig. 3.6). The plots shown in Figs. 3.3, 3.4, 3.5 show how the different protist variants provide for quite different response curves relating light and prey abundance to protist growth rate. These are all assuming all other features of physiology are held constant, that only the different selected functions are operational. In reality this is not so. For example, GNCMs are ciliates which have very different escape responses from predators than do non-ciliates. There are also differences in size ranges (Flynn et al., 2019) with CMs typically being smaller. More fundamentally, mixoplankton grow in mature ecosystems (typified by the temperate summer), while non-mixoplankton can exploit immature systems (typified by temperate spring bloom conditions). Organisms evolve to match the supply of resources (Flynn, 2009), so (mixo)plankton growing in mature systems will inevitably have lower maximum growth rates. Set against these caveats, below we compare configurations assuming that indeed all else is equal.

3.4.4 protoZ and protP

Microzooplankton (protoZ) display a fast "boom-and-bust" dynamic, with their growth rapidly depleting the prey and then the protoZ quickly died through starvation. The consequences are that subsequent blooms of algal prey and protoZ are also large dynamic events. In higher nutrient-loaded systems, these boom-and-bust cycles are further exaggerated. What protoZ have as an advantage over their mixoplankton counterparts is that they are not constrained by the need for photosynthesis (Hansen et al., 2013).

Most mixoplankton appear to be capable of only survival in darkness (Caron et al., 1993; Kim et al., 2008; Brutemark and Granéli, 2011; Hansen, 2011; Hansen et al., 2013), presumably because they need some products of photosynthesis for active growth. The protP (phytoplankton) can only compete with the algae for nutrients and light, but exert no grazing impact on them. In the model, protP thus does not exert any control over its competition, as does CM. In reality, allelopathy has the potential to reshape community structure (Granéli et al., 2008b; Granéli et al., 2008a). The protP only compete equally with CMs where there are insufficient prey, or for protP species that have evolved cell cycles that can be uncoupled from the diel light–dark cycle (Nelson and Brand, 1979), where maximum growth rates are higher. Importantly this applies to protP as diatoms, which are also structurally highly robust and grow well in turbulent waters, while those same water conditions inhibit the growth of flagellates (Margalef, 1978; Thomas and Gibson, 1990), which comprise the CMs. The other critical factor for diatom growth is, of course, the need for silicate.

3.4.5 GNCM and SNCM

Both GNCMs and SNCMs have an advantage over protoZ, as they are not limited to just heterotrophy and therefore not as directly affected by lower prey biomass as the protoZ. At the same time, they are ultimately both constrained by an obligatory need for phagotrophy and for phototrophy. Prey consumption by GNCM is highest during daytime (Supplemental Material Fig. S7), when the products of photosynthesis mitigate against the loss of N associated with SDA. On the contrary, however, GNCMs have a lower growth rate than the protoZ when light is limiting, because they are slowed down by the need for some level of phototrophy (competition for nutrients with algae). Under prey limitation and in shallow water without light limitation, GNCMs may have a decided advantage over protoZ as they can compensate for low prey abundance with phototrophy as long as enough prey are available to support their chloroplast demands (Figs. 3.6, 3.9). GNCMs produce a greater biomass (mgN m^{-3}) in shallow water (Fig. 3.6) because primary production rates are higher and so in consequence are encounter rates of prey. This effect equally applies to the protoZ, which however lacks the ability to directly exploit external inorganic nitrogen. The SNCM variant has two advantages over the GNCM.

1. It needs to ingest prey much less frequently making it more independent of the biomass of its prey; this is of most importance at low prey abundance (Fig. 3.4) but critically assumes that the prey that are available include the special prey that can supply photosystems (e.g. *Teleaulax*, *Mesodinium* and *Dinophysis*; Johnson and Stoecker, 2005; Smith and Hansen, 2007; Park et al., 2008; Nielsen et al., 2012). However, because of the ability of SNCMs to continue grazing and photosynthesising for some time after the source of their acquired phototrophy (here, Alg1) has been all but eliminated, the SNCM scenarios do not have a second bloom (Fig. 3.6) as the population size of Alg1 is grazed so low that it is too small to recover. The

dynamics of an SNCM bloom thus requires the presence of sufficient special prey, and the very success of the SNCM bloom can be its undoing when the collective grazing on that special prey effectively eliminates it. We can thus expect that blooms of the CM *Teleaulax*, SNCM ciliate *Mesodinium* and the SNCM dinoflagellate *Dinophysis* (Minnhagen et al., 2011; Anderson et al., 2012; Reguera et al., 2012) will show a complex linkage to temporal physico-chemical ecology dynamics. With an ability to last a long time between photosystem acquisition, prey and SNCM may not even need to bloom simultaneously if the SNCM has obtained its chloroplasts from a prey bloom many weeks earlier. The SNCM receive its chloroplasts during the prey bloom and then bloom later when conditions that are favourable for it to bloom. This type of information may be highly relevant for ecosystem models driving at the prediction of harmful algae blooms caused by SNCMs like *Dinophysis*. The linkage between GNCM and its prey is much more closely matched in this context, with the need for frequent chloroplast acquisition acting to prevent a situation where the prey are eliminated. So, while on initial inspection one may think that the SNCM are advantaged by only needing to occasionally top up with acquired photosystems, the simulations show that this may not actually contribute to an ability to form repeat blooms (Figs. 3.6 and 3.9).

2. SNCMs can use nitrate granting them access to an additional source of nitrogen (Fig. 3.1, 3.2, 3.6, 3.8). This ability gives the SNCM an edge over the GNCM especially under oligotrophic conditions, but only under conditions of good light. The ability to use nitrate may be acquired at the same time they acquire their phototrophic potential from their prey. If it is an inherent ability, reduction of nitrate to usable ammonium requires both the enzymes nitrate and nitrite reductase plus significant reductant. An advantage of the ability to use nitrate needs to be weighed against the biochemical costs (see **faure_co-_1991**; Syrett, 1981; Solomonson and Barber, 1990); if their prey are already using the nitrate then the cost and dangers of operating that biochemistry are borne by the prey, to the benefit of the NCM.

Feeding frequency is highly dependent on the NCMs ability to maintain the chloroplasts. In the simulation, the GNCM needs to ingest one prey cell minimum per day to receive its required chloroplasts, whereas the SNCM only needs to feed once every 30 days. The consequential impact upon growth dynamics differs between these functional types in different environmental conditions, as seen by difference in the prey ingestion index (*PiI*; Fig. 3.9). These critical feeding rates can be readily altered in the model by adjustment of the maximum period of time between the ingestion of one prey cell per predator (*Crit_IR*). The maximum photosynthetic rate of the GNCM is also dependent on the nutrient status of the prey from which they acquire chloroplasts, because they cannot repair them. In the GNCM variant, characteristics of the photosystem of the prey are inherited from the prey, while the SNCM variant has its own photosynthesis parameters (*maxGPS*, *alpha*, *ChlC*). SNCMs that use the prey nucleus alongside the ingested chloroplast and are proven to

have some innate genetic information for chloroplast maintenance of certain prey species will have to acquire new chloroplasts at a much lower rate than a GNCM that cannot repair any damages to the chloroplasts caused by photooxidation for example or prevent damage via photoregulation (Hansen et al., 2016).

While the SNCM ciliate *Mesodinium* reportedly needs to ingest a minimum of one specific prey cell per day to maintain maximum growth rate, it can survive up to 50 days without ingesting any of its special prey, the CM cryptophyte *Teleaulax*, at all (Smith and Hansen, 2007). In fact, *Mesodinium* may feed so infrequently, that it was long believed to be a normal autotrophic phytoplankton (Olli, 1999), which in our model would be described as a protP. Then, it was discovered that they had to steal their chloroplasts from cryptophytes (Gustafson et al., 2000). The ability for kleptochloroplast maintenance lowers the need for frequent ingestion and a recent study even reported division of kleptochloroplasts in *Dinophysis* spp. (Rusterholz et al., 2017). Photoacclimation, as proven in *Mesodinium* (Moeller et al., 2011), also decreases photo-oxidative stress on chloroplasts and makes them last longer.

3.4.6 CM

The CM configuration appears the most successful variant in all scenarios. It yields the most biomass and maintains growth much longer than other protist variants. The only exception is in shallow oligotrophic water, where the SNCM attains an equally high biomass yield for as long as suitable prey are available to provide plastids. The CM yields the most biomass because it is not dependent on access to photosynthetic prey but can supplement its own photosynthesis by ingestion. It can therefore not only outcompete the algae for nutrients, but also remove its algal competitors that cause shading under low light conditions by resorting to phagotrophy. Once nutrients and prey are removed, the population of the CM does not collapse because it does not starve and can exploit diverse nutrient options. What makes the CM so successful is that it can eat its competition and still keep growing after its prey is depleted, because it does not rely on it to provide for acquired phototrophy (as do the NCMs). This raises the question as to why CMs are not dominant everywhere all the time. For that, we need to consider conditions required for these organisms to thrive, and those critically exclude highly turbulent systems (Margalef, 1978; Thomas and Gibson, 1990). Those conditions favour diatoms, which coincidentally have decoupled their cell cycle from the diel cycle, replaced a C-wall with one made of Si, and also have evolved such that they cannot engage in phagotrophy. There is thus a sharp differential between protP such as diatoms and the CMs, as described by Margalef's mandala (Margalef, 1978). Between CMs and SNCMs, competitive advantage is also related to the types of organism; CMs are flagellates, while some plastidic SNCMs are flagellates, and others are ciliates. There are various reasons why mixotrophs do not dominate in all waters, related to fragility of motile forms, a lack of prey (physiological traits that are not used are more likely lost by evolution), differences in prey-predator

selections and dependencies (especially for NCMs), and differences in maximum growth rates (which are functions of system maturity, as mentioned above; Flynn (2009)).

3.4.7 Further model development

This is a simple single nutrient (N)-based construct describing mixoplankton using two state variables; it contrasts greatly with the variable stoichiometric "perfect beast" construct of Flynn (2009). Inevitably, the lack of variable stoichiometry places limitations on deployment of the model we describe in this work; that is especially so when considering issues linked with ecological stoichiometry. Aside from that, the most obvious feature of protist plankton that is missing, and that has scope for profound effects on plankton dynamics, is the formation of resting stages. Resting stages are particularly important in boom-and bust plankton systems but are rarely considered in models. In our model, protoZ and both GNCMs and SNCMs begin to die once their growth rate falls below a certain level (Caron et al., 1990). Many GNCMs and SNCMs (e.g. Dinophyceae) are known to form resting cysts when conditions become unfavourable (Berland et al., 1995; Balkis et al., 2016). These cysts sink to the sediment but blooms can rapidly form from these cysts once conditions improve again (Balkis et al., 2016). Many cyst-forming organisms are also associated with harmful algae blooms (Reguera et al., 2012; Balkis et al., 2016). Cysts are also important life cycle components for CMs, such as the HAB-forming *Prymnesium parvum* and *Karlodinium micrum* (Faure et al., 2019) as well as many groups of protP, such as diatoms (Hallegraeff and Bolch, 1992; McQuoid and Hobson, 1996; Cremer et al., 2007). In addition, while largely inactive some of these cysts in for example *Alexandrium tamarense* are known to affect their environment by their toxicity (Oshima et al., 1992). We will explore variable stoichiometry and the dynamics of resting stages in mixoplankton growth dynamics in future works.

Funding This research was supported by the EU-funded H2020 Marie Skłodowska-Curie Actions ITN MixITiN 766327 funding.

Author contributions AAA and KJF conceived, built and ran the model. AAA and KJF equally shared the analysis of the results and writing of the paper.

Chapter 4

Acquired phototrophy and its implications for bloom dynamics of the cryptophyte-*Mesodinium*-*Dinophysis*-complex

Abstract

Certain species of the dinoflagellate genus *Dinophysis* are responsible for causing diarrheic shellfish poisoning (DSP) and consequently severe economic damage to shellfish aquaculture around the world. Most *Dinophysis* species are mixoplankton, combining phagotrophy with acquired phototrophy. *Dinophysis* acquires phototrophy through a food chain linkage that includes a cryptophyte (often the constitutive mixoplankton *Teleaulax* sp.), the non-constitutive mixoplankton ciliate *Mesodinium* sp., and then *Dinophysis* itself. *Mesodinium* acquires its chloroplasts from the *Teleaulax*/*Plagioselmis*/*Geminigera* clade with a preference for *Teleaulax* while *Dinophysis* relies exclusively on *Mesodinium* for its phototrophic potential. Despite the necessity of this linkage, the temporal dynamics of the blooms of *Teleaulax* and *Mesodinium* as precursors for *Dinophysis* blooms have not been explored in simulation models explicitly describing this exchange of plastids between the three organisms. Using a nitrogen-based model we explored these dynamics under different ecological settings. Temperature, nutrient load, mixed layer depth and irradiance all greatly influence the timing and magnitude of the species succession and thence the timing and magnitude of *Dinophysis* blooms. The key factors for *Dinophysis* growth are both availability of *Mesodinium* and the timing of its growth phase with that of its predator, with the potential for affecting *Dinophysis* blooms up to three months later. *Dinophysis* has a very complex relationship with its abiotic and biotic environment. Fitting this model that simulates the biological factor of *Dinophysis* bloom formation with existing hydrodynamic models could greatly improve our understanding of bloom formation and aid monitoring and forecasting of *Dinophysis* HAB events. Future monitoring of *Dinophysis* would likely be enhanced by monitoring also for its precursor prey species, *Teleaulax* and *Mesodinium*, which are rarely accorded the same effort as the dinoflagellate.

4.1 Introduction

Dinophysis is a harmful dinoflagellate in many coastal regions that harbour shellfish aquaculture, where it notoriously forms often low-density (10^3 cells L^{-1}) blooms that are the causative agents for diarrhetic shellfish poisoning (DSP) leading to the closure of these aquaculture facilities (review by Reguera et al., 2012). Significant effort has been expended on understanding the dynamics behind the occurrence of these, and other HAB, events to find ways to forecast them (Velo-Suárez et al., 2010; Raine et al., 2010; Moita et al., 2016; Pinto et al., 2016; Ajani et al., 2016). Many monitoring programs target toxigenic *Dinophysis* species (Campbell et al., 2010). Traditional methods of monitoring by counting cells and using satellite chlorophyll concentrations are not robust for forecasting *Dinophysis* (Ruiz-Villarreal et al., 2016). The cell concentration threshold for *Dinophysis*, at which it can pose a threat, is at 200 cells L^{-1} (Yasumoto et al., 1985), a cell abundance level that can be very difficult to detect (Berdalet et al., 2017). Satellite imagery is not ideal because blooms often occur in subsurface water layers and are therefore not detectable with this method (e.g., *D. acuta*; Ruiz-Villarreal et al., 2016).

Modelling offers tools to forecast blooms and also to aid understanding of the dynamics behind their occurrence (Cusack et al., 2016; Ruiz-Villarreal et al., 2016; Flynn and McGillicuddy, 2018). Most models for *Dinophysis* bloom formation emphasise physical oceanographic drivers (Velo-Suárez et al., 2010; Raine et al., 2010; Moita et al., 2016; Pinto et al., 2016), with a particular focus on upwelling and downwelling processes and coastal advection that bring *Dinophysis* cells into coastal waters from offshore, or into surface waters from deeper water layers (Tab. 4.1). Such models help to explain the occurrences of *Dinophysis* and demonstrate the significance of hydrodynamics for the formation of blooms of the dinoflagellate. However, there is still a lack of predictive power in the existing hydrodynamic models suggesting that there is a key element missing from these models which could be the biological component (Moita et al., 2016; Ajani et al., 2016).

TABLE 4.1: Publications on modelling the growth dynamics of *Dinophysis* and *Mesodinium*.

Region	**Role**	**Model Description**	***Target* species**	**Author**
Bantry Bay (Ireland)	Hindcasting & forecasting	3D Physical model (wind); no explicit mixoplankton	*D. acuminata*	Raine et al. (2010)
Bay of Biscay (France)	forecasting	3D Lagrangian Particle-Tracking Model + IBM; no explicit mixoplankton	*D. acuminata*	Velo-Suárez et al. (2010)
Galician Rías Baixas, NW Spain	conceptual	2D Physics (wind, up- & downwelling); mismatch of *D. acuminata* and *M. rubrum*	*D. acuminata*	Velo-Suárez et al. (2014)
Thermaikos Gulf (NW Aegean Sea)	forecasting	2D hydrodynamic model coupled with transport model simulating HAB dispersion including some biological processes with temperature, light and nutrients	*D. spp*	Savvidis et al. (2011)
Bantry Bay (Ireland)	forecasting	3D physical model: BANTRY model (200–250 m horizontal resolution with 20 vertical levels; no explicit mixoplankton	*D. spp*	Cusack et al. (2016)
Iberian coast	forecasting	3D Lagrangian particle-tracking model	*D. acuminata*	Pinto et al. (2016)
Western Andalucía, Spain)	forecasting	Artificial neural network approach	*D. acuminata*	Velo-Suárez and Gutiérrez-Estrada (2007)
NW Iberia	forecasting	3D Lagrangian offline model + IBM; no explicit mixoplankton	*D. acuminata, D. acuta*	Moita et al. (2016)
SE Australia	Physico-chemical	Generalised additive models	*D. acuminata, D. caudata, M. rubrum*	Ajani et al. (2016)
general	conceptual exploration	Biological simulation comparing phototroph and heterotroph with acquired phototroph	*M. rubrum*	Moeller et al. (2016)
N-based	conceptual exploration	Biological simulation of the entire TMD-complex	*Teleaulax* spp. *M. rubrum* *D. acuminata*	This work

A key aspect of *Dinophysis* is that most of the toxigenic species are mixoplankton (Anderson et al., 2002; Park et al., 2006; Jaén and Mamán, 2009; Nishitani et al., 2010; Rodríguez et al., 2012). Mixoplankton are protists that photosynthesise and eat (Flynn et al., 2019), and there are important differences between mixoplankton functional types.

Thus, *Dinophysis* sp. are plastidic specialist non-constitutive mixoplankton (pSNCM, defined by Mitra et al., 2016, modified by Flynn et al., 2019) that acquire their phototrophic ability from ingestion of the ciliate *Mesodinium rubrum* (Park et al., 2006). That ciliate itself is also a pSNCM and acquires its' phototrophic capacity from consumption of the *Teleaulax*/*Plagioselmis*/*Geminigera* (TPG) cryptophytes (Gustafson et al., 2000; Johnson et al., 2006). *Teleaulax* spp. are constitutive mixoplankton (a CM as per Mitra et al., 2016) that have their own, innate, photosystems and can feed on picoplankton (Yoo et al., 2017). While both the pSNCM ciliate and dinoflagellate are capable of maintaining their acquired phototrophy (kleptoplastids) for some time, ultimately they rely on this trophic linkage to proliferate (Hansen et al., 2013).

Blooms of *Mesodinium* and *Dinophysis* can occur a couple of weeks apart, assuming that sufficient prey in the form of a *Mesodinium* bloom was available so support the initial *Dinophysis* growth (Moita et al., 2016). This is possible because *M. rubrum* retains prey nuclei with a half-life of ten days and retain plastids for months (Hansen and Fenchel, 2006; Johnson and Stoecker, 2005; Smith and Hansen, 2007; Johnson et al., 2007). It has been suggested (Harred and Campbell, 2014) to use *M. rubrum* as an important indicator for blooms of *D. ovum* in the Gulf of Mexico and a conceptual model for the Rias in NW Spain also combines physical changes with *Mesodinium*-*Dinophysis* encounter (Velo-Suárez et al., 2014). Others have also suggested including *Mesodinium* and their cryptophyte prey in the modelling of *Dinophysis* (e.g., Glibert et al., 2010).

To further explore the dynamics of this linkage between *Teleaulax*-*Mesodinium*-*Dinophysis* (hereafter TMD) requires a simulation model that focusses on the unique physiology of the three organisms. The development of *Dinophysis* blooms is strongly connected to changes in hydrodynamics but also to prey availability and the unique relationship they have with it as SNCMs. It is therefore important to join hydrodynamic models with biological models to understand the full picture. Such models could help to explain bloom events that could not be explained by the physical models alone, and perhaps in due course may help us better understand when and why *Dinophysis* blooms may exceed the 200 cells L^{-1} action level (Berdalet et al., 2017), why blooms attain different sizes and how long blooms could potentially last. The here presented model allows exploring the dynamics of *Mesodinium* and *Dinophysis* in response to prey-predator ratios, different conditions of nutrient concentrations, irradiance and temperature under culture conditions while being simple enough to be joined with a hydrodynamic model.

4.2 Methods

What follows is a general description of the simulation model. The complete equations of the model are provided in the appendix A. Some of the methods below are described in more detail in chapter 2.

4.2.1 Mixoplankton food web of the model

The TMD model is an adapted version of the N-based systems-dynamics (ordinary differential equation-driven) model of mixoplankton functional types of Anschütz and Flynn (2020). For this work, the original model was extended to describe 2 protist models for the pSNCM functional type (configured for *M. rubrum* and *Dinophysis* sp.) and one as a CM for *Teleaulax sp.*. From here on, these organisms are referred to by their genus name only.

Teleaulax was fed with *Synechococcus* (Fig. 4.1). A larger sized (ESD = 6 µm), unspecified, phytoplankton (termed "Alga") was also included as an additional prey for *Mesodinium*, and to provide competition for nutrients and light in phototrophic growth. So, in full the foodweb comprised, *Teleaulax* feeding only on *Synechococcus* (Yoo et al., 2017). *Mesodinium* feeding on *Teleaulax*, *Synechococcus* and Alga (Myung et al., 2006; Jeong et al., 2015), while *Dinophysis* fed only on *Mesodinium*. *Dinophysis* was configured so that it could not use NO_3^- (García-Portela et al., 2020), while all others could do so. The full construct is shown in Fig. 4.1. Nutrient regeneration occurs in the model by an implicit regeneration term. Bacteria and the microbial loop components are not explicitly described.

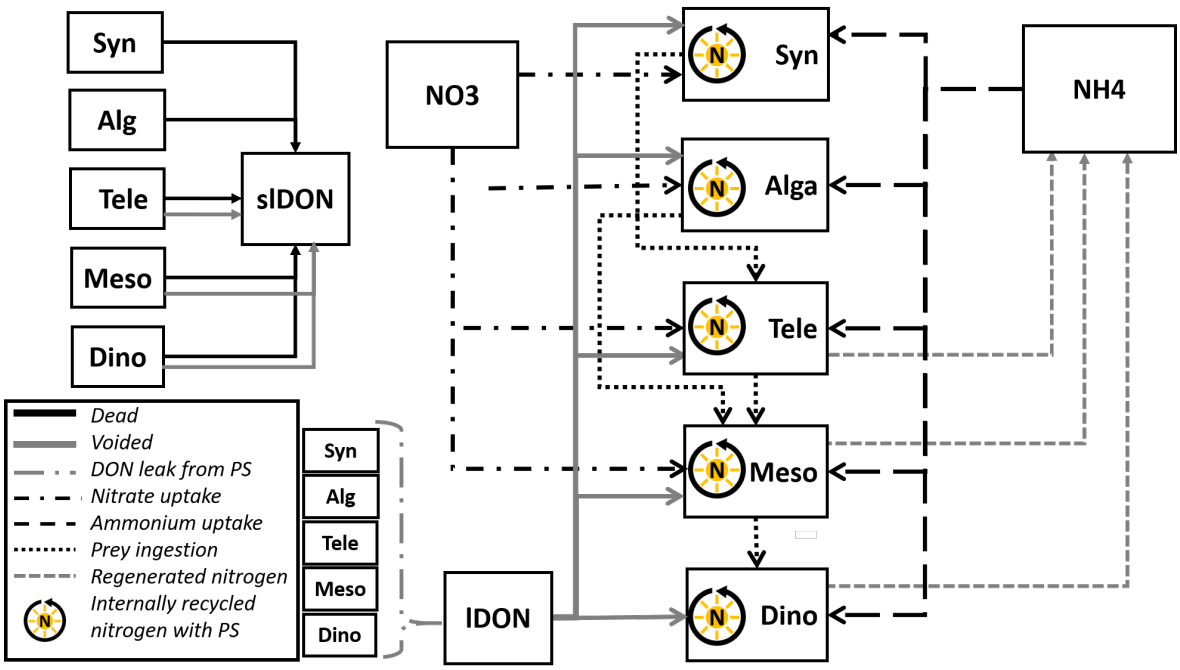

FIGURE 4.1: Schematic of the main model and its state variables. *Teleaulax* is configured as a constitutive mixoplankton (CM), while *Mesodinium* and *Dinophysis* are configured as specialist non-constitutive mixoplankton (SNCM), as described in Anschütz and Flynn (2020). Also shown are the phytoplankton *Synechococcus* and an unassigned protist "Alga". These are mixotrophic by virtue of being able to use dissolved organic N (DON), as the mixoplankton, but these phytoplankton cannot eat. All organisms leak DON. Nitrate (NO_3^-) is available for use by all but the *Dinophysis*. Voided and dead organic material contributes to the sem-labile DON pool, which degrades to contribute to the ammonium (NH_4^+) pool via an implicit microbial loop.

4.2.2 Model modifications from Anschütz and Flynn (2020)

The delay pipeline functions (which operate in Powersim Studio akin to a conveyor belt thus providing for the tracking of historic events) of the earlier model (Anschütz and Flynn, 2020) were replaced. These were used in the functions for averaging growth rate (*uAVd*), delaying the nutrient status (*Nu_T*) and the ingestion rate of specific prey in the pSNCMs (*lig_T*). Here they were replaced by functions that more readily allow for implementation in other modelling platforms. The state variables for the parameter being averaged have a start value of zero and an inflow of only that additional amount to the original state variable calculated in the preceding timestep. If that amount is zero, the flow is changed to a very small number ($1e^{-12}$) to avoid the potential for division by zero error. For example, growth of *Synechococcus* (*uTP_Syn*) would have an alternative averaged growth function (*uAV_Syn_alt*) with a flow of

$$uAV\_Syn\_alt = MAX((uTP\_Syn - uAV\_Syn\_alt)\cdot 10, 1e^{-12}) \tag{4.1}$$

Photosynthesis is calculated with reference to the depth-averaged available light in the water column (*avgPFD*), computed from the surface light (*Light_surf*) and average light attenuation through the water column (*att_tot*), which is itself a function of the pigmented plankton biomass and water attenuation:

$$avgPFD = \frac{Light\_surf}{att\_tot\cdot(1 - EXP(-att\_tot))} \tag{4.2}$$

Photosynthesis (*PS*) of each organism is defined using the Smith (1936) equation, with reference to the initial slope of the PE curve (*alphau*, with time units in seconds) and the maximum gross photosynthetic rate which is related to the nutrient status (*PSqmax*) as:

$$PS = PSqmax\cdot 1 - e^{\frac{-alphau\cdot avgPFD\cdot 24\cdot 60\cdot 60}{PSqmax}} \tag{4.3}$$

4.2.3 Sub-model additions to the model by Anschütz and Flynn (2020)

The operational maximum growth rate (*UmT*) is calculated with reference to the current temperature (*T*), the reference temperature (RT) at which the reference growth rate is stated (UmRT) and the Q_{10} factor.

$$UmT = UmRT \cdot Q_{10}^{\frac{T - RT}{10}} \tag{4.4}$$

A constant mortality rate (0.05 d^{-1}) was applied to all organisms. In the case of *Mesodinium* and *Dinophysis*, this constant mortality adds to the mortality rate described in the original model that accounts for a failure in photosystem activity (see Anschütz and Flynn, 2020).

In addition to nutrients being described as state variables for nitrate and ammonium, a state variable was added for dissolved organic nitrogen (*DON*), which receives the outflows of voided material from predation, released organic nitrogen due to mortality and DON leakage concurrent with photosynthesis (Alldredge et al., 1993; Bronk, 1999; Passow, 2002). Both labile DON and semi-labile DON are decomposed to ammonium at a rate of 0.5 d^{-1}. The exact value does not affect the outcomes of simulations, just the concentrations of DON vs NH_4^+.

Cyanobacteria, including *Synechococcus* (Wawrik et al., 2009), and most if not all protist plankton (Flynn and Butler, 1986; Flynn et al., 2019) are capable of exploiting labile DON to support their growth. Thus, we enabled all organisms to use DON with a modification of the routine used by Fasham et al. (1990). The use of labile DON (*lDON*) is described with a Michaelis-Menten kinetic as

$$DON\_up = \frac{0.1 \cdot UmT \cdot lDON}{Knh4\_Syn + lDON} \tag{4.5}$$

where *UmT* is the maximum growth rate dependent on temperature, *lDON* is the pool of labile DON and *Knh4* is the half-saturation for the uptake of NH_4^+. In the case of *Mesodinium* and *Dinophysis* this uptake rate was co-controlled by the plastid ingestion index (*Pil*). This describes the relative competence of the photosystems in these pSNCMs (see Anschütz and Flynn, 2020).

4.2.4 Model parametrisation

All constants defining activity of *Synechococcus*, *Teleaulax*, *Mesodinium* and *Dinophysis* were accorded values consistent with literature data (Tab. 4.2). Cellular nitrogen to carbon ratios (*NC*) vary among species, with the availability of external nutrients and (for predators) with prey quantity and quality. In this N-based model, NC value is constant with a value based on literature data of organisms grown in balanced nutrient conditions. In Anschütz and Flynn (2020), the prey-predator encounter model assumed swimming speeds calculated with reference to cell radius. As the speed (v) of the TMD organisms is well studied, and in the case of *Mesodinium* also unique with a high escape swimming speed, the auxiliary was changed to a constant reflecting literature values (Tab. 4.2). The

two pSNCM organisms, *Mesodinium* and *Dinophysis*, have different abilities to maintain optimal functionality of their photosystems which they acquire from their prey (parameter, *crit_IR*). These were configured with literature values listed in Tab. 4.3.

The model presented here is configured to represent *D. acuminata*, as it is a common toxigenic species and sufficient physiological data are available to aid model configuration. There are, however, differences between species of *Dinophysis* (Tab. 4.4) that should be born in mind if the model is used to simulate other species.

TABLE 4.2: Values of constants used to configure the *Synechococcus* (Syn), *Teleaulax* (Tele), *Mesodinium* (Meso) and *Dinophysis* (Dino) submodels. If not listed, the values for the respective organism was not found in the literature and the standard value from the old model was used. These values were kept constant in all simulations and during the DSA.

Parameter	Description	Unit	Species	Value	Reference
alpha	Slope of Chl-specific photosynthetic efficiency curve	(m2 g-1 chl.a)* (gC µmol-1 photon)	Syn	5.56e-06	Prézelin and Schofield, 1989
			Tele	2.31e-06	Anschütz (unpublished)
			Meso	5.05e-06	Johnson and Stoecker, 2005
			Dino	4.22e-06	Hansen et al., 2016
BR	Basal respiration	dl	Syn	ca 5 % of the umax	Grobbelaar et al., 1991
ChlC	Chlorophyll to carbon ratio	gChl (gC)-1	Syn	0.042	Broddrick et al., 2019
			Meso	0.055	Rial et al., 2013; Hansen et al., 2016
			Dino	0.045	Olenina et al., 2006; Hansen et al., 2016
Crit_IR	max time between ingestions of 1 prey cell per SNCM cell to enable max PS	d-1	Meso	25	Johnson and Stoecker, 2005; Smith and Hansen, 2007
			Dino	5	Rusterholz et al., 2017
Kno3	half saturation constant for nitrate	mgN m-3	Syn	20.02	Franck et al., 2003
NC	Nitrogen to carbon ratio	gN gC-1	Syn	0.133	Turpin and Miller, 1985
			Tele	0.167	Meunier et al., 2013
			Meso	0.265	Moeller et al., 2011
			Dino	0.125	Rao and Pan, 1993
r	equivalent spherical radius	µm	Syn	0.98	Zubkov and Tarran, 2005; Yoo et al., 2017
			Tele	6/2	Olenina et al., 2006; Yoo et al., 2017; Anschütz (unpublished)
			Meso	36/2	Olenina et al., 2006; Montagnes et al., 2008

Table 4.2 continued from previous page

Parameter	Description	Unit	Species	Value	Reference
			Dino	127/2	Larsen and Moestrup, 1992; Bérard-Therriault et al., 1999; Suzuki et al., 2009; Garcia-Cuetos et al., 2010; Rodríguez et al., 2012
relMaxPrey	maximum prey:predator size ratio	dl	Tele	1/3	Yoo et al., 2017; Anschütz (unpublished)
			Meso	5.6/13	Yoo et al., 2017
			Dino	60/78	Olenina et al., 2006; Montagnes et al., 2008
relMinPrey	minimum prey:predator size ratio	dl	Tele	0.9/7.5	Yoo et al., 2017; Anschütz (unpublished)
			Meso	3.9/36	Olenina et al., 2006
			Dino	15/176	Olenina et al., 2006; Montagnes et al., 2008
relOpPrey	optimal prey:predator size ratio	dl	Tele	0.95/6	Yoo et al., 2017; Anschütz (unpublished)
			Meso	2.2/60	Olenina et al., 2006; Yoo et al., 2017
			Dino	36/127	Olenina et al., 2006; Montagnes et al., 2008
Umax	Maximum growth rate	N/N/d	Syn	0.7	Campbell and Carpenter, 1986
			Tele	0.85	Hamilton et al., 2017; Anschütz (unpublished)
			Meso	0.52	Yih et al., 2004
			Dino	0.535	Kim et al., 2008; Smith et al., 2018
v	speed of motility	m s-1	Tele	5.55e-05	Meunier et al., 2013
			Meso	5.00e-03	Riisgård and Larsen, 2009
			Dino	1.04e-04	Jiang et al., 2018

TABLE 4.3: Abiotic parameters of the model that were varied in the dynamic risk analysis and simulations. The numbers in bold font are the values used by default in simulations. The nutrient load levels were the same as in Anschütz and Flynn (2020) and are 5 µM N, 20 µM N and 50 µM N.

Parameter name	Description	unit	values
critIR_Meso (DSA)	Critical plastid retention time	d	15; **25**
critIR_Dino (DSA)	Critical plastid retention time	d	**5**; 15; 30
LD	Fraction of daylight	dl	0.7
MLD	Mixed layer depth	m	3; **10**; 20
N_load	Nutrient load	mg N m^{-3}	70; 280; **700**
Opt_CR_Meso	proportion of prey of optimal characteristics captured by starved Mesodinium	dimension less	**0.2**; 0.5
Opt_CR_Dino	proportion of prey of optimal characteristics captured by starved Dinophysis	dimension less	**0.2**; 0.5
PFD	Surface light irradiance	µmol m^{-2} s^{-1}	50; 100; **500**; 1000
T	Temperature	°C	5; 10; **15**; 20

Synechococcus (S)
Alga (A)
Teleaulax (T)
Mesodinium (M)
Dinophysis (D)

Organism inoculations tested, shown in the format S-A-T-M-D, with initials indicating species as shown

% of initial DIN (mg N m^{-3})

	S	A	T	M	D
Original	2	2	1.5	0.1	0.01
+ S	10	2	1.5	0.1	0.01
- T	2	2	0.5	0.1	0.01
- M	2	2	1.5	0.01	0.01
+ M	2	2	1.5	1	0.01
+ D	2	2	1.5	0.1	0.1

TABLE 4.4: List of physiological values of different species of *Dinophysis* from the literature that are relevant for the model. The model is configured with literature values of *D. acuminata*. The ESD was determined by calculating the equivalent spherical diameter from width and length of *Dinophysis* spp. found in the literature. The parameters and their description are fully documented in Tab. A.1 containing all equations and constants of the model. See also Tab. 4.2

Species	Parameter	Value	Unit	Reference
D. acuta	alpha	1.16e-07 - 8.3e-06	(m^2 g^{-1} chl.a)*(gC μmol^{-1} photon)	Hansen et al., 2016
D. acuta	BR	50	% of gross photosynthesis	Hansen et al., 2016
D. norvegica	BR	2.08 $\pm$ 0.38	ng C $cell^{-1}$ d^{-1}	Carpenter et al., 1995
D. acuta	ChlC	40	pg Chl a $cell^{-1}$	Hansen et al., 2016
D. acuminata	crit_IR	5	d	Rusterholz et al., 2017
D. acuta	crit_IR	5	d	Rusterholz et al., 2017
D. caudata	crit_IR	17	d	Park et al., 2008
D. norvegica	NC_plank	0.1 - 0.115	µg µg-1	Rao and Pan, 1993
D. acuta	opmaxIng	1.49	ng C $cell^{-1}$ d^{-1}	Granéli et al., 1997
D. norvegica	opmaxIng	2.59	ng C $cell^{-1}$ d^{-1}	Granéli et al., 1997
D. acuminata	opmaxIng	2	ng C $cell^{-1}$ d^{-1}	Hansen, 2011
D. acuminata	ESD*	70 - 101	µm	Garcia-Cuetos et al., 2010; Bérard-Therriault et al., 1999
D. acuta	ESD*	111 - 134	µm	Bérard-Therriault et al., 1999
D. caudata	ESD*	111	µm	Kim et al., 2012b
D. fortii	ESD*	109 - 129	µm	Larsen and Moestrup, 1992
D. norvegica	ESD*	90 - 153	µm	Larsen and Moestrup, 1992
D. sacculus	ESD*	77 - 100	µm	Larsen and Moestrup, 1992
D. tripos	ESD*	83 - 190	µm	Rodríguez et al., 2012
D. acuminata	Umax	0.59	d^{-1}	Granéli et al., 1997
D. acuta	Umax	0.41	d^{-1}	Granéli et al., 1997
D. norvegica	Umax	0.63	d^{-1}	Granéli et al., 1997
D. caudata	Umax	0.1	d^{-1}	Park et al., 2008
D. fortii	Umax	0.7	d^{-1}	Nagai et al., 2011
D. sacculus	Umax	0.21 - 0.35	d^{-1}	Aissaoui et al., 2014
D. tripos	Umax	0.37	d^{-1}	Rodríguez et al., 2012
D. acuminata	v	170	µm s^{-1}	Jiang et al., 2018
D. acuta	v	104 $\pm$ 36	µm s^{-1}	Nielsen and Kiørboe, 2015

4.2.5 Dynamic Sensitivity Analysis

The dynamic sensitivity analysis of this model was performed in the same manner as described in Anschütz and Flynn (2020) and chapter 2. This was undertaken using the risk assessment tool in Powersim Studio 10, in which the ”decisions” (environmental conditions) are set with respect to the range of value for each tested parameter (assumptions). These fixed decision conditions under which the model was run are listed in Tab. 4.5. The parameters tested for sensitivity are listed in Tab. 4.6.

TABLE 4.5: Minimum, maximum and center (”actual”) values used for the decisions of the dynamic sensitivity analysis.

Decisions	**min**	**actual**	**max**
LD	0.35	0.7	1
MLD	1	10	40
N_load	70	280	700
NO3	62.02	248.1	620.19
NH4	6.21	24.8	62.08
Alg	1.75	7	17.5
Syn	3.5	14	35
Tele	1.75	7	17.5
Meso	0.875	3.5	8.75
Dino	0.044	1.75	0.44
PFD	50	100	500
w	0	0.001	0.003

TABLE 4.6: Tested Assumptions for dynamic sensitivity analysis. Each assumption was first tested alone, and then all assumptions were varied together.

organism	**parameter**	**Value Pn (literature)**	**decreased value PN**	**increased value PN**
Dino	*critIR*	5	3	15
Meso	*critIR*	22	15	30
Dino	*opt_CR*	0.2	0.05	0.5
Meso	*opt_CR*	0.2	0.05	0.5
Dino	*injectTime*	20	5	30

4.2.6 Simulations, caveats and general settings

The model was developed and run within Powersim Studio 10 (www.Powersim.com) using an Euler integration routine of step size 0.0625 d^{-1}. Simulations were run with default conditions (unless otherwise noted) of 15 °C and surface PFD 500 µmol m^{-2} s^{-1}. Other abiotic conditions are set as described in Tab. 4.3. Steady-state and dynamic sensitivity analyses (see chapter 2) were conducted as in Anschütz and Flynn, 2020).

For most simulations, the mixed layer depth (MLD) was set to 10 m. *Dinophysis* often forms high-density blooms in thin sub-surface layers as a result of stratification (Gentien et al., 1995; Anderson et al., 2005; Farrell et al., 2012; Moita et al., 2016). To simulate the physical conditions of a thin layer the MLD was set to 1 m and irradiance (de facto at the top of that thin layer) to 50 µmol m^{-2} s^{-1} to account for the light attenuation in the overlying water.

The *Dinophysis* sub-model is not subjected to grazing by another sub-model as the other organism sub-models are (e.g. *Mesodinium* grazing on *Teleaulax*. This work is aimed at studying the specific interactions within the TMD-complex and describes a mesocosm rather than a complete food web. To test the impact of a grazer of *Dinophysis* on the overall bloom dynamics of the TMD-complex, a simple *Dinophysis* specific grazing function was added. The simulations at different nutrient loadings were run with and without this grazing function. All other simulations were run without this grazing function.

4.3 Results

The model is based on nitrogen biomass. In order to aid contextual understanding, the biomass of *Dinophysis* was transformed from gN to cells. *Dinophysis* here is configured as *D. acuminata* assuming a nitrogen content of 2,318 pg N $cell^{-1}$.

4.3.1 Dynamic Sensitivity Analysis

In general, the model is stable and responses to changes in parameter values were all in the expected direction and of the expected magnitude (Fig. 4.2). The dynamic sensitivity analysis (Fig. 4.2) showed slight differences in the amplitude of *Dinophysis* abundance and of both labile and semi-labile DON in response to changes in the critical retention time of plastids by *Dinophysis* (*crit_IR_Dino*). Variations in the value of *crit_IR_Meso* (which defines the maximum retention time of kleptopastids with maximum photosynthetic capacity) changes the amplitude of the cumulative production and in consequence the concentration of dissolved nutrients and the abundances of *Mesodinium* and *Dinophysis*. Variations of the optimal capture rate of *Mesodinium* (*opt_CR_Meso*) causes minor changes in the amplitude of nitrate and ammonium concentrations while changes in capture rate of *Dinophysis* (*opt_CR_Dino*) impact cumulative production as well as DON, ammonium and the abundances of *Mesodinium* and *Dinophysis* in particular.

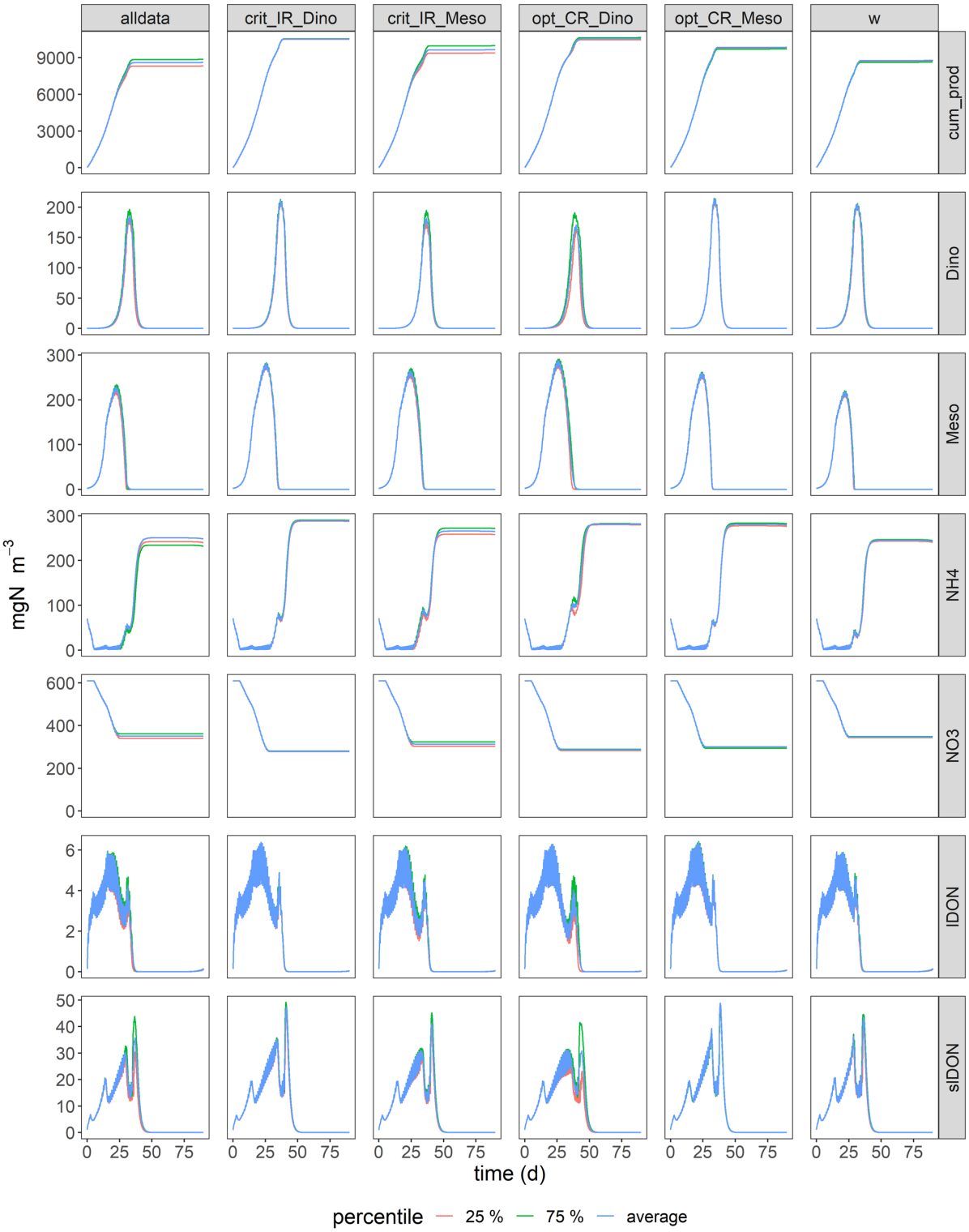

FIGURE 4.2: Results from the dynamic sensitivity analysis. Horizontal labels: tested parameters. Vertical labels: state variables tested for variations of the tested parameters. In "allData" all input parameters (constants) were varied. The plots show the average output, and then the 25% and 75% percentiles (i.e., average +/- 25%). Displayed are only those state variables that showed any response to the variations of the tested parameters.

4.3.2 Biotic interactions

All simulations share a common pattern of organism succession where *Synechococcus* is grazed down early to low residual biomass, followed by growths of "Alga" and *Teleaulax* which were then followed by *Mesodinium* (Fig. 4.3 - 4.8). The accumulating *Mesodinium* biomass not only outcompetes these species for nutrients but also exerts grazing pressure upon them. It is always the organism to generate the highest biomass. *Dinophysis* begins to grow during the active growth phase of *Mesodinium* and then exerts grazing pressure on *Mesodinium* accelerating its eventual decline. Ultimately, both *Mesodinium* and *Dinophysis* decline as their growth rates decrease due to the sequential loss of their source of kleptochloroplasts over time.

Ammonium is used preferentially over nitrate, along with labile DON (Fig. 4.3 - 4.8). Both labile and semi-labile DON accumulate and ammonium begins to increase due to the decomposition of these organic forms. High levels of ammonium later in the simulations cannot be used by *Mesodinium* and *Dinophysis* because the ultimate source of their chloroplasts, *Teleaulax*, is depleted and thus the two pSNCMs lose their ability for photosynthesis and hence exploit inorganic nutrients. Depending on the timing of events within the 90 d simulation period, in some simulations, this crash of the pSNCMs allows *Synechococcus*, the Alga and *Teleaulax* to bloom again.

By the time that *Dinophysis* blooms, nitrate concentrations are already much lower or depleted due to prior use by the other organisms (Fig. 4.3 - 4.8). However, as the (initial) nutrient load greatly affects the bloom development of those earlier organisms, it affects the timing and magnitude of the much later occurring *Dinophysis* bloom (Fig. 4.3). Also, the earlier plankton activity causes ammonium to accumulate, which *Dinophysis* can use while it cannot use nitrate. Oligotrophic conditions (i.e. DIN $<$ 5 µM) do not enable any significant growth of *Dinophysis* nor of any blooms (Fig. 4.3). *Teleaulax* and *Mesodinium* consume the population of *Synechococcus*. *Teleaulax* and Alga appear together and are followed by *Mesodinium*. Mesotrophic conditions in the same depth give rise to a bloom of *Mesodinium* as well as *Dinophysis* (Fig. 4.3). Inorganic nutrient concentrations decline most rapidly when *Mesodinium* reaches large biomasses. Eutrophic conditions result in the highest cell numbers of *Dinophysis* (Fig. 4.3).

The simulations presented here feature no grazing pressure on *Dinophysis*, in order to focus on the trophodynamics of the cryptophyte-*Mesodinium*-*Dinophysis* complex. In reality, *Dinophysis* experiences grazing pressure from copepods and other microzooplankton like *Fragilidium duplocampanaeforme* (Kozlowsky-Suzuki et al., 2006; Lee and Park, 2017). Fig. 4.4 shows the same simulations as Fig. 4.3 with an added generic grazing function for *Dinophysis*. The bloom dynamics of the complex including biomass yield of *Teleaulax* and *Mesodinium* and the timing of the blooms are affected very little by the grazing on *Dinophysis*. The *Mesodinium* bloom lasts slightly longer in eutrophic conditions. Neither the timing nor the length of the *Dinophysis* blooms change when grazing on *Dinophysis* is activated. Only the biomass yield of the dinoflagellate is much

lower and closer to the values found in field suggesting that grazing is the factor that keeps the cell numbers of*Dinophysis* low in the field.

The proportions and concentrations of each organism at the start of simulations changes both the maximum cell numbers of all organisms and bloom dynamics in terms of bloom cycles and length to varying degrees (Fig. 4.5). Initial higher proportions of *Synechococcus* greatly increases the biomass of *Teleaulax* and to a small extent also that of *Mesodinium* while it has a negligible effect on *Dinophysis* growth. Small initial concentrations of *Mesodinium* in proportion to *Dinophysis* result in the largest biomass of *Mesodinium* and the smallest biomass of *Dinophysis*, as *Dinophysis* cannot develop and initially decline (die) due to low prey availability. In consequence, *Dinophysis* cannot exert significant grazing pressure on *Mesodinium* later on in the simulation. In contrast, a high initial concentration of the ciliate promotes a more rapid sequence of events that eventually (because both *Mesodinium* and *Dinophysis* blooms crash) leads to a later bloom of *Synechococcus* that uses the available regenerated ammonium. High concentrations of *Dinophysis* at inoculum promote a quick bloom succession with smaller maximum biomasses of all organisms and no succeeding blooms.

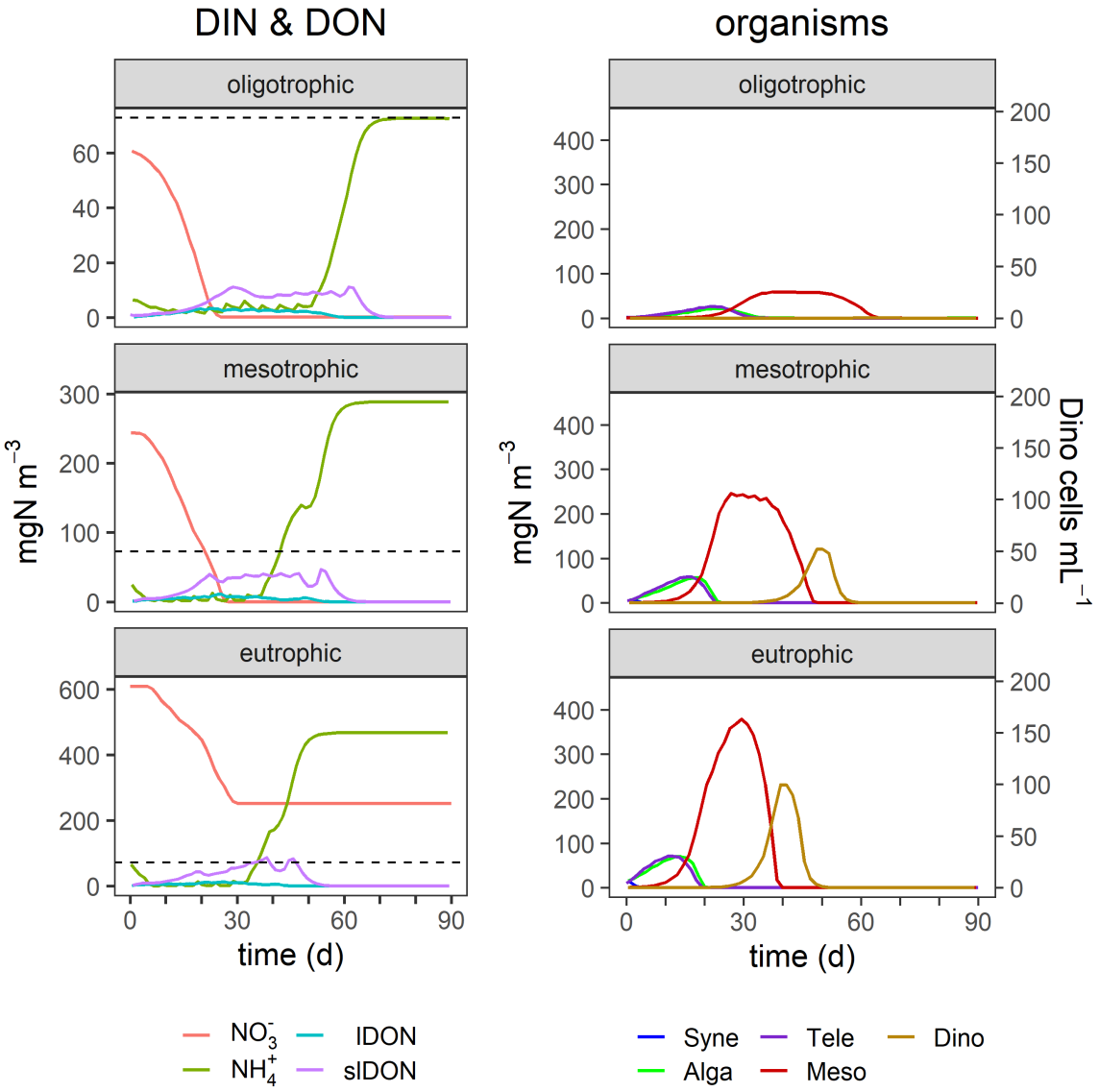

FIGURE 4.3: Dynamic changes in biomass and nutrient concentrations in simulated systems of different nutrient loadings at a mixed layer depth (MLD) of 10 m, irradiance (PFD) of 500 µmol photons m^{-2} s^{-1} and 15 ℃. The nitrogen concentrations levels were 5 µM (oliogtrophic), 20 µM (mesotrophic) and 50 µM (eutrophic). The reference temperature is 15 ℃. The organisms *Synechococcus* ("Syne"), unassigned phytoplankton "Alga", *Teleaulax* ("Tele"), *Mesodinium* ("Meso"), and *Dinophysis* ("Dino") are inoculated at biomass abundances equivalent to 2, 2, 1.5, 0.1 and 0.01 % of initial DIN concentrations, respectively. Inorganic nutrients (DIN) are supplied as nitrate (NO_3^-) and ammonium (NH_4^+). DON is present as labile (lDON) and semi-labile DON (slDON). The biomass of all organisms is shown in nitrogen biomass. *Dinophysis* numbers are transforms from the model output in mgN m^{-3}, configured to represent for *D. acuminata*, assuming an average cell size (ESD) of 70 m and a N content of 2,318 pgN $cell^{-1}$. The dashed line indicates the total nitrogen loading under oligotrophic conditions as a reference for the other simulations that have a different y-axis scale. The complete test conditions are listed in Tab. 4.3.

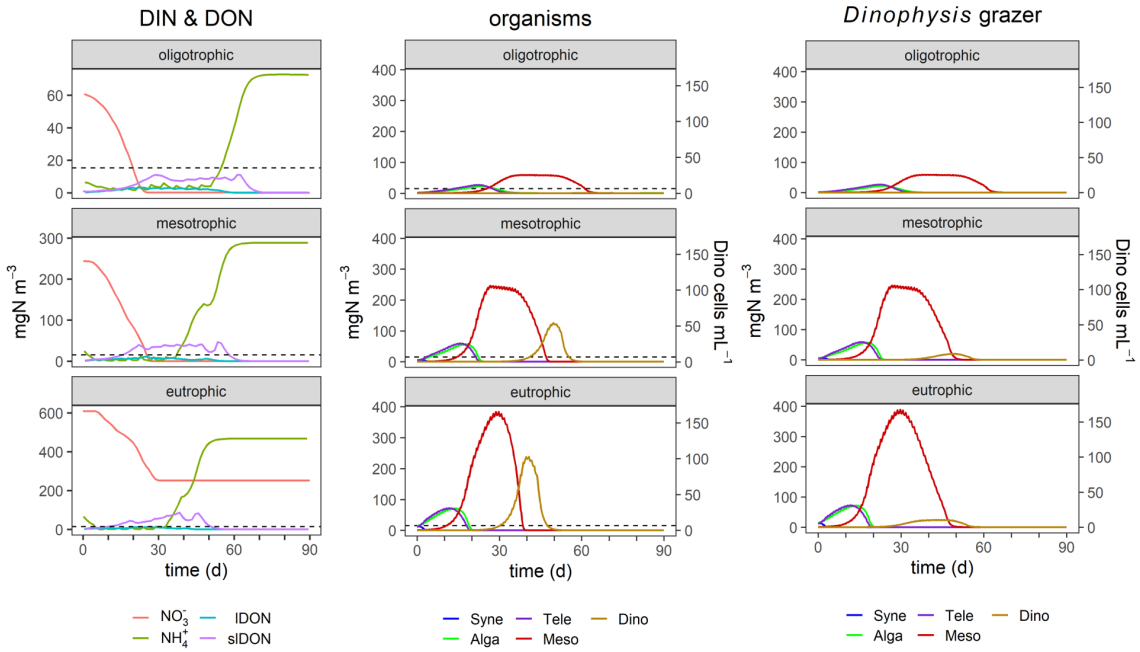

FIGURE 4.4: Dynamic changes in biomass and nutrient concentrations in simulated systems of different nutrient loadings at a mixed layer depth (MLD) of 10 m, irradiance (PFD) of 500 µmol photons m^{-2} s^{-1} and 15 ℃. The nitrogen concentrations levels were 5 µM (oliogtrophic), 20 µM (mesotrophic) and 50 µM (eutrophic). The organisms *Synechococcus* ("Syne"), unassigned phytoplankton "Alga", *Teleaulax* ("Tele"), *Mesodinium* ("Meso"), and *Dinophysis* ("Dino") are inoculated at biomass abundances equivalent to 2, 2, 1.5, 0.1 and 0.001 % of initial DIN concentrations, respectively. Inorganic nutrients (DIN) are supplied as nitrate (NO_3^-) and ammonium (NH_4^+). DON is present as labile (lDON) and semi-labile DON (slDON). The biomass of all organisms is shown in nitrogen biomass. *Dinophysis* numbers are transforms from the model output in mgN m^{-3}, configured to represent for *D. acuminata*, assuming an average cell size (ESD) of 70 µm and a N content of 2 318 pg N $cell^{-1}$. The dashed line indicates the total nitrogen loading under oligotrophic conditions as a reference for the other simulations that have a different y-axis scale.

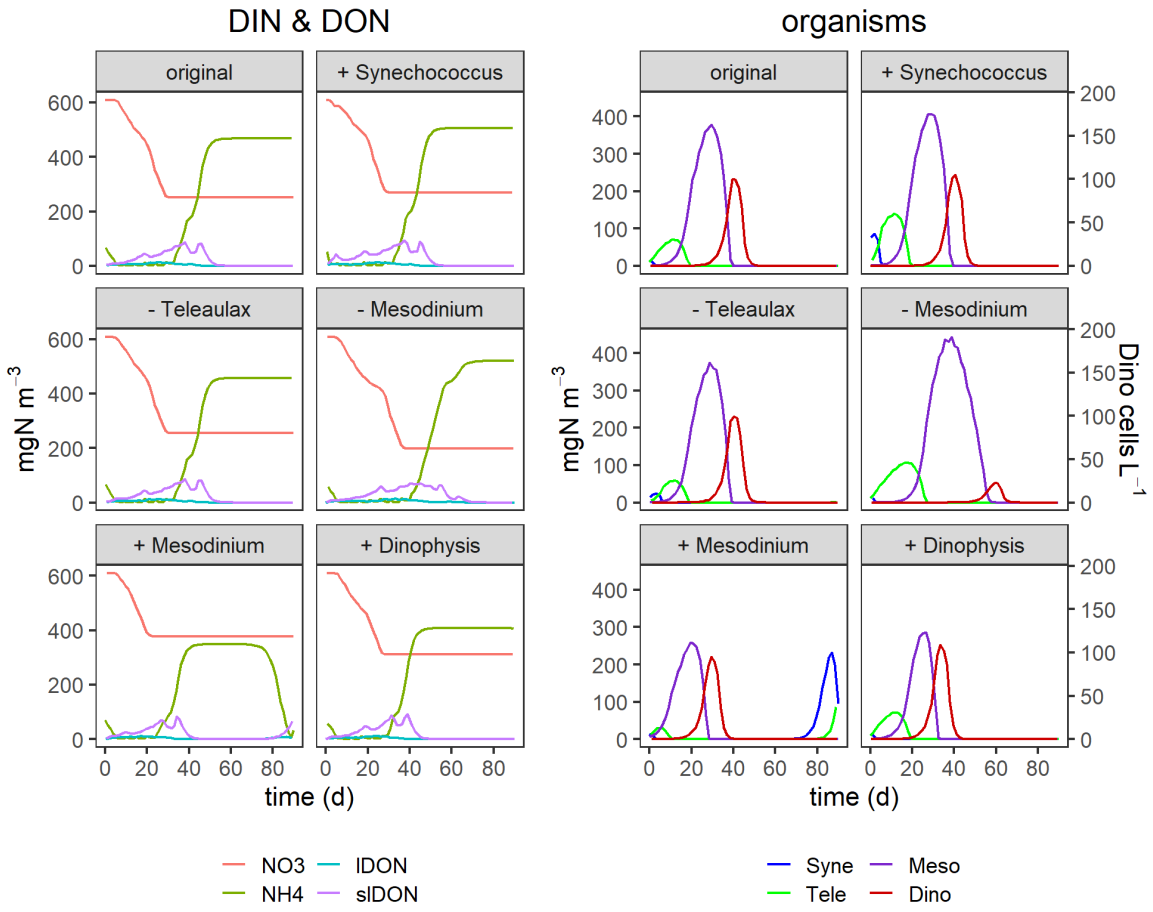

FIGURE 4.5: As Fig. 4.3 this figure shows the dynamic changes in biomass and nutrient concentrations in a simulated system, but with different initial organism inoculum ratios. The simulations were run with a mixed layer depth (MLD) of 10 m, irradiance (PFD) of 500 µmol photons m^{-2} s^{-1} and 15 °C. The reference temperature is 15 °C. The organisms *Synechococcus* ("Syne"), unassigned phytoplankton "Alga", *Teleaulax* ("Tele"), *Mesodinium* ("Meso"), and *Dinophysis* ("Dino") are inoculated at biomass abundances equivalent to 2, 2, 1.5, 0.1 and 0.01 % of initial DIN concentrations, respectively. Inorganic nutrients (DIN) are supplied as nitrate (NO_3^-) and ammonium (NH_4^+). DON is present as labile (lDON) and semi-labile DON (slDON). The biomass of all organisms is shown in nitrogen biomass. *Dinophysis* numbers are transforms from the model output in mgN m^{-3}, configured to represent for *D. acuminata*, assuming an average cell size (ESD) of 70 m and a N content of 2,318 pgN $cell^{-1}$. The dashed line indicates the total nitrogen loading under oligotrophic conditions as a reference for the other simulations that have a different y-axis scale. The complete test conditions are listed in Tab. 4.3.

4.3.3 Abiotic interactions

Higher irradiance increased the peak size of blooms of each organism type, but the timing of their blooms does not change (Fig. 4.6). In contrast, temperature increases have a large effect on the outcome of the *Dinophysis* bloom with the potential to accelerate the appearance of its bloom as well as decrease its duration (Fig. 4.7). In addition, they promote earlier blooms of *Dinophysis* and shorter growth cycles, but they can also lower the maximum cell numbers. The lower the temperature the more the peak of *Dinophysis* is delayed (several days or weeks). The cell numbers of the *Dinophysis* bloom vary with the phase of the *Mesodinium* bloom in which *Dinophysis* begins to grow.

The maximum biomass of all organisms is lower at 10 m MLD, except *Synechococcus* which is grazed away early in all simulations (Fig. 4.8). The duration of the individual blooms remains broadly similar but in 10 m MLD nitrate does not get as low as in 1 m depth. The predator-prey encounter rates are higher in 1 m depth. While the encounter rates between *Teleaulax* and *Synechococcus* are roughly the same in 1 m and 10 m depth, the encounter rate of *Mesodinium* and *Teleaulax* is almost double at 1 m. The encounter between *Dinophysis* and *Mesodinium* is also higher in 1 m depth and begins to increase earlier than in 10 m.

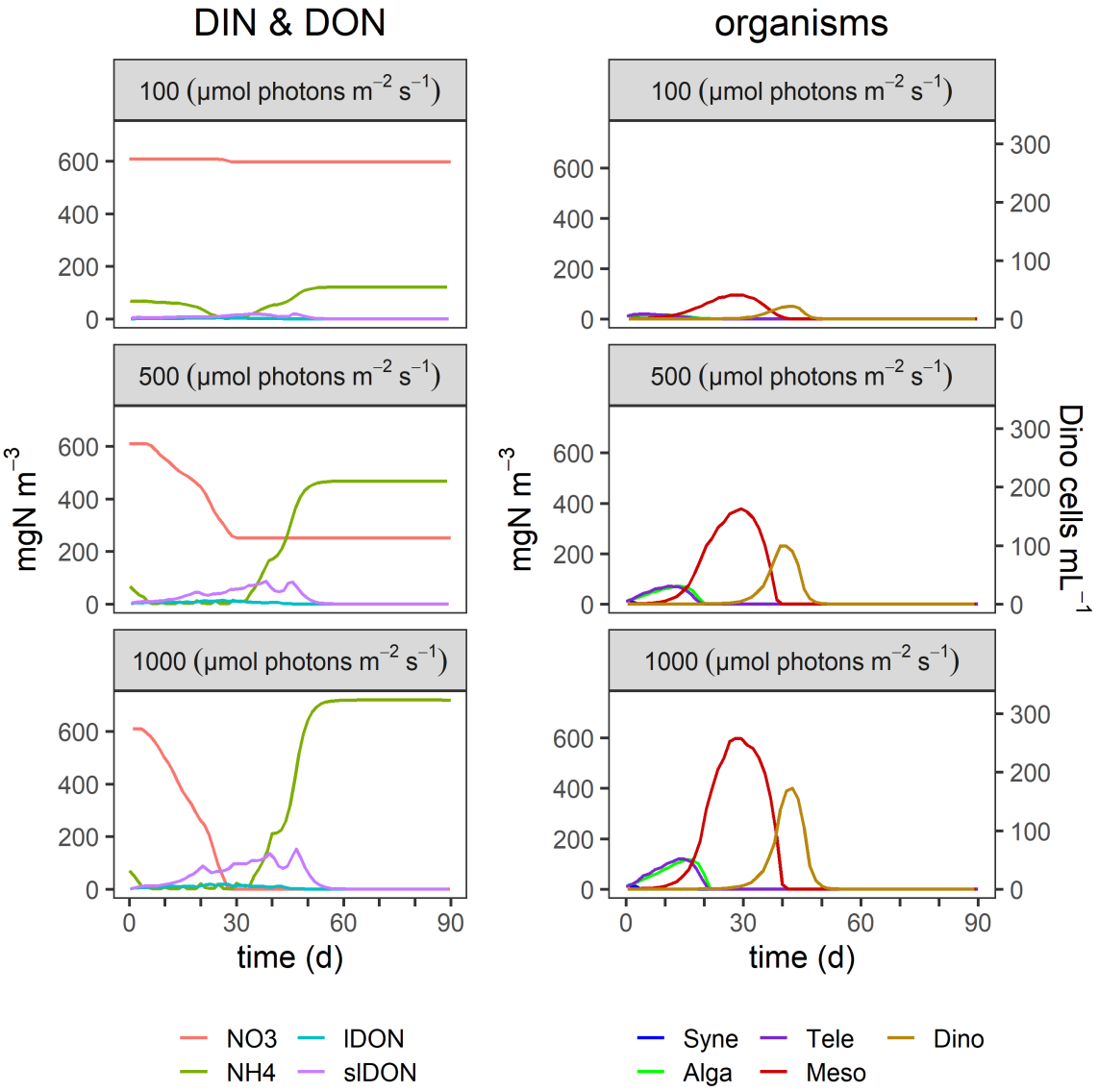

FIGURE 4.6: As Fig. 4.3 this figure shows the dynamic changes in biomass and nutrient concentrations in a simulated system, but with different irradiances. The simulations were run with a mixed layer depth (MLD) of 10 m, irradiance (PFD) of 500 µmol photons m^{-2} s^{-1} and 15 °C. The reference temperature is 15 °C. The organisms *Synechococcus* ("Syne"), unassigned phytoplankton "Alga", *Teleaulax* ("Tele"), *Mesodinium* ("Meso"), and *Dinophysis* ("Dino") are inoculated at biomass abundances equivalent to 2, 2, 1.5, 0.1 and 0.01 % of initial DIN concentrations, respectively. Inorganic nutrients (DIN) are supplied as nitrate (NO_3^-) and ammonium (NH_4^+). DON is present as labile (lDON) and semi-labile DON (slDON). The biomass of all organisms is shown in nitrogen biomass. *Dinophysis* numbers are transforms from the model output in mgN m^{-3}, configured to represent for *D. acuminata*, assuming an average cell size (ESD) of 70 m and a N content of 2,318 pgN $cell^{-1}$. The dashed line indicates the total nitrogen loading under oligotrophic conditions as a reference for the other simulations that have a different y-axis scale. The complete test conditions are listed in Tab. 4.3.

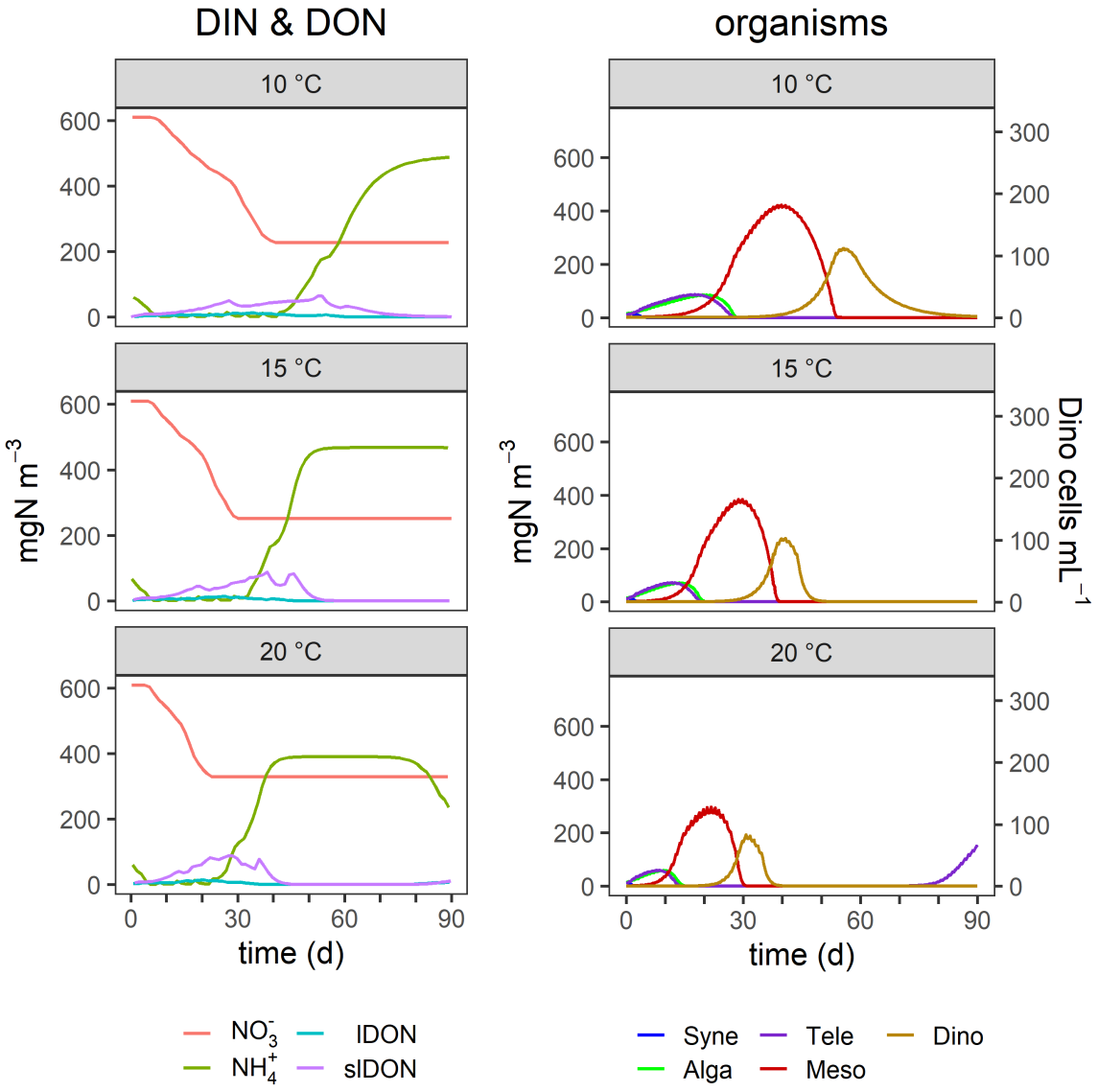

FIGURE 4.7: As Fig. 4.3 this figure shows the dynamic changes in biomass and nutrient concentrations in a simulated system, but with different temperatures. The simulations were run with a mixed layer depth (MLD) of 10 m, irradiance (PFD) of 500 µmol photons m^{-2} s^{-1} and 15 °C. The reference temperature is 15 °C. The organisms *Synechococcus* ("Syne"), unassigned phytoplankton "Alga", *Teleaulax* ("Tele"), *Mesodinium* ("Meso"), and *Dinophysis* ("Dino") are inoculated at biomass abundances equivalent to 2, 2, 1.5, 0.1 and 0.01 % of initial DIN concentrations, respectively. Inorganic nutrients (DIN) are supplied as nitrate (NO_3^-) and ammonium (NH_4^+). DON is present as labile (lDON) and semi-labile DON (slDON). The biomass of all organisms is shown in nitrogen biomass. *Dinophysis* numbers are transforms from the model output in mgN m^{-3}, configured to represent for *D. acuminata*, assuming an average cell size (ESD) of 70 m and a N content of 2,318 pgN $cell^{-1}$. The dashed line indicates the total nitrogen loading under oligotrophic conditions as a reference for the other simulations that have a different y-axis scale. The complete test conditions are listed in Tab. 4.3.

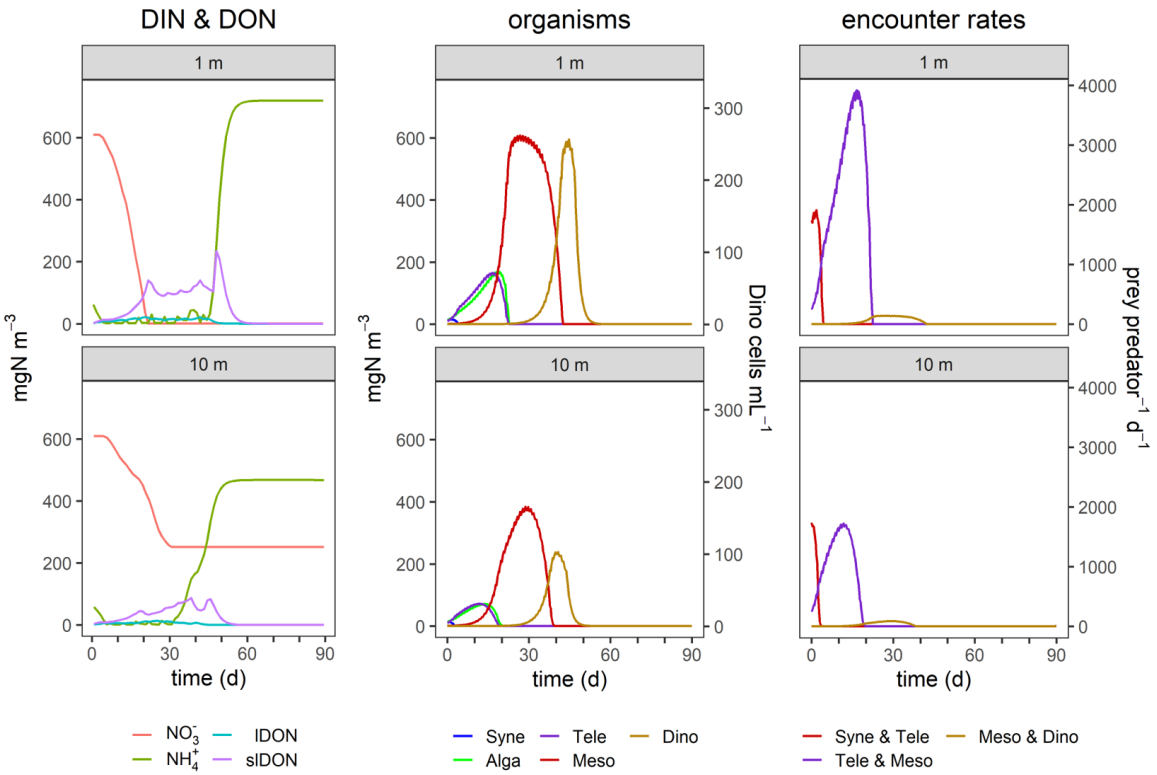

FIGURE 4.8: Dynamic changes in biomass and nutrient concentrations in simulated systems at mixed layer depths (MLD) of 10 m simulating a mesocosm and 1 m simulating a thin layer. *Dinophysis* is often found in thin layers in stratified water columns where it much easier to capture its fast prey *Mesodinium* due to much higher encounter rates. The plots of the encounter rates show predator-prey encounters of the three mixoplankton with their respective prey. The simulations were run with an irradiance (PFD) of 500 µmol photons m^{-2} s^{-1} and 15 °C. The reference temperature is 15 °C. The organisms *Synechococcus* ("Syne"), unassigned phytoplankton "Alga", *Teleaulax* ("Tele"), *Mesodinium* ("Meso"), and *Dinophysis* ("Dino") are inoculated at biomass abundances equivalent to 2, 2, 1.5, 0.1 and 0.01 % of initial DIN concentrations, respectively. Inorganic nutrients (DIN) are supplied as nitrate (NO_3^-) and ammonium (NH_4^+). DON is present as labile (lDON) and semi-labile DON (slDON). The biomass of all organisms is shown in nitrogen biomass. *Dinophysis* numbers are transforms from the model output in mgN m^{-3}, configured to represent for *D. acuminata*, assuming an average cell size (ESD) of 70 µm and a N content of 2,318 pgN $cell^{-1}$. The dashed line indicates the total nitrogen loading under oligotrophic conditions as a reference for the other simulations that have a different y-axis scale. The complete test conditions are listed in Tab. 4.3.

4.4 Discussion

The challenge in understanding the bloom dynamics of the cryptophyte-*Mesodinium*-*Dinophysis* complex is the complexity and multitude of factors affecting it including stratification, advection, salinity, predator-prey interaction and the mixoplankton nature of the organisms. This model focuses on the interaction between the organisms of the complex under the exclusion of hydrodynamics, DVM and predators. It assumes mesocosm conditions rather than field conditions as a simplification.

The model allows for an exploration of the bloom dynamics of the toxigenic mixoplankton dinoflagellate *Dinophysis* and the key organisms *Teleaulax* and *Mesodinium* that enable *Dinophysis* growth with a focus on the biological interactions. In general terms, *Dinophysis* depends mostly on the availability of *Mesodinium* at the right time. Abiotic factors directly and indirectly shape the timing and magnitude of *Dinophysis* blooms as they influence the phase of the *Mesodinium* bloom in which *Dinophysis* itself starts to proliferate. The effects of the initial conditions accumulate over time and lead to sometimes counter-intuitive results. The collective interactions of the organisms of prey and predator and competitors for nutrients alongside nutrient regeneration all impact the dynamics.

The organisms in this model were configured as *Teleaulax amphioxeia*, *Mesodinium rubrum* and *Dinophysis acuminata* as those were the species with the most physiological data available. However, the model can be configured as any species of the genus *Teleaulax*, *Mesodinium* or *Dinophysis* provided there are available data. The dynamic risk analysis showed the model to be sensitive to variations in the maximum growth rate (which is sensitive to temperature) as well as the pSNCM maximum plastid retention time (*crit_IR*) and the optimal prey capture rates. Different species of *Dinophysis* are known to vary in their physiology (Tab. 4.2) and ecology and toxin production (Reguera et al., 2012; García-Portela et al., 2018). Also, the plastid retention time may differ between species of *Dinophysis*. With more data becoming available on different species of the TMD-complex the model can be used for comparisons of the theoretical implications of physiological differences between species.

Apart from physiological and morphological variations, species of *Dinophysis* differ in seasonality, geographical distribution (Fig. 4.9) and the hydrodynamics that are ideal for their growth (Reguera et al., 2012; Cusack et al., 2016; García-Portela et al., 2018). For example, species differed in Australia, where seasonal stratification and nutrient loads were found to be triggers for blooms of *D. acuminata*, while growths of *D. caudata* were linked to nutrients, salinity and dissolved oxygen (Ajani et al., 2016). A common trait of most species of *Dinophysis* is that they seem more dependent on the availability of their prey *Mesodinium* than on light availability (Reguera et al., 2012). *Dinophysis* is often found in high densities in thin layers at a larger depth that is limited in light but passed by twice a day by *Mesodinium* during its DVM (Sjöqvist and Lindholm, 2011). DVM by *Dinophysis* often appears to be associated with the DVM pattern of *Mesodinium*.

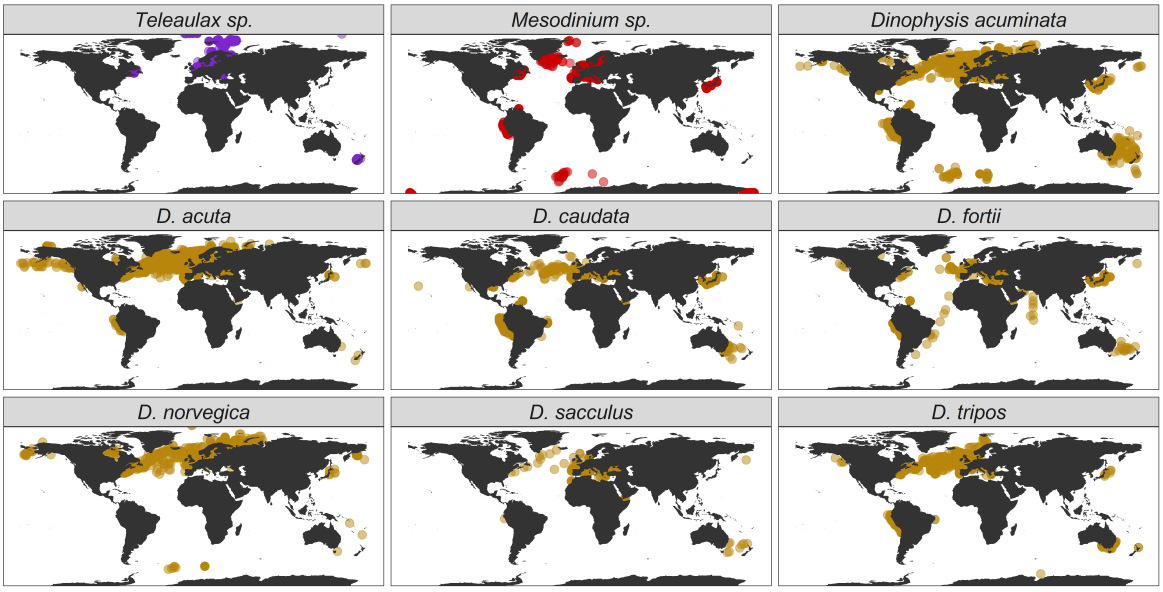

FIGURE 4.9: Global distribution of *Teleaulax* sp., *Mesodinium* sp. and of mixoplankton *Dinophysis* species that are known to form toxic algae blooms that can lead to the closure of shellfish aquacultures. The data were obtained from the Ocean Biogeographic Information System (OBIS) database. Each dot represents a recorded observation. Records of *D. ovum* are joined with *D. acuminata* as they are likely the same species (Park et al., 2019). That *Teleaulax* sp. and *Mesodinium* sp. are globally distributed is due to a sampling bias. *Dinophysis* is much more sampled and targeted in monitoring due to being a HAB species. The dinoflagelate is also larger and more robust than the cryptophyte and ciliate. As *Dinophysis* receives its cryptophyte plastids via the ciliate, the presence of *Dinophysis* implies the presence of *Teleaulax* sp. and *Mesodinium* sp..

4.4.1 Eutrophication

The model suggests that eutrophic conditions increase the potential for *Dinophysis* blooms, because they prepare the system for larger *Mesodinium* blooms which then increase the potential for *Dinophysis* blooms (Fig. 4.3). The importance of prey abundance for *Dinophysis* has been observed in the field (Moita et al., 2016; Smith et al., 2018) and DSP events have been related to high levels of dissolved organic and inorganic nutrients (Hattenrath-Lehmann and Gobler, 2015; Hattenrath-Lehmann et al., 2015). In the simulations, by the time *Dinophysis* starts to bloom, levels of nitrate can already be very low with ammonium starting to accumulate as a result of decomposition of labile and semi-labile DON which support the growth of *Dinophysis* that had access to plenty of *Mesodinium* as a source for plastids. *Dinophysis* itself appears either unable or poorly equipped to use nitrate (Hattenrath-Lehmann et al., 2015; García-Portela et al., 2020) and the ability for nitrate use was, therefore, disabled for *Dinophysis* in this model. In any case, the intracellular regeneration of ammonium within *Dinophysis* on account of its feeding and then later the increasing availability of external DON and ammonium would repress any usage of nitrate. *Dinophysis* was found successful in nitrogen-depleted waters (Seeyave et al., 2009). Levels of nitrate therefore may not have any direct effect on *Dinophysis* blooms. However, via their impact on *Mesodinium* growth, eutrophic conditions have significant scope to affect coasts that are vulnerable to harmful *Dinophysis* blooms several weeks after the nutrient input occurred. This duality of direct and indirect effects of eutrophication on *Dinophysis* blooms also finds support by experimental studies on *D. acuminata* and *M. rubrum* (Hattenrath-Lehmann et al., 2015; Hattenrath-Lehmann and Gobler, 2015).

In the aforementioned thin water layers, *Dinophysis* often reaches very high cell concentrations that are almost similar to a monoculture (Farrell et al., 2012). These water layers contain almost no predators. In reality, *Mesodinium* exercises large scale diel vertical migration (DVM) through water layers of up to 30 m, while *Dinophysis* accumulates in thin layers capturing *Mesodinium* when it passes through the layer twice a day (Sjöqvist and Lindholm, 2011). The current model does not capture this and rather simulates a large mesocosm with homogeneously distributed organisms.

With the exception of the simulations at different nutrient loads shown in Fig. 4.4 the simulations were run without grazing on *Dinophysis* to focus on the effect of the interactions of *Teleaulax*, *Mesodinium* and *Dinophysis* on their respective bloom dynamics.

In the field, *Dinophysis* is subjected to grazing by microzooplankton like *Fragilidium* (Park and Kim, 2010) and zooplankton like copepods (Kozlowsky-Suzuki et al., 2006) which keeps their cell numbers lower and is the main reason for the decline of *Dinophysis* blooms apart from hydrodynamic events of water displacement like advection and downwelling (Escalera et al., 2010; Velo-Suárez et al., 2010). A generic encounter-based grazing rate was applied specifically to *Dinophysis* in a second run (Fig. 4.4) of the simulations shown in Fig. 4.3 to test the effect of grazing on *Dinophysis* on the overall dynamics. Grazing on *Dinophysis* did not affect the maximum biomass of *Synechococcus*,

Teleaulax and *Mesodinum* and only prolonged the bloom phase of *Mesodinium* for a few days in eutrophic conditions. The timing and length of bloom of *Dinophysis* did not change but the maximum cell numbers were lower by a magnitude. However, the magnitude will change with the grazing rate and whether the grazers are themselves grazed. For implementation in larger ecosystem models with the aim to simulate conditions in the field, this grazing rate can easily be implemented permanently. In any case, the model suggests that the mixotrophic nutrition mode is a key to explaining the seasonal lag of these blooms (Salgado et al., 2011).

4.4.2 Predator-prey ratio

The initial ratio of inoculated organisms has a considerable impact on the following bloom dynamics (Fig. 4.5). The concentrations of *Mesodinium* in comparison to the other organisms appear to have the biggest impact on overall bloom dynamics as the ciliate is both an important grazer to *Teleaulax* as well as being the specialist prey to *Dinophysis*. The results are sometimes counter-intuitive as low initial concentrations of *Mesodinium* can result in comparatively low biomasses of *Dinophysis* while the ciliate itself subsequently grows to larger numbers. *Mesodinium* starts out in low numbers in comparison to *Dinophysis*, the dinoflagellate is starved of sufficient plastids to support its population early on. At the same time, *Teleaulax* can develop larger cell numbers due to a lower grazing pressure by *Mesodinium*. By the time the cell numbers of *Mesodinium* increase, the ciliate finds itself in perfect conditions of a high biomass of its prey *Teleaulax* and low grazing pressure by *Dinophysis*. The size of the impact that the initial concentration of *Mesodinium* has on the other organisms and especially *Dinophysis* show a high level of complexity of the dynamics that seem chaotic at first glance. Models can help to understand the complex processes behind these dynamics. While *Mesodinium* is considered non-toxic, it is known to form large blooms (red tides) that can lead to oxygen depletion and thus suffocation of other organisms (Yoo et al., 1998). *Dinophysis* is dependent both on the concentration of *Mesodinium* as well as the timing of its appearance. Prey availability early on in the growth phase of *Dinophysis* appears to be crucial as the pSNCM will be able to maintain its chloroplasts for a time.

4.4.3 Irradiance

The model by Moeller et al. (2016) on *M. rubrum* found that acquired phototrophy affects the coexistence of the organism with its *Teleaulax* prey (and supplier of plastids) and that an increase in irradiance shifts a stable coexistence to boom and bust cycles. Our model shows that such an interaction extends further to *Dinophysis*. However, while the maximum biomass of *Teleaulax*, *Mesodinium* and *Dinophysis* increase significantly with elevated irradiance, the boom and bust dynamic did not repeat in cycles (Fig. 4.6). Without a recurring reseeding (in nature, for example, by advection) *Teleaulax* and *Mesodinium*

were grazed to extinction and *Dinophysis* thus cannot take advantage of the reappearing nutrients.

The model by Anschütz and Flynn (2020) showed that good growth conditions allow blooms of SNCMs of such a magnitude that the essential provider of acquired phototrophy (e.g., *Teleaulax* for *Mesodinium*) is driven to extinction and the SNCM bloom will then subsequently also become extinct (or be forced to encyst). Lower nutrient systems prevent boom-and-bust dynamics and thus can support lower (but perhaps still actionable) levels of *Dinophysis*. The implication is that decreasing sources of eutrophication need not necessarily remove the potential for HABs of *Dinophysis*.

Higher irradiance decreases the time that *Dinophysis* can operate its kleptochloroplasts (Rusterholz et al., 2017). Irradiance may impact pSNCM growth by triggering photoacclimation while decreasing their longevity due to photodamage. A higher level of photodamage may raise the demand for their specific prey to resupply on plastids. Further developments of the model could include an irradiance dependence of *crit_IR* and photoacclimation could be simulated by changing the chlorophyll to carbon ratio (*ChlC*). Photoacclimation is known to be important to pSNCM growth in variable light (Moeller et al., 2016) but doing justice to this process and the decline of acquired phototrophy linked to both light and nutrient status requires models that better describe food quality impacts on mixoplankton activity (e.g., Lundgren et al. (2016); Lin et al. (2018)). This requires the use of full variable stoichiometric (C:N:P:Chl) models.

4.4.4 Temperature

Temperature is known to have a substantial effect on the frequency of *Dinophysis* blooms in a season and their maximum biomass (Escalera et al., 2006; Díaz et al., 2016; Pitcher et al., 2017). Temperature impacts are both abiotic and biotic. Warmer waters lead to a more stratified and stable water column that favours *Dinophysis*. The results of this model show that temperature moves the time frame of the blooms of the critical species of *Teleaulax, Mesodinium* and *Dinophysis* due to their physiological response to temperature and that the timing consequentially impacts the likelihood and size of *Dinophysis* blooms (Fig. 4.7). Interestingly, the simulations show that elevated temperature does not necessarily result in the largest blooms of *Dinophysis* as it accelerates the growth phase of *Mesodinium* and so *Dinophysis* has less exposure time to its specific prey. The right timing of the bloom of *Dinophysis* with that of *Mesodinium* appears a critical factor for *Dinophysis*. While hydrodynamic events of stratification, advection and up-welling are crucial factors for *Dinophysis* bloom events (Escalera et al., 2010; Raine et al., 2010; Díaz et al., 2016; Ajani et al., 2016), the components of the TMD chain need to be present in the appropriate magnitude at the right time for *Dinophysis* blooms to develop and produce high cell abundances (González-Gil et al., 2010; Sjöqvist and Lindholm, 2011).

4.4.5 Mixed layer depth

The simulations were run at eutrophic conditions that are high in DIN and light-limited due to a larger biomass suspended in the water that attenuates light. Light attenuation by organic matter builds up over depth leaving the organisms in 30 m MLD with less light for photosynthesis and therefore a lower capacity to use nitrate. Both pSNCMs (*Mesodinium* and *Dinophysis*) encounter much more prey at 1 m. For *Mesodinium* and especially *Dinophysis* this leads to a much higher biomass yield.

Events that increase the proximity of organisms have important implications for bloom development. This applies particularly to predator-prey interactions that are critical for mixoplankton food webs, and here for the progression of the TMD chain. The simulations returned a higher biomass for *Dinophysis* at 1 m depth as predator-prey encounters are enhanced (Fig. 4.8). *Dinophysis* often aggregates in very high abundances in thin layers (Campbell et al., 2010; González-Gil et al., 2010; Sjöqvist and Lindholm, 2011; Hattenrath-Lehmann et al., 2013; Díaz et al., 2016; Berdalet et al., 2017) that resemble monocultures (Farrell et al., 2012). This strategy increases encounter rates with their much faster prey enabling *Dinophysis* to launch its ambush-style attacks on *Mesodinium* (Jiang et al., 2018). Turbulence damages ciliates (Smayda, 2002) and *M. rubrum* is documented to actively avoid turbulence (Cloern et al., 1994). In fact, vertical stability of the water column is essential to enable *M. rubrum* to reach the highest cell abundances (Sanders, 1995; Herfort et al., 2011). Thus, stable water conditions may coincidentally favour the growth of their *Dinophysis* predator.

4.4.6 Current input and advection

DSP events are often associated with the physical transport of *Dinophysis* populations by wind-driven advection and coastal counter-currents (Escalera et al., 2010; Raine et al., 2010; Reguera et al., 2012), hence the forecasting power of physical models for HAB events linked to hydrodynamics (Velo-Suárez et al., 2010; Raine et al., 2010; Savvidis et al., 2011; Cusack et al., 2016; Moita et al., 2016; Pinto et al., 2016). In addition to horizontal currents, blooms have also been related to upwellings potentially bringing populations of *Dinophysis* from shelf bottom waters to the surface water and into contact with their *M. rubrum* prey (Velo-Suárez et al., 2014).

The effective dilution of a system, as a result of water exchange during advection, changes temperature, MLD and turbulence as well as to the availability of nutrients. It also seeds the surface water with different organisms. These are conditions that influence factors which this model suggests can promote the development of *Dinophysis* blooms. Impacts of each member of the TMD chain (and of course additional interaction upon those members, such as predation and competition) all play parts in the story. The increase in stratification and mixed layer depths in the summertime due to climate change (Sallée et al., 2021) will likely affect the bloom potential of *Dinophysis*. A changing ocean may challenge the reliability of existing forecasting models that are based on time series

data of hydrodynamic events. A solution could be mechanistic models that combine hydrodynamics and the biology of *Dinophysis* and the species it depends on.

4.5 Conclusion

While the model shows the importance of prey availability for the growth of *Dinophysis*, it also shows that the timing of prey availability has a significant effect on cell number development. The mixoplanktonic activity of *Dinophysis* and its prey *Mesodinium* play an important role in the dynamics of bloom formation and potential DSP events. The simulations indicate that eutrophication sets conditions that enable *Dinophysis* blooms weeks later after the nutrient injection. Both high *Mesodinium* to *Dinophysis* ratios and the growth phase in which *Dinophysis* meets *Mesodinium* affect cell abundances of *Dinophysis* in consecutive blooms. Monitoring programs could therefore benefit from including *Mesodinium*, which has the advantage that *Mesodinium* appears in much larger numbers making it easier to detect than *Dinophysis*.

The disparity between the monitoring and research effort expended on just the terminal end of the TMD chain, on *Dinophysis*, is notable. The other critical components, namely *Mesodinium* and *Teleaulax*, receive far less attention (Fig. 4.9) and yet their success and timing set the scene for blooms of the toxigenic species. The dynamics shown by the simulations will perhaps act to prompt more attention in monitoring these other species. For aquacultures, it is not only important to know when the blooms will occur but also their duration. The main reasons for the decline in *Dinophysis* blooms are dispersion (Velo-Suárez et al., 2010), grazing (Kozlowsky-Suzuki et al., 2006) and infections with parasites like *Amoebophrya* sp. (Velo-Suárez et al., 2014).

Finally, models of the form we used here may help to test sensitive parameters of different species and theoretically explore their behaviour and inspire future experiments. The model thus provides a tool to explore reasons for differences in bloom dynamics between species. As a nitrogen-based model this model is also suitable for implementation in larger nitrogen-based ecosystem models and therefore exploration in a larger context.

The model presented here does not replace a hydrodynamic model and on its own is not sufficient as a predicting tool for *Dinophysis* blooms occurring in the field. It is however the first biological model featuring *Teleaulax*, *Mesodinium* and *Dinophysis*. This model could deliver useful results in combination with a hydrodynamic model that can account for stratification and *Dinophysis* input via currents from the outside (from offshore or up the coastline).

Funding This research was supported by EC MSCA-ITN 2019 funding to the project MixITiN (grant number 766327).

Author contributions Anna-Adriana Anschütz and Kevin J. Flynn conceived, built and ran the model. Anna-Adriana Anschütz and Kevin J. Flynn shared the analysis of the results and writing of the manuscript. Nathalie Gypens, Aditee Mitra and Kevin J Flynn provided comments and advice on draft versions of this chapter.

Chapter 5

Growth and stoichiometry of *T. amphioxeia* in phosphorous limiting conditions – a combined experimental-modelling approach

Abstract

A growing body of research has revealed the frequency of mixoplankton in plankton communities and the variety of trophic modes and physiology that can be found among mixoplankton. How external and internal stoichiometry drives the synergism of photo- and phagotrophy in mixoplankton is still not completely understood and very few models feature mixoplankton and their variable stoichiometry. *Teleaulax amphioxeia* is a ubiquitous constitutive mixoplankton species that is the source of kleptochloroplasts for the specialist non-constitutive mixoplankton *Mesodinium* spp. and the HAB genus *Dinophysis* spp.. In addition to phototrophy, *T. amphioxeia* preys on heterotrophic bacteria and *Synechococcus*. This is the first experimental data set on *T. amphioxeia* growing in various nutrient conditions and showing the impact they have on its internal stoichiometry. The mechanistic variable stoichiometric model "Perfect Beast" was tuned to those experimental data. Results from the tuning process strongly suggest that *T. amphioxeia* feeds on bacteria as a response to phosphorous limitation as a compensation for the missing nutrient, but otherwise does not heavily rely on phagotrophy to grow.

5.1 Introduction

Teleaulax amphioxeia is a globally occurring cryptophyte that can be found in a wide variety of different environmental conditions (Clay, 2015). It is very frequently encountered and can occasionally form large blooms (Needham et al., 2018). It holds quite a substantial role in marine food webs. As a constitutive mixotroph, it both contributes to primary production and exerts grazing pressure on cyanobacteria (*Synechococcus* sp.) and heterotrophic bacteria (Yoo et al., 2017). In addition, *T. amphioxeia* is an important prey species to many types of microzooplankton and mixoplankton (Yoo et al., 2017).

Both the red tide ciliates, *Mesodinium* spp. (Gustafson et al., 2000), and the HAB dinoflagellates, *Dinophysis* spp. (Garcia-Cuetos et al., 2010; Nishitani et al., 2010; Sjöqvist and Lindholm, 2011; Hernández-Urcera et al., 2018) use kleptochloroplasts from the *Teleaulax*/*Geminigera*/*Plagioselmis* clade with *T. amphioxeia* often being the preferred cryptophyte species (Peltomaa and Johnson, 2017; Hernández-Urcera et al., 2018).

Ciliates belonging to the *Mesodinium* genus are an important food for copepods and fish larvae (Lindholm, 1985). Species of the *Mesodinium rubrum*/*major* complex form prominent red tides as first documented off the coast of Peru by Charles Darwin (Lindholm, 1985). They may substantially affect the oxygen regime of their environment during blooms and as a result, their potential to harm aquacultures has been debated (Hayes et al., 1989; Liu et al., 2012).

The dinoflagellate genus *Dinophysis* is notorious for the causation of harmful algae blooms and its associated poisoning of shellfish aquacultures (Reguera et al., 2012; Reguera et al., 2014). Due to the diarrheic shellfish poisoning caused by ingestion of shellfish contaminated with *Dinophysis*, blooms caused by the toxic members of this species have repeatedly caused the shutdown of aquacultures and therefore significant economic damage (Reguera et al., 2014). Apart from *Dinophysis*, several other toxic protist species use *T. amphioxeia* as prey (Yoo et al., 2017), like the mixoplankton dinoflagellates *Karlodinium armiger*, *Prorocentrum micans*, *Alexandrium tamarense* and *Akashiwo sanguinea* and the heterotrophic dinoflagellate *Pfiesteria piscicida*. Despite its connection in newfound complex mixotrophic relationship with potentially toxic algae, its importance as a prey species and therefore factor in the food web and higher trophic levels, little is known about the ecophysiology of this cryptophyte.

Grazing experiments with the heterotrophic dinoflagellate *Oxyrrhis marina* under various nutrient regimes showed that grazing rates on *Teleaulax* sp. increased in phosphate deplete conditions (Meunier et al., 2013). This suggests that the predator compensates for prey that is of low nutritious value by increasing the ingested quantity. Nutrient loadings and consequent differences in nutrients status in *Teleaulax* sp. could thus potentially affect grazing rates and stoichiometry that travel up the trophic levels in the food web. Experimental research on the nutrient demands and general ecophysiology of the cryptophyte is however scarce and generally do not exceed the use as feed for other organisms like *Mesodinium* and *Dinophysis* that the actual experiment is focused on.

The importance of mixoplankton to nutrient cycling in marine environments has been shown by experimental (Dolan and Pérez, 2000; Ptacnik et al., 2004) and modelling studies (Mitra et al., 2014; Ward and Follows, 2016; Leles et al., 2018; Anschütz and Flynn, 2020; Leles et al., 2021). Mixoplankton is now recognised to contribute substantially to grazing on bacteria across various types of marine ecosystems (Stoecker et al., 2016; Edwards, 2019).

Considering stoichiometry is important to understand trophic levels and triggers for mixotrophy as predation in some mixoplankton may be triggered by limitation in a certain nutrient as an additional source of that nutrient (Stoecker, 1998; Stoecker et al., 2016). Few models so far describe mixoplankton and the implications of limitation of different nutrients for its physiology (Flynn and Mitra, 2009). The drivers of bacterivory in *T. amphioxeia* are still unclear and there is a lack in mixoplankton models that feature variable stoichiometry and have been fit to experimental data.

The "Perfect Beast" model is a mechanistic model that describes the variable stoichiometry of carbon, nitrogen and phosphorous in a mixotrophic protist (Flynn and Mitra, 2009). Rather than as a simple addition of phagotrophy and phototrophy, mixotrophy is described as a synergism of photosynthesis, inorganic nutrient uptake and prey consumption. The protist can be configured as a pure autotroph, heterotroph or different types of mixoplankton. Ingestion is controlled by a food vacuole that competes with the chloroplast for volume in the cell. As the model also describes different triggers for feeding in a mixotroph, such as the acquisition of a limiting nutrient like phosphorous, the variable stoichiometric model allows for a more accurate description of a mixoplankton ecological behaviour in a chemically variable environment.

Feeding in *T. amphioxeia* as a response to phosphorous limitation can only be described in a model that features variable stoichiometry, which is not the case in a nitrogen-based model that assumes a fixed ratio of nitrogen to phosphorous. Combining the results from the experiments on *T. amphioxeia* described above and results on grazing by (Yoo et al., 2017) with the “Perfect Beast” model is expected to deliver insights into the triggers and implications of bacterial grazing in *T. amphioxeia*.

This study was aimed at generating the first data set on physiology and stoichiometry of *T. amphioxeia* under different conditions of external stoichiometry. Ecophysiological response in cell stoichiometry, respiration rates, growth rates and rates of photosynthesis were monitored among other physiological parameters. Provided here is the first data set on the variable stoichiometry of *T. amphioxeia* to this extent.

In addition, the capability of the "Perfect Beast" model was tested to accurately reproduce experimental data of biomass development and internal stoichiometry of *T. amphioxeia* when grown in different conditions of nutrient availability. Furthermore, it was tested which role bacterivory plays in the mixotrophic physiology of *T. amphioxeia* and under which conditions feeding on bacteria provides a benefit to this constitutive mixotroph.

5.2 Methods

The experiment was specifically designed to acquire physiological data suitable for configuring a variable stoichiometric model of the organism. For that purpose, *T. amphioxeia* was grown in three treatments of varying ratios of nitrogen and phosphate: a control that was equal to the Redfield ratio, a nitrogen limiting condition and a phosphate limiting conditions. Nutrient concentrations were measured daily. The general concept of the following methods and experiment set-up are described in more detail in chapter 2.

5.2.1 Cultures and culture conditions

Stock cultures of the cryptophyte *T. amphioxeia* (strain isolated in Øresund in 1990; Riisgaard and Hansen, 2009) were grown on *f*/20 medium (Guillard, 1975) at 15.0 °C $\pm$ 1.0 °C in a temperature-regulated room in Pyrex media bottles (1 L). Medium was prepared with filtered (Whatmann GF/F) and autoclaved seawater with a salinity of 33. Light was provided by cool white fluorescent tubes (OSRAM 58W, 840) at an intensity of 350 µmol photons m^{-2} s^{-1} (PAR, 400-700 nm) in a light:dark cycle of 16:8 h. Photon irradiance was measured (in air, inside the bottle) with a light meter equipped with a spherical quantum sensor (ULM & US-SQS/L, Walz GmbH, Germany). All cultures were xenic and frequently checked under the microscope for contamination with heteroflagellates.

5.2.2 Experiment

Three types of media (control, nitrogen-limiting and phosphate-limiting) were inoculated in duplicates with the stock culture. In all three conditions, the $NaNO_3$ concentration was 50 µM and vitamin and trace metal concentrations remained that of *f*/20 medium. The NaH_2PO_4 concentration was 3.125 µM (Redfield, 1:16) in the control, 12.5 µM (1:4) in the nitrogen-limiting treatment and 0.78 µM (1:64) in the phosphorous-limiting treatment. The cultures were kept in 5 L Pyrex media bottles and except for organic nutrients sampled daily for every parameter. The bottles were sealed with a silicon stopper. Sampling was carried out with tubing on which a negative pressure was applied. Before sampling, the tubing was rinsed with ca. 10 mL sample which were discarded. To avoid limitation by carbon dioxide (Hansen, 2002), the bottles were aerated with filtered air (0.2 µm) to keep a pH of 8.3 $\pm$ 0.1 and a DIC of 26.8 $\pm$ 1 g C m^{-3}. A total of 120 mL was taken daily from the culture flasks and given directly into 200 mL Pyrex media bottles from which any further sub-samples for analysis were taken.

5.2.2.1 Cell numbers and biovolume

T. amphioxeia cell numbers from the three treatments were measured in 3 mL samples with a flow cytometer (Beckmann Coulter, Cytoflex). The flow rate was determined with QC standardization beads (CytoFlex Daily QC fluorospheres). *T. amphioxeia* cells were

detected based on cell complexity (SSC), cell size (FSC) and pigment fluorescence (chlorophyll and phycoerythrin).

In addition, cell numbers and biovolume were measured in a Coulter counter (Beckmann Coulter counter) with a 100 µm aperture. For this purpose, 5 mL samples were diluted with filtered seawater (GF/F, salinity 33) by a factor 3. Two replicates of each sample were measured. The range of *T. amphioxeia* cells to detect was chosen based on the biovolume output and the size range of *T. amphioxeia* (4-9 µm). Cell volumes were calculated by dividing biovolume by cell numbers.

5.2.2.2 Bacterial cell numbers

Bacterial abundance was determined using CytoFLEX flow cytometer (Beckman Coulter) according to the method described in Gasol and Giorgio (2000). Bacteria samples were gently vortexed and 5 µm of SYBR^{TM} green I (ThermoFisher Scientific) diluted 1:200 was added in 500 mL of the sample. After 10 min incubation in the dark bacteria concentration were determined using the plot of green fluorescence (FITC) against the side scatter (FSC). The bacteria population had more green fluorescence than the other particles like debris or background noise. The concentration of bacteria was determined by gating and looking at the count events/µL.

5.2.2.3 Inorganic carbon uptake - ^{14}C incorporation

Inorganic carbon uptake was measured as described by Hansen et al. (2016). To yield a carbon-specific growth rate this rate was divided by the average cell carbon content calculated with carbon biomass data and cell numbers determined with the flow cytometer. Every 24 h two samples of 2 mL were incubated in a scintillation vial for 3 h with one sample in the dark and the other at experimental light conditions.

5.2.2.4 Dissolved inorganic carbon (DIC)

DIC concentrations were measured on 25 mL subsamples using a combustion catalytic oxidation method (TOC-L Shimadzu, ASI-L). The samples were filled in glass vials that were closed with aluminium foil and a screw cap allowing no air space and run to a previously executed calibration. The samples were run together with a control of 20 mg L^{-1} DIC and a cleaning sample with MilliQ between treatments. The samples pH was lowered to 2 with 3 % of 25 % H_2SO_4 to remove organic carbon by changing it to CO_2. The sample was then oxidized in a platinum-packed catalysator at 720 ℃ and turned into gas-form. Unwanted particles were stopped in a moisture-chamber and halogens removed in a halogen-scrubber. Finally, inorganic carbon was measured by the NDIR-detector.

5.2.2.5 Dissolved inorganic nitrogen and phosphorous

Dissolved inorganic phosphorous (DIP) was reduced to a phospho-molybdenum complex with ascorbic acid (pH$<$1) following Murphy and Riley, 1962). The complex was measured spectophotometrically at 880 nm (Seal Analytical Analyser). Nitrate was first reduced to nitrite and then made to react with sulphanilamide and couples with N-1-naphthylethylenediamine dihydrochloride (NEDD) under acidic conditions. The resulting azo dye was measured at 520 – 560 nm.

5.2.2.6 Cellular organic carbon, nitrogen & phosphorous (C, N, P)

The cellular contents of carbon, nitrogen and phosphorous content were measured by filtering a sample volume containing a total of $\sim$ 10,000 cells (ashed Whatman GF/C filters) to obtain sufficient material for analysis. The filters were placed in a petri dish and dried in the oven (< 50 ℃) overnight. Apart from the petri dishes all material getting in contact with the filter was burned. Carbon and nitrogen were analysed on a FLASH 2000 organic elemental analyser with sulphanilamide being used as reference material. For the analysis of phosphorous, the sample was first digested with 2.5% potassium persulfate solution and then measured with QuAAtro segmented flow analyser Waal et al. (2013).

5.2.2.7 Chl *a*

For Chl *a*, 10 mL of sample were filtered (Whatman GF/F) 0.2 mbar on a filtration rack and the filter was placed in a scintillation vial filled with 5 mL of 97 % EtOH and kept in the fridge ($\sim$ 4 ℃) overnight in the dark. After 24 h, the samples were taken out of the fridge 5 min prior to analysis to allow the samples to reach room temperature and thus avoid condensation on the cuvette. Then, 2 mL of pigment dissolved in EtOH were pipetted into cuvettes and measured spectrophotometrically (Trilogy Turner fluorometer) at excitation of 436 nm and emission of 685 nm Skovgaard et al. (2000). For cell-specific chlorophyll total chlorophyll was divided by cell numbers detected in the flow cytometer.

5.2.3 Model

5.2.3.1 Model description

The variable stoichiometric model "Perfect Beast" (Fig. 5.1) was originally developed by Flynn and Mitra (2016). Here, the version described in Mitra et al. (2014) was deployed that was extended with the Satiation-Controlled-Encounter-Based (SCEB) model (Flynn and Mitra, 2016) and the prey optimality model (Flynn, 2018), which are described in 3.2.1. The model by Mitra et al. (2014) describes a food web with bacteria, non-motile algae, mixoplanktonic nanoflagellates, heterotrophic nanoflagellates and microzooplankton (Fig. 5.2). Higher trophic levels are described with a closure function. The model is carbon biomass-based, but allows for stoichiometric calculations of the respective nitrogen and

phosphorous contents. Dissolved inorganic nutrients are provided as ammonium, nitrate, dissolved inorganic phosphorous (DIP) and dissolved inorganic carbon (DIC). Dissolved organics are described as dissolved organic carbon (DOC) and semi-labile dissolved organics of carbon, nitrogen and phosphorous (sDOMC, sDOMN, sDOMP), which support bacterial growth. In addition, physical forcings like light and temperature etc. can be altered.

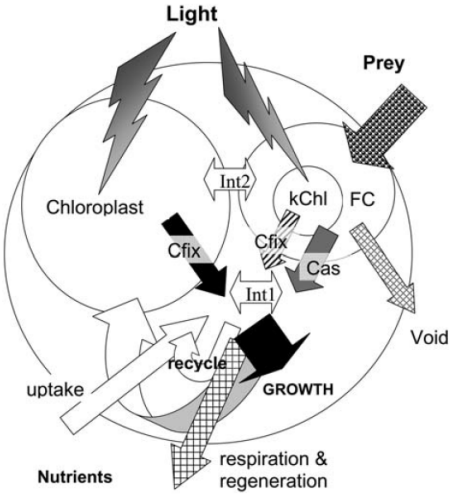

FIGURE 5.1: Schematic of processes and interactions described in the model. Photoautotrophic growth uses inorganic nutrients and light via the mixotrophs own photosystems. A proportion of activity leading to growth is required to support synthesis of those photosystems. Predation brings prey material into the food vacuole, FC, in entirety into the confines of the mixotroph cell itself (phagotrophy), piecewise through peduncle feeding or held within a palium feeding veil outside of the cell proper. A portion of the material is assimilated (Cas), a portion voided (void). If applicable, C is fixed also via kleptochloroplasts (kChl). Interactions between phototrophic and heterotrophic nutrition (Int1) and for space within the mixotroph (Int2) shape the growth of the mixotroph. Taken from Flynn and Mitra (2009) with original figure legend.

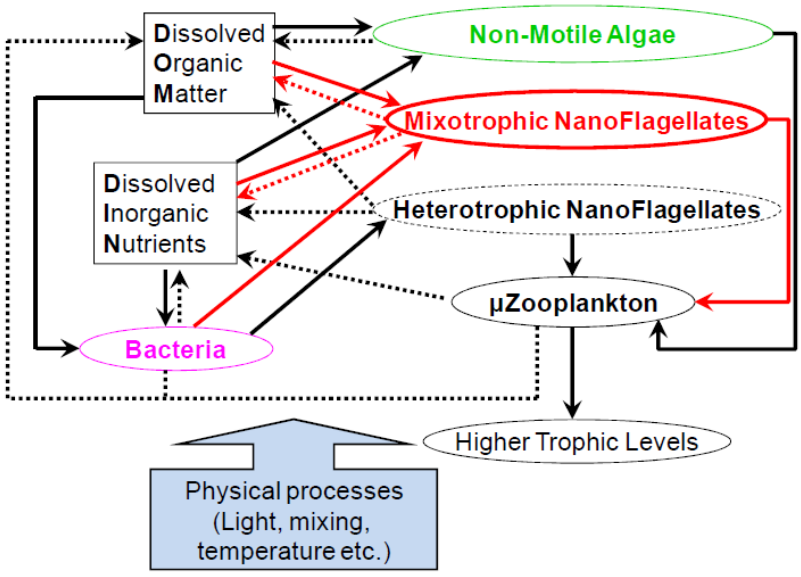

FIGURE 5.2: The MNFs are capable of eating bacteria (red-lined black arrow), and hence deriving nutrients for the support of their growth, and of their primary production, directly. Dashed arrows indicate functions contributing to nutrient pools (blue for inorganic, brown for organic). Heavy black arrows indicate predatory links. Taken from Mitra et al. (2014) with shortened legend.

5.2.3.2 Configuration of the ”Perfect Beast” model as *T. amphioxeia*

The food web of the model here is structurally the same as in Mitra et al. (2014) except that it does not have heterotrophic nanoflagellates, microzooplankton nor a higher trophic level closure function. In addition, the non-motile algae were disabled by setting their inoculum to almost zero ($1e^{-21}$) and their maximum growth rate to zero to simulate the monoculture of *T. amphioxeia* in the experiment. The only organisms in the model were *T. amphioxeia* and bacteria (Fig. 5.3). The mixoplankton model was configured as a constitutive mixoplankton (CM) with the ability to feed on bacteria (Fig. 5.3 & Tab. 5.1). *T. amphioxeia* can use ammonium, nitrate, DIP and DIC and is able to internally recycle nutrients. The cryptophyte contributes to the pools of DOC and semi-labile organic matter as well as the inorganic nutrient pools. Bacteria use the inorganic as well as the organic pools of nutrients while they contribute to both. The model consists of several submodels that describe individual parts of the organisms physiology. The *T. amphioxeia* model has state variables for each cellular carbon, nitrogen, phosphorous and chlorophyll biomass. Digestion of prey (bacteria) is described in the food vacuole model and the carbon, nitrogen, phosphorous and chlorophyll biomass are relative to the overall biomass of the mixoplankton and contribute to it. Light attenuation and photosynthesis by *T. amphioxeia* are described by a submodel that functions as described in chapter 3. The capture of bacteria as prey by *T. amphioxeia* is described in the SCEB submodel (for description see chapter 3.2.1). The stoichiometry of bacteria is fixed in this model and there is no nitrogen and phosphorous state variable for bacteria in addition to the state variable for carbon biomass. Nutrient usage and regeneration by bacteria are calculated using constants for nitrogen to carbon (NC) and phosphorous to carbon (PC) ratio for nitrogen and phosphorous specific uptake. Due to the small size of bacteria, data of the biomass of bacteria and thus their stoichiometry are difficult to measure and where therefore excluded from this study.

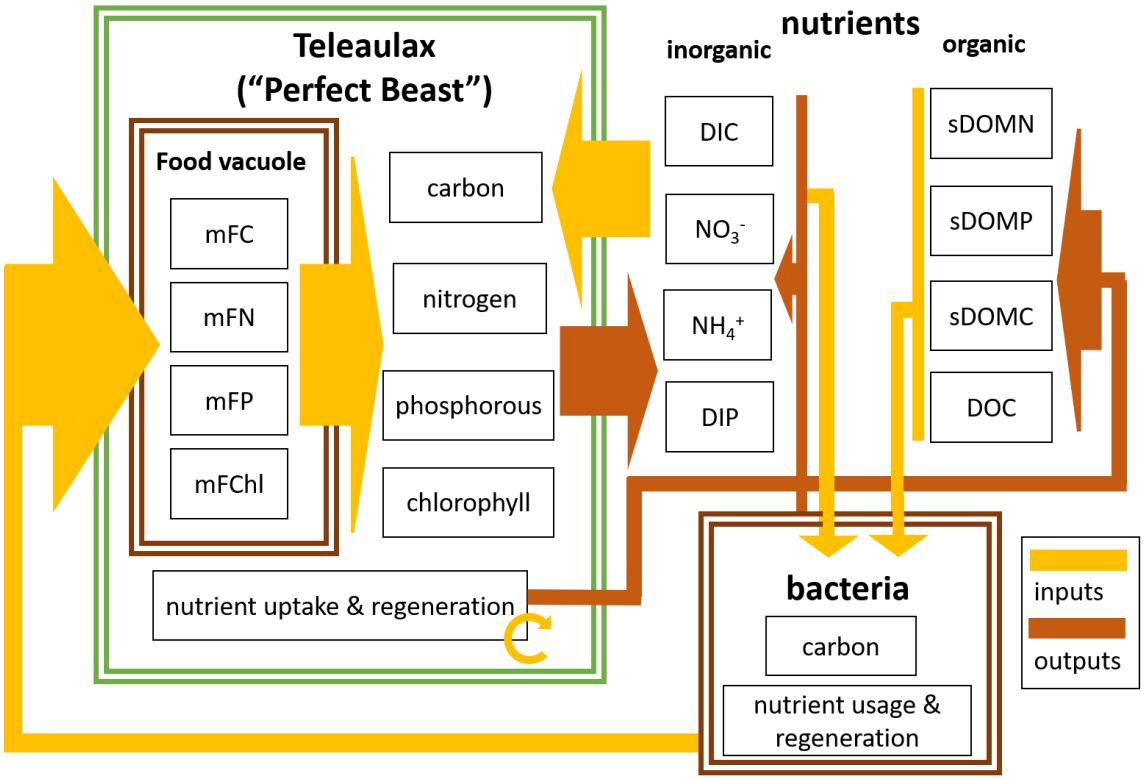

FIGURE 5.3: Food web schematic of configured *T. amphioxeia* model derived from the "Perfect Beast" model described in Mitra et al. (2014). This model does not feature micro-zooplankton, heterotrophic nanoflagellates, non-motile algae nor a closure function for higher trophic levels. For bacteria, only carbon biomass is described and their stoichiometry is fixed in the model. Not shown here are the submodels for PFD and photosynthesis. Note that bacteria do not use DIC.

TABLE 5.1: Constants of the "Perfect Beast" model (Flynn and Mitra, 2009) describing the external conditions of the experiment and constants that configure the model as a constitutive mixoplankton.

Constant	description	Value	Unit
Stype	Growth in response to grazing	1	Switch
Spd	C-fixation does not affect digestion	0	Switch
Smix	Carbon contribution from mixotrophy additive to growth	1	Switch
Fcabs	Max possible digestive vacuole size	1	gC/gC
Pbalcrit	Min required contribution of photo Cfix to total C for growth	0.1	dl
SVol	Volume sharing	0	Switch
LD	fraction of day illuminated	16/24	dl
PAR	Surface PAR	350	µmol photon m^{-2} s^{-1}
Mix_depth	mixed layer depth	0.2	m

5.2.3.3 Tuning the model to the experimental data

For the tuning process, the experimental data were processed, and missing data were interpolated to achieve a continuously spaced data set over time that is suitable for tuning. The carbon, nitrogen and phosphorous biomass were calculated from the results of the elemental analysis and the biovolume of *T. amphioxeia* by using a conversion factor derived from the slope of a linear regression of biovolume over the respective elemental biomass.

The model was tuned (see chapter 2) to a set of two replicates per each of the three treatments by manually adjusting the physiological constants (Tab. 5.3) and the initial concentrations of nutrient concentrations and inoculated cell numbers (Tab. 5.2) to fit the maximum biomass and growth curve recorded in the experiment in each treatment equally. Tuning involved the use of a generic algorithm of the software to minimise the standard deviation between data and model (see chapter 2). In a manual post-edit the visual optimal fit of the model output with the experimental data was improved. Both the model and the experiment are closed systems for all state variables of the model where no nutrients or biomass can enter or leave. The only exception is that the flasks in the experiment were aerated to prevent the pH of the medium from increasing too high. The model was run for the same amount of time as the experiment (14 days) at a step size of 0.03125 d^{-1} with the Euler routine.

TABLE 5.2: Initial concentrations of inorganic nutrients and inoculated organisms of the experiment. For the model, the initial concentrations of inorganic nutrients and inoculated organisms were tuned to the experimental data. For the tuning process, it was assumed that there were no bacteria suitable for feeding in the control, nitrogen-limiting and phosphorous-limiting treatment. The bacteria biomass was set to a very low value rather than zero to avoid an error in the model simulation generated by division by zero. The initial values of the nutrient concentrations differ between the model and the experiment because the model was also tuned to the initial concentrations due to the variance in the experimental data and a potential lack in their accuracy. The initial nutrient concentrations of the model were tuned to the overall trend of all data while taking into account the initial concentration of intended in the experimental set-up. Note that the bacteria carbon biomass in the P-limiting treatment experiment data are calculated from cell numbers based on a conservative estimate of the per cell carbon content of the bacteria in the culture.

parameter	**unit**	**type**	**replicate**	**Control**	**Nlim**	**Plim Bac/ no Bac**
initNO3	mg N m^{-3}	model	A	438.3	492.3	405.4
		experiment	A	258.4	453.1	402.9
		model	B	578.9	580.7	462.8
		experiment	B	361.0	580.7	381.3
initPO4	mg P m^{-3}	model	A	55.4	323.4	15
		experiment	A	40.2	198.4	30.7
		model	B	81.9	385.0	15
		experiment	B	60.1	302.5	9.3
initmC	mg C m^{-3}	model	A	112.1	91.7	60.8
		experiment	A	114.0	90.5	110.6
		model	B	105.1	120.0	54.0
		experiment	B	106.8	131.4	108.5
initbC	mg C m^{-3}	model	A	1e-21	1e-21	150/1e-21
		experiment	A	52.7	10.7	52.8
		model	B	1e-21	1e-21	150/1e-21
		experiment	B	73.5	128.5	57.3

TABLE 5.3: Physiological constants of the "Perfect Beast" model of *T. amphioxeia* and bacteria. The values were acquired by fitting the model to the experimental data of the three treatments (control, Nlim and Plim). Each treatment had two replicates. The maximum chlorophyll to carbon ratio (mChlCabs) may be low here, because *T. amphioxeia* also contains phycoerythrin as a photoactive pigment like other cryptophytes (Jeffrey et al., 2011). This also affected the tuning of the Chl *a*-specific initial slope to PI curve (malpha).

Constant	**description**	**Value**	**unit**
ESD_M	ESD of *Teleaulax*	5	µm
mNCo	min N:C	0.12	gN/gC
mNCm	max N:C that affects phototrophic growth	0.22	gN/gC
Ncabs	absolute max possible organic N:C	0.25	gN/gC
mPCo	min P:C	0.01	gP/gC
mPCm	max P:C quota that affects growth	0.02	gP/gC
PCabs	absolute max P:C	0.035	gP/gC
mChlCabs	max possible constitutive Chl:C ratio	0.006	gChl/gC
mBR	basal respiration	0.019	dl
malpha	Chl-specific initial slope to PI curve, giving gC fixed per gChl. *a* per photon	0.00006	(m^2 g^{-1} Chl *a*)(gC µmol^{-1} photon)
mUphot	*Teleaulax* maximum rate of photosynthesis-driven growth	0.47	d^{-1}
death	specific mortality rate	0.1	gC/gC/d
bUm	Bacterial maximum net growth rate	0.501	(gC/gC/d)
bbNC	Bacterial N:C	0.12	(g/g)
bBPC	Bacterial P:C	0.045	(g/g)
optimal_CR	proportion of prey of optimal characteristics captured by starved *Teleaulax*	0.2	dl

5.2.3.4 Dynamic Sensitivity Analysis of the "Perfect Beast" model configured as *T. amphioxeia*

The size and maximum growth rate of the bacteria in the experiment were not measured and could therefore cause variation in the data provided for the model. In order to determine the sensitivity of the biomass calculated for *T. amphioxeia* by the model to different sizes of bacteria and growth rate, a dynamic sensitivity analysis was performed (see chapter 2). The range of tested values is given in Tab. 5.4. The nutrient conditions under which the analyses were run are listed in Tab. 5.5.

TABLE 5.4: Constants that were tested in the dynamic sensitivity analysis. The objective was to assess the effect size of the parameters related to predation on bacteria that could not be measured in the experiment and therefore have to be estimated.

tested constants	**min**	**max**	**unit**
bacteria size	0.5	1	µm
bacteria max. growth rate	0.5	2	d^{-1}
Optimal capture rate	0.1	0.3	dimensionless

TABLE 5.5: The dynamic sensitivity analysis was run at two different levels of nitrogen on phosphorous input. The results of each analysis are displayed in Fig. 5.5

Plot	**Decisions**	**Value**	**Unit**	**N:P**
A)	PO_4^-	23.4	µg P L^{-1}	16
	bacteria	128	µg C L^{-1}	
	NH_4^+	0	µg N L^{-1}	
	NO_3^-	350	µg N L^{-1}	
B)	PO_4^-	5.9	µg P L^{-1}	60
	bacteria	128	µg C L^{-1}	
	NH_4^+	0	µg N L^{-1}	
	NO_3^-	350	µg N L^{-1}	

5.2.3.5 Effect of phosphorus stored in bacteria on growth and biomass yield of *T. amphioxeia*

After the tuning process, the contribution of grazing on bacteria to growth in *T. amphioxeia* was tested in the model in various conditions of phosphorous availability. The effects of bacterial prey were tested at different levels of dissolved inorganic phosphorous (DIP), nitrogen limiting (Nlim) and phosphorous limiting (Plim) conditions. To an inoculum of 100

mg C m^{-3} *T. amphioxeia* carbon biomass, 500 mg NO_3^- m^{-3} were added in all treatments. The different levels of DIP were provided as 3 µM DIP, 6 µM DIP and 3 µM DIP with an inoculum of bacterial phosphor of 3 µM phosphorous. The initial concentration of DIP was 300 mg DIP m^{-3} in the nitrogen-limiting treatment and 10 mg DIP m^{-3} in the phosphorous-limiting treatment. The data on *T. amphioxeia* carbon, nitrogen, phosphorous and chlorophyll biomass was exported as well as levels of nitrate and DIP.

5.3 Results

5.3.1 Effect of bacteria as prey on nutrient levels and *T. amphioxeia* biomass

The analysis of the impact of phosphorous bound in bacterial prey in the model (Fig. 5.4) shows that the form in which phosphorous is available (PO_4^- or bacteria) matters. The treatment of 3 µM DIP and 3 µM bacterial phosphorous generated a much higher biomass yield and higher growth rates than an initial DIP of 6 µM P without bacteria. The phosphorous biomass in the treatment with bacteria did not reach a higher yield than the treatment with 6 µM P, but the growth was accelerated. *T. amphioxeia* reaches a higher nitrogen biomass with bacteria as the bacteria are also an additional source of nitrogen. In the comparison of bacteria in the nitrogen-limited treatment and the phosphorous limited treatment, the mixoplankton is able to deplete the nitrate levels in the phosphorous limiting treatment. Bacteria being available as prey result in both a higher biomass yield of *T. amphioxeia* and a faster development of that biomass (Fig. 5.4). Both nitrate and phosphate levels are depleted quicker. Nitrate levels in the phosphorous limiting conditions get depleted further than without bacteria. The same is true for phosphate levels in the nitrogen limiting conditions. Larger biomasses are achieved when half of the available phosphorous is supplied as bacteria.

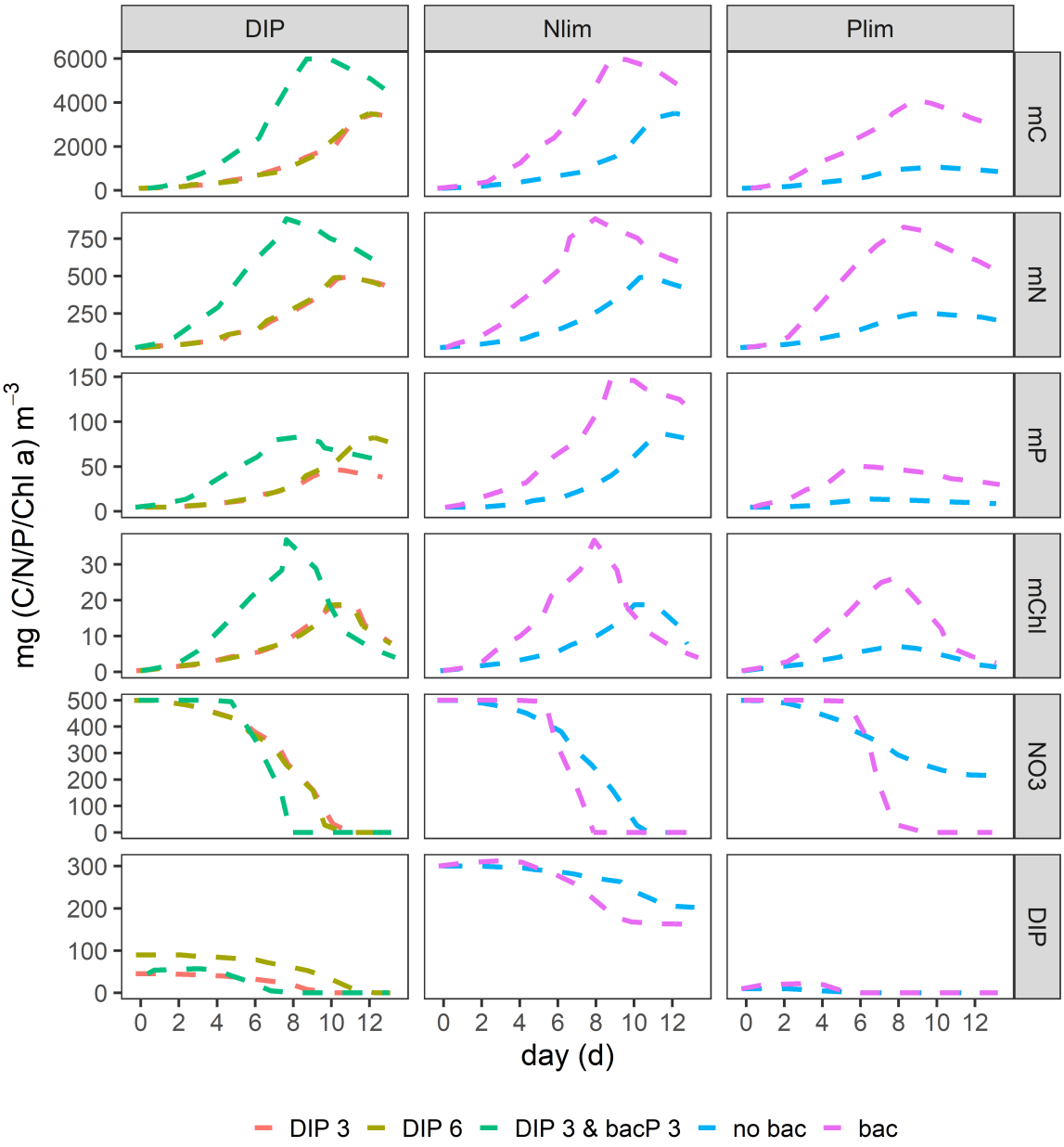

FIGURE 5.4: Results of the analysis of the impact size of phosphorus stored in bacteria on growth and biomass yield of *T. amphioxeia*. The effect of bacterial prey were tested at different levels of dissolved inorganic phosphorous (DIP column), nitrogen limiting (Nlim column) and phosphorous limiting (Plim column) conditions. NO_3^- = 500 µg N m^{-3}, inoculum *T. amphioxeia* carbon biomass = 100 µg C m^{-3}, DIP = PO_4^-, mC = *T. amphioxeia* carbon biomass, mN = *T. amphioxeia* nitrogen biomass, mP = *T. amphioxeia* phosphor biomass, mChl = *T. amphioxeia* chlorophyll biomass. The treatments were DIP 3 = initial PO_4^- of 3 µM P, DIP 6 = initial PO_4^- of 6 µM P and DIP 3 & bacP 3 = initial PO_4^- of 3 µM P and inoculum of bacterial phosphor of 3 µM P. The initial concentration of DIP was 300 mg DIP m^{-3} in the nitrogen-limiting treatment and 10 mg DIP m^{-3} in the phosphorous-limiting treatment

5.3.2 Dynamic Sensitivity Analysis

The results of the dynamic sensitivity analysis show that neither bacteria size, bacterial maximum growth rate nor the optimal capture rate by *T. amphioxeia* cause variation in the carbon biomass of *T. amphioxeia* during its growth phase (Fig. 5.5). Some small variation occurs in the stationary growth phase of the cryptophyte.

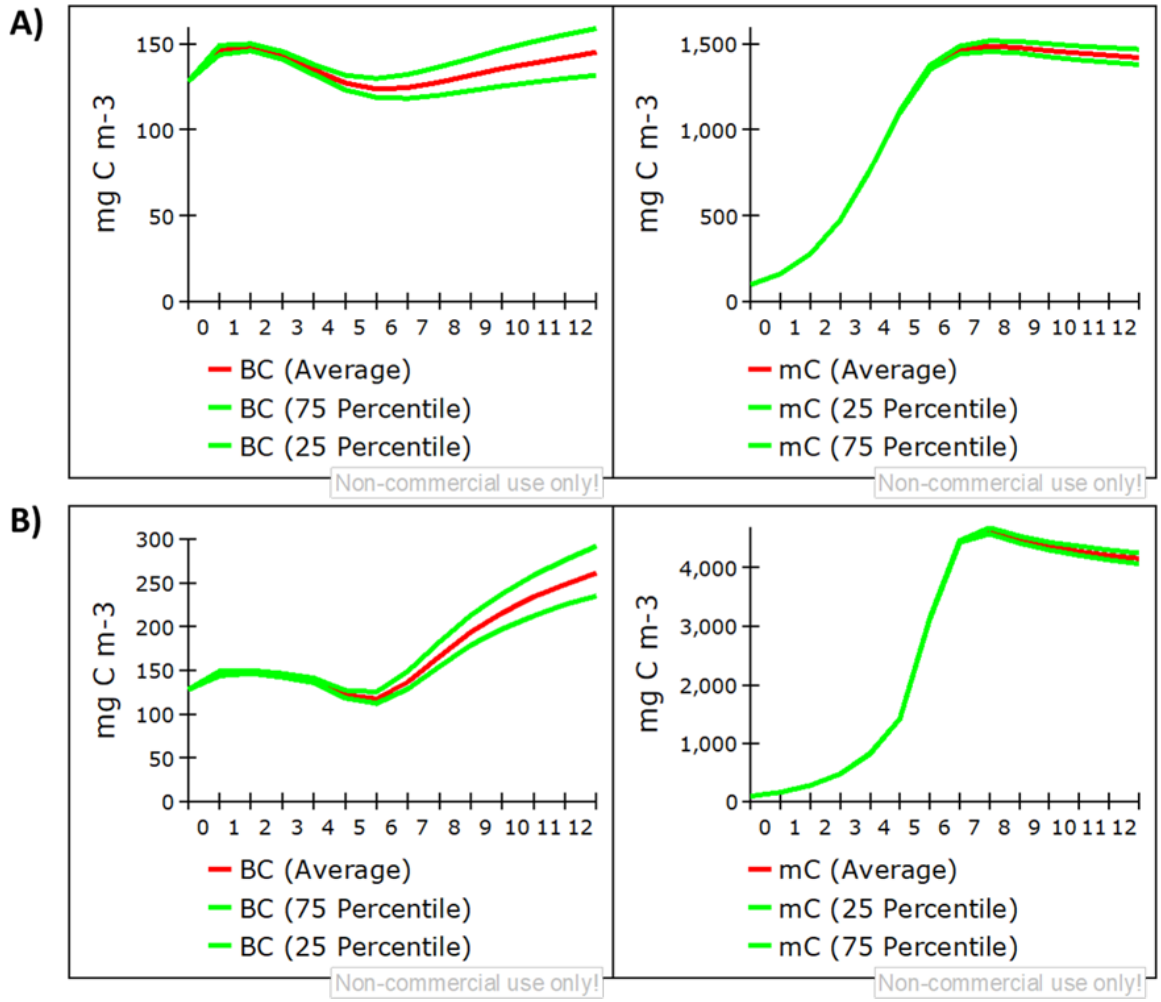

FIGURE 5.5: Results from the dynamic sensitivity analysis of the "Perfect Beast" model configured as *T. amphioxeia* and tuned to experimental data. The analysis was run under two different initial settings of nutrients (Tab. 5.4 & 5.5). BC = bacterial carbon biomass, mC = *T. amphioxeia* biomass.

5.3.3 Model fit to biomass data

The experiment was successful at generating suitable data for model configuration, tuning and validation. The model could be fitted to the biomass and growth curves of the experiment in each the control and N-deplete treatment. The model generates a good fit of maximum biomass with the results of the experiment in the control and nitrogen limiting treatments (Fig. 5.6). At the same time, phosphate and nitrate concentrations reach the

same minimum levels (Fig. 5.7). In the P-deplete conditions, the model underestimates the phosphorous biomass of *T. amphioxeia* in the experiment. In the P-deplete treatment, the biomass development predicted by the model is much faster by 8 days than the actual data recorded in the experiment. Overall, the model has a good fit of carbon, nitrogen, phosphorous and Chl *a* biomass in all treatments and for the increase rate in that biomass in the control and nitrogen limiting treatment. In Fig. 5.9 the beginning of the growth phase of the model and the experimental data were synchronised by removing the data of the first eight days of the experimental data and plotting the all data to begin at day zero. This shows that the model matches the experimental data also in the growth rate and development of biomass.

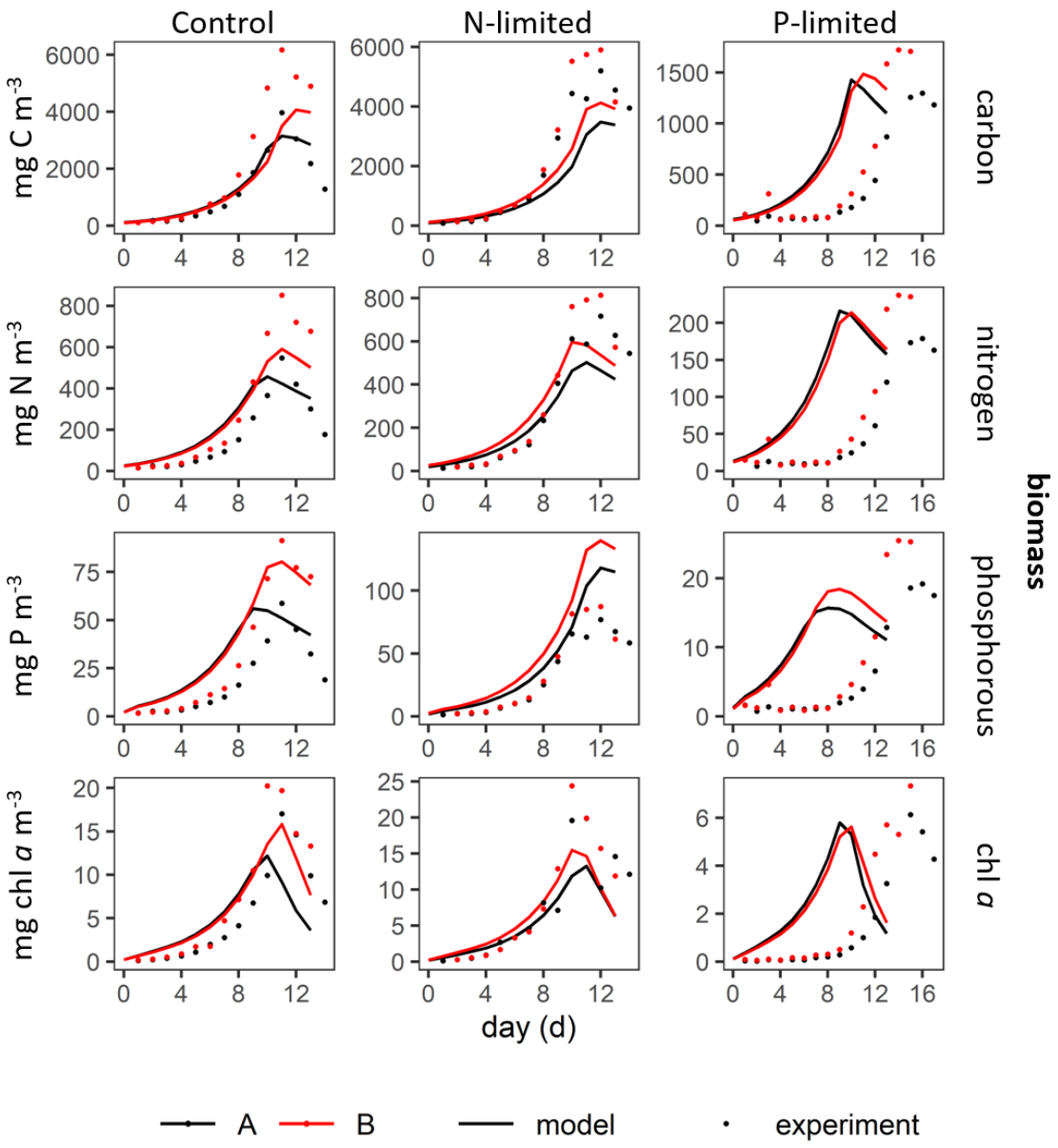

FIGURE 5.6: Fit of the model (lines) to experimental data (dots) to the biomass of *T. amphioxeia* grown in Redfield ratio of nutrients, nitrogen limiting conditions and phosphorous limiting conditions. The initial values were set to the same conditions as measured in the experiment. Note that the time axis for the phosphorous limiting conditions is longer than for the other conditions. The model was run without any bacteria as prey for *T. amphioxeia*. A continuous time series of elemental biomass was calculated with a coefficient from a linear regression of continuous biovolume data over biomass data. Note the outlier in the carbon, nitrogen and phosphorous biomass on day 3 in the P-limited treatment. It appears that the P-limited treatment was much more nutrient limited than the N-limited treatment in comparison to the control due to the much lower maximum biomass yield.

5.3.4 Model fit to external nutrients and internal stoichiometry

The model's prediction of nitrate and phosphate depletion has a good fit with the experimental data in all treatments except for nitrate levels in the phosphorous limiting conditions (Fig. 5.7). Here, the initial value of nitrate estimated by the model is half ($\sim$200 mg m^{-3}) of what was measured in the experiment ($\sim$400 mg m^{-3}). The model also matches the nitrogen to carbon (NC) and the phosphorous to carbon ratio (PC) of the experiment in all treatments. In the phosphorous limiting conditions, the model is again much faster than the real events of the experiment.

5.3.5 Chlorophyll to carbon ratio and photosynthesis

The model overestimated the chlorophyll to carbon ratio of *T. amphioxeia* by 0.001 g Chl *a* g C^{-1} and in timing by 2 days (Fig. 5.8). The fit of chlorophyll to carbon ratio of the modelling data to experimental data is best in nitrogen-limiting conditions. In phosphorous-limiting conditions, the model is too quick in comparison with the experimental data as displayed for the other parameters also. The photosynthetic rate is estimated too high by the model in both the control and the phosphorous-limiting treatment. The model matches the overall pattern of the photosynthetic rate the best in the control.

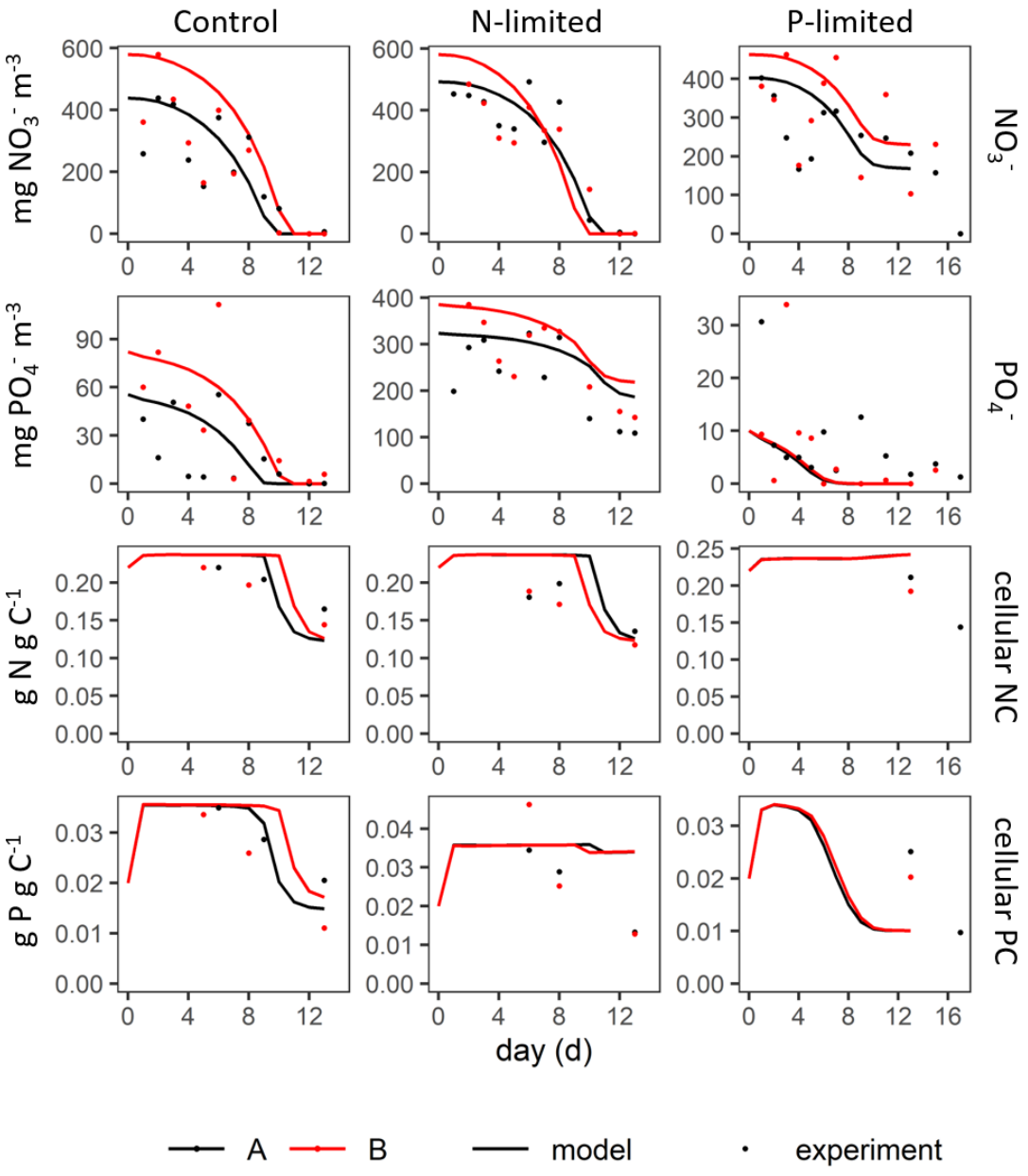

FIGURE 5.7: Fit of the model (lines) to experimental data (dots) of external nutrients and the cellular nitrogen to carbon (NC) and phosphorous to carbon ratio (PC) of *T. amphioxeia* grown in Redfield ratio of nutrients, nitrogen limiting conditions and phosphorus limiting conditions. The initial values were set to the same conditions as measured in the experiment. Note that the time axis for the phosphorous limiting conditions is longer than for the other conditions. The model was run without any bacteria as prey for *T. amphioxeia*. The variance in the inorganic nutrient data suggests that there was some unexplained biological activity in the system.

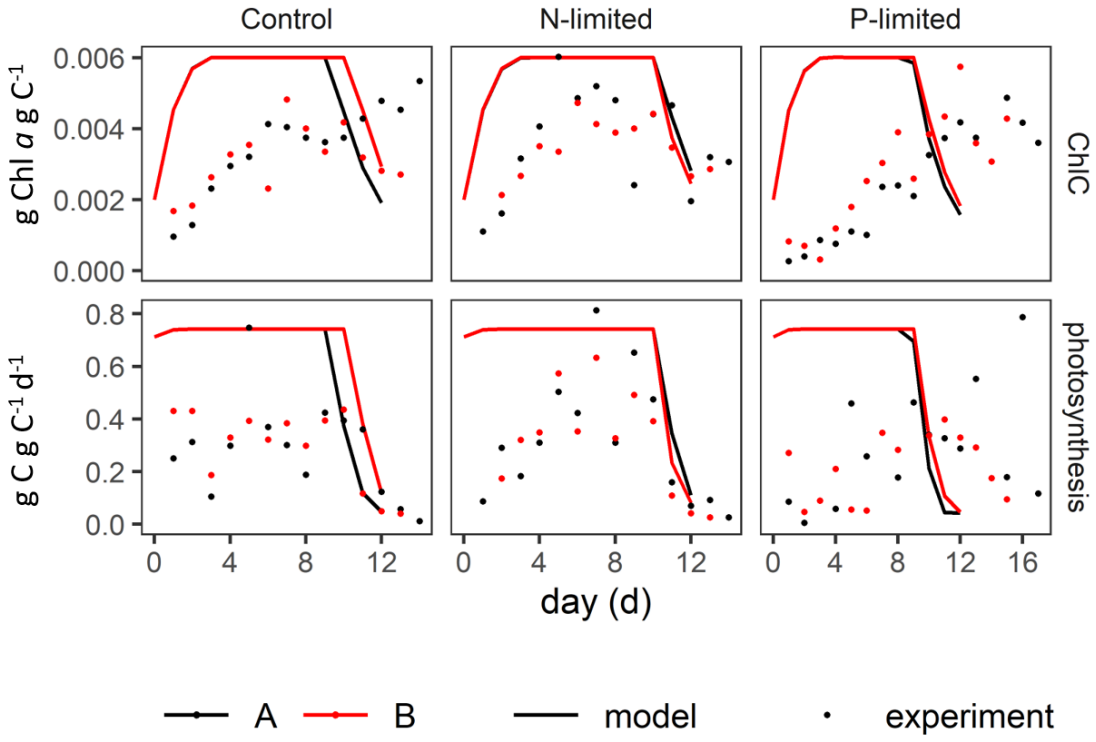

FIGURE 5.8: Fit of the model (lines) to experimental data (dots) of the cellular chlorophyll to carbon (ChlC) and the daily photosynthetic rate of *T. amphioxeia* grown in Redfield ratio of nutrients, nitrogen limiting conditions and phosphorous limiting conditions. The initial values were set to the same conditions as measured in the experiment. Note that the time axis for the phosphorous limiting conditions is longer than for the other conditions. The model was run without any bacteria as prey for *T. amphioxeia*.

5.3.6 Potential contribution of bacterivory to growth in *T. amphioxeia*

There was a decided temporal mismatch in the biomass development between model and experiment in the phosphorous-limiting treatment (Fig. 5.6). As this mismatch may be due to a culture effect where the cells initially grow on the walls of the culture flasks and re-enter the medium later on, the biomass development during the exponential growth phase in the experiment was compared with that predicted by the model on a log scale. Fig. 5.9 a) shows a comparison of the biomass development during the exponential growth phase in the phosphorous-limiting treatment in the experiment with the model. The exponential growth was faster in the experiment than in the model.

The model was run for all treatments and replicates without bacteria. In Fig. 5.9 the results of these runs for the phosphorous-limiting treatment are compared with a simulation that was inoculated with a small number of bacteria that was measured initially in the experiments. In the experiment, bacteria concentrations did not change much over time with only a small increase to the very end of the experiment. In the simulation, bacteria are grazed out early on, but begin to increase again by the time that the biomass of *T. amphioxeia* reaches saturation. Including a small number of bacteria as prey in the model increases the fit of the model's predicted phosphorous biomass of *T. amphioxeia* with the experimental data.

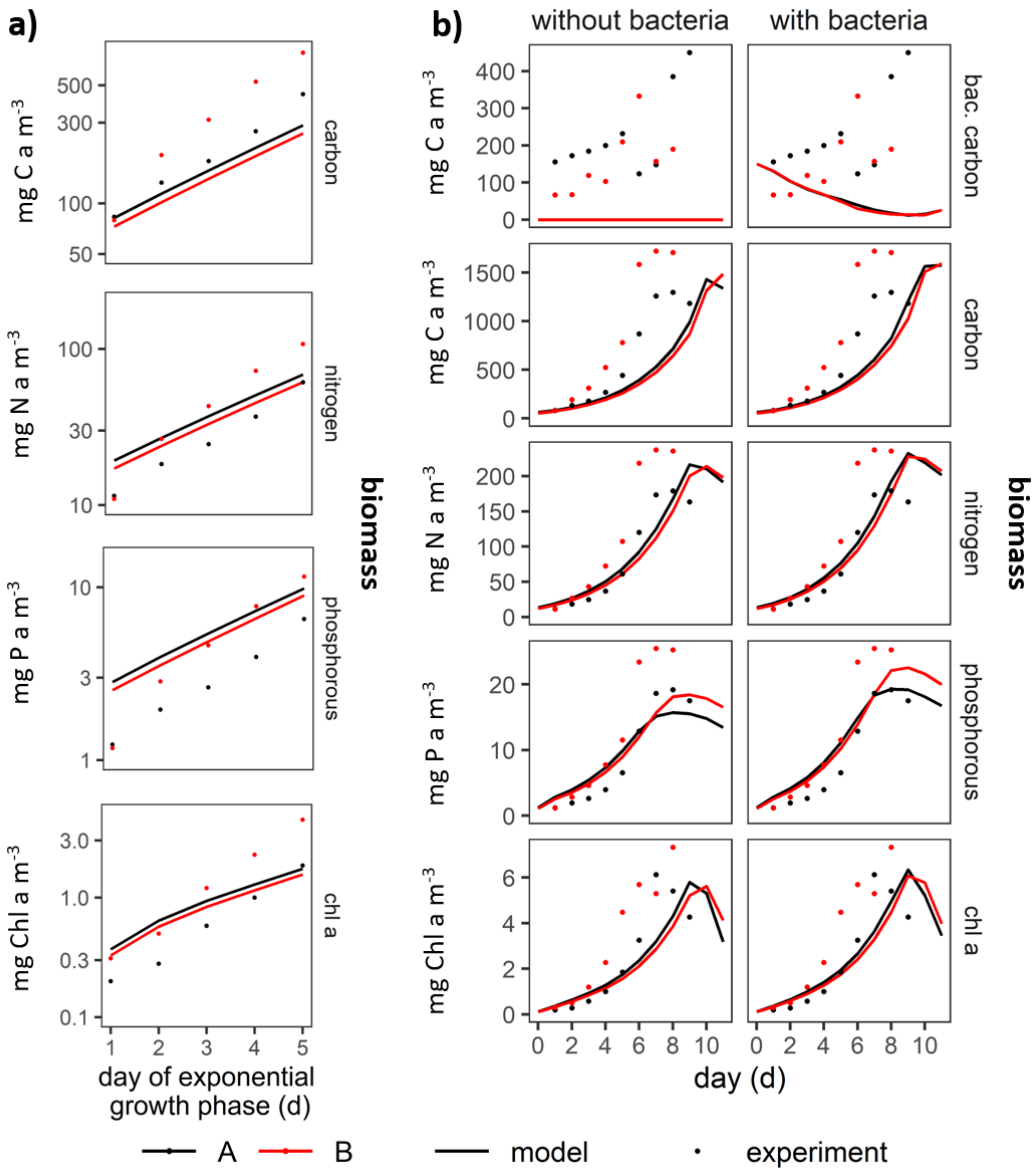

FIGURE 5.9: a) Comparison of the fit of the model (lines) to experimental data (dots) of *T. amphioxeia* biomass during the growth phase of *T. amphioxeia*. The y-axis is a log scale. The data here is the replotted data in the growth phase of the phosphorous limiting treatment shown in Fig. 5.6. b) Comparison of the fit of the model (lines) to experimental data (dots) of *T. amphioxeia* biomass when the model was started with available bacteria as prey and without. The model was rerun with a small amount of bacteria as prey to test if it improves the fit of phosphorous biomass between model and experiment data. There was a decided mismatch in timing between model and experiment data (Fig. 5.6). To visualise the match biomass any experimental data before the begin of the growth phase was deleted. Note that the scales of the y-axes differ.

5.4 Discussion

Under the current configuration, the model predicts reasonably well the growth and decline of *T. amphioxeia* carbon, nitrogen, phosphorous and chlorophyll biomass, as well as the use of nitrate and phosphate of the nitrogen-limiting and control conditions of the experiment (Fig. 5.6– 5.8). There is a decided temporal mismatch of the model and the experimental data in the phosphate limiting treatment, yet both arrive at the same maximum biomass yield (Fig. 5.6). When the biomass finally increases in the experimental data, it does so at an unrealistically fast rate. At the same time nutrient concentrations of the experiment match those of the model and begin to decrease from the beginning of the experiment implying that nutrients are being taken up from the start.

The delay in the development of biomass in the phosphorous-limiting treatments could have been caused by a shock from transfer during inoculation where a large portion of the transferred cells died. Alternatively, the reason could be a culture effect, where the cells of *T. amphioxeia* attach to the wall of the glassware after transfer to the culture bottle. They continue to grow on the wall where they elude sampling and only re-enter the culture medium later on in the experiment explaining the sudden spike in biomass. *T. amphioxeia* may do this to graze on a biofilm of bacteria growing on the walls of the glassware to compensate for limitations in phosphorous. This would also explain why the time mismatch appears only in the phosphorous-limiting treatment. Indeed, the growth rate was higher during the exponential phase in the experiment than in the model (Fig. 5.9). However, the experimental data still show exponential growth, which may suggest a very fast growth rate by *T. amphioxeia* in the medium rather than a sudden re-entering of a developed population into the medium from the glass wall. In any case, the mismatch in timing of the model with the experimental data in the phosphorous-limiting conditions appear to be an artefact of the experiment rather than an issue with the model.

As a small addition of bacteria biomass within the measured range improves the fit of phosphorous biomass of *T. amphioxeia* in the phosphorous-limiting treatment (Fig. 5.9) while carbon, nitrogen and Chl. *a* biomass remain unaffected. Thus, the model suggests that bacterivory may contribute to biomass in phosphorous-limiting conditions, but not in nitrogen-limiting conditions. Grazing on bacteria by *T. amphioxeia*, therefore, may be triggered by phosphorous limitation. In the nitrogen-limiting condition, on the other hand, bacteria only allow the mixoplankton to marginally use more dissolved phosphate with the additional source of nitrogen from bacteria. This indicates that bacteria are more important as a phosphorous source for *T. amphioxeia* than a source of nitrogen.

The discovery of the mixotrophic nature of *T. amphioxeia* is fairly recent (Yoo et al., 2017) and the significance of predation for the cryptophyte's growth is not well understood and neither are the reasons for predation. Triggers for phagotrophy and its proportion to phototrophy in mixoplankton can be scarcity of light or a certain key nutrient like nitrogen or phosphorous when phagotrophy may support phototrophic growth. *T. amphioxeia* possibly resorts to feeding on bacteria in phosphorous limiting conditions as an

additional source for the limiting nutrient. Since adding a small amount of bacteria biomass to the phosphorous-limiting conditions improved the fit of nitrogen and phosphorous biomass, the model supports the idea of supplementary bacterivory in phosphorous limiting conditions. Grazing rates of *T. amphioxeia* and therefore the pressure it exerts over bacteria populations may thus vary significantly in different nutrient regimes.

It is not just the nutrient availability that is relevant to the growth, behaviour and physiology of the organism, but also their proportion of the limiting nutrient to other nutrients. In nutrient limiting conditions, the stoichiometry of plankton matches that of its environment and reaches the optimum for the organism when nutrients are available in abundance (Klausmeier et al., 2004; Bi et al., 2012). Furthermore, organisms are fixed by their stoichiometric limits. When one nutrient is overly abundant in comparison to a limiting nutrient, the limiting nutrient may hinder or even prevent further uptake of the available nutrient (Gülzow et al., 2018). Stoichiometry impacts nutrient uptake rates, grazing and trophic levels in mixoplankton, while mixoplankton, in turn, change the biochemical signature of their environment. The availability of one nutrient alone as for example described in nitrogen-based models incompletely reflects phytoplankton quality for higher trophic levels in marine food webs (Bi et al., 2017). Models that describe variable stoichiometry are therefore needed to describe this aspect of marine food webs.

Relevant factors in predator-prey interaction are not only size ratio, speed and capture success, but also the palatability of the captured prey. Palatability depends on both toxicity and stoichiometry of the prey. Prey of low nutritious value may lead to rejection of the prey altogether, but it can also increase grazing rates by the predator to compensate for the lack of nutrient in the prey (Meunier et al., 2013). Changes in the stoichiometry of such a basal prey species as *T. amphioxeia* may hence impact stoichiometry and grazing rates in much higher trophic levels in the marine food web. The implementation of the here presented model on the variable stoichiometry of *T. amphioxeia* in larger multi-nutrient food web models could help improve the accuracy of these models and gauge the effect size of the mixoplankton cryptophyte on such food webs.

T. amphioxeia is also the source of kleptochloroplasts of the ciliates in the *Mesodinium rubrum/major* species complex (Hansen et al., 2012) and the toxigenic HAB genus *Dinophysis* (Janson, 2004). It is unknown what effect the stoichiometry of *T. amphioxeia* has on its predator *Mesodinium* and how this is passed on to the *Dinophysis* which preys on *Mesodinium*. The importance of prey abundance for *Dinophysis* has been observed in the field (Moita et al., 2016; Smith et al., 2018) and diarrheic shellfish poisoning events caused by *Dinophysis* have been related to high levels of dissolved organic and inorganic nutrients (Hattenrath-Lehmann and Gobler, 2015; Hattenrath-Lehmann et al., 2015). The retention time of kleptochloroplast of cryptophytic origin varies with light and nutrient composition. There is a lack of an adequate description of the impact of food quality on mixoplantonic activity (e.g., Lundgren et al., 2016; Lin et al., 2018) in full variable stoichiometric (C:N:P:Chl) models. The variable stoichiometric model of *T. amphioxeia* described here can be an adequate first element of such a variable

stoichiometric *Teleaulax-Mesodinium-Dinophysis* model.

The proposed model adequately predicts growth curves of *T. amphioxeia* in nitrogen and phosphorous limiting conditions, if bacterivory in *T. amphioxeia* is considered to be triggered by phosphorous limitation. Theoretically, *T. amphioxeia* may divide once when it feeds on heterotrophic bacteria for 31 days even when its growth efficiency is assumed to be 50%. Thus, heterotrophic bacteria may not be a critical growth factor, but a supplementary factor (Yoo et al., 2017).

This configuration of the model is thus an accurate simulation of the growth behaviour of *T. amphioxeia* under various nutrient conditions. It is the first variable stoichiometric model of the constitutive mixotroph *T. amphioxeia* and can be used for further application and exploration of the organism in different ecological conditions.

The next step will be the development of a complete variable stoichiometric *Teleaulax-Mesodinium-Dinophysis* model that will allow for the exploration of the complex interactions under changing nutrient conditions. A stoichiometric model of the TMD complex will allow us to explore stoichiometric dynamics in and between the organisms such as the effect of nutrient limitation on photosynthesis and grazing rates and the effect of prey with higher and lower nutritious value. These are mechanisms that cannot be explored with the nitrogen-based model and new results are therefore expected to come from such a new model. In addition, a variable stoichiometric model can be implemented in larger ecosystem plankton models that account for variable stoichiometry such as the ERSEM model (Butenschön et al., 2016).

5.5 Conclusion

The variable stoichiometric model ("Perfect Beast") could successfully be tuned with the experimental data on *T. amphioxeia* generated in the experiment here. The physiological constants of the mixoplankton model were adjusted in the tuning process so that the model now represents the CM *T. amphioxeia* specifically and reproduces its growth dynamics under different nutrient conditions. The model can find application in further specific studies or be embedded in more complex food web models. Questions regarding external and internal stoichiometry concerning *T. amphioxeia* and their effects on feeding on bacteria by the CM could not be conclusively resolved. This was due to limitations in the experimental data and the unresolved issue of the temporal mismatch between model and experiment data in the phosphorous-limiting treatment. It is uncertain whether the reason was a culture effect where *T. amphioxeia* initially grew on the culture flask wall and re-entered the medium later on or whether *T. amphioxeia* suffered a shock after inoculation where many cells died and only recovered from it much later during the experiment. The results of this joint modelling and experiment study suggests that feeding on bacteria by *T. amphioxeia* may be triggered by limitations in phosphorous. However, this question can only be answered by further experimental studies.

Funding This research was supported by EC MSCA-ITN 2019 funding to the project MixITiN (grant number 766327).

Acknowledgements Aditee Mitra developed the food-web model from an updated "Perfect Beast" model (Flynn and Mitra, 2009; Mitra et al., 2014) and co-supervised this component. Nikola Medić analysed the bacteria samples. Dedmer Van der Waal did the analysis of the cellular carbon, nitrogen and phosphorous content samples. Ayoe Lüchau analysed the samples of inorganic nutrients (DIN and DIP). Kevin J. Flynn and Per Juel Hansen supervised Anna-Adriana Anschütz in the design and execution of the experiment and the subsequent analysis. The experiments were conducted in the laboratory of Per Juel Hansen (UCPH). Nathalie Gypens, Aditee Mitra and Kevin J Flynn provided comments and advice on draft versions of this chapter.

Chapter 6

Global discussion

6.1 Introduction

The aim of this thesis was to explore different mixoplankton functional types with regard to their ecological niches and response to different environmental factors such as nutrient load. The implications of such niche separations were further studied on a species level with the example of the TMD-complex. The complex also allowed the study of the implications of different mixoplankton types as in the case of *Teleaulax*, *Mesodinium* and *Dinophysis*. The aim was achieved by combining eco-physiological models and experimental data. Specifically, the generic nitrogen-based mixoplankton model in chapter 3 was built to compare different mixoplankton types and the results strongly suggest a niche separation of the different types. On a species level, a nitrogen-based TMD-model was used to explore the effect of prey availability and nutrient load on the succession of different mixoplankton functional types. For the CM *T. amphioxeia* it was possible to tune the variable stoichiometric model "Perfect Beast" (Flynn and Mitra, 2009) to data from an experiment on the cryptophyte in different nutrient conditions, which was carried out in the scope of this thesis.

First, a summary of thesis results is provided for each chapter with a brief overview of how these findings advance the field (sections 6.2-6.4). Second, these findings are brought together to contextualise them with current ecological models. Then the limitations of this study and the general study of mixoplankton will be addressed followed by a discussion of the challenges that the scientific community will face to advance our understanding of mixoplankton ecology (section 6.6). Finally, I will address the implications for environmental management and highlight key questions (section 6.7).

6.2 Niche separation of mixoplankton functional types (chapter 3)

Hypothesis 1: Distinguishing between different mixoplankton types in nitrogen-based plankton models makes a difference to the outcome of the biomass predictions.

The results of the model in chapter 3 show that mixoplankton behave distinctly different regarding nutrient uptake, biomass production and growth phases than strict phototrophs and autotrophs in a nitrogen-based model. Furthermore, there is a niche separation between the mixoplankton type GNCM, SNCM and CM confirming the first hypothesis listed in 1.8. This niche separation persists across different conditions of water depth, nutrient load and irradiance and has also been shown in experiments (Wilken et al., 2020). Internal nutrient recycling from prey affects nutrient acquisition from external nutrient sources in addition to differences in the ability to use different forms of nitrogen (NO_3^- vs. NH_4^+). The internal synergism of heterotrophy and phototrophy is here an important factor in the different performance of the distinct mixoplankton types and is often omitted from existing mixoplankton models (e.g. Ward and Follows, 2016).

What is new in this nitrogen-based model is the distinction between different mixoplankton types and the treatment of mixotrophy as a synergism while it also includes an encounter sub-model of prey and predator that considers allometry. A few models consider mixotrophy as a synergism and also feature different mixoplankton functional types (Flynn and Mitra, 2009; Ghyoot et al., 2017a; Livanou et al., 2020), for example, the "Perfect Beast" model. However, they are variable stoichiometric models and therefore not compatible with larger nitrogen-based ecosystem models. The design of future general plankton models should include an evaluation of the relevance of different mixoplankton types to the system. Species-specific models should consider the functional type of the species to increase the accuracy of the model output. The simulation of complex mixoplankton interaction such as displayed in the TMD complex need to respect the different mixoplankton functional types and cannot assume a generic mixoplankton type.

With an increasing amount of physiological data arising on different mixoplankton species (Lundgren et al., 2016; Lin et al., 2018; Maselli et al., 2020; Traboni et al., 2020), the model can also be configured as different mixoplankton species of different functional types and can be used for comparative studies. However, it is important to consider the organism's specific response to hydrodynamic events like stratification, as this is not featured in this model. As 40 - 60 % of microzooplankton may indeed be NCM (Leles et al., 2017), considering mixoplankton in plankton models may be crucial for accurate representation of trophic links, energy transfer and primary production.

The generic nitrogen-based mixoplankton model here could be implemented in a larger nitrogen-based plankton ecosystem of "intermediate complexity" such as MEDUSA (Yool et al., 2011; Yool et al., 2013). This model was designed to study how the anthropogenic change to the global ocean may impact the biological pump and overall biochemical

response. Such models are important to estimate the pressure that anthropogenic climate change has on the marine habitat and predicting future climate change under the consideration of plankton activity. MEDUSA does not currently include mixoplankton and predominantly features strict photoautotrophic diatoms as phytoplankton. Including a mixoplankton model as described here could improve and rectify the calculated rates of carbon export by the biological carbon pump. Important questions to explore with such a combined model are, for example, how much new production from inorganic nutrients there is versus the production from recycled nutrients (f-ratio). Especially, when GNCM are considered that are capable of phototrophy but often cannot use nitrate and therefore do not contribute to the new production at all. Heterotrophy and photosynthesis are split into two antagonist groups (phytoplankton vs zooplankton) regarding their impact on the biological carbon pump. How may the estimates of photosynthesis to heterotrophy ratios change in such a model when including mixoplankton that are capable of both trophic modes in one cell? What will the effect size be of considering different mixoplankton types?

Furthermore, the role of mixoplankton and the different types on nutrient cycling and the competition for nutrients can be explored. Important questions from an anthropocentric perspective regarding ecosystem services are the role that mixoplankton play in energy transfer to higher trophic levels and how that may impact fish stocks, for instance. The model in chapter 3 suggests that mixoplankton have fewer boom and bust cycles and longer more stable bloom phases. How mixoplankton may thus influence ecosystem and food stability and what this quality means regarding mixoplankton HAB species are further questions that can be explored in more complex models.

Fig. 6.1 gives suggestions on how to integrate mixoplankton into large ecosystem models and eventually coastal management. New information on the physiology of mixoplankton can be used to build small flexible mixoplankton models. These models can be integrated into more complex ecosystem models exploring environmental pressures with a new paradigm. The knowledge derived from these models can eventually be incorporated into coastal management and monitoring.

Finally, the generic nitrogen-based mixoplankton model can easily be developed further into an individual based model (IBM). A mixoplankton IBM could be used to explore crucial questions regarding the population dynamics of NCM. Mixoplankton types that acquire their phototrophic abilities rely on obtaining and maintaining a minimum number of functional plastids per individual. When the right prey runs out, NCM of the same species could thus become intra-guild competitors for prey. What this means on a population level is not completely understood, yet. For example, the SNCM *Mesodinium* and *Dinophysis* will only divide a few times upon sudden starvation of specific prey (Hansen et al., 2013). Therefore, what does starvation pressure on the individual cell mean for the growth dynamics of the whole population?

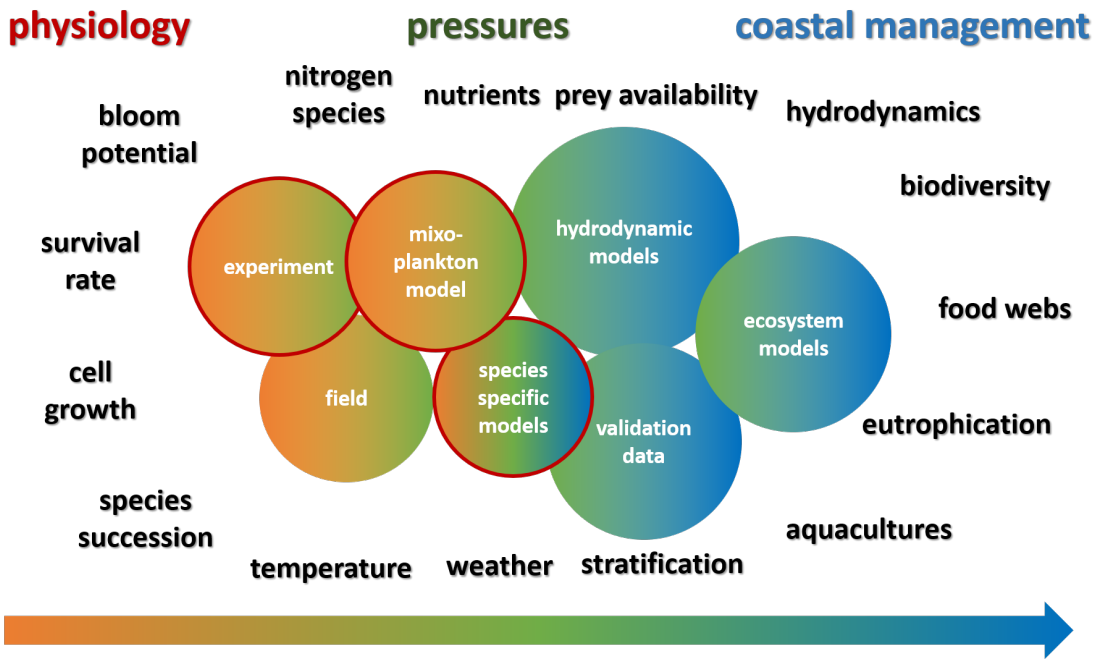

FIGURE 6.1: Bottom-up benefits of trophodynamic mixoplankton models for the improvement of coastal management. Revelations about the cell physiology of harmful mixoplankton species relevant to the ecosystem and human health as well as socioeconomics can give cues on what needs to be monitored more closely and which aspects should be included in predictive models. The here developed mixoplankton models can also be integrated into larger ecosystem models that study for example the effect of global warming on the biological carbon pump. For specifics on the models of this study can be integrated in larger models see sections 6.2 - 6.4. The circles framed in red indicate the components of this process that this work has provided material for. The newly derived knowledge can be used to improve the implementation of existing regulative directives on national and regional levels.

6.3 Implications of nutrient and prey availability for the mixoplankton types in the TMD complex (chapter 4)

Hypothesis 2: Prey and nutrient availability influence the bloom dynamics and the HAB potential of *Dinophysis*. Specialised mixotrophic relationships significantly influence the bloom dynamics of multi-organism mixoplankton complexes like the TMD complex.

The nitrogen-based TMD model presented here was a development of the generic N-based mixoplankton model from chapter 3. The model focuses on the effect of the unique biology and interactions between the different mixoplankton types of the complex. The results strongly suggest that the amount and timing of prey availability directly affect the bloom potential of *Mesodinium* and *Dinophysis*. In addition, eutrophication directly promotes the growth of *Mesodinium* and thus indirectly also the growth of *Dinophysis*. Therefore, the results support the second hypothesis stated in 1.8. The model does not include hydrodynamic processes like upwelling and stratification nor currents which are

key factors in the bloom formation of *Mesodinium* and *Dinophysis*, respectively (Velo-Suárez et al., 2014; Moita et al., 2016). It does therefore not simulate real-life conditions, but gives a clear indication that future models that aim at simulating the bloom dynamics of the TMD complex should include the biology and specifically the mixoplankton nature of these organisms. The stepwise inclusion of physiological data on mixoplankton complexes from experiments and field samples into smaller models and eventually large ecosystem models has the potential to greatly improve the reliability and accuracy of such models and improve coastal management (Fig. 6.1).

Thus, a next step in modelling the bloom dynamics of the TMD-complex should be the integration of the here proposed nitrogen-based model from chapter 4 into a suitable hydrodynamic model that describes stratification and current input and allows for the implementation of dial vertical migration (DVM) by *Mesodinium*. *Mesodinium* and *Dinophysis* have very different strategies. While *Mesodinium* is a fast swimmer that exhibits DVM of up to 30 m a day (Sjöqvist and Lindholm, 2011; Olli, 1999), *Dinophysis* is more of a stealth predator (Jiang et al., 2018) that takes advantage of thin stable water layers caused by stratification and waits for its prey (Sjöqvist and Lindholm, 2011). These differences cannot be captured in a model that assumes homogeneous distribution of all organisms throughout the simulated water mass. The fact that *Mesodinium* may only pass through a thin layer with a very dense population of *Dinophysis* twice a day probably results in very different encounter and thus feeding rates by *Dinophysis* than estimated by a model that assumes a completely mixed water layer.

Existing hydrodynamic models on *Dinophysis* blooms seem more reliable in their predictions, when DSP events mainly happen by populations of *Dinophysis* that developed elsewhere and were then transported to the site of the prediction. Reliably simulating the development of a *Dinophysis* bloom *in situ* at the vulnerable coast, bay or fjord remains a challenge. In these cases, a combination of a biological model with a hydrodynamic model could prove very useful. Such modelling study on joining two models should ideally be conducted with a focus on a target region of a sheltered marine water body like a fjord that is also notorious for DSP events for a number of reasons. An ideal region for such a model study would be the Puyuhuapi Fjord, for example (Díaz et al., 2021). The fjord is sheltered from major ocean currents decreasing variability in the hydrodynamic model. It also has a long history of DSP events causing damage to local aquacultures. Therefore, *Dinophysis acuta* has been intensively monitored along with various other environmental parameters providing a time series and rich data set ideal for tuning and validation of the targeted model. The data set comprises cell numbers of *D. acuta*, concentrations of Chl *a* and nutrients like nitrate (also phosphate and silicate) that are crucial for tuning and validating the biological model. In addition, there are data on temperature and salinity depth profiles as well as fresh water input via riverine inflow and rainfall that can used for the hydrodynamic model.

However, there is no time series on *Teleaulax* and *Mesodinium* in this data set, which is a problem that applies to many regions prone to DSP events. A data set that comprises

the prey species would be useful to study the impact of warming on the bloom dynamics of the complex. Chapter 4 suggest that the temporal match is important for the bloom potential of *Mesodinium* and *Dinophysis*. Results from this chapter also show that as temperature lowers or raises the maximum growth rates of the organisms, the timing of the blooms changes. In this model the same effect size and direction were applied to each organisms maximum growth rate. What are the implications of changes in timing due to temperature for the interaction and bloom dynamics in this tiered mixoplankton complex in the light of ocean warming? Do *Teleaulax*, *Mesodinium* and *Dinophysis* differ in their response to temperature and if yes, how? Then, how could warming of the oceans affect the temporal match of the different components of the complex? Lastly, what could that mean for the HAB potential by *Dinophysis*?

The TMD complex is likely not the only complex species-specific dependency between different mixoplankton types, but it is the best studied. The resulting bulk of available data on all three organisms thus provide a good ground to use these organisms as model systems. They can be used to improve our understanding of such a new found complex mixoplankton interaction where plastids change their owner several times. It is unlikely that this interaction is unique to the TMD complex. In the future, the model can thus also be parametrised with physiological data from other species that have formed a similar complex.

The model here specifically describes the species *T. amphioxeia*, *M. rubrum* and *D. acuminata* where the prey dependency regarding kleptoplasty is well-studied (Gustafson et al., 2000; Park et al., 2006; Kim et al., 2012a; Reguera et al., 2012). It may be possible that even though the species of *Dinophysis* are globally distributed that there are regional differences with respect to which prey species they are specific. In Japanese waters, *D. acuminata* and *D. norvegica* contained plastids more similar to *T. acuta* and *Geminigera cryophila* (Nishitani et al., 2010). *Geminigera cryophila* is rather associated with colder climates and may be the preferred species as a source for plastids in boreal regions (Minnhagen and Janson, 2006). In Korea, sequences of the raphidophyte *Heterosigma akashiwo* and the prasinophyte *Pyramimonas* sp. were found (Kim et al., 2012a). Kleptoplastids coming from the *Rhodomonas*/*Storeatula* clade were found in *Dinophysis* of the coast of Chile (Díaz et al., 2020). The authors argue that the mediating ciliate might be tintinnids (Díaz et al., 2020). These findings may indicate *Dinophysis* can resort to an alternative prey genus than the cryptophyte-*Mesodinium* chain (Rial et al., 2015).

6.4 The first variable stoichiometric model of the CM *T. amphioxeia* tuned to experimental data (chapter 5)

Hypothesis 3: *T. amphioxeia* feeds on bacteria in conditions of low inorganic phosphorous to compensate for the missing nutrient.

The hypothesis that *T. amphioxeia* feeds on bacteria to compensate for limitations in dissolved phosphorous (chapter 1.8) could not be conclusively tested here.

In chapter 5 it was speculated that the reasons for the temporal mismatch between model and experiment in the P-limiting treatment may be due to either a culture effect or a shock to the population upon inoculation. That apart from the temporal mismatch the model was still capable of reproducing both growth rate and biomass yield of *T. amphioxeia* in this treatment suggests that they may be a third explanation. As a CM *T. amphioxeia* has a lower time pressure for nutrient uptake in nutrient limiting conditions as in the case of bacteria, the cryptophyte has the ability to acquire the nutrients from its competitor later on. Another explanation for the temporal mismatch in the P-limiting treatment could be internal physiological processes that delayed both nutrient uptake and especially the growth phase. *T. amphioxeia* changes from a diploid genome to a haploid genome (*P.* prolonga) in conditions with low inorganic nutrients (Altenburger et al., 2020b). If *T. amphioxeia* indeed changed from a diploid to a haploid stage as a response to the nutrient limiting environment possible to decrease the nutrient demand, it could explain why the cells started dividing much later than predicted by the model while still displaying the predicted growth rate and maximum biomass.

To what degree feeding on bacteria by *T. amphioxeia* is triggered by limitation in certain nutrients is therefore still unclear. In order to address this question, the here described experiment could be repeated with the inclusion of a feeding experiment with an axenic culture of *T. amphioxeia* as a control. If in fact feeding is triggered by compensation for a limiting nutrient, the trophic level of certain mixoplankton types may change depending on the nutrient availability of their environment. In that case, models that describe trophic levels and the transfer of nutrients and energy between them need to consider mixoplankton as for example done by Leles et al. (2018) and Leles et al. (2021). Furthermore, the food web structure and associated trophic levels may change, if the proportion of mixoplankton increases in an ecosystem compared to strict autotrophs. In an estuary in Portugal for example, the ratio of cryptophytes to diatoms shifted towards cryptophytes (Brito et al., 2015). Here, both nutrient cycling and trophic levels could have changed due to this shift. In addition, the risk for harmful blooms caused by *Dinophysis* could have increased, if the shift involved an increase in their plastid source *Teleaulax*. Such potential implications need to be tested with more data and possibly a variable stoichiometric TMD model that can account for the response of *Teleaulax* to limitations in different types of nutrients.

As useful as a nitrogen-based model is as a first approximation, these models have a decided caveat as they are only applicable to environments, where nitrogen is the limiting nutrient. Where another nutrient is limiting such as phosphorous, a nitrogen-based model can potentially overestimate biomass yields and growth phases. Furthermore, nitrogen-based models assume a fixed stoichiometry as they only assign one nutrient. In reality, variable stoichiometry affects feeding rates, nutrient uptake, growth rates and trophic levels (Katechakis et al., 2005; Riisgaard and Hansen, 2009; Hansen, 2011). In the

case of mixoplankton, a nitrogen-based model may further misrepresent the behaviour of certain functional types. In chapter 5, a variable stoichiometric model of *T. amphoxeia* was successfully tuned to experimental data derived from a growth experiment with the cryptophyte in different conditions of external nutrient concentrations. The model can thus be applied in further studies on the cryptophyte or as an element in food web models (Fig. 6.1). It can further find application in a variable stoichiometric model of the TMD complex, where stoichiometric data are scarce, especially of the cryptophytes that are the plastid source.

In the context of stoichiometry another question is whether the quality of the prey and specifically their plastids changes with the nutrient conditions and if that is of importance to the bloom potential of *Mesodinium* and *Dinophysis*. Further experiments on the effect of stoichiometry on the growth dynamics of the TMD-complex in combination with a variable stoichiometric model could advance our understanding of this. A first experiment could be an expansion of the aforementioned feeding experiment with *T. amphioxeia* by adding a feeding experiment with *M. rubrum*. The ciliate could be fed with *T. amphioxeia* of the different treatments (non-limiting, N-limiting, P-limiting, with and without bacterial grazing) to test whether growth conditions of the *T. amphioxeia* affect the feeding rates of *M. rubrum*. Such experimental data would make a variable stoichiometric TMD-model more robust. The model could further be implemented as described for the nitrogen-based TMD-model described in and tuned with the proposed data set from the Chilean fjord as it contains data on phosphate concentrations (Díaz et al., 2021).

6.5 Perceptions of the modelling process

All models come with the caveat that they are an approximation of the real world and are too simple or wrong for the purpose they were designed for. In order to build sensible models that have relevance for real-life scenarios, it is important to have as good an understanding as possible of the process and to keep a close exchange with experts on the topic. It is crucial to keep up with the current literature on the topic, but also the development of knowledge. A way to keep models close to reality is to configure the models with existing data. A good way to bring a model closer to reality is to tune it to a suitable continuous set of data and it is best to validate the model with a different set of such data. However, suitable data for tuning are hard to find and it is thus even harder to find data for validation. Bearing all caveats in mind, a good model can be a great tool for many purposes. For example, the nitrogen-based model here enables the theoretical exploration of different mixoplankton types where physiological data for big comparative studies are still limited (chapter 3). If the model is tuned and reliable, it can produce continuous data of parameters that are otherwise difficult or costly to sample. In conjunction with experimental or time series data, the model can help in explaining experimental results and make them more conclusive (Moita et al., 2016; Ajani et al., 2016). Models can help us to understand very complex processes that are hard to grasp

and lead us to the hypothesis that may be counter-intuitive but lead in the right direction. For example, the TMD-model predicted the highest peak biomass of *Mesodinium* at their lowest relative inoculum concentration (chapter 4).

By rebuilding a concept from scratch the modeller takes a different perspective. Questions need answers that normally do not arise during experiments. The system balance for carbon, nitrogen and phosphorous are rarely tested in experiments. The main reason for this is feasibility as in most growth experiments cell numbers are counted and biomass is not measured, due to the cost and difficulty of the sampling procedure. Indeed, the acquisition of biomass data also posed a challenge for generating tuning data for the variable stoichiometric *T. amphioxeia* model in this study (chapter 5).

In summary, models can improve understanding, produce useful data from minimal sampling data that can lead to forecasting (data of today make data of tomorrow) and lastly models can inspire new experiments if they leave us with questions that neither model nor experiments could answer. Regarding mixoplankton, modelling has great potential as a tool, but also comes with caveats. As the omnipresence of mixoplankton becomes increasingly apparent, models can be used to test new concepts. The term mixoplankton applies to a diversity of forms of plankton whose implications for the current understanding of marine food webs and nutrient cycling has yet to be discovered. Models that were built under the dichotomic plankton model may still be adequate for their purpose, but their validity needs to be verified by testing the effect size of mixoplankton to such systems. However, data for testing mixoplankton models on a large scale (food webs) and small scale (species level) are still scarce in comparison to data on autotrophs and heterotrophs (Flynn et al., 2019).

6.6 Limitations of study

The generic nitrogen-based model does not yet feature the mixoplankton functional type eSNCM (chapter 3). A comparison of the functional types GNCM, pSNCM and CM with eSNCM are thus currently not possible with this nitrogen-based model. The study of a niche separation of eSNCM against other mixoplankton functional types remains thus unexplored. As eSNCM differ in their global spatial distribution from other mixoplankton functional types (Leles et al., 2017), there is some indication for a niche separation. Even though the model distinguishes between three mixoplankton functional types in addition to the "standard" strict phototrophs and heterotrophs it is still a generalisation. There is distinct variation in each mixoplankton functional type as for example in the case of the pSNCM *Mesodinium* and *Dinophysis*. But also CMs can vary greatly in their proportion of phototrophy and phagotrophy in addition to size (Leles et al., 2019). Despite covering three different mixoplankton functional types, the model still does not cover the full complexity of the diversity of mixoplankton functional types.

While the model developed in chapter 4 is the first biological model of the full TMD complex, there are certain shortcomings of it, as it does neither describe hydrodynamics

nor DVM by *Mesodinium*. The next step should be the integration of the here described biological model into a hydrodynamic model and to include DVM to build a comprehensive model that represents the hydrodynamic and biological factors that drive the bloom dynamics of the TMD complex. Including DVM of *Mesodinium* will also likely affect capture rates by *Dinophysis*, if the availability of *Mesodinium* is reduced to short periods twice a day. As for the nitrogen-based model described in chapter 3 of which this model is a development, the same caveats regarding the absence of other nutrients apply. A variable stoichiometric model of the *Teleaulax-Mesodinium-Dinophysis* interactions will allow to explore stoichiometric dynamics in and between the organisms such as the effect of nutrient limitation on photosynthesis and grazing rates and the effect of prey with higher and lower nutritious values. These are mechanisms that cannot be explored with the nitrogen based model, unless we are sure that N is the only limiting nutrient, and new results are therefore expected to come from such a new model. In addition, a variable stoichiometric model can be implemented in larger ecosystem plankton models that account for variable stoichiometry such as the ERSEM model (Butenschön et al. 2016).

A key question for aquacultures and public health is still the toxicity of different species of *Dinophysis* in different regions. *Dinophysis* produces the lipophilic toxins okadaic acid (OA), dinophysistoxins (DTX) and pectenotoxins (PTX), which can be detected even in cell concentrations lower than 10^3 cells L^{-1} (Yasumoto et al., 1985; Reguera et al., 2012; Reguera et al., 2014). Ocadaic acid and dinophysistoxins are acid polyether lactones that inhibit the protein phosphatase. The physiological factors and environmental triggers for toxin production are still under debate (Nielsen et al., 2012; Hansen et al., 2013; García-Portela et al., 2018; John and Flynn, 2002; Hernández-Urcera et al., 2018; Kamiyama et al., 2010; García-Portela et al., 2018).

The reasons *T. amphioxeia* feeding on bacteria could not be definitely found out with this chapter, due to limitations of the experimental data set (chapter 5). It could not be determined what the reasons were for the temporal mismatch between modelling and experimental data. Effects of stoichiometry of *T. amphioxeia* on its physiology and biomass development under different nutrient conditions need to be researched in further studies with a focus on experimental work. Apart from *Synechococcus* being a confirmed prey of *T. amphioxeia* (Yoo et al., 2017) it is unknown how selective the cryptophyte is in feeding on bacteria. Future experiments could follow the same set-up as described in chapter 5, but with larger culture volumes to allow for more sampling points for the analysis of carbon, nitrogen and phosphorous biomass. This method requires large sampling volumes due to a high detection limit relative to the carbon content of a single cell. More data points also increases the robustness of the data for potential statistical analysis. Ideally, a feeding experiment would be carried out in conjunction with an axenic culture of *T. amphioxeia* that excludes any phagotrophic activity and allows monitoring of the cryptophyte as a pure autotroph. Photosynthesis, respiration and feeding need to be measured to quantify the relative contribution of phototrophy and phagotrophy to

carbon growth. In this case, feeding on bacteria by *T. amphioxeia* and its associated physiological processes could be quantified in comparison with the purely phototrophic growth in the bacteria free (axenic) treatment. Such an experimental set-up is challenging, because it is difficult to keep large culture volumes bacteria free. However, the results could be promising. Bacteria communities in long existing stock cultures such as the *T. amphioxeia* culture used here will likely have changed and may be different from the bacteria community the cryptophyte will be exposed to in the wild. How this could have affected the experiment described in chapter 5 is difficult to assess. The type of bacteria used as prey may therefore need to be evaluated for a feeding experiment. The inevitable selection to lab conditions and therefore comparability of these cultures with field organisms is a general caveat associated with culture experiments.

6.6.1 Future study of mixoplankton

Going forward the study of mixoplankton faces challenges from various sources. There is a lack of time series of mixoplankton in plankton samples as many established sampling methods like net samples miss mixoplankton. In addition, these organisms have long not been recorded as such. Net samples have a bias towards larger more robust plankton types such as the purely autotrophic diatoms and crustaceans like copepods in comparison to mixoplankton that are often fragile ciliates and flagellates (Flynn et al., 2019; Biard et al., 2016). This causes a relative over-representation of pure autotrophs in the samples. In addition, there is a sampling bias toward large size classes of plankton (Leles et al., 2019). The sampling bias becomes apparent when bulk plankton sampling is compared with more targeted sampling (Leles et al., 2019). Another sampling bias may be in the sampled water layer. Many plankton samples are taken standardly in the deep chlorophyll maximum (DCM). This however, may routinely miss mixoplankton like *Dinophysis* which are often found outside of the DCM (Reguera et al., 2012) and are thus captured by this method.

The parameter chlorophyll is also problematic in the context of satellite imagery. The method is a powerful tool for gathering data on phototrophic activity on a global scale. However, satellite chlorophyll imagery only captures near surface phototrophically active organisms, but not organisms deeper in the surface ocean. This again applies to organisms such as *Dinophysis* that are often found in deeper water layers. Furthermore, chlorophyll is often linked to primary producers. In the case of mixoplankton, the presence of chlorophyll gives no information on whether the organism is predominantly phototrophically or heterotrophically active nor whether the primary production is new production from inorganic nutrients. Mixoplankton research would benefit greatly, if we could use satellite data to distinguish mixoplankton from strict phototrophs, but it is still unclear how this can be done.

Field samples mainly give information of what is there and when. What the organisms are doing often needs be studied with experiments of these organisms in culture. The very

nature of mixoplankton however, makes it often very difficult to keep these organisms in culture. Mixoplankton with high prey specificity can not be cultured until their special prey is known as for example in the case of the SNCM *Mesodinium* (Gustafson et al., 2000) and *Dinophysis* (Park et al., 2006). Keeping these organisms in culture therefore requires that their special prey is also kept in culture, which can easily get very complicated when their special prey also has specific prey requirements as in the case of *Dinophysis*.

Feeding by mixoplankton can be studied with transmission electron microscopy (TEM) of the food vacuole, fluorescently labelled surrogate prey or fluorescent microspheres (Wilken et al., 2019). However, these methods reach their limits with particularly small mixoplankton (Wilken et al., 2019). The use of rotenone in estimating mixoplankton growth against strict heterotrophs may also be problematic (Ferreira and Calbet, 2020).

Molecular techniques that analyse the genetic material need to consider that many mixoplankton retain genetic material from their prey as *Mesodinium* retains the nucleomorph of its cryptophyte prey. However, specific genes can also serve as tracers for the origin of kleptoplastids (Rial et al., 2015). Single cell amplified genomes in combination with metatranscriptomics and metaproteomics may help to develop methods for the acquisition of quantitative data on mixoplankton activity (Wilken et al., 2019).

Even though there are already many methods for gathering qualitative data on mixoplankton activity, they often do not work on a larger scale and there is thus a lack of quantitative methods (Wilken et al., 2019). Quantitative data is however needed both for estimating the impact size of mixoplankton processes in marine environments and for tuning and validating associated models.

The problem persists that the data gathered in field and laboratory are often not suitable for tuning or validation of models, whether it is the spacing of the data or the very parameter itself. Cell numbers are an important and easily measured parameter. However, it does not give the same level of information on growth as organisms can gain biomass ergo grow without division and therefore increase in cell numbers. Biomass data is expensive and difficult to measure but more suitable for tuning and validation of biomass models.

Despite the challenges of studying mixoplankton and implementing them in models they should no longer be excluded from them. As stated by Flynn et al. (2019) and supported by the findings of this thesis, it is important to not only consider mixoplankton in models, but also recognise their functional diversity.

6.7 What next?

Mixoplankton types differ greatly and upon a closer look, we see that even the division of mixoplankton into the major group GNCM, SNCM and CM does not do the diversity justice. In the case of the two pSNCM *Mesodinium* and *Dinophysis* it already becomes apparent that there are substantial differences in plastid retention time, nutrient uptake and movement in the water and the bloom potential regarding biomass. Apart from pSNCM

there are also eSNCM that harbour permanent endosymbionts as the dinoflagellate *Noctiluca scintillans* (Hansen et al., 2004). Thus, the model could be extended to comprise eSNCM as an additional mixoplankton functional type and the model could be used to theoretically explore their ecological niche compared with the other types. As a next step, the generic N-based model could be implemented in a larger N-based ecosystem model such as the MEDUSA model (Yool et al., 2013) as it was done with the "Perfect Beast" model by Leles et al. (2018). The behaviour of the nitrogen-based mixoplankton models could then be explored in a wider ecological context in a similar fashion. Here, a challenge is that many of these large plankton models are validated with satellite chlorophyll data (Yool et al., 2013), which cannot separate mixoplankton from strict phytoplankton as mentioned above. Including mixoplankton in such models should probably go hand in hand with considering new ways for validation.

The advantage of the N-based TMD model is its simplicity in a first approach to understanding the complex trophodynamics of the three-tiered mixoplankton complex of *Teleaulax*, *Mesodinium* and *Dinophysis*. The importance of timing of blooms and prey availability for a subsequent Dinophysis bloom emerge from the N-based model. A variable stoichiometric TMD model offers the potential to give a much more realistic simulation due to its ability to simulate variable stoichiometry (C:N:P:Chl). Not only should a variable stoichiometric model be applied in environments where dissolved inorganic phosphorous (DIP) is potentially limiting, but also where light attenuation could be important (as is most likely in the coastal systems where *Dinophysis* blooms cause HABs). Low DIP areas which would necessitate a variable stoichiometric model approach include the Mediterranean Sea where *Dinophysis* is also a widespread genus (Caroppo et al., 2001; Koukaras, 2004; García-Altares et al., 2016; Bazzoni et al., 2018) and which is known to be limited in DIP rather than DIN (Krom et al., 1991; Thingstad et al., 2005). Since the toxicity of *Dinophysis* may vary with the growth phase and environmental factors, it may also be useful to fit the model with a submodel that simulates toxicity. This model could then be tuned to experimental data on the toxicity of *Dinophysis* to test different hypotheses for the triggers of toxicity. As prey availability is crucial for pSNCM on a cell based level due to the necessity of individual plastid acquisition, an individual based model of the current model could deliver interesting results in comparison with the biomass model. The question here would be, what effect the plastid shortage for some cells has on the whole population.

The variable stoichiometric *T. amphioxeia* model could next be implemented in a larger variable stoichiometric ecosystem model, because it bears certain reliability as a tuned variable stoichiometric model of a CM cryptophyte. It could prove useful to test the effects of an opportunistically feeding CM on nutrient cycling and trophic levels in a larger systemic context. The model could further be used as a base model to construct a variable stoichiometric model of the TMD complex. Alternatively, the *T. amphioxeia* model could be used as a prey model for another mixoplankton predator such as *Karlodinium venificum*, where a similar study was done with *Rhodomonas salina* as prey and where the "Perfect

Beast" model was used (Lin et al., 2018). Once the question of the relationship between feeding and external nutrient availability in *T. amphioxeia* is solved, the model can find use in forecasting models of HAB events that consider nutrient composition in relation to eutrophication and prey availability. For example, the mixoplankton *K. veneficum* showed higher growth rates when feeding in environments that have high N:P ratios raising the potential risk for HAB formations (Lin et al., 2018). In addition, limitation in nitrogen and phosphorous increase the toxin content per cell in this HAB species (Adolf et al., 2009). In turn, *K. veneficum* growing under nitrogen limitation and thus developing a high carbon to nitrogen ratio become unpalatable for higher trophic level grazers due to their changed biochemistry (Lin et al., 2018).

6.7.1 Possible implications of mixoplankton for environmental management

With the emerging knowledge on mixoplankton and their role in primary production, nutrient cycling and grazing, environmental management may also need to be rethought concerning mixoplankton. Several HAB species that are already being monitored are now known to be mixoplankton (Smayda, 1997; Heisler et al., 2008; Anderson et al., 2012). However, certain challenges are associated with monitoring mixoplankton beginning with sampling. Many of these caveats also apply to the TMD complex. Many mixoplankton species are fragile like the ciliate *Mesodinium* and get lost in standard net samples. In the case of *Dinophysis*, sampling and the quantification of cell numbers and species identification are difficult due to the morphological plasticity of each species during their life cycle. There is no solid molecular or morphological marker and observation require species-specific sampling strategies (Reguera et al., 2012).

Biodiversity and food webs

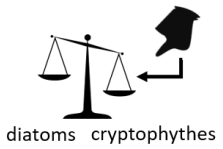

Does mixoplankton promote biodiversity? Does it boost or disrupt food webs? In Tagus estuary in Portugal, the local plankton community changed as chryptophytes became more abundant than diatoms from the 1980s to 2006-2007 (Brito et al., 2015). Higher nutrient loadings were here suspected as the cause as similar events have been linked to this potential cause in other regions next to grazing by an invasive bivalve. As a plastid source for the HAB genus *Dinophysis*, such changes in the plankton community could have farther-reaching consequences than anticipated when some species of *Dinophysis* were still considered autotroph.

Eutrophication

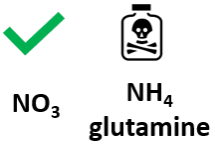

Will HABs become more frequent with eutrophication? Experiments on *Dinophysis* in oligotrophic (only nitrate) and eutrophic (ammonia) conditions in Florida revealed that *Dinophysis* forms non-toxic blooms in oligotrophic conditions and produces toxins (DSP) in the presence of available ammonia, urea and the amino acid glutamine (Hattenrath-Lehmann et al., 2015). *Dinophysis* is an example of a mixotroph that does not use nitrate, but is capable of phototrophy which may be the case for many NCM. For these organisms, monitoring for eutrophication needs to be more specific to the nitrogen species as nitrate may not have the same effect.

Aquacultures

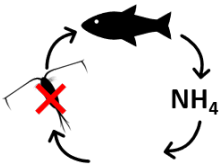

How may mixoplankton impact aquaculture? As aquacultures are naturally a source of ammonia, they may be epicentres for the formation of HABs by phytoplankton and mixoplankton alike. Additionally, potential predators like copepods may be heavily grazed upon by a large number of fish in the aquaculture. Mixoplankton may have an advantage here as they can cope with lower light conditions than phytoplankton. For the Baltic Sea, the expansion of shellfish aquacultures as a sustainable and supplementary alternative to fisheries on wild stocks is promoted by the EU (Joyce et al., 2013). In 2017, almost all of the Baltic have been identified as eutrophic (HELCOM, 2017). This level of eutrophication may be problematic for aquacultures. In Denmark, DSP events in shellfish aquacultures have already been associated with *Dinophysis* (Jørgensen and Andersen, 2007). If shellfish aquacultures shall indeed be the future of fisheries and a strong economic factor in the Baltic associated Scandinavia, monitoring of nutrient input with a distinction of nitrogen species may need to be implemented.

Hydrographical condition: stratification and upwelling

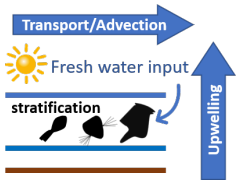

As hydrodynamics are changing with global warming (Sallée et al., 2021), can our understanding be improved on how hydrodynamics affect bloom formation? Harmful blooms by Dinophysis are often linked to stratification (Reguera et al., 2012; Souza et al., 2014; Ajani et al., 2016). *Dinophysis* blooms are heavily influenced by weather, because of their dependence on upwelling/stratification status, which is determined by weather (Reguera et al., 2012). Hence, hydrodynamics may also play a significant role in prey availability. *Mesodinium* is much faster than *Dinophysis* and able to vertically migrate 30 m daily. As a result, *Teleaulax*, *Mesodinium* and *Dinophysis* need to be in the same thin water layer for *Dinophysis* to successfully grow (Velo-Suárez et al., 2014). Climate change and the associated warming of surface water are predicted to lead to more stratification and to a decrease in upwelling events (García-Reyes et al., 2015).

Microbial carbon pump and carbon flux

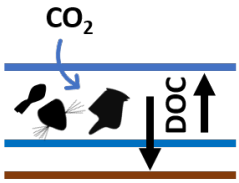

How does mixoplankton influence the carbon cycle in marine ecosystem? How much do they contribute to the biological carbon pump and how much do they impact the microbial carbon pump? Mixoplankton are photosynthetically active to varying degrees and thus contribute to the biological carbon pump by fixing CO_2 and thus exporting it to the deep ocean when they sink. As grazers they may also impact the microbial carbon pump that counter acts the carbon sink. Grazing on bacteria by mixoplankton like *T. amphioxeia* (Yoo et al., 2017) may decrease the microbial carbon pump. The production of labile DOC may also change the the presence of mixoplankton (Leles et al., 2021). It is thus important to assign the trophic status of plankton communities beyond the dichotomy of strict phototrophy and heterotrophy in carbon cycling models.

Increasing the body of research on mixoplankton physiology and the associated trophodynamics and using models as tools can help in the bottom-up process of improving our understanding of marine plankton and ultimately feed into improving coastal management (Fig. 6.1). There are still many challenging questions ahead. What role does mixoplankton play in carbon cycling? Is mixoplankton the better food with a higher nutritional value? How many more mixoplankton complexes like the TMD complex are out there? What would that mean in terms of how we view biodiversity in ecosystems. What does biodiversity mean in this context for coastal management? Models can help us explore and maybe answer many of these questions. Variable stoichiometric models as presented in this study can be used for exploring the role of mixoplankton in carbon cycling, trophic levels and food quality. Mixoplankton models that describe complex interactions as in the nitrogen-based TMD model can be used to study the diversity in mixoplankton interaction.

Bibliography

Adolf, J. E., T. Bachvaroff, and A. R. Place (2008). “Can cryptophyte abundance trigger toxic *Karlodinium veneficum* blooms in eutrophic estuaries?” In: *Harmful Algae* 8.1, pp. 119–128. ISSN: 15689883. DOI: 10.1016/j.hal.2008.08.003.

Adolf, J. E., T. R. Bachvaroff, and A. R. Place (2009). “Environmental modulation of karlotoxin levels in strains of the cosmopolitan dinoflagellate *Karlodinium veneficum* (Dinophyceae)”. In: *Journal of Phycology* 45.1, pp. 176–192. ISSN: 00223646, 15298817. DOI: 10.1111/j.1529-8817.2008.00641.x.

Aissaoui, A., A. Dhib, B. Reguera, et al. (2014). “First evidence of cell deformation occurrence during a *Dinophysis* bloom along the shores of the Gulf of Tunis (SW Mediterranean Sea)”. In: *Harmful Algae* 39, pp. 191–201. ISSN: 15689883. DOI: 10.1016/j.hal.2014.07.017.

Ajani, P., M. E. M. Larsson, A. Rubio, et al. (2016). “Modelling bloom formation of the toxic dinoflagellates *Dinophysis acuminata* and *Dinophysis caudata* in a highly modified estuary, south eastern Australia”. In: *Estuarine, Coastal and Shelf Science* 183, pp. 95–106. DOI: 10.1016/J.ECSS.2016.10.020.

Alldredge, A. L., U. Passow, and B. E. Logan (1993). “The abundance and significance of a class of large, transparent organic particles in the ocean”. In: *Deep Sea Research Part I: Oceanographic Research Papers* 40.6, pp. 1131–1140. DOI: 10.1016/0967-0637(93)90129.

Altenburger, A., H. Cai, Q. Li, et al. (2020a). “Dimorphism in cryptophytes—The case of *Teleaulax amphioxeia*/*Plagioselmis prolonga* and its ecological implications”. In: *Science Advances* eabb1611.6.

Altenburger, A., H. Cai, Q. Li, et al. (2020b). “Limits to the cellular control of sequestered cryptophyte prey in the marine ciliate *Mesodinium rubrum*”. In: *The ISME Journal*. DOI: 10.1101/2020.07.14.202424.

Anderson, D. M., A. Cembella, and G. M. Hallegraeff (2012). “Progress in understanding harmful algal blooms (HABs): Paradigm shifts and new technologies for research, monitoring and management”. In: *Annual Review of Marine Science* 4, pp. 143–176. ISSN: 0953797104. DOI: 10.1146/annurev-marine-120308-081121.

Anderson, D. M., P. M. Glibert, and J. M. Burkholder (2002). “Harmful algal blooms and eutrophication: nutrient sources, compositions, and consequences”. In: *Estuaries* 25.4, pp. 704–726. ISSN: 0160-8347. DOI: 10.1016/j.hal.2008.08.017.

Anderson, D. M., G. C. Pitcher, and M. Estrada (2005). “The comparative "Systems" approach to HAB research”. In: *Oceanography* 18.2, pp. 148–157.

Anschütz, A. A. and K. J. Flynn (2020). “Niche separation between different functional types of mixoplankton: results from NPZ - style N - based model simulations”. In: *Marine Biology* 167.3, pp. 1–21. ISSN: 0123456789. DOI: 10.1007/s00227-019-3612-3.

Archibald, J. M. (2007). “Nucleomorph genomes: Structure, function, origin and evolution”. In: *BioEssays* 29.4, pp. 392–402. DOI: 10.1002/bies.20551.

Arias, A., E. Saiz, and A. Calbet (2017). “Diel feeding rhythms in marine microzooplankton: effects of prey concentration, prey condition, and grazer nutritional history”. In: *Marine Biology* 164.10, pp. 205–205. ISSN: 0123456789. DOI: 10.1007/s00227-017-3233-7.

Azam, F., T. Fenchel, J. G. Field, et al. (1983). “The ecological role of water-column microbes in the sea”. In: *Marine Ecology Progress Series* 10.3, pp. 257–263. ISSN: 0171-8630. DOI: 10.3354/meps010257.

Balkis, N., M. Balci, A. Giannakourou, A. Venetsanopoulou, and P. Mudie (2016). “Dinoflagellate resting cysts in recent marine sediments from the Gulf of Gemlik (Marmara Sea, Turkey) and seasonal harmful algal blooms”. In: *Phycologia* 55.2, pp. 187–209. DOI: 10.2216/15-93.1.

Balrow, S. B. and P. Krugens (2002). “Cryptomonads from the Salton Sea, California”. In: *Hydrobiologia* 473, pp. 129–137. DOI: 10.1023/A:1016585818665.

Baretta-Bekker, J., J. Baretta, A. Hansen, and B Riemann (1998). “An improved model of carbon and nutrient dynamics in the microbial food web in marine enclosures”. In: *Aquatic Microbial Ecology* 14, pp. 91–108. ISSN: 0948-3055, 1616-1564. DOI: 10.3354/ame014091.

Bazzoni, A. M., A. G. Mudadu, G. Lorenzoni, et al. (2018). “Detection of *Dinophysis* species and associated okadaic acid in farmed shellfish: a two-year study from the western Mediterranean area”. In: *Journal of Veterinary Research* 62.2, pp. 137–144. ISSN: 2450-8608. DOI: 10.2478/jvetres-2018-0022.

Berdalet, E., B. Reguera, S. Roy, et al. (2017). “Harmful algal blooms in fjords, coastal embayments, and stratified systems: recent progress and future research”. In: *Oceanography* 30.1, pp. 46–57. ISSN: 10428275. DOI: 10.5670/oceanog.2017.109.

Berge, T., S. Chakraborty, P. J. Hansen, and K. H. Andersen (2017). “Modeling succession of key resource-harvesting traits of mixotrophic plankton”. In: *The ISME Journal* 11.1, pp. 212–223. ISSN: 0711218005. DOI: 10.1038/ismej.2016.92.

Berland, B. R., S. Y. Maestrini, and D. Grzebyk (1995). “Observation on possible life cycle stages of the dinoflagellates *Dinophysis cf. acuminata*, *Dinophysis acuta* and *Dinophysis pavillardi*”. In: *Aquatic Microbial Ecology* 9, pp. 183–189.

Bi, R., C. Arndt, and U. Sommer (2012). “Stoichiometric responses of phytoplankton species to the interactive effect of nutrient supply ratios and growth rate”. In: *Journal of Phycology* 48.3, pp. 539–549. ISSN: 00223646. DOI: 10.1111/j.1529-8817.2012.01163.x.

Bi, R., S. Ismar, U. Sommer, and M. Zhao (2017). “Environmental dependence of the correlations between stoichiometric and fatty acid-based indicators of phytoplankton nutritional quality”. In: *Limnology and Oceanography* 62.1, pp. 334–347. DOI: 10.1002/lno.10429.

Biard, T., L. Stemmann, M. Picheral, et al. (2016). “*In situ* imaging reveals the biomass of giant protists in the global ocean”. In: *Nature* 532.7600, pp. 504–507. DOI: 10.1038/nature17652.

Bils, F., M. Moyano, N. Aberle, et al. (2017). “Exploring the microzooplankton-ichthyoplankton link: A combined field and modeling study of Atlantic herring (*Clupea harengus*) in the Irish sea”. In: *Journal of Plankton Research* 39.1, pp. 147–163. DOI: 10.1093/plankt/fbw074.

Blanco, J., J Correa, S. Muñíz, et al. (2013). “Evaluación del impacto de los métodos y niveles utilizados para el control de toxinas en el mejillón”. In: *Revista Galega dos Recursos Marinos (Art. Inf. Tecn.)* 3, pp. 1–55.

Blauw, A., P Anderson, M Estrada, et al. (2006). “The use of fuzzy logic for data analysis and modelling of European harmful algal blooms: results of the HABES project”. In: *African Journal of Marine Science* 28.2, pp. 365–369. ISSN: 1814-232X, 1814-2338. DOI: 10.2989/18142320609504179.

Bérard-Therriault, L., M. Poulin, and L. Bossé (1999). *Guide d’identification du phytoplancton marin de l’estuaire et du golfe du Saint-Laurent: incluant également certains protozoaires*. Publication spéciale canadienne des sciences halieutiques et aquatiques 128. Ottawa: Les Presses Scientifiques du CNRC. 387 pp. ISBN: 978-0-660-96057-9.

Bristow, L. A., W. Mohr, S. Ahmerkamp, and M. M. Kuypers (2017). “Nutrients that limit growth in the ocean”. In: *Current Biology* 27.11, R474–R478. ISSN: 09609822. DOI: 10.1016/j.cub.2017.03.030.

Brito, A. C. A., T. Moita, C. Gameiro, et al. (2015). “Changes in the phytoplankton composition in a temperate estuarine system (1960 to 2010)”. In: *Estuaries and Coasts* 38.5, pp. 1678–1691. ISSN: 0035121750. DOI: 10.1007/s12237-014-9900-8.

Broddrick, J. T., D. G. Welkie, D. Jallet, et al. (2019). “Predicting the metabolic capabilities of *Synechococcus elongatus* PCC 7942 adapted to different light regimes”. In: *Metabolic Engineering* 52, pp. 42–56. ISSN: 10967176. DOI: 10.1016/j.ymben.2018.11.001.

Bronk, D (1999). “Rates of NH_4^+ uptake, intracellular transformation and dissolved organic nitrogen release in two clones of marine *Synechococcus* spp”. In: *Journal of Plankton Research* 21.7, pp. 1337–1353. ISSN: 14643774. DOI: 10.1093/plankt/21.7.1337.

Brutemark, A. and E. Granéli (2011). “Role of mixotrophy and light for growth and survival of the toxic haptophyte *Prymnesium parvum*”. In: *Harmful Algae* 10.4, pp. 388–394. ISSN: 1568-9883. DOI: 10.1016/j.hal.2011.01.005.

Burkholder, J. A. M., P. M. Glibert, and H. M. Skelton (2008). “Mixotrophy, a major mode of nutrition for harmful algal species in eutrophic waters”. In: *Harmful Algae* 8.1, pp. 77–93. ISSN: 1568-9883. DOI: 10.1016/j.hal.2008.08.010.

Butenschön, M., J. Clark, J. N. Aldridge, et al. (2016). “ERSEM 15.06: a generic model for marine biogeochemistry and the ecosystem dynamics of the lower trophic levels”. In: *Geoscientific Model Development* 9.4, pp. 1293–1339. ISSN: 1991-959X. DOI: https://doi.org/10.5194/gmd-9-1293-2016.

Calbet, A. (2008). “The trophic roles of microzooplankton in marine systems”. In: *ICES Journal of Marine Science* 65, pp. 325–331. DOI: 10.1093/icesjms/fsn013.

Calbet, A., R. A. Martínez, S. Isari, et al. (2012). “Effects of light availability on mixotrophy and microzooplankton grazing in an oligotrophic plankton food web: Evidences from a mesocosm study in Eastern Mediterranean waters”. In: *Journal of Experimental Marine Biology and Ecology* 424-425, pp. 66–77. DOI: 10.1016/j.jembe.2012.05.005.

Campbell, L. and E. J. Carpenter (1986). “Diel patterns of cell division in marine *Synechococcus spp.* (Cyanobacteria): use of the frequency of dividing cells technique to measure growth rate”. In: *Marine Ecology Progress Series* 32, pp. 139–148.

Campbell, L., R. J. Olson, H. M. Sosik, et al. (2010). “First harmful *Dinophysis* (Dinophyceae, Dinophysiales) bloom in the U.S. is revealed by automated imaging flow cytometry”. In: *Journal of Phycology* 46.1, pp. 66–75. DOI: 10.1111/j.1529-8817.2009.00791.x.

Caron, D. A., A. Goldman, and T. Fenchel (1990). “Protozoan respiration and metabolism”. In: *Ecology of marine protozoa*. Ed. by G. M. Capriulo, pp. 307–322.

Caron, D. A., R. W. Sanders, E. L. Lim, et al. (1993). “Light-dependent phagotrophy in the freshwater mixotrophic chrysophyte *Dinobryon cylindricum*”. In: *Microbial Ecology* 25.1, pp. 93–111. ISSN: 0095-3628. DOI: 10.1007/BF00182132.

Caroppo, C., R. Congestri, and M. Bruno (2001). “Dynamics of *Dinophysis* sensu lato species (Dinophyceae) in a coastal Mediterranean environment (Adriatic Sea)”. In: *Continental Shelf Research* 21.16, pp. 1839–1854. ISSN: 02784343. DOI: 10.1016/S0278-4343(01)00028-0.

Carpenter, E. J., S. Janson, R. Boje, F. Pollehne, and J. Chang (1995). “The dinoflagellate *Dinophysis norvegica*: biological and ecological observations in the Baltic Sea”. In: *European Journal of Phycology* 30.1, pp. 1–9. DOI: 10.1080/09670269500650751.

Carvalho, W. F. and E. Granéli (2010). “Contribution of phagotrophy versus autotrophy to *Prymnesium parvum* growth under nitrogen and phosphorus sufficiency and deficiency”. In: *Harmful Algae* 9.1, pp. 105–115. ISSN: 15689883. DOI: 10.1016/j.hal.2009.08.007.

Cerino, F. and A. Zingone (2006). “A survey of cryptomonad diversity and seasonality at a coastal Mediterranean site”. In: *European Journal of Phycology* 41.4, pp. 363–378. DOI: 10.1080/09670260600839450.

Chawla, A., D. A. Jay, A. M. Baptista, M. Wilkin, and C. Seaton (2008). “Seasonal variability and estuary-shelf interactions in circulation of a river-dominated dynamics estuary”. In: *Civil and Environmental Engineering* 31, pp. 269–288. ISSN: 1223700790227. DOI: 10.1007/S12237-007-9022-7.

Clay, B. L. (2015). “Cryptomonads”. In: *Freshwater Algae of North America (Second Edition)*. Ed. by J. D. Wehr, R. G. Sheath, and J. P. Kociole. Second Edi. Boston: Academic Press, pp. 809–850. ISBN: 978-0-12-385877-1. DOI: 10.1016/B978-0-12-385876-4.00018-9.

Cloern, J. E. (2001). “Our evolving conceptual model of the coastal eutrophication problem”. In: *Marine Ecology Progress Series* 210, pp. 223–253.

Cloern, J. E., B. E. Cole, and S. W. Hager (1994). “Notes on a *Mesodinium rubrum* red tide in San Francisco Bay (California, USA)”. In: *Journal of Plankton Research* 16.9, pp. 1269–1276. ISSN: 0142-7873, 1464-3774. DOI: 10.1093/plankt/16.9.1269.

Crane, K. W. and J. P. Grover (2010). “Coexistence of mixotrophs, autotrophs, and heterotrophs in planktonic microbial communities”. In: *Journal of Theoretical Biology* 262.3, pp. 517–527. ISSN: 00225193. DOI: 10.1016/j.jtbi.2009.10.027.

Crawford, D. W., D. A. Purdie, A. P. M. Lockwood, and P Weissman (1997). “Recurrent red-tides in the Southampton Water Estuary caused by the phototrophic ciliate *Mesodinium rubrum*”. In: *Estuarine, Coastal and Shelf Science* 45, pp. 799–812.

Cremer, H., F. Sangiorgi, F. Wagner-Cremer, et al. (2007). “Diatoms (Bacillariophyceae) and Dinoflagellate Cysts (Dinophyceae)”. In: *Caribbean Journal of Science* 43.1, pp. 23–58. DOI: 10.1007/s11116-014-9521-x.

Curtis, B. A., G. Tanifuji, S. Maruyama, et al. (2012). “Algal genomes reveal evolutionary mosaicism and the fate of nucleomorphs”. In: *Nature* 492.7427, pp. 59–65. DOI: 10.1038/nature11681.

Cusack, C., T. Dabrowski, K. Lyons, et al. (2016). “Harmful algal bloom forecast system for SW Ireland. Part II: Are operational oceanographic models useful in a HAB warning system”. In: *Harmful Algae* 53, pp. 86–101. ISSN: 15689883. DOI: 10.1016/j.hal.2015.11.013.

Díaz, P. A., C. Fernández-Pena, I. Pérez-Santos, et al. (2020). “*Dinophysis* Ehrenberg (Dinophyceae) in Southern Chile harbours red cryptophyte plastids from *Rhodomonas*/*Storeatula* clade”. In: *Harmful Algae* 99, p. 101907. ISSN: 15689883. DOI: 10.1016/j.hal.2020.101907.

Díaz, P. A., I. Peréz-Santos, G. Álvarez, et al. (2021). “Multiscale physical background to an exceptional harmful algal bloom of *Dinophysis acuta* in a fjord system”. In: *Science of The Total Environment* 773, p. 145621. ISSN: 00489697. DOI: 10.1016/j.scitotenv.2021.145621.

Díaz, P. A., M. Ruiz-Villarreal, Y. Pazos, T. Moita, and B. Reguera (2016). “Climate variability and *Dinophysis acuta* blooms in an upwelling system”. In: *Harmful Algae* 53, pp. 145–159. DOI: 10.1016/j.hal.2015.11.007.

Dolan, J. R. and M. T. Pérez (2000). “Costs, benefits and characteristics of mixotrophy in marine oligotrichs”. In: *Freshwater Biology* 45.2, pp. 227–238. DOI: 10.1046/j.1365-2427.2000.00659.x.

Donk, E. V., M. Lürling, D. O. Hessen, and G. M. Lokhorst (1997). “Altered cell wall morphology in nutrient-deficient phytoplankton and its impact on grazers”. In: *Limnology and Oceanography* 42.2, pp. 357–364. ISSN: 00243590. DOI: 10.4319/lo.1997.42.2.0357.

Douglas, S. E., C. A. Murphy, D. F. Spencer, and M. W. Gray (1991). “Cryptomonad algae are evolutionary chimaeras of two phylogenetically distinct unicellular eukaryotes”. In: *Nature* 350.6314, pp. 148–151. DOI: 10.1038/350148a0.

Dugdale, R. C. and J. J. Goering (1967). “Uptake of new and regenerated forms of nitrogen in primary productivity”. In: *Limnology and Oceanography* 12.2, pp. 196–206. ISSN: 00243590. DOI: 10.4319/lo.1967.12.2.0196.

Edwards, K. F. (2019). “Mixotrophy in nanoflagellates across environmental gradients in the ocean”. In: *Proceedings of the National Academy of Sciences* 116.13, pp. 6211–6220. ISSN: 0027-8424, 1091-6490. DOI: 10.1073/pnas.1814860116.

Elser, J. J. and R. P. Hassett (1994). “A stoichiometric analysis of the zooplankton–phytoplankton interaction in marine and freshwater ecosystems”. In: *Nature* 370.6486, pp. 211–213.

Escalera, L, B Reguera, Y Pazos, A Moroño, and J. M. Cabanas (2006). “Are different species of *Dinophysis* selected by climatological conditions?” In: *African Journal of Marine Science* 28.2, pp. 283–288. DOI: 10.2989/18142320609504163.

Escalera, L., B. Reguera, T. Moita, et al. (2010). “Bloom dynamics of *Dinophysis acuta* in an upwelling system: In situ growth versus transport”. In: *Harmful Algae* 9.3, pp. 312–322. DOI: 10.1016/j.hal.2009.12.002.

European Parliament, Council of the European Union, E. Parliament, and C. o. t. E. Union (2008). “Directive 2008/56/EC of the European Parliament and of the Council”. In: *Official Journal of the European Union* 164, pp. 19–40. ISSN: 0308-597X. DOI: 10.1016/j.biocon.2008.10.006.

Farrell, H., P. Gentien, L. Fernand, et al. (2012). “Scales characterising a high density thin layer of *Dinophysis acuta* Ehrenberg and its transport within a coastal jet”. In: *Harmful Algae* 15, pp. 36–46. ISSN: 15689883. DOI: 10.1016/j.hal.2011.11.003.

Fasham, M. J. R., H. W. Ducklow, and S. M. McKelvie (1990). “A nitrogen-based model of plankton dynamics in the oceanic mixed layer”. In: *Journal of Marine Research* 48.3, pp. 591–639. DOI: 10.1357/002224090784984678.

Faure, E., F. Not, A.-S. Benoiston, et al. (2019). “Mixotrophic protists display contrasted biogeographies in the global ocean”. In: *The ISME Journal*. DOI: 10.1038/s41396-018-0340-5.

Fenchel, T. and P. J. Hansen (2006). “Motile behaviour of the bloom-forming ciliate *Mesodinium rubrum*”. In: *Marine Biology Research* 2.1, pp. 33–40. DOI: 10.1080/17451000600571044.

Ferreira, G. D. and A. Calbet (2020). “Caveats on the use of rotenone to estimate mixotrophic grazing in the oceans”. In: *Scientific Reports* 10.3899, p. 11. DOI: 10.1038/s41598-020-60764-2.

Flynn, K. J., M. J. R. Fasham, and C. R. Hipkin (1997). “Modelling the interactions between ammonium and nitrate uptake in marine phytoplankton”. In: *Philosophical Transactions Royal Society B* 352, pp. 1625–1645.

Flynn, K. J. (2009). “Going for the slow burn: Why should possession of a low maximum growth rate be advantageous for microalgae?” In: *Plant Ecology and Diversity* 2.2, pp. 179–189. DOI: 10.1080/17550870903207268.

— (2018). *Dynamic Ecology - an introduction to the art of simulating trophic dynamics*. Ed. by K. J. Flynn. Swansea, UK: Swansea University, UK. ISBN: 978-0-9567462-9-0.

Flynn, K. J. and I. Butler (1986). “Nitrogen sources for the growth of marine microalgae: role of dissolved free amino acids”. In: *Marine Ecology Progress Series* 34.1958, pp. 281–304. DOI: 10.3354/meps034281.

Flynn, K. J. and P. J. Hansen (2013). “Cutting the canopy to defeat the "Selfish Gene"; Conflicting selection pressures for the integration of phototrophy in mixotrophic protists”. In: *Protist* 164.6, pp. 1–13. ISSN: 1434-4610. DOI: 10.1016/j.protis.2013.09.002.

Flynn, K. J. and D. J. McGillicuddy (2018). “Modeling marine harmful algal blooms: current status and future prospects”. In: *Harmful Algal Blooms*. Ed. by S. E. Shumway, J. M. Burkholder, and S. L. Morton. Chichester, UK: John Wiley & Sons, Ltd, pp. 115–134. ISBN: 978-1-118-99467-2 978-1-118-99465-8. DOI: 10.1002/9781118994672.ch3.

Flynn, K. J. and A. Mitra (2009). “Building the "perfect beast": Modelling mixotrophic plankton”. In: *Journal of Plankton Research* 31.9, pp. 965–992. ISSN: 0142-7873. DOI: 10.1093/plankt/fbp044.

— (2016). “Why plankton modelers should reconsider using rectangular hyperbolic (Michaelis-Menten, Monod) descriptions of predator-prey interactions”. In: *Frontiers in Marine Science* 3.165. DOI: 10.3389/fmars.2016.00165.

Flynn, K. J., A. Mitra, K. Anestis, et al. (2019). “Mixotrophic protists and a new paradigm for marine ecology: where does plankton research go now?” In: *Journal of Plankton Research* 00.0. DOI: 10.1093/plankt/fbz026.

Flynn, K. J., D. K. Stoecker, A. Mitra, et al. (2013). “Misuse of the phytoplankton-zooplankton dichotomy: The need to assign organisms as mixotrophs within plankton functional types”. In: *Journal of Plankton Research* 35.1, pp. 3–11. ISSN: 0142-7873. DOI: 10.1093/plankt/fbs062.

Franck, V., K. Bruland, D. Hutchins, and M. Brzezinski (2003). “Iron and zinc effects on silicic acid and nitrate uptake kinetics in three high-nutrient, low-chlorophyll (HNLC) regions”. In: *Marine Ecology Progress Series* 252, pp. 15–33. ISSN: 0171-8630, 1616-1599. DOI: 10.3354/meps252015.

Franks, P. J. (2002). “NPZ models of plankton dynamics: Their construction, coupling to physics, and application”. In: *Journal of Oceanography* 58.2, pp. 379–387. DOI: 10.1023/A:1015874028196.

Fux, E., S. Gonzalez-Gil, M. Lunven, P. Gentien, and P. Hess (2010). “Production of diarrhetic shellfish poisoning toxins and pectenotoxins at depths within and below the euphotic zone”. In: *Toxicon* 56.8, pp. 1487–1496. DOI: 10.1016/j.toxicon.2010.09.007.

Gao, H., X. An, L. Liu, et al. (2017). “Characterization of *Dinophysis acuminata* from the Yellow Sea, China, and its response to different temperatures and *Mesodinium* prey”. In: *Oceanological and Hydrobiological Studies* 46.4, pp. 439–450. DOI: 10.1515/ohs-2017-0043.

García-Altares, M., A. Casanova, M. Fernández-Tejedor, J. Diogène, and P. de la Iglesia (2016). “Bloom of *Dinophysis spp.* dominated by *D. sacculus* and its related diarrhetic shellfish poisoning (DSP) outbreak in Alfacs Bay (Catalonia, NW Mediterranean Sea): Identification of DSP toxins in phytoplankton, shellfish and passive samplers”. In: *Regional Studies in Marine Science* 6, pp. 19–28. ISSN: 23524855. DOI: 10.1016/j.rsma.2016.03.009.

García-Portela, M., B. Reguera, J. Gago, M. Le Gac, and F. Rodríguez (2020). “Uptake of inorganic and organic nitrogen sources by *Dinophysis acuminata* and *D. acuta*”. In: 8.187. DOI: 10.3390/microorganisms8020187.

García-Portela, M., P. Riobó, B. Reguera, et al. (2018). “Comparative ecophysiology of *Dinophysis acuminata* and *D. acuta* (Dinophyceae, Dinophysiales): effect of light intensity and quality on growth, cellular toxin content, and photosynthesis”. In: *Journal of Phycology* 917, pp. 899–917. DOI: 10.1111/jpy.12794.

García-Reyes, M., W. J. Sydeman, D. S. Schoeman, et al. (2015). “Under pressure: climate change, upwelling, and eastern boundary upwelling ecosystems”. In: *Frontiers in Marine Science* 2. ISSN: 2296-7745. DOI: 10.3389/fmars.2015.00109.

Garcia-Cuetos, L., j. Moestrup, J. Hansen, et al. (2010). “The toxic dinoflagellate *Dinophysis acuminata* harbors permanent chloroplasts of cryptomonad origin, not kleptochloroplasts”. In: *Harmful Algae* 9.1, pp. 25–38. ISSN: 1568-9883. DOI: 10.1016/j.hal.2009.07.002.

Gasol, J. M. and P. A. D. Giorgio (2000). “Using flow cytometry for counting natural planktonic bacteria and understanding the structure of planktonic bacterial communities”. In: *Scientia Marina* 64.2, pp. 197–224.

Gentien, P., M. Lunven, M. Lehaître, and J. Duvent (1995). “*In-situ* depth profiling of particle sizes”. In: *Deep Sea Research Part I: Oceanographic Research Papers* 42.8, pp. 1297–1312. ISSN: 09670637. DOI: 10.1016/0967-0637(95)00058-E.

Gerritsen, J. and J. R. Strickler (1977). “Encounter probabilities and community structure in zooplankton: a mathematical model”. In: *Journal of the Fisheries Board of Canada* 34.1, pp. 73–82.

Ghyoot, C., K. J. Flynn, A. Mitra, C. Lancelot, and N. Gypens (2017a). “Modeling plankton mixotrophy: a mechanistic model consistent with the Shuter-type biochemical approach”. In: *Frontiers in Ecology and Evolution* 5, p. 78. ISSN: 2296-701X. DOI: 10.3389/fevo.2017.00078.

Ghyoot, C., N. Gypens, K. J. Flynn, and C. Lancelot (2015). “Modelling alkaline phosphatase activity in microalgae under orthophosphate limitation: the case of *Phaeocystis globosa*”. In: *Journal of Plankton Research* 37.5, pp. 869–885. ISSN: 0142-7873. DOI: 10.1093/plankt/fbv062.

Ghyoot, C., C. Lancelot, K. J. Flynn, A. Mitra, and N. Gypens (2017b). “Introducing mixotrophy into a biogeochemical model describing an eutrophied coastal ecosystem: The Southern North Sea”. In: *Progress in Oceanography*, pp. 1–11. DOI: 10.1016/j.pocean.2017.08.002.

Giménez Papiol, G., V. Beuzenberg, A. I. Selwood, L. MacKenzie, and M. A. Packer (2016). “The use of a mucus trap by *Dinophysis acuta* for the capture of *Mesodinium rubrum* prey under culture conditions”. In: *Harmful Algae* 58, pp. 1–7. ISSN: 1568-9883. DOI: 10.1016/j.hal.2016.07.001.

Glibert, P. M., J. I. Allen, A. F. Bouwman, et al. (2010). “Modeling of HABs and eutrophication: status, advances, challenges”. In: *Journal of Marine Systems* 83.3, pp. 262–275. DOI: 10.1016/j.jmarsys.2010.05.004.

Glibert, P. M. and J. A. M. Burkholder (2011). “Harmful algal blooms and eutrophication: "strategies" for nutrient uptake and growth outside the Redfield comfort zone”. In: *Chinese Journal of Oceanology and Limnology* 29.4, pp. 724–738. ISSN: 0254-4059. DOI: 10.1007/s00343-011-0502-z.

Gülzow, N., Y. Wahlen, and H. Hillebrand (2018). “Metaecosystem dynamics of marine phytoplankton alters resource use efficiency along stoichiometric gradients”. In: *The American Naturalist* 193.1, pp. 000–000. DOI: 10.1086/700835.

Gobler, C. J., D. L. Berry, S. T. Dyhrman, et al. (2011). "Niche of harmful alga *Aureococcus anophagefferens* revealed through ecogenomics". In: *Proceedings of the National Academy of Sciences* 108.11, pp. 4352–4357. ISSN: 0027-8424, 1091-6490. DOI: 10.1073/pnas.1016106108.

González-Gil, S., L. Velo-Suárez, P. Gentien, I. Ramilo, and B. Reguera (2010). "Phytoplankton assemblages and characterization of a *Dinophysis acuminata* population during an upwelling-downwelling cycle". In: *Aquatic Microbial Ecology* 58.3, pp. 273–286. DOI: 10.3354/ame01372.

Granéli, E, D. Anderson, P Carlsson, and S. Maestrini (1997). "Light and dark carbon uptake by *Dinophysis* species in comparison to other photosynthetic and heterotrophic dinoflagellates". In: *Aquatic Microbial Ecology* 13, pp. 177–186. ISSN: 0948-3055, 1616-1564. DOI: 10.3354/ame013177.

Granéli, E. and J. T. Turner (2006). *Ecological of Harmful Algae*. 95 pp. ISBN: 978-3-540-32209-2.

Granéli, E., P. S. Salomon, and G. O. Fistarol (2008a). "The role of allelopathy for harmful algae bloom formation". In: *Algal Toxins: Nature, Occurrence, Effect and Detection*. Springer, pp. 159–178. ISBN: 978-1-4020-8479-9. DOI: 10.1007/978-1-4020-8480-5.

Granéli, E., M. Weberg, and P. S. Salomon (2008b). "Harmful algal blooms of allelopathic microalgal species: The role of eutrophication". In: *Harmful Algae* 8, pp. 94–102. DOI: 10.1016/j.hal.2008.08.011.

Grobbelaar, N., W.-T. Li, and T.-C. Huang (1991). "Relationship between the nitrogenase activity and dark respiration rate of *Synechococcus* RF-1". In: *FEMS Microbiology Letters* 83.1, pp. 99–102. ISSN: 03781097, 15746968. DOI: 10.1111/j.1574-6968.1991.tb04396.x.

Guillard, R. R. L. (1975). "Culture of phytoplankton for feeding marine invertebrates". In: *Culture of marine invertebrate animals*. Ed. by C. J. Berg. Springer.

Gustafson, D. E., D. K. Stoecker, M. D. Johnson, W. F. Van Heukelem, and K. Sneider (2000). "Cryptophyte algae are robbed of their organelles by the marine ciliate *Mesodinium rubrum*". In: *Nature* 405, pp. 1049–1052. ISSN: 9780511735066. DOI: 10.1177/0956247816647344.

Hackett, J. D., L. Maranda, H. S. Yoon, and D. Bhattacharya (2003). "Phylogenetic evidence for the cryptophyte origin of the plastid of *Dinophysis* (Dinophysiales, Dinophyceae)". In: *Journal of Phycology* 39.2, pp. 440–448. ISSN: 00223646. DOI: 10.1046/j.1529-8817.2003.02100.x.

Haefner, J. (1996). *Modeling Biological Systems*. New York: Chapman & Hall. ISBN: 0-412-04201-0. DOI: 10.1007/b106568.

Hallegraeff, G. M. and C. J. Bolch (1992). "Transport of diatom and dinoflagellate resting spores in ships' ballast water: implications for plankton biogeography and aquaculture". In: *Journal of Plankton Research* 14.8, pp. 1067–1084.

Hallegraeff, G. M. and I. A. N. Lucas (1988). "The marine dinoflagellate genus *Dinophysis* (Dinophyceae): photosynthetic, neritic and non-photosynthetic, oceanic species". In: *Phycologia* 27.1, pp. 25–42. DOI: 10.2216/i0031-8884-27-1-25.1.

Hamilton, M., G. M. Hennon, R. Morales, et al. (2017). "Dynamics of *Teleaulax*-like cryptophytes during the decline of a red water bloom in the Columbia River Estuary". In: *Journal of Plankton Research* 39.4, pp. 589–599. ISSN: 0021-9258. DOI: 10.1093/plankt/fbx029.

Hammer, A. C. and J. W. Pitchford (2005). "The role of mixotrophy in plankton bloom dynamics, and the consequences for productivity". In: *ICES Journal of Marine Science* 62.5, pp. 833–840. DOI: 10.1016/j.icesjms.2005.03.001.

Hansen, B., P. K. Bjornsen, and P. J. Hansen (1994). "The size ratio between planktonic predators and their prey". In: *Limnology and Oceanography* 39.2, pp. 395–403. ISSN: 0024-3590. DOI: 10.4319/lo.1994.39.2.0395.

Hansen, P. J., K. Ojamäe, T. Berge, et al. (2016). "Photoregulation in a kleptochloroplastidic dinoflagellate, *Dinophysis acuta*". In: *Frontiers in Microbiology* 7.785. DOI: 10.3389/fmicb.2016.00785.

Hansen, P. J. (2011). "The role of photosynthesis and food uptake for the growth of marine mixotrophic dinoflagellates". In: *Journal of Eukaryotic Microbiology* 58.3, pp. 203–214. DOI: 10.1111/j.1550-7408.2011.00537.x.

Hansen, P. J. and T. Fenchel (2006). “The bloom-forming ciliate *Mesodinium rubrum* harbours a single permanent endosymbiont”. In: *Marine Biology Research* 2.3, pp. 169–177. ISSN: 1745-1000, 1745-1019. DOI: 10.1080/17451000600719577.

Hansen, P. J., L. Miranda, and R. Azanza (2004). “Green *Noctiluca scintillans*: a dinoflagellate with its own greenhouse”. In: *Marine Ecology Progress Series* 275, pp. 79–87. ISSN: 0171-8630. DOI: 10.3354/meps275079.

Hansen, P. J., L. T. Nielsen, M. Johnson, T. Berge, and K. J. Flynn (2013). “Acquired phototrophy in *Mesodinium* and *Dinophysis* - A review of cellular organization, prey selectivity, nutrient uptake and bioenergetics”. In: *Harmful Algae* 28, pp. 126–139. ISSN: 1568-9883. DOI: 10.1016/j.hal.2013.06.004.

Hansen, P. (2002). “Effect of high pH on the growth and survival of marine phytoplankton: implications for species succession”. In: *Aquatic Microbial Ecology* 28, pp. 279–288.

Hansen, P., M Moldrup, W Tarangkoon, L Garcia-Cuetos, and. Moestrup (2012). “Direct evidence for symbiont sequestration in the marine red tide ciliate *Mesodinium rubrum*”. In: *Aquatic Microbial Ecology* 66.1, pp. 63–75. ISSN: 0948-3055, 1616-1564. DOI: 10.3354/ame01559.

Harred, L. B. and L. Campbell (2014). “Predicting harmful algal blooms: A case study with *Dinophysis ovum* in the Gulf of Mexico”. In: *Journal of Plankton Research* 36.6, pp. 1434–1445. DOI: 10.1093/plankt/fbu070.

Hattenrath-Lehmann, T. and C. J. Gobler (2015). “The contribution of inorganic and organic nutrients to the growth of a North American isolate of the mixotrophic dinoflagellate, *Dinophysis acuminata*”. In: *Limnology and Oceanography* 60, pp. 1588–1603. ISSN: 00243590. DOI: 10.1002/lno.10119.

Hattenrath-Lehmann, T. K., M. A. Marcoval, D. L. Berry, et al. (2013). “The emergence of *Dinophysis acuminata* blooms and DSP toxins in shellfish in New York waters”. In: *Harmful Algae* 26, pp. 33–44. DOI: 10.1016/j.hal.2013.03.005.

Hattenrath-Lehmann, T. K., M. A. Marcoval, H. Mittlesdorf, et al. (2015). “Nitrogenous nutrients promote the prowth and toxicity of *Dinophysis acuminata* during estuarine bloom events”. In: *PLoS ONE* 10.4. Ed. by H. G. Dam, e0124148. ISSN: 1932-6203. DOI: 10.1371/journal.pone.0124148.

Hayes, G. C., D. A. Purdie, and J. A. Williams (1989). “The distribution of ichthyoplankton in Southampton Water in response to low oxygen levels produced by a *Mesodinium rubrum* bloom”. In: *Journal of Fish Biology* 34.5, pp. 811–813. ISSN: 0022-1112, 1095-8649. DOI: 10.1111/j.1095-8649.1989.tb03363.x.

Heaney, S. I. and R. W. Eppley (1981). “Light, temperature and nitrogen as interacting factors affecting diel vertical migrations of dinoflagellates in culture”. In: *Journal of Plankton Research* 3.2, pp. 331–344. DOI: 10.1093/plankt/3.2.331.

Heisler, J., P. Glibert, J. Burkholder, et al. (2008). “Eutrophication and harmful algal blooms: A scientific consensus”. In: *Harmful Algae* 8.1, pp. 3–13. ISSN: 15689883. DOI: 10.1016/j.hal.2008.08.006.

HELCOM (2017). *The integrated assessment of eutrophication - supplementary report to the first version of the ‘State of the Baltic Sea’ report 2017*. URL: http://stateofthebalticsea.helcom.fi/about-helcom-and-the-assessment/downloads-and-data/.

Herfort, L., T. D. Peterson, V. Campbell, S. Futrell, and P. Zuber (2011). “*Myrionecta rubra* (*Mesodinium rubrum*) bloom initiation in the Columbia River estuary”. In: *Estuarine, Coastal and Shelf Science* 95.4, pp. 440–446. DOI: 10.1016/j.ecss.2011.10.015.

Hernández-Urcera, J., P. Rial, M. García-Portela, et al. (2018). “Notes on the cultivation of two mixotrophic *Dinophysis* species and their ciliate prey *Mesodinium rubrum*”. In: *Toxins* 10.12, pp. 505–505. DOI: 10.3390/toxins10120505.

Hood, R. R., E. A. Laws, R. A. Armstrong, et al. (2006). “Pelagic functional group modeling: Progress, challenges and prospects”. In: *Deep Sea Research Part II: Topical Studies in Oceanography* 53.5, pp. 459–512. ISSN: 09670645. DOI: 10.1016/j.dsr2.2006.01.025.

Izaguirre, I., R. Sinistro, M. R. Schiaffino, et al. (2012). “Grazing rates of protists in wetlands under contrasting light conditions due to floating plants”. In: *Aquatic Microbial Ecology* 65.3, pp. 221–232. DOI: 10.3354/ame01547.

Jacobson, D. and R. Andersen (1994). “*Dinophysis* (Dinophyceae): light and electron microscopical observations of food vacuoles in *Dinophysis acuminata*, *D. norvegica* and two heterotrophic dinophysoid”. In: *Phycologia* 33, pp. 97–110.

Jaén, D. and L. Mamán (2009). “First report of *Dinophysis acuta* in culture”. In: *Harmful Algae News* 39, pp. 1–2.

Janson, S. (2004). “Molecular evidence that plastids in the toxin-producing dinoflagellate genus *Dinophysis* originate from the free-living cryptophyte *Teleaulax amphioxeia*”. In: *Environmental Microbiology* 6.10, pp. 1102–1106. ISSN: 1462-2912. DOI: 10.1111/j.1462-2920.2004.00646.x.

Jeffrey, S., S. W. Wright, and M. Zapata (2011). “Microalgal classes and their signature pigments”. In: *Phytoplankton Pigments*. Ed. by S. Roy, C. Llewellyn, E. S. Egeland, and G. Johnsen. Cambridge: Cambridge University Press, pp. 3–77. ISBN: 978-0-511-73226-3. DOI: 10.1017/CBO9780511732263.004.

Jeong, H. J., A. S. Lim, P. J. Franks, et al. (2015). “A hierarchy of conceptual models of red-tide generation: Nutrition, behavior, and biological interactions”. In: *Harmful Algae* 47, pp. 97–115. ISSN: 1568-9883. DOI: 10.1016/j.hal.2015.06.004.

Jeong, H. J., Y. D. Yoo, K. H. Lee, et al. (2013). “Red tides in Masan Bay, Korea in 2004-2005: I. Daily variations in the abundance of red-tide organisms and environmental factors”. In: *Harmful Algae* 30, S75–S88. DOI: 10.1016/j.hal.2013.10.008.

Jiang, H. and M. D. Johnson (2017). “Jumping and overcoming diffusion limitation of nutrient uptake in the photosynthetic ciliate *Mesodinium rubrum*”. In: *Limnology and Oceanography* 62.2, pp. 421–436. DOI: 10.1002/lno.10432.

Jiang, H., D. M. Kulis, M. L. Brosnahan, and D. M. Anderson (2018). “Behavioral and mechanistic characteristics of the predator-prey interaction between the dinoflagellate *Dinophysis acuminata* and the ciliate *Mesodinium rubrum*”. In: *Harmful Algae* 77, pp. 43–54. DOI: 10.1016/j.hal.2018.06.007.

Jimenez, R. and P. Intriago (1987). “Observations on blooms of *Mesodinium rubrum* in the upwelling area off Ecuador”. In: *Oceanologica Acta, Special issue*.

John, E. H. and K. J. Flynn (2002). “Modelling changes in paralytic shellfish toxin content of dinoflagellates in response to nitrogen and phosphorus supply”. In: *Marine Ecology Progress Series* 225, pp. 147–160.

Johnson, M. D., D. J. Beaudoin, A. Laza-Martinez, et al. (2016). “The genetic diversity of *Mesodinium* and associated cryptophytes”. In: *Frontiers in Microbiology* 7, pp. 1–16. DOI: 10.3389/fmicb.2016.02017.

Johnson, M. D., D. Oldach, C. F. Delwiche, and D. K. Stoecker (2007). “Retention of transcriptionally active cryptophyte nuclei by the ciliate *Myrionecta rubra*”. In: *Nature* 445.7126, pp. 426–428. ISSN: 0028-0836. DOI: 10.1038/nature05496.

Johnson, M. D. and D. K. Stoecker (2005). “Role of feeding in growth and photophysiology of *Myrionecta rubra*”. In: *Aquatic Microbial Ecology* 39.3, pp. 303–312. DOI: 10.3354/ame039303.

Johnson, M. D., D. K. Stoecker, and H. G. Marshall (2013). “Seasonal dynamics of *Mesodinium rubrum* in Chesapeake Bay”. In: *Journal of Plankton Research* 35.4, pp. 877–893. DOI: 10.1093/plankt/fbt028.

Johnson, M. D., T. Tengs, D. Oldach, and D. K. Stoecker (2006). “Sequestration, performance, and functional control of cryptophyte plastids in the ciliate *Myrionecta rubra* (ciliophora)”. In: *Journal of Phycology* 42.6, pp. 1235–1246. ISSN: 0022-3646. DOI: 10.1111/j.1529-8817.2006.00275.x.

Jones, H. L. J., P. Durjun, B. S. C. Leadbeater, and J. C. Green (1995). “The relationship between photoacclimation and phagotrophy with respect to chlorophyll a, carbon and nitrogen content, and cell size of *Chrysochromulina brevifilum (Prymnesiophyceae)*”. In: *Phycologia* 34.2, pp. 128–134. ISSN: 0031-8884. DOI: 10.2216/i0031-8884-34-2-128.1.

Jones, H. L. J., B. S. C. Leadbeater, and J. C. Green (1993). “Mixotrophy in marine species of *Chrysochromulina* (Prymnesiophyceae): ingestion and digestion of a small green flagellate”. In: *Journal of Marine Biological Association* 73, pp. 283–296. DOI: 10.1017/S0025315400032859.

Jost, C., C. A. Lawrence, F. Campolongo, et al. (2004). “The effects of mixotrophy on the stability and dynamics of a simple planktonic food web model”. In: *Theoretical Population Biology* 66.1, pp. 37–51. ISSN: 00405809. DOI: 10.1016/j.tpb.2004.02.001.

Joyce, A., S. Lindegarth, J. K. Petersen, and C. Murphy (2013). “Strategic approaches for aquaculture industry development: Flat oyster cultivation in Scandinavia”. In: *DTU Library*.

Jørgensen, K. and P. Andersen (2007). “Relation between the concentration of *Dinophysis acuminata* and diarrheic shellfish poisoning toxins in Blue Mussels (*Mytilus edulis*) during a toxic episode in the Limfjord (Denmark), 2006”. In: *Journal of Shellfish Research* 26.4, pp. 1081–1087. DOI: 10.2983/0730-8000(2007)26[1081:RBTCOD]2.0.CO;2.

Kamiyama, T., S. Nagai, T. Suzuki, and K. Miyamura (2010). “Effect of temperature on production of okadaic acid, dinophysistoxin-1, and pectenotoxin-2 by *Dinophysis acuminata* in culture experiments”. In: *Aquatic Microbial Ecology* 60.2, pp. 193–202. DOI: 10.3354/ame01419.

Katechakis, A., T. Haseneder, R. Kling, and H. Stibor (2005). “Mixotrophic versus photoautotrophic specialist algae as food for zooplankton: The light:nutrient hypothesis might not hold for mixotrophs”. In: *Limnology and Oceanography* 50.4, pp. 1290–1299. ISSN: 00243590. DOI: 10.4319/lo.2005.50.4.1290.

Kenny, P. and K. J. Flynn (2016). “Coupling a simple irradiance description to a mechanistic growth model to predict algal production in industrial-scale solar-powered photobioreactors”. In: *Journal of Applied Phycology* 28.6, pp. 3203–3212. DOI: 10.1007/s10811-016-0892-6.

Kim, J. I., H. S. Yoon, G. Yi, et al. (2015a). “The plastid genome of the cryptomonad *Teleaulax amphioxeia*”. In: *PLoS ONE* 10.6. DOI: 10.1371/journal.pone.0129284.

Kim, M., S. Kim, W. Yih, M. G. Park, and M. Gil Park (2012a). “The marine dinoflagellate genus *Dinophysis* can retain plastids of multiple algal origins at the same time”. In: *Harmful Algae* 13, pp. 105–111. ISSN: 1568-9883. DOI: 10.1016/j.hal.2011.10.010.

Kim, M., S. W. Nam, W. Shin, D. W. Coats, and M. G. Park (2012b). “*Dinophysis caudata* (Dinophyceae) sequesters and retains plastids from the mixotrophic ciliate prey *Mesodinium rubrum*”. In: *Journal of Phycology* 48.3, pp. 569–579. ISSN: 1529-8817. DOI: 10.1111/j.1529-8817.2012.01150.x.

— (2015b). “Fate of green plastids in *Dinophysis caudata* following ingestion of the benthic ciliate *Mesodinium coatsi*: Ultrastructure and psbA gene”. In: *Harmful Algae* 43, pp. 66–73. DOI: 10.1016/j.hal.2015.02.004.

Kim, M. and M. G. Park (2019). “Unveiling the hidden genetic diversity and chloroplast type of marine benthic ciliate *Mesodinium* species”. In: *Scientific Reports* 9.1, p. 14081. ISSN: 2045-2322. DOI: 10.1038/s41598-019-50659-2.

Kim, S., Y. G. Kang, H. S. Kim, et al. (2008). “Growth and grazing responses of the mixotrophic dinoflagellate *Dinophysis acuminata* as functions of light intensity and prey concentration”. In: *Aquatic Microbial Ecology* 51.3, pp. 301–310. ISSN: 0948-3055. DOI: 10.3354/ame01203.

Klausmeier, C. A., E. Litchman, and S. A. Levin (2004). “Phytoplankton growth and stoichiometry under multiple nutrient limitation”. In: *Limnology and Oceanography* 49.4, pp. 1463–1470.

Koukaras, K. (2004). “*Dinophysis* blooms in Greek coastal waters (Thermaikos Gulf, NW Aegean Sea)”. In: *Journal of Plankton Research* 26.4, pp. 445–457. ISSN: 1464-3774. DOI: 10.1093/plankt/fbh042.

Kozlowsky-Suzuki, B., P. Carlsson, A. Rühl, and E. Granéli (2006). “Food selectivity and grazing impact on toxic *Dinophysis spp.* by copepods feeding on natural plankton assemblages”. In: *Harmful Algae* 5.1, pp. 57–68. ISSN: 15689883. DOI: 10.1016/j.hal.2005.05.002.

Krom, M. D., N. Kress, S. Brenner, and L. I. Gordon (1991). “Phosphorus limitation of primary productivity in the eastern Mediterranean Sea”. In: *Limnology and Oceanography* 36.3, pp. 424–432. ISSN: 00243590. DOI: 10.4319/lo.1991.36.3.0424.

Lalli, C. M. and T. R. Parsons (2006). *Biological oceanography: an introduction*. 2. ed., reprinted. Open University oceanography series. Amsterdam: Elsevier Butterworth-Heinemann. 314 pp. ISBN: 978-0-7506-3384-0.

Landry, M. R. (2002). "Integrating classical and microbial food web concepts: evolving views from the open-ocean tropical Pacific". In: *Hydrobiologia* 480, pp. 29–39.

Larsen, J. and j. Moestrup (1992). "Potentially toxic phytoplankton. 2. Genus *Dinophysis* (Dinophyceae)". In: *ICES Identification Leaflets for Plankton 180. International Council for the Exploration of the Sea*. Ed. by J. A. Lindley. 180 vols. Copenhagen, Denmark, pp. 1–12.

Laza-Martínez, A., J. Arluzea, I. Miguel, and E. Orive (2012). "Morphological and molecular characterization of *Teleaulax gracilis* sp. nov. and *T. minuta* sp. nov. (Cryptophyceae)". In: *Phycologia* 51.6, pp. 649–661. DOI: 10.2216/11-044.1.

Lee, B. and M. G. Park (2017). "Different life cycle strategies of the dinoflagellates *Fragilidium duplocampanaeforme* and its prey *Dinophysis acuminata* may explain their different susceptibilities to the infection by the parasite Parvilucifera infectans". In: *Harmful Algae* 65, pp. 1–8. ISSN: 15689883. DOI: 10.1016/j.hal.2017.04.002.

Leles, S. G., A. Mitra, K. J. Flynn, et al. (2017). "Oceanic protists with different forms of acquired phototrophy display contrasting biogeographies and abundance". In: *Proceedings of the Royal Society B: Biological Sciences* 284.1860, pp. 20170664–20170664. ISSN: 0000000227681. DOI: 10.1098/rspb.2017.0664.

Leles, S. G., J. Bruggeman, L. Polimene, et al. (2021). "Differences in physiology explain succession of mixoplankton functional types and affect carbon fluxes in temperate seas". In: *Progress in Oceanography* 190, p. 102481. ISSN: 00796611. DOI: 10.1016/j.pocean.2020.102481.

Leles, S. G., A. Mitra, K. J. Flynn, et al. (2019). "Sampling bias misrepresents the biogeographical significance of constitutive mixotrophs across global oceans". In: *Global Ecology and Biogeography* 28.4, pp. 418–428. DOI: 10.1111/geb.12853.

Leles, S. G., L. Polimene, J. Bruggeman, et al. (2018). "Modelling mixotrophic functional diversity and implications for ecosystem function". In: *Journal of Plankton Research* 40.6, pp. 627–642. DOI: 10.1093/plankt/fby044.

Lin, C.-H., K. J. Flynn, A. Mitra, and P. M. Glibert (2018). "Simulating effects of variable stoichiometry and temperature on mixotrophy in the harmful dinoflagellate *Karlodinium veneficum*". In: *Frontiers in Marine Science* 5, p. 320. ISSN: 2296-7745. DOI: 10.3389/fmars.2018.00320.

Lindholm, T. (1985). "*Mesodinium rubrum*-a unique photosynthetic ciliate". In: *Advances in aquatic mirobiology* 3, p. 48.

Lindholm, T., P. Lindroos, and A. C. Mörk (1988). "Ultrastructure of the photosynthetic ciliate *Mesodinium rubrum*". In: *BioSystems* 21.2, pp. 141–149. DOI: 10.1016/0303-2647(88)90007-X.

Liu, H., X. Song, L. Huang, et al. (2012). "Potential risk of *Mesodinium rubrum* bloom in the aquaculture area of Dapeng'ao cove, China: diurnal changes in the ciliate community structure in the surface water". In: *Oceanologia* 54.1, pp. 109–117. ISSN: 00783234. DOI: 10.5697/oc.54-1.109.

Livanou, E., K. Barsakis, S. Psarra, and K. Lika (2020). "Modelling the nutritional strategies in mixotrophic nanoflagellates". In: *Ecological Modelling* 428, p. 109053. ISSN: 03043800. DOI: 10.1016/j.ecolmodel.2020.109053.

Lundgren, V. M., P. M. Glibert, E. Granéli, et al. (2016). "Metabolic and physiological changes in *Prymnesium parvum* when grown under, and grazing on prey of, variable nitrogen:phosphorus stoichiometry". In: *Harmful Algae* 55, pp. 1–12. ISSN: 15689883. DOI: 10.1016/j.hal.2016.01.002.

Mafra, L., S. Nagai, H. Uchida, et al. (2016). "Harmful effects of *Dinophysis* to the ciliate *Mesodinium rubrum*: Implications for prey capture". In: *Harmful Algae* 59, pp. 82–90. ISSN: 15689883. DOI: 10.1016/j.hal.2016.09.009.

Margalef, R. (1978). "Life-forms of phytoplankton as survival alternatives in an unstable environment". In: *Oceanologica Acta* 1.4, pp. 493–509.

Maselli, M., A. Altenburger, D. K. Stoecker, and P. J. Hansen (2020). “Ecophysiological traits of mixotrophic *Strombidium spp*”. In: *Journal of Plankton Research* 42.5. Ed. by J. Dolan, pp. 485–496. ISSN: 0142-7873, 1464-3774. DOI: 10.1093/plankt/fbaa041.

McFadden, G. I. (1993). “Second-hand chloroplasts: evolution of cryptomonad algae”. In: *Advances in Botanical Research*. Ed. by J. A. Callow. Vol. 19. C vols. London: Academic Press Limited, pp. 189–230. DOI: 10.1016/S0065-2296(08)60205-0.

McKie-Krisberg, Z. M., R. J. Gast, and R. W. Sanders (2015). “Physiological responses of three species of Antarctic mixotrophic phytoflagellates to changes in light and dissolved nutrients”. In: *Microbial Ecology* 70.1, pp. 21–29. ISSN: 1432-184X. DOI: 10.1007/s00248-014-0543-x.

McManus, G. B., H. Zhang, and S. Lin (2004). “Marine planktonic ciliates that prey on macroalgae and enslave their chloroplasts”. In: *Limnology and Oceanography* 49.1, pp. 308–313. DOI: 10.4319/lo.2004.49.1.0308.

McQuoid, M. R. and L. A. Hobson (1996). “Diatom resting stages”. In: *Journal of Phycology* 32.6, pp. 889–902. ISSN: 0022-3646. DOI: 10.1080/01418619108213945.

Meunier, C. L., K. Schulz, M. Boersma, and A. M. Malzahn (2013). “Impact of swimming behaviour and nutrient limitation on predator-prey interactions in pelagic microbial food webs”. In: *Journal of Experimental Marine Biology and Ecology* 446, pp. 29–35. ISSN: 0022-0981. DOI: 10.1016/j.jembe.2013.04.015.

Minnhagen, S., W. F. Carvalho, P. S. Salomon, and S. Janson (2008). “Chloroplast DNA content in *Dinophysis* (Dinophyceae) from different cell cycle stages is consistent with kleptoplasty”. In: *Environmental Microbiology* 10.9, pp. 2411–2417. DOI: 10.1111/j.1462-2920.2008.01666.x.

Minnhagen, S. and S. Janson (2006). “Genetic analyses of *Dinophysis spp.* support kleptoplastidy”. In: *FEMS Microbiology Ecology* 57.1, pp. 47–54. ISSN: 0168-6496. DOI: 10.1111/j.1574-6941.2006.00096.x.

Minnhagen, S., M. Kim, P. S. Salomon, et al. (2011). “Active uptake of kleptoplastids by *Dinophysis caudata* from its ciliate prey *Myrionecta rubra*”. In: *Aquatic Microbial Ecology* 62.1, pp. 99–108. DOI: 10.3354/ame01459.

Mitra, A., K. J. Flynn, J. M. Burkholder, et al. (2014). “The role of mixotrophic protists in the biological carbon pump”. In: *Biogeosciences* 11.4, pp. 995–1005. ISSN: 1726-4170. DOI: 10.5194/bg-11-995-2014.

Mitra, A. and K. J. Flynn (2005). “Predator-prey interactions: Is ’ecological stoichiometry’ sufficient when good food goes bad?” In: *Journal of Plankton Research* 27.5, pp. 393–399. DOI: 10.1093/plankt/fbi022.

Mitra, A. and K. J. Flynn (2006). “Promotion of harmful algal blooms by zooplankton predatory activity”. In: *Biology Letters* 2.2, pp. 194–197. DOI: 10.1098/rsbl.2006.0447.

Mitra, A. and K. J. Flynn (2010). “Modelling mixotrophy in harmful algal blooms: More or less the sum of the parts?” In: *Journal of Marine Systems* 83.3, pp. 158–169. ISSN: 09247963. DOI: 10.1016/j.jmarsys.2010.04.006.

Mitra, A., K. J. Flynn, U. Tillmann, et al. (2016). “Defining planktonic protist functional groups on mechanisms for energy and nutrient acquisition: incorporation of diverse mixotrophic strategies”. In: *Protist* 167.2, pp. 106–120. DOI: 10.1016/j.protis.2016.01.003.

Moeller, H. V., M. D. Johnson, and P. G. Falkowski (2011). “Photoacclimation in the phototrophic marine ciliate *Mesodinium rubrum* (ciliophora)”. In: *Journal of Phycology* 47.2, pp. 324–332. ISSN: 1529-8817. DOI: 10.1111/j.1529-8817.2010.00954.x.

Moeller, H. V., E. Peltomaa, M. D. Johnson, and M. G. Neubert (2016). “Acquired phototrophy stabilises coexistence and shapes intrinsic dynamics of an intraguild predator and its prey”. In: *Ecology Letters* 19.4, pp. 393–402. ISSN: 1461-0248. DOI: 10.1111/ele.12572.

Moestrup, j., L. Garcia-Cuetos, P. J. Hansen, and T. Fenchel (2012). “Studies on the genus *Mesodinium* I: Ultrastructure and description of *Mesodinium chamaeleon* n. sp., a benthic marine species with green or red chloroplasts”. In: *Journal of Eukaryotic Microbiology* 59.1, pp. 20–39. DOI: 10.1111/j.1550-7408.2011.00593.x.

Moita, M. T., L. Sobrinho-Gonçalves, P. B. Oliveira, S. Palma, and M. Falcão (2006). "A bloom of *Dinophysis acuta* in a thin layer off North-West Portugal". In: *African Journal of Marine Science* 28.2, pp. 265–269. ISSN: 1814232060. DOI: 10.2989/18142320609504160.

Moita, M. T., Y. Pazos, C. Rocha, R. Nolasco, and P. B. Oliveira (2016). "Toward predicting *Dinophysis* blooms off NW Iberia: A decade of events". In: *Harmful Algae* 53, pp. 17–32. DOI: 10.1016/J.HAL.2015.12.002.

Montagnes, D. J., J. Allen, L. Brown, et al. (2008). "Factors controlling the abundance and size distribution of the phototrophic ciliate *Myrionecta rubra* in open waters of the North Atlantic". In: *Journal of Eukaryotic Microbiology* 55.5, pp. 457–465. ISSN: 1066-5234. DOI: 10.1111/j.1550-7408.2008.00344.x.

Moorthi, S., R Ptacnik, R. Sanders, et al. (2017). "The functional role of planktonic mixotrophs in altering seston stoichiometry". In: *Aquatic Microbial Ecology* 79.3, pp. 235–245. ISSN: 0948-3055, 1616-1564. DOI: 10.3354/ame01832.

Morden, C. W. and A. R. Sherwood (2002). "Continued evolutionary surprises among dinoflagellates". In: *Proceedings of the National Academy of Sciences of the United States of America* 99.18, pp. 11558–11560. DOI: 10.1073/pnas.192456999.

Murphy, J. and J. P. Riley (1962). "A modified single solution method for the determination of phosphate in natural waters". In: *Analytica chimica acta* 27, pp. 31–36.

Myung, G, W Yih, H. Kim, J. Park, and B. Cho (2006). "Ingestion of bacterial cells by the marine photosynthetic ciliate *Myrionecta rubra*". In: *Aquatic Microbial Ecology* 44, pp. 175–180. ISSN: 0948-3055, 1616-1564. DOI: 10.3354/ame044175.

Nagai, S., T. Suzuki, T. Nishikawa, and T. Kamiyama (2011). "Differences in the production and excretion kinetics of okadaic acid, dinophysistoxin-1, and pectenotoxin-2 between cultures of *Dinophysis acuminata* and *Dinophysis fortii* isolated from western japan". In: *Journal of Phycology* 47.6, pp. 1326–1337. DOI: 10.1111/j.1529-8817.2011.01076.x.

Nam, S. W., W. Shin, M. Kang, W. Yih, and M. G. Park (2015). "Ultrastructure and molecular phylogeny of *Mesodinium coatsi* sp. nov., a benthic marine ciliate". In: *Journal of Eukaryotic Microbiology* 62.1, pp. 102–120. DOI: 10.1111/jeu.12150.

Needham, D. M., E. B. Fichot, E. Wang, et al. (2018). "Dynamics and interactions of highly resolved marine plankton via automated high-frequency sampling". In: *The ISME Journal* 12.10, pp. 2417–2432. ISSN: 1751-7362, 1751-7370. DOI: 10.1038/s41396-018-0169-y.

Nelson, D. M. and L. E. Brand (1979). "Cell division periodicity in 13 species of marine phytoplankton on a light:dark cycle". In: *Journal of Phycology* 15, pp. 67–75.

Nielsen, L. T. and T. Kiørboe (2015). "Feeding currents facilitate a mixotrophic way of life". In: *The ISME Journal* 9.10, pp. 2117–2127. DOI: 10.1038/ismej.2015.27.

Nielsen, L. T., B. Krock, and P. J. Hansen (2012). "Effects of light and food availability on toxin production, growth and photosynthesis in *Dinophysis acuminata*". In: *Marine ecology progress series.* 471, pp. 37–50. ISSN: 0171-8630. DOI: 10.3354/meps10027.

— (2013). "Production and excretion of okadaic acid, pectenotoxin-2 and a novel dinophysistoxin from the DSP-causing marine dinoflagellate *Dinophysis acuta* - Effects of light, food availability and growth phase". In: *Harmful Algae* 23, pp. 34–45. DOI: 10.1016/j.hal.2012.12.004.

Nishitani, G., K. Miyamura, and I. Imai (2003). "Trying to cultivation of *Dinophysis caudata* (Dinophyceae) and the appearance of small cells". In: *Plankton Biology and Ecology* 50.2, pp. 31–36.

Nishitani, G., S. Nagai, K. Baba, et al. (2010). "High-level congruence of *Myrionecta rubra* prey and *Dinophysis* species plastid identities as revealed by genetic analyses of isolates from Japanese coastal waters". In: *Applied and Environmental Microbiology* 76.9, pp. 2791–2798. DOI: 10.1128/AEM.02566-09.

Nishitani, G. and M. Yamaguchi (2018). "Seasonal succession of ciliate *Mesodinium* spp. with red, green, or mixed plastids and their association with cryptophyte prey". In: *Scientific reports* 8.1, pp. 17189–17189. DOI: 10.1038/s41598-018-35629-4.

Norén, F., j. Moestrup, and A.-S. Rehnstam-Holm (1999). "*Parvilucifera infectans* norén et moestrup gen. et sp. nov. (perkinsozoa phylum nov.): a parasitic flagellate capable of killing toxic microalgae". In: *European Journal of Protistology* 35.3, pp. 233–254. ISSN: 0932-4739. DOI: 10.1016/S0932-4739(99)80001-7.

Nézan, E. and N. Chomérat (2009). "*Fragilidium duplocampanaeforme* sp. nov. (Dinophyceae): A new phagotrophic dinoflagellate from the French Atlantic coast". In: *European Journal of Protistology* 45.1, pp. 2–12. ISSN: 09324739. DOI: 10.1016/j.ejop.2008.04.002.

Ojamäe, K., P. J. Hansen, and I. Lips (2016). "Mass entrapment and lysis of *Mesodinium rubrum* cells in mucus threads observed in cultures with *Dinophysis*". In: *Harmful Algae* 55, pp. 77–84. ISSN: 1568-9883. DOI: 10.1016/j.hal.2016.02.001.

Olenina, I., S. Hajdu, L. Edler, et al. (2006). "Biovolumes and size-classes of phytoplankton in the Baltic Sea". In: *HELCOM Baltic Sea Environment Proceedings* 106.357, pp. 144–144.

Olli, K. (1999). "Diel vertical migration of phytoplankton and heterotrophic flagellates in the Gulf of Riga". In: *Journal of Marine Systems* 23.1, pp. 145–163. ISSN: 0924-7963. DOI: 10.1016/S0924-7963(99)00055-X.

Oshima, Y., C. J. Bolch, and G. M. Hallegraeff (1992). "Toxin composition of resting cysts of *Alexandrium tamarense* (Dinophyceae)". In: *Toxicon* 30.12, pp. 1539–1544.

Packard, T. T., D. Blasco, and R. T. Barber (1978). "*Mesodinium rubrum* in the Baja California upwelling system". In: *Upwelling ecosystems*. Springer, pp. 73–89.

Park, J. H., M. Kim, H. J. Jeong, and M. G. Park (2019). "Revisiting the taxonomy of the "*Dinophysis acuminata* complex" (Dinophyta)". In: *Harmful Algae* 88, pp. 101657–101657. DOI: 10.1016/j.hal.2019.101657.

Park, J. S., G. Myung, H. S. Kim, B. C. Cho, and W. Yih (2007). "Growth responses of the marine photosynthetic ciliate *Myrionecta rubra* to different cryptomonad strains". In: *Aquatic Microbial Ecology* 48.1, pp. 83–90. ISSN: 0948-3055. DOI: 10.3354/ame048083.

Park, M., J. Park, M. Kim, and W. Yih (2008). "Plastid dynamics during survival of *Dinophysis caudata* without its ciliate prey". In: *Journal of Phycology* 44.5, pp. 1154–1163. DOI: 10.1111/j.1529-8817.2008.00579.x.

Park, M. G. and M. Kim (2010). "Prey specificity and feeding of the thecate mixotrophic dinoflagellate *Fragilidium duplocampanaeforme*". In: *Journal of Phycology* 46.3, pp. 424–432. ISSN: 00223646, 15298817. DOI: 10.1111/j.1529-8817.2010.00824.x.

Park, M. G., M. Kim, S. Kim, and W. Yih (2010). "Does *Dinophysis caudata* (Dinophyceae) have permanent plastids?" In: *Journal of Phycology* 46.2, pp. 236–242. ISSN: 0022-3646. DOI: 10.1111/j.1529-8817.2009.00777.x.

Park, M. G., S. Kim, H. S. Kim, et al. (2006). "First successful culture of the marine dinoflagellate *Dinophysis acuminata*". In: *Aquatic Microbial Ecology* 45.2, pp. 101–106. ISSN: 0948-3055. DOI: 10.3354/ame045101.

Passow, U (2002). "Transparent exopolymer particles (TEP) in aquatic environments". In: *Progress in Oceanography* 55.3, pp. 287–333. DOI: 10.1016/S0079-6611(02)00138-6.

Peltomaa, E. and M. D. Johnson (2017). "*Mesodinium rubrum* exhibits genus-level but not species-level cryptophyte prey selection". In: *Aquatic Microbial Ecology* 78.3, pp. 147–159. DOI: 10.3354/ame01809.

Peterson, T. D., R. L. Golda, M. L. Garcia, et al. (2013). "Associations between *Mesodinium rubrum* and cryptophyte algae in the Columbia River estuary". In: *Aquatic Microbial Ecology* 68, pp. 117–130. DOI: 10.3354/ame01598.

Pinto, L., M. Mateus, and A. Silva (2016). "Modeling the transport pathways of harmful algal blooms in the Iberian coast". In: *Harmful Algae* 53, pp. 8–16. ISSN: 15689883. DOI: 10.1016/j.hal.2015.12.001.

Pitcher, G. C., A. Jiménez, and B. Reguera (2017). "Harmful algal blooms in eastern boundary upwelling systems: A GEOHAB Core Research Project". In: *Oceanography* 30.1, pp. 22–35. DOI: 10.5670/oceanog.2017.107..

Pitta, P., A. Giannakourou, and U. Christaki (2001). “Planktonic ciliates in the oligotrophic Mediterranean Sea: Longitudinal trends of standing stocks, distributions and analysis of food vacuole contents”. In: *Aquatic Microbial Ecology* 24.3, pp. 297–311. DOI: 10.3354/ame024297.

Prézelin, B. B. and O Schofield (1989). “Blue-green light effects on light-limited rates of photosynthesis: relationship to pigmentation and productivity estimates for *Synechococcus* populations from the Sargasso Sea”. In: *Marine Ecology Progress Series* 54, pp. 121–139.

Ptacnik, R., U. Sommer, T. Hansen, and V. Martens (2004). “Effects of microzooplankton and mixotrophy in an experimental planktonic food web”. In: *Limnology and Oceanography* 49.4, pp. 1435–1445. ISSN: 0024-3590. DOI: 10.4319/lo.2004.49.4_part_2.1435.

Raine, R., G. McDermott, J. Silke, et al. (2010). “A simple short range model for the prediction of harmful algal events in the bays of southwestern Ireland”. In: *Journal of Marine Systems* 83.3, pp. 150–157. ISSN: 09247963. DOI: 10.1016/j.jmarsys.2010.05.001.

Rao, D. and Y. Pan (1993). “Photosynthetic characteristics of *Dinophysis norvegica* Claparede & Lachmann, a red-tide dinoflagellate”. In: *Journal of Plankton Research* 15.8, pp. 965–976. ISSN: 0142-7873, 1464-3774. DOI: 10.1093/plankt/15.8.965.

Raven, J. A. and P. G. Falkowski (1999). “Oceanic sinks for atmospheric CO_2”. In: *Plant, Cell and Environment* 22.6, pp. 741–755. ISSN: 0140-7791, 1365-3040. DOI: 10.1046/j.1365-3040.1999.00419.x.

Redfield, A. C., B. H. Ketchum, and F. A. Richards (1963). “The influence of organisms on the composition of sea water”. In: *The sea: ideas and observations on progress in the study of the seas* 2, pp. 26–77. ISSN: 9780674017283.

Reguera, B. and S. González-Gil (2001). “Small cell and intermediate cell formation in species of *Dinophysis* (Dinophyceae, Dinophysiales)”. In: *Journal of Phycology* 37.2, pp. 318–333. ISSN: 0022-3646. DOI: 10.1046/j.1529-8817.2001.037002318.x.

Reguera, B. and S. González-Gil (2007). “*Dinophysis diegensis* is a life history stage of *Dinohysis caudata* (Dinophycae, Dinophysiales)”. In: *Phycological Society of America* 43, pp. 1083–1093.

Reguera, B., P. Riobó, F. Rodríguez, et al. (2014). “*Dinophysis* toxins: Causative organisms, distribution and fate in shellfish”. In: *Marine Drugs* 12.1, pp. 394–461. ISSN: 1660-3397. DOI: 10.3390/md12010394.

Reguera, B., L. Velo-Suárez, R. Raine, and M. G. Park (2012). “Harmful *Dinophysis* species: A review”. In: *Harmful Algae* 14, pp. 87–106. ISSN: 1568-9883. DOI: 10.1016/j.hal.2011.10.016.

Reynolds, C. S. (2006). “Pelagic Ecology”. In: *Encyclopedia of Environmetrics*. DOI: 10.1002/9780470057339.vap008.pub2.

Rial, P., J. L. Garrido, D. Jaén, and F. Rodríguez (2013). “Pigment composition in three *Dinophysis* species (Dinophyceae) and the associated cultures of *Mesodinium rubrum* and *Teleaulax amphioxeia*”. In: *Journal of Plankton Research* 35.2, pp. 433–437. ISSN: 0142-7873. DOI: 10.1093/plankt/fbs099.

Rial, P., A. Laza-Martínez, B. Reguera, N. Raho, and F. Rodríguez (2015). “Origin of cryptophyte plastids in *Dinophysis* from Galician waters: Results from field and culture experiments”. In: *Aquatic Microbial Ecology* 76.2, pp. 163–174. DOI: 10.3354/ame01774.

Riisgaard, K. and P. J. Hansen (2009). “Role of food uptake for photosynthesis, growth and survival of the mixotrophic dinoflagellate *Dinophysis acuminata*”. In: *Marine Ecology Progress Series* 381, pp. 51–62. ISSN: 0171-8630. DOI: 10.3354/meps07953.

Riisgård, H. U. and P. S. Larsen (2009). “Ciliary-propelling mechanism, effect of temperature and viscosity on swimming speed, and adaptive significance of ’jumping’ in the ciliate *Mesodinium rubrum*”. In: *Marine Biology Research* 5.6, pp. 585–595. ISSN: 1745-1000. DOI: 10.1080/17451000902729704.

Riobó, P., B. Reguera, J. Franco, and F. Rodríguez (2013). “First report of the toxin profile of *Dinophysis sacculus* Stein from LC–MS analysis of laboratory cultures”. In: *Toxicon* 76, pp. 221–224. ISSN: 00410101. DOI: 10.1016/j.toxicon.2013.10.012.

Rodríguez, F., L. Escalera, B. Reguera, et al. (2012). “Morphological variability, toxinology and genetics of the dinoflagellate *Dinophysis tripos* (Dinophysiaceae, Dinophysiales)”. In: *Harmful Algae* 13, pp. 26–33. DOI: 10.1016/j.hal.2011.09.012.

Rothschild, B. J. and T. R. Osborn (1988). “Small-scale turbulence and plankton contact rates”. In: *Journal of Plankton Research* 10.3, pp. 465–474. ISSN: 0142-7873. DOI: 10.1093/plankt/10.3.465.

Ruiz-Villarreal, M., L. M. García-García, M. Cobas, P. A. Díaz, and B. Reguera (2016). “Modelling the hydrodynamic conditions associated with *Dinophysis* blooms in Galicia (NW Spain)”. In: *Harmful Algae* 53, pp. 40–52. ISSN: 15689883. DOI: 10.1016/j.hal.2015.12.003.

Rusterholz, P. M., P. J. Hansen, and N. Daugbjerg (2017). “Evolutionary transition towards permanent chloroplasts? - Division of kleptochloroplasts in starved cells of two species of *Dinophysis* (Dinophyceae)”. In: *PLoS ONE* 12.5. DOI: 10.1371/journal.pone.0177512.

Salgado, X. Álvarez, F. Figueiras, M. Fernández-Reiriz, et al. (2011). “Control of lipophilic shellfish poisoning outbreaks by seasonal upwelling and continental runoff”. In: *Harmful Algae* 10.2, pp. 121–129. ISSN: 15689883. DOI: 10.1016/j.hal.2010.08.003.

Sallée, J.-B., V. Pellichero, C. Akhoudas, et al. (2021). “Summertime increases in upper-ocean stratification and mixed-layer depth”. In: *Nature* 591.7851, pp. 592–598. DOI: 10.1038/s41586-021-03303-x.

Sanders, R. W., K. G. Porter, and D. A. Caron (1990). “Relationship between phototrophy and phagotrophy in the mixotrophic chrysophyte *Poterioochromonas malhamensis*”. In: *Microbial Ecology* 19.1, pp. 97–109. DOI: 10.1007/BF02015056.

Sanders, R. (1995). “Seasonal distributions of the photosynthesizing ciliates *Laboea strobila* and *Myrionecta rubra* (= *Mesodinium rubrum*) in an estuary of the Gulf of Maine”. In: *Aquatic Microbial Ecology* 9, pp. 237–242. ISSN: 0948-3055, 1616-1564. DOI: 10.3354/ame009237.

Savvidis, Y. G., D. P. Patoucheas, G Nikolaidis, and C. G. Koutitas (2011). “Modelling the dispersion of harmful algal bloom (HAB) in the Thermaikos Gulf (NW Aegean Sea)”. In: *Global Nest Journal* 13.2, pp. 119–129. ISSN: 1790-7632. DOI: 10.30955/gnj.000670.

Schoener, D. M. and G. B. McManus (2012). “Plastid retention, use, and replacement in a kleptoplastidic ciliate”. In: *Aquatic Microbial Ecology* 67.3, pp. 177–187. DOI: 10.3354/ame01601.

Schoener, D. M. and G. B. McManus (2017). “Growth, grazing, and inorganic C and N uptake in a mixotrophic and a heterotrophic ciliate”. In: *Journal of Plankton Research* 39.3, pp. 379–391. DOI: 10.1093/plankt/fbx014.

Seeyave, S, T. A. Probyn, G. C. Pitcher, M. I. Lucas, and D. A. Purdie (2009). “Nitrogen nutrition in assemblages dominated by *Pseudo-nitzschia* spp., *Alexandrium catenella* and *Dinophysis acuminata* off the west coast of South Africa”. In: *Marine Ecology Progress Series* 379, pp. 91–107. ISSN: 0171-8630. DOI: 10.3354/meps07898.

Sekerci, Y. and R. Ozarslan (2020). “Oxygen-plankton model under the effect of global warming with nonsingular fractional order”. In: *Chaos, Solitons & Fractals* 132, p. 109532. ISSN: 09600779. DOI: 10.1016/j.chaos.2019.109532.

Sjöqvist, C. O. and T. J. Lindholm (2011). “Natural co-occurrence of *Dinophysis acuminata* (Dinoflagellata) and *Mesodinium rubrum* (Ciliophora) in thin layers in a coastal inlet”. In: *Journal of Eukaryotic Microbiology* 58.4, pp. 365–372. DOI: 10.1111/j.1550-7408.2011.00559.x.

Skovgaard, A. (1996). “Mixotrophy in *Fragilidium subglobosum* (Dinophyceae): growth and grazing responses as functions of light intensity”. In: *Marine Ecology Progress Series* 143, pp. 247–253.

Skovgaard, A., P. J. Hansen, and D. K. Stoecker (2000). “Physiology of the mixotrophic dinoflagellate *Fragilidium subglobosum*. I. Effects of phagotrophy and irradiance on photosynthesis and carbon content”. In: *Marine Ecology Progress Series* 201, pp. 129–136. DOI: 10.3354/meps201129.

Smayda, T. J. (1997). “Harmful algal blooms: Their ecophysiology and general relevance to phytoplankton blooms in the sea”. In: *Limnology and Oceanography* 42.5, pp. 1137–1153.

— (2002). “Turbulence, watermass stratification and harmful algal blooms: an alternative view and frontal zones as “pelagic seed banks””. In: *Harmful Algae* 1.1, pp. 95–112. ISSN: 15689883. DOI: 10.1016/S1568-9883(02)00010-0.

Smith, E. L. (1936). “Photosynthesis in relation to light and carbon dioxide”. In: *Proceedings of the National Academy of Sciences* 22.8, pp. 504–511. DOI: 10.1073/pnas.22.8.504.

Smith, J. L., M. Tong, D. Kulis, and D. M. Anderson (2018). “Effect of ciliate strain, size, and nutritional content on the growth and toxicity of mixotrophic *Dinophysis acuminata*”. In: *Harmful Algae* 78, pp. 95–105. ISSN: 15689883. DOI: 10.1016/j.hal.2018.08.001.

Smith, M. and P. J. Hansen (2007). “Interaction between *Mesodinium rubrum* and its prey: Importance of prey concentration, irradiance and pH”. In: *Marine Ecology Progress Series* 338.1954, pp. 61–70. ISSN: 0171-8630. DOI: 10.3354/meps338061.

Soetaert, K. and P. M. J. Herman (2009). *A practical guide to ecological modelling: using R as a simulation platform*. Dordrecht: Springer. 372 pp. ISBN: 978-1-4020-8623-6 978-1-4020-8624-3.

Solomonson, L. P. and M. J. Barber (1990). “Assimilatory nitrate reductase: functional properties and regulation”. In: *Annual review of plant biology* 41.1, pp. 225–253.

Souza, C. Alves-de, D. Varela, C. Contreras, et al. (2014). “Seasonal variability of *Dinophysis* spp. and *Protoceratium reticulatum* associated to lipophilic shellfish toxins in a strongly stratified Chilean fjord”. In: *Deep-Sea Research Part II: Topical Studies in Oceanography* 101, pp. 152–162. DOI: 10.1016/j.dsr2.2013.01.014.

Stern, R. F., A. L. Amorim, and E. Bresnan (2014). “Diversity and plastid types in *Dinophysis acuminata* complex (Dinophyceae) in Scottish waters”. In: *Harmful Algae* 39, pp. 223–231. DOI: 10.1016/j.hal.2014.07.013.

Sterner, R. W. and J. J. Elser (2002). *Ecological stoichiometry: the biology of elements from molecules to the biosphere*. Princeton university press. ISBN: 0-691-07491-7.

Stickney, H. L., R. R. Hood, and D. K. Stoecker (2000). “The impact of mixotrophy on planktonic marine ecosystems”. In: *Ecological Modelling* 125, pp. 203–230.

Stoecker, D. K. (1998). “Conceptual models of mixotrophy in planktonic protists and some ecological and evolutionary implications”. In: *European Journal of Protistology* 34.3, pp. 281–290. ISSN: 0932-4739. DOI: 10.1016/S0932-4739(98)80055-2.

Stoecker, D. K., P. J. Hansen, D. A. Caron, and A. Mitra (2016). “Mixotrophy in the marine plankton”. In: *Annual Review of Marine Science* 9.1, pp. 311–335. DOI: 10.1146/annurev-marine-010816-060617.

Stoecker, D. K., M. D. Johnson, C. De Vargas, and F. Not (2009). “Acquired phototrophy in aquatic protists”. In: *Aquatic Microbial Ecology* 57.3, pp. 279–310. ISSN: 0948-3055. DOI: 10.3354/ame01340.

Stoecker, D. K. and P. J. Lavrentyev (2018). “Mixotrophic plankton in the polar seas: a pan-Arctic review”. In: *Frontiers in Marine Science* 5.292. DOI: 10.3389/fmars.2018.00292.

Strom, S. L. (2001). “Light-aided digestion, grazing and growth in herbivorous protists”. In: *Aquatic Microbial Ecology* 23, pp. 253–261. ISSN: 0948-3055. DOI: 10.1088/0256-307X/23/7/022.

Suzuki, T., A. Miyazono, K. Baba, R. Sugawara, and T. Kamiyama (2009). “LC-MS/MS analysis of okadaic acid analogues and other lipophilic toxins in single-cell isolates of several *Dinophysis* species collected in Hokkaido, Japan”. In: *Harmful Algae* 8.2, pp. 233–238. DOI: 10.1016/j.hal.2008.06.001.

Syrett, P. J. (1981). “Nitrogen metabolism of microalgae”. In: *Physiological bases of phytoplankton ecology. Canadian Bulletin of Fisheries and Aquatic Science* 210. Ed. by T. Platt, pp. 182–210.

Takishita, K., K. Kolke, T. Maruyama, and T. Ogata (2002). “Molecular evidence for plastid robbery (kleptoplastidy) in *Dinophysis*, a dinoflagellate causing diarrhetic shellfish poisoning”. In: *Protist*. ISSN: 1434-4610. DOI: 10.1078/1434-4610-00106.

Tamar, H. (1979). “The movements of jumping ciliates”. In: *Archiv für Protistenkunde* 122.3, pp. 290–327. DOI: 10.1016/S0003-9365(79)80040-8.

Tang, E. P. Y. (1995). “The allometry of algal growth rates”. In: *Journal of Plankton Research* 17.6, pp. 1325–1335.

Taylor, F. J. R (1976). “Dinoflagellates from the international Indian Ocean expedition”. In: *Bibliotheca Botanica* 43, pp. 234–234.

Taylor, F. J. R., D. J. Blackbourn, and J. Blackbourn (1971). “The red-water ciliate *Mesodinium rubrum* and its "incomplete symbionts": A review including new ultrastructural observations”. In: *Journal of Fisheries Research Board of Canada* 28, 391:407.

Thingstad, T. F., M. Krom, R. F. C. Montoura, et al. (2005). “Nature of phosphorus limitation in the ultraoligotrophic Eastern Mediterranean”. In: *Science* 309.5737, pp. 1068–1071. ISSN: 0036-8075, 1095-9203. DOI: 10.1126/science.1112632.

Thingstad, T. F., H. Havskum, K. Garde, and B. Riemann (1996). “On the strategy of "eating your competitor": a mathematical analysis of algal mixotrophy”. In: *Ecology* 77.7, pp. 2108–2118. DOI: 10.2307/2265705.

Thomas, W. H. and C. H. Gibson (1990). “Effects of small-scale turbulence on microalgae”. In: *Journal of Applied Phycology* 2, pp. 71–77.

Tong, M., Q. Zhou, K. M. David, et al. (2010). “Culture techniques and growth characteristics of *Dinophysis acuminata* and its prey”. In: *Chinese Journal of Oceanology and Limnology* 28.6, pp. 1230–1239. ISSN: 0254-4059\R1993-5005. DOI: 10.1007/s00343-010-9960-y.

Traboni, C., A. Calbet, and E. Saiz (2020). “Effects of prey trophic mode on the gross-growth efficiency of marine copepods: the case of mixoplankton”. In: *Scientific Reports* 10.1, p. 12259. ISSN: 2045-2322. DOI: 10.1038/s41598-020-69174-w.

Turpin, D. H. and A. G. Miller (1985). “Predicting the kinetics of dissolved inorganic carbon limited growth from the short-term kinetics of photosynthesis in *Synechococcus leopliensis* (Cyanophyta)”. In: *Journal of Phycology* 21, pp. 409–418.

Šupraha, L., S. Bosak, Z. Ljubešić, et al. (2014). “Cryptophyte bloom in a Mediterranean estuary: High abundance of *Plagioselmis cf. prolonga* in the Krka River estuary (eastern Adriatic Sea)”. In: *Scientia Marina* 78.3, pp. 329–338. ISSN: 1886-8134, 0214-8358. DOI: 10.3989/scimar.03998.28C.

Vale, P., M. J. Botelho, S. M. Rodrigues, S. S. Gomes, and M. A. d. M. Sampayo (2008). “Two decades of marine biotoxin monitoring in bivalves from Portugal (1986–2006): A review of exposure assessment”. In: *Harmful Algae* 7.1, pp. 11–25. ISSN: 15689883. DOI: 10.1016/j.hal.2007.05.002.

Velo-Suárez, L., S. González-Gil, Y. Pazos, and B. Reguera (2014). “The growth season of *Dinophysis acuminata* in an upwelling system embayment: A conceptual model based on in situ measurements”. In: *Deep-Sea Research Part II: Topical Studies in Oceanography* 101, pp. 141–151. DOI: 10.1016/j.dsr2.2013.03.033.

Velo-Suárez, L. and J. Gutiérrez-Estrada (2007). “Artificial neural network approaches to one-step weekly prediction of *Dinophysis acuminata* blooms in Huelva (Western Andalucía, Spain)”. In: *Harmful Algae* 6.3, pp. 361–371. ISSN: 15689883. DOI: 10.1016/j.hal.2006.11.002.

Velo-Suárez, L., B. Reguera, S. González-Gil, et al. (2010). “Application of a 3D Lagrangian model to explain the decline of a *Dinophysis acuminata* bloom in the Bay of Biscay”. In: *Journal of Marine Systems* 83.3, pp. 242–252. DOI: 10.1016/j.jmarsys.2010.05.011.

Velo-Suárez, L., S. G. Gil, P. Gentien, et al. (2008). “Thin layers of *Pseudo-nitzschia* spp. and the fate of *Dinophysis acuminata* during an upwelling-downwelling cycle in a Galician Ría”. In: *Limnology and Oceanography* 53.5, pp. 1816–1834. ISSN: 00243590. DOI: 10.4319/lo.2008.53.5.1816.

Våge, S., M. Castellani, J. Giske, and F. Thingstad T (2013). “Successful strategies in size structured mixotrophic food webs”. In: *Aquatic Ecology* 47.123, pp. 329–347. DOI: 10.1007/s10452-013-9447-y.

Waal, D. B. Van de, U. John, P. Ziveri, et al. (2013). “Ocean acidification reduces growth and calcification in a marine dinoflagellate”. In: *PLoS ONE* 8.6, pp. 65987–65987. DOI: 10.1371/journal.pone.0065987.

Waal, D. B. Van de, A. M. Verschoor, J. M. Verspagen, E. Van Donk, and J. Huisman (2010). “Climate-driven changes in the ecological stoichiometry of aquatic ecosystems”. In: *Frontiers in Ecology and the Environment* 8.3, pp. 145–152. ISSN: 1540-9295. DOI: 10.1890/080178.

Ward, B. A., S. Dutkiewicz, A. D. Barton, and M. J. Follows (2011). “Biophysical aspects of resource acquisition and competition in algal mixotrophs”. In: *The American Naturalist* 178.1, pp. 98–112. DOI: 10.1086/660284.

Ward, B. A. and M. J. Follows (2016). “Marine mixotrophy increases trophic transfer efficiency, mean organism size, and vertical carbon flux”. In: *Proceedings of the National Academy of Sciences* 113.11, pp. 2958–2963. DOI: 10.1073/pnas.1517118113.

Wawrik, B., A. V. Callaghan, and D. A. Bronk (2009). “Use of inorganic and organic nitrogen by *Synechococcus* spp. and diatoms on the West Florida Shelf as measured using stable isotope probing”. In: *Applied and Environmental Microbiology* 75.21, pp. 6662–6670. ISSN: 0099-2240, 1098-5336. DOI: 10.1128/AEM.01002-09.

Wilken, S., C. J. Choi, and A. Z. Worden (2020). “Contrasting mixotrophic lifestyles reveal different ecological niches in two closely related marine protists”. In: *Journal of Phycology* 56.1, pp. 52–67. ISSN: 0022-3646, 1529-8817. DOI: 10.1111/jpy.12920.

Wilken, S., C. C. M. Yung, M. Hamilton, et al. (2019). “The need to account for cell biology in characterizing predatory mixotrophs in aquatic environments”. In: *Philosophical Transactions of the Royal Society B* 375.20190090, p. 13. DOI: 10.1098/rstb.2019.009.

Wilkerson, F. P. and G. Grunseich (1990). “Formation of blooms by the symbiotic ciliate *Mesodinium rubrum*: the significance of nitrogen uptake”. In: *Journal of Plankton Research* 12.5, pp. 973–989.

Yasumoto, T., M. Murata, Y. Oshima, et al. (1985). “Diarrhetic shellfish toxins”. In: *Tetrahedron* 41.6, pp. 1019–1025. DOI: 10.1016/S0040-4020(01)96469-5.

Yih, W., S. K. Hyung, J. J. Hae, G. Myung, and G. K. Young (2004). “Ingestion of cryptophyte cells by the marine photosynthetic ciliate *Mesodinium rubrum*”. In: *Aquatic Microbial Ecology* 36.2, pp. 165–170. DOI: 10.3354/ame036165.

Yih, W., H. S. Kim, G. Myung, et al. (2013). “The red-tide ciliate *Mesodinium rubrum* in Korean coastal waters”. In: *Harmful Algae* 30 (SUPPL.1), S53–S61. ISSN: 1568-9883. DOI: 10.1016/j.hal.2013.10.006.

Yoo, J. S., I. K. Lee, and Y. H. Kim (1991). “Recolonization of the disturbed benthic algal community in Inchon Dock”. In: *The Korean Journal of Botany (Korea Republic)*.

Yoo, J.-S., J.-H. Lee, and Y. Fukuyo (1998). “Red Tide Organism: Ciliate *Mesodinium rubrum rubrum* (Lohmann) Hamburger et Buddenbrock”. In: *Algae* 13.1, pp. 143–149.

Yoo, Y. D., K. A. Seong, H. J. Jeong, et al. (2017). “Mixotrophy in the marine red-tide cryptophyte *Teleaulax amphioxeia* and ingestion and grazing impact of cryptophytes on natural populations of bacteria in Korean coastal waters”. In: *Harmful Algae* 68, pp. 105–117. DOI: 10.1016/j.hal.2017.07.012.

Yool, A., E. E. Popova, and T. R. Anderson (2011). “Medusa-1.0: a new intermediate complexity plankton ecosystem model for the global domain”. In: *Geoscientific Model Development* 4.2, pp. 381–417. ISSN: 1991-9603. DOI: 10.5194/gmd-4-381-2011.

Yool, A, E. E. Popova, and T. R. Anderson (2013). “MEDUSA-2.0: an intermediate complexity biogeochemical model of the marine carbon cycle for climate change and ocean acidification studies”. In: *Geoscientific Model Development* 6.5, pp. 1767–1811. DOI: 10.5194/gmd-6-1767-2013.

Zingel, P., H. Agasild, K. Karus, L. Buholce, and T. Nõges (2019). “Importance of ciliates as food for fish larvae in a shallow sea bay and a large shallow lake”. In: *European Journal of Protistology* 67, pp. 59–70. DOI: 10.1016/j.ejop.2018.10.004.

Zubkov, M. and G. Tarran (2005). “Amino acid uptake of *Prochlorococcus* spp. in surface waters across the South Atlantic Subtropical Front”. In: *Aquatic Microbial Ecology* 40, pp. 241–249. ISSN: 0948-3055, 1616-1564. DOI: 10.3354/ame040241.

Appendix A

Supplementary Material for N-based TMD-model - model equations

TABLE A.1: Equations of the nitrogen-based *Teleaulax-Mesodinium-Dinophysis* model. The equations are sorted in first order by organisms they apply to in column O (S = *Synechococcus*, A = alga, T = *Teleaulax amphioxeia*, M = *Mesodinium rubrum*, D = *Dinophysis acuminata*). The equations are sorted by variable type (VT; A = auxiliary, C = constant, SV = state variable) in second order, by the submodel they belong to in third order and by the variable name (VN) in fourth order.

o	vn	vt	equations and values	unit	description
S	NC_	C	0.133	gN gC-1	Redfield ratio for N:C (mole 16:105) for *Synechococcus* (Turpin et al. 2004)
S	percent_	C	15*5/100		proportion of nitrogen *Synechococcus* of total nutrient load
S	BR_	C	1.5*0.05	dl	Scaler for basal respiration rate in *Synechococcus* for reference to maximum growth rate (on the basis that faster growing species have inherent higher BR rates); ca 5 % of the umax_Syn (Grobbelaar et al. 1991)
S	Umax_	C	0.86	gN (gN)-1 d-1	*Synechococcus* maximum N-specific growth rate at neutral temperature, 1.5 d-1 (Campbell & Carpenter 1986)
S	ChlC_	C	0.042	gChl (gC)-1	Mass ratio content of chlorophyll:C in Alg. No photoacclimation is assumed, so this is de facto the maximum content. *Synechococcus* (Broddrick et al. 2019)
S	Knh4_	C	14	mgN m-3	*Synechococcus* half saturation constant for ammonium
S	Kno3_	C	20.02	mgN m-3	*Synechococcus* half saturation constant for nitrate (Franck et al. 2003)
S	alpha_Chl_	C	5.56E-06	(m2 g-1 chl.a)* (gC µmol-1 photon)	Slope of Chl-specific PE curve (Prézelin and Schofield), *Synechococcus*
S	thres_	C	1.46E-03	mgN m-3	Threshold for predation on *Synechococcus* (1000 cells per mL = 10e6 cells L-1) *Synechococcus* builds clusters
S	tox_	C	0	dl	Toxicity factor for *Synechococcus*; 0 not toxic

Continued on next page

Table A.1 continued from previous page

o	vn	vt	equations and values	unit	description
S	r_	C	0.98/2	µm	radius of *Synechococcus* cell (ESD devided by 2), average = 1.15 (Zubkov and Tarran 2005; Yoo et al 2017)
S	Ccell_	A	a*(4/3*PI*(r_Syn)^3)^b	pgC cell-1	C content of Alg
S	Ncell_	A	Ccell_Syn*NC_Syn	pg N cell-1	N content per cell of *Synechococcus*
S	nos_	A	10^9**Synechococcus*/Ncell_Syn	Alg cells (m3)-1	Cell abundance of *Synechococcus*
S	v_	A	(10^-6)*(38.542*(r_Syn*2)^0.5424)*0	m s-1	speed of motility of *Synechococcus*
S	Inoc_	A	N_load*percent_Syn/100	µg N L-1	nitrogen initial inoculation of Alg1
S	death_	A	IF(*Synechococcus*>1e-9, *Synechococcus**death_con,0)	mgN m-3 d-1	*Synechococcus* continous death rate
S	DON_	A	IF(*Synechococcus*>1e-9,vDON_up**Synechococcus*)	mgN m-3 d-1	Synechoccus population growth rate supported by labile DON
S	DONout_	A	IF(*Synechococcus*>1e-9,*Synechococcus**DON_leak,0)	mgN m-3 d-1	DON leak from Synechoccus
S	Nu_Syn_rate	A	(Nu_Syn-Nu_Syn_alt)*10	dl	N-status of Synechoccus (averaged)
S	U_Syn_alt	A	(uTP_Syn-uAV_Syn_alt)*10	gN (gN)-1 d-1	growth rate of Synechoccus (average intermediate)
S	upnh4_	A	IF(*Synechococcus*>1e-9, IF(netRegN_Syn<Vnh4_Syn, *Synechococcus**(Vnh4_Syn-netRegN_Syn),0) ,0)	mgN m-3 d-1	Synechoccus population growth rate supported by ammonium. NOTE the release of NH4 during darkness with reg_Syn!
S	upno3_	A	IF(*Synechococcus*>1e-9, *Synechococcus**Vno3_Syn)	mgN m-3 d-1	Synechoccus population growth rate supported by nitrate
S	wash_	A	dil**Synechococcus*	mgN m-3 d-1	*Synechoccus* washout by dilution
S	washin_	A	dil*(Inoc_Syn)*0.2*Sw_land_runoff	mgN m-3 d-1	Synechoccus washin by dilution
S	maxGPS_	A	UmT_Syn*(1+BR_Syn)	N/N/d	gross assimilation needed to support UmT_Syn
S	abco_	A	abco_Chl*ChlC_Syn/NC_Syn	m2 (mgN)-1	Phytoplankton-N2 specific coefficient for light absorbance

Continued on next page

Table A.1 continued from previous page

o	vn	vt	equations and values	unit	description
S	attco_	A	*Synechococcus**abco_Syn	m-1	Attenuation coefficient to phytoplankton2 N-biomass
S	Ndem_	A	PS_Syn*(1-MR)	N/N/d N	demand to satisfy concurrent photosynthesis corrected for MR costs; Synechoccus
S	netRegN_	A	IF(RegN_Syn>Ndem_Syn, RegN_Syn-Ndem_Syn,0)	N/N/d	net regeneration of N which occurs if internal regeneration of N exceeds the concurrent demands driven by incoming PS; Synechoccus
S	PAss_	A	PS_Syn*(1-MR)	N/N/d	net phototrophy, from gross phototrophy minus the cost of anabolism required for incorportion of DIN. This is set by MR, but in reality it is affected by the f-ratio as far more effort is required to reduce NO3 to NH4 within the cell. Synechoccus
S	PVnh4_	A	IF(NH4>(14*0.01), maxGPS_Syn*TGnh4_Syn*NH4/ (NH4+Knh4_Syn),0)	gN (gN)-1 d-1	Synechoccus potential NH4 supply as transport PLUS the current internal regeneration of NH4
S	PVno3_	A	IF(NO3>(14*0.01), maxGPS_Syn*TGno3_Syn*NO3/ (NO3+Kno3_Syn),0)	gN (gN)-1 d-1	Synechoccus potential nitrate transport; light dependent
S	RegN_	A	UmT_Syn*BR_Syn	N/N/d	regeneration rate through basal respiration for Synechoccus
S	TGnh4_	A	Umax_Syn*NC_Syn*10	dl	*Synechococcus* transport:growth needs ratio for ammonium
S	TGno3_	A	Umax_Syn*NC_Syn*2	dl	*Synechococcus* transport:growth needs ratio for nitrate
S	Vnh4_	A	MIN(uTP_Syn,PVnh4_Syn)	gN (gN)-1 d-1	Synechoccus potential usage of ammonium
S	Vno3_	A	IF(uTP_Syn>PVnh4_Syn, MIN((uTP_Syn-PVnh4_Syn),PVno3_Syn),0)	gN (gN)-1 d-1	Synechoccus potential usage of nitrate
S	uTP_	A	IF(RegN_Syn<Ndem_Syn, Ndem_Syn-RegN_Syn,0)	N/N/d	net incorporation of DIN with phototrophy after usage of internally regenerated NH4 for Synechoccus

Continued on next page

Table A.1 continued from previous page

o	vn	vt	equations and values	unit	description
S	alphau_	A	alpha_Chl_Syn*ChlC_Syn	(m2)*(µmol-1 photon)	Specific slope of PE curve; Synechoccus
S	Nu_	A	MIN(1, (RegN_Syn+PVnh4_Syn+PVno3_Syn)/PS_Syn)	dl	N-status of Synechoccus
S	PS_	A	PSqmax_Syn*(1-EXP(-alphau_Syn*avgPFD*24*60*60/ PSqmax_Syn))	N/N/d	gross PS for Synechoccus ;uses averaged light over watercolumn NOT Smith integration
S	PSqmax_	A	maxGPS_Syn*Nu_Syn_alt	d-1	Maximum photosynthetic rate down-regulated by nutrient stress; Synechoccus
S	CR_	A	Enc_Syn*PR_Syn*palat_syn*opt_CR_Tele	Alg Prot-1 d-1	potential capture of *Synechococcus* taking into account all factors
S	CRC_	A	CR_Syn*Ncell_Syn/Ncell_Tele	gN gN-1 d-1	Potential N-specific ingestion of *Synechococcus* by *Teleaulax*
S	palat_	A	(NC_Syn+1e-6)^tox_Syn	dl	Palatability index for *Synechococcus* (0 not palatable)
S	PR_	A	IF((relMaxPrey_Tele>rel_Syn AND rel_Syn>relMinPrey_Tele), IF (rel_Syn<relOpPrey_Tele,(rel_Syn-relMinPrey_Tele)/ (relOpPrey_Tele-relMinPrey_Tele), (relMaxPrey_Tele-rel_Syn)/ (relMaxPrey_Tele-relOpPrey_Tele)),0)	dl	Prey handling index for *Synechococcus* by *Teleaulax*
S	rel_	A	r_Syn/r_Tele	dl	prey:pred radius for *Synechococcus*:*Teleaulax*
S	av_fratio_	A	SLIDINGAVERAGE(fratio_Syn,1,0)	dl	daily average of protist f-ratio
S	fratio_	A	IF(N_tot_Syn>0,Vno3_Syn/N_tot_Syn,0)	dl	f-ratio of Protist
S	N_tot_	A	IF(RegN_Syn<Ndem_Syn, RegN_Syn,Ndem_Syn)+Vnh4_Syn+Vno3_Syn	N/N/d	total nitrogen use of Protist

Continued on next page

Table A.1 continued from previous page

o	vn	vt	equations and values	unit	description
S	nosL_	A	nosML_Syn*1000	cells L-1	cell concentration of *Synechococcus*
S	nosML_	A	nos_Syn/10^6	Alg cells ml-1	Cell abundance of *Synechococcus*
S	thres_cell_	A	(10^6*thres_Syn)/Ncell_Syn	cells L-1	miniumum cells that can be ingested
S	UmT_	A	Umax_Syn*Q10^((T-RT)/10)	gN gN-1 d-1	Umax at current temperature; this is the maximum possible growth rate which may only be achieved growing mixotrophically
S	Nu_Syn_alt	SV	0 + Nu_Syn_rate	dl	N-status of Synechoccus (averaged intermediate)
S	uAV_Syn_alt	SV	0 + U_Syn_alt	gN (gN)-1 d-1	
S	Synecho-coccus	SV	Inoc_Syn - death_Syn - DONout_Syn - ing_Tele - lig_Syn_Meso - wash_Syn + DON_Syn + upnh4_Syn + upno3_Syn + washin_Syn	mgN m-3	Synechoccus sp.-biomass (bacterial prey of *Teleaulax*)
A	NC_	C	(16*14)/(105*12)	gN gC-1	Redfield ratio for N:C (mole 16:105) for plankton
A	percent_	C	2*5/100		proportion of nitrogen N_Alg of total nutrient load
A	BR_	C	0.1	dl	Scaler for basal respiration rate in Alg for reference to maximum growth rate (on the basis that faster growing species have inherent higher BR rates)

Continued on next page

Table A.1 continued from previous page

o	vn	vt	equations and values	unit	description
A	Umax_	C	0.693	gN (gN)-1 d-1	Alg maximum N-specific growth rate at neutral temperature
A	ChlC_	C	0.06	gChl (gC)-1	Mass ratio content of chlorophyll:C in Alg. No photoacclimation is assumed, so this is de facto the maximum content.
A	Knh4_	C	14	mgN m-3	Alg half saturation constant for ammonium
A	Kno3_	C	7	mgN m-3	Alg half saturation constant for nitrate
A	alpha_Chl_	C	2.50E-06	(m2 g-1 chl.a)* (gC µmol-1 photon)	Slope of Chl-specific PE curve
A	thres_	C	3.26e-06*1000*50	mgN m-3	Threshold for predation on Alga (50 cells mL-1)
A	tox_	C	0	dl	Toxicity factor for Phy1; 0 not toxic
A	r_	C	6/2	µm	radius of Alg cell (ESD devided by 2)
A	DON_leak_	A	SUM(Vnh4_Alg,Vno3_Alg)*PS_leakage+ (DON_up_Alg*SDA+BR_Alg*uTP_Alg)	gN (gN)-1 d-1	loss of Alga nh4 is SDA of DON uptake and basal respiration of growth rate (specific dynamic action + basal respiration + PS leak
A	DON_up_	A	MAX(1e-9, ((0.1*UmT_Alg)*lDON)/ (Knh4_Alg+lDON))	gN (gN)-1 d-1	Alga potential usage of DON (Fasham et al. 1990), DON*0.1 is for using only 10% of DON, which is labile and usable DON will only be taken up, if the alga is photosynthesising. According to Fasham, DON is supplying carbon for photosynthesis
A	Ccell_	A	a*(4/3*PI*(r_Alg)^3)^b	pgC cell-1	C content of Alg
A	Ncell_	A	Ccell_Alg*NC_Alg	pg N cell-1	N content per cell of Alg
A	nos_	A	10^9 * N_Alg/Ncell_Alg	Alg cells (m3)-1	Cell abundance of Alg
A	v_	A	(10^-6)*(38.542*(r_Alg*2)^0.5424)	m s-1	speed of motility of Alg

Continued on next page

Table A.1 continued from previous page

o	vn	vt	equations and values	unit	description
A	Inoc_	A	N_load*percent_Alg/100	µg N L-1	nitrogen initial inoculation of Syn (mg m-3)
A	death_	A	IF(N_Alg>1e-9,N_Alg*death_con,0)	mgN m-3 d-1	Alga continous death rate
A	DON_	A	IF(N_Alg>1e-9,DON_up_Alg*N_Alg)	mgN m-3 d-1	Alga population growth rate supported by labile DON
A	DONout_	A	IF(N_Alg>1e-9,N_Alg*DON_leak_Alg,0)	mgN m-3 d-1	DON leak from Alg
A	Nu_Alg_rate	A	(Nu_Alg-Nu_Alg_alt)*10	dl	N-status of Alg (averaged intermediate)
A	U_Alg_alt	A	(uTP_Alg-uAV_Alg_alt)*10	gN (gN)-1 d-1	growth rate of Alg (average intermediate)
A	upnh4_	A	IF(N_Alg>1e-9, N_Alg*(Vnh4_Alg-netRegN_Alg),0)	mgN m-3 d-1	Alg population growth rate supported by ammonium. NOTE the release of NH4 during darkness with reg_Alg!
A	upno3_	A	IF(N_Alg>1e-9,N_Alg*Vno3_Alg)	mgN m-3 d-1	Alg population growth rate supported by nitrate
A	wash_	A	dil*N_Alg	mgN m-3 d-1	Alg washout by dilution
A	washin_	A	dil*(Inoc_Alg)*0.2*Sw_land_runoff	mgN m-3 d-1	Alga washin by dilution
A	maxGPS_	A	UmT_Alg*(1+BR_Alg)	N/N/d	gross assimilation needed to support UmT_Alg
A	abco_	A	abco_Chl*ChlC_Alg/NC_Syn	m2 (mgN)-1	Phytoplankton-N specific coefficient for light absorbance
A	attco_	A	abco_AlgN*N_Alg	m-1	Attenuation coefficient to phytoplankton N-biomass
A	Ndem_	A	PS_Alg*(1-MR)	N/N/d N	demand to satisfy concurrent photosynthesis corrected for MR costs
A	netRegN_	A	IF(RegN_Alg>Ndem_Alg,RegN_Alg-Ndem_Alg,0)	N/N/d	net regeneration of N which occurs if internal regeneration of N exceeds the concurrent demands driven by incoming PS

Continued on next page

Table A.1 continued from previous page

o	vn	vt	equations and values	unit	description
A	PAss_	A	PS_Alg*(1-MR)	N/N/d	net phototrophy, from gross phototrophy minus the cost of anabolism required for incorportion of DIN. This is set by MR, but in reality it is affected by the f-ratio as far more effort is required to reduce NO3 to NH4 within the cell.
A	PVnh4_	A	IF(NH4>(14*0.01), maxGPS_Alg*TGnh4_Alg*NH4/ (NH4+Knh4_Alg),0)	gN (gN)-1 d-1	Algal potential NH4 supply as transport PLUS the current internal regeneration of NH4
A	PVno3_	A	IF(NO3>(14*0.01), maxGPS_Alg*TGno3_Alg*NO3/ (NO3+Kno3_Alg),0)	gN (gN)-1 d-1	Alg potential nitrate transport; light dependent
A	RegN_	A	UmT_Alg*BR_Alg	N/N/d	regeneration rate through basal respiration for Alg
A	TGnh4_	A	Umax_Alg*NC_Alg*10	N/C/d	Alg transport:growth needs ratio for ammonium
A	TGno3_	A	Umax_Alg*NC_Alg*2	N/C/d	Alg transport:growth needs ratio for nitrate
A	Vnh4_	A	MIN(uTP_Alg,PVnh4_Alg)	gN (gN)-1 d-1	Alga potential usage of ammonium
A	Vno3_	A	IF(uTP_Alg>PVnh4_Alg, MIN((uTP_Alg-PVnh4_Alg),PVno3_Alg),0)	gN (gN)-1 d-1	Alg potential usage of nitrate
A	uTP_	A	IF(RegN_Alg<Ndem_Alg,Ndem_Alg-RegN_Alg,0)	N/N/d	net incorporation of DIN with phototrophy after usage of internally regenerated NH4 for alga
A	alphau_	A	alpha_Chl_Alg*ChlC_Alg	(m2)* (µmol-1 photon)	Specific slope of PE curve
A	Nu_	A	MIN(1,(RegN_Alg+PVnh4_Alg+PVno3_Alg)/PS_Alg)	dl	N-status of Alg
A	PS_	A	PSqmax_Alg*(1-EXP(-alphau_Alg*avgPFD*24*60*60/ PSqmax_Alg))	N/N/d	gross PS for Prot; uses averaged light over watercolumn NOT Smith integration

Continued on next page

Table A.1 continued from previous page

o	vn	vt	equations and values	unit	description
A	PSqmax_	A	maxGPS_Alg*Nu_Alg_alt	d-1	Maximum photosynthetic rate down-regulated by nutrient stress
A	lig_	A	IF(CRC_Alg_Meso=0,0, ingN_Meso*CRC_Alg_Meso/SCRC_Meso)	gN (gN)-1 d-1	ingestion rate of Alg by *Mesodinium*
A	palat_	A	(NC_Alg+1e-6)^tox_Alg	dl	Palatability index for Alg (0 not palatable)
A	C_	A	N_Alg/NC_Alg	mgC m-3	Alg C-biomass
A	nosL_	A	nosML_Alg*1000	cells L-1	cell concentration of Alg
A	nosML_	A	nos_Alg/10^6	Alg cells ml-1	Cell abundance of Alg
A	thres_cell_	A	(10^6*thres_Alg)/Ncell_Alg	cells L-1	miniumum cells that can be ingested
A	UmT_	A	Umax_Alg*Q10^((T-RT)/10)	gN gN-1 d-1	Umax at current temperature; this is the maximum possible growth rate which may only be achieved growing mixotrophically
A	N_Alga	SV	Inoc_Alg - death_Alg - DONout_Alg - ing_Alg_Meso - wash_Alg + DON_Alg + upnh4_Alg + upno3_Alg + washin_Alg	µmgN m-3	Alg N-biomass (specific algal prey for SNCM)
A	Nu_Alg_alt	SV	0 + Nu_Alg_rate	dl	N-status of Alg (averaged)
A	uAV_Alg_alt	SV	0 + U_Alg_alt	gN (gN)-1 d-1	growth rate of Alg (averaged)

Continued on next page

Table A.1 continued from previous page

o	vn	vt	equations and values	unit	description
T	v_	C	5.55E-04	m s-1	speed of motility of *Teleaulax* (Meunier et al 2013)
T	NC_	C	0.167	gN gC-1	Redfield ratio for N:C (mole 16:105) for *Teleaulax*
T	percent_	C	2*5/100		proportion of nitrogen *Teleaulax* of total nutrient load
T	AEN_	C	0.6	dl	Assimilation efficiency for N entering from prey (food) ingestion, *Teleaulax*
T	BR_	C	0.1	dl	Scaler for basal respiration rate in *Teleaulax* for reference to maximum growth rate (on the basis that faster growing species have inherent higher BR rates)
T	Umax_	C	0.693	N/N/d	*Teleaulax* maximum possible N-specific growth rate at neutral temperature (Hamilton et al. 2017)
T	ChlC_	C	0.06	gChl (gC)-1	Mass ratio content of chlorophyll:C in *Teleaulax*. No photoacclimation is assumed, so this is de facto the maximum content.
T	Knh4_	C	14	mgN m-3	*Teleaulax* half saturation constant for ammonium
T	Kno3_	C	7	mgN m-3	*Teleaulax* half saturation constant for nitrate
T	alpha_Chl_	C	2.31E-06	(m2 g-1 chl.a)* (gC µmol-1 photon)	Slope of Chl-specific PE curve (AA Anschuetz); *Teleaulax*
T	opt_CR_	C	0.2	dl	proportion of prey of optimal characteristics captured by starved *Teleaulax*
T	thres_	C	3.26E-05	mgN m-3	Threshold for predation on *Teleaulax* (100 cells mL-1)
T	r_	C	36/2	µm	radius of *Teleaulax* cell (AA Anschuetz)

Continued on next page

Table A.1 continued from previous page

o	vn	vt	equations and values	unit	description
T	relMaxPrey_	C	1/3	dl	maximum prey:*Teleaulax* size ratio
T	relMinPrey_	C	0.9/7.5	dl	minimum prey:*Teleaulax* size ratio
T	relOpPrey_	C	0.95/6	dl	optimal prey:*Teleaulax* size ratio
T	DON_leak_	A	SUM(Vnh4_Tele,Vno3_Tele)*PS_leakage+ (DON_up_Tele*SDA+BR_Tele*uTP_Tele)	gN (gN)-1 d-1	loss of *Teleaulax* nh4 is SDA of DON uptake and basal respiration of growth rate (specific dynamic action + basal respiration + PS leak; *Teleaulax*
T	DON_up_	A	MAX(1e-9, ((0.1*UmT_Tele)*lDON)/ (Knh4_Tele+lDON))	gN (gN)-1 d-1	*Teleaulax* potential usage of DON (Fasham et al. 1990), DON*0.1 is for using only 10% of DON, which is labile and usable DON will only be taken up, if *Teleaulax* is photosynthesising. According to Fasham, DON is supplying carbon for photosynthesis
T	Ccell_	A	a*(4/3*PI*(r_Tele)^3)^b	pgC cell-1	C content of Prot
T	Enc_Syn	A	(24*60*60)*PI*(r_Syn/1E6+r_Tele/1E6)^2* nos_Syn*(v_Syn^2+3*v_Tele^2+4*w^2)* ((v_Tele^2+w^2)^-0.5)*3^-1	Alg Prot-1 d-1	encounter rate of a cell of *Synechococcus* by a cell of *Teleaulax*
T	Ncell_	A	Ccell_Tele*NC_Tele	pg N cell-1	N content per cell of protist
T	Inoc_	A	N_load*percent_Tele/100	µg N L-1	nitrogen initial inoculation of Protist
T	death_	A	IF(N_Teleaulax>1e-9, N_Teleaulax*death_con,0)	mgN m-3 d-1	*Teleaulax* death rate when growth rate falls beneath a limit and a continous death rate
T	DON_	A	IF(N_Teleaulax>1e-9, DON_leak_Tele*N_Teleaulax,0)	gN (gN)-1 d-1	DON leak by *Teleaulax*
T	DONout_	A	SUM(death_Tele,void_Tele)	mgN m-3 d-1	DON leak from Tele

Continued on next page

Table A.1 continued from previous page

o	vn	vt	equations and values	unit	description
T	DONup_	A	IF(N_Teleaulax>1e-9, DON_up_Tele*N_Teleaulax)	mgN m-3 d-1	*Teleaulax* population growth rate supported by labile DON
T	ing_	A	IF(N_Teleaulax>1e-9, N_Teleaulax*ingN_Tele,0)	mgN m-3 d-1	*Teleaulax* population ingestion rate
T	Nu_Tele_rate	A	(Nu_Tele-Nu_Tele_alt)*10	dl	N-status of *Teleaulax* (averaged intermediate)
T	reg_	A	IF(N_Teleaulax>1e-9, N_Teleaulax*netRegN_Tele,0)	mgN m-3 d-1	*Teleaulax* population N-regeneration rate
T	U_Tele_alt	A	(u_Tele-uAV_Tele_alt)*10	gN (gN)-1 d-1	growth rate of *Teleaulax* (average intermediate)
T	upnh4_	A	IF(N_Teleaulax>1e-9, N_Teleaulax*(Vnh4_Tele),0)	mgN m-3 d-1	*Teleaulax* population growth rate supported by ammonium
T	upno3_	A	IF(N_Teleaulax>1e-9, N_Teleaulax*Vno3_Tele,0)	mgN m-3 d-1	*Teleaulax* population growth rate supported by nitrate
T	void_	A	IF(N_Teleaulax>1e-9, N_Teleaulax*voidN_Tele,0)	mgN m-3 d-1	*Teleaulax* population N-voiding rate
T	wash_	A	dil*N_Teleaulax	mgN m-3 d-1	*Teleaulax* washout by dilution
T	washin_	A	dil*(Inoc_Tele)*0.2*Sw_land_runoff	mgN m-3 d-1	*Teleaulax* washin by dilution
T	assN_	A	ingN_Tele*AEN_Tele	gN (gN)-1 d-1	Assimilation rate of prey-N into *Teleaulax*-N
T	maxGPS_	A	maxGU_Tele*pCritMax	gN (gN)-1 d-1	*Teleaulax* maximum N-specific growth rate as supported by phototrophy
T	maxGU_	A	UmT_Tele*(1+BR_Tele)	N/N/d	gross assimilation needed to support umax_Tele
T	maxIAss_	A	maxGU_Tele-(maxGU_Tele*pCritMin)	N/N/d	maximum assimilation of ingested material, taking into account the maximum gross growth rate, and the critical proportion that must come via phototrophy (set by pCritMin); *Teleaulax*

Continued on next page

Table A.1 continued from previous page

o	vn	vt	equations and values	unit	description
T	opmaxIAss_	A	MAX((UmT_Tele*BR_Tele), MIN(possU_Tele-PAss_Tele,maxIAss_Tele))	N/N/d	operational maximum possible assimilation of ingested material; this cannot exceed possU-grossPS, nor can it exceed maxgrossU/pCritmin. However, as a minimum level survival grazing is allowed; *Teleaulax*
T	opmaxIng_	A	opmaxIAss_Tele/(AEN_Tele*(1-SDA))	N/N/d	maximum possible Ingestion rate to satisfy the maximum possible assimilation rate, taking into account SDA and AE; *Teleaulax*
T	possU_	A	MIN((PAss_Tele+1e-6)/pCritMin,maxGU_Tele)	N/N/d	shortfall in N that could be covered by assimilation of ingested materials, taking into account any proportion of nutrition that must come via phototrophy (defined by pCritMin); inclusion of 1e-6 is to prevent a problem with PAss_Prot being 0; *Teleaulax*
T	regNsda_	A	assN_Tele*SDA	gN (gN)-1 d-1	*Teleaulax* N-specific N-release rate; this amount may be regenerated, or potentially (for a mixotroph) re-assimilated
T	abco_	A	abco_Chl*ChlC_Tele/NC_Tele	m2 (mgN)-1	Phytoplankton-N specific coefficient for light absorbance
T	attco_	A	abco_Tele*N_Teleaulax	m-1	Attenuation coefficient to phytoplankton N-biomass
T	Ndem_	A	PS_Tele*(1-MR)	N/N/d	N demand to satisfy concurrent photosynthesis corrected for MR costs of *Teleaulax*
T	netRegN_	A	IF(RegN_Tele>Ndem_Tele, RegN_Tele-Ndem_Tele,0)	N/N/d	net regeneration of N which occurs if internal regeneration of N exceeds the concurrent demands driven by incoming PS; *Teleaulax*
T	PAss_	A	PS_Tele*(1-MR)	N/N/d	net phototrophy, from gross phototrophy minus the cost of anabolism required for incorportion of DIN. This is set by MR, but in reality it is affected by the f-ratio as far more effort is required to reduce NO3 to NH4 within the cell; *Teleaulax*

Continued on next page

Table A.1 continued from previous page

o	vn	vt	equations and values	unit	description
T	PVnh4_	A	IF(NH4>(14*0.01), maxGPS_Tele*TGnh4_Tele*NH4/(NH4+Knh4_Tele),0)	gN (gN)-1 d-1	*Teleaulax* potential NH4 supply as transport PLUS the current internal regeneration of NH4. Limit is set to the limitation of NH4 detection. (Mol nitrogen, 14)
T	PVno3_	A	IF(NO3>(14*0.01), maxGPS_Tele*TGno3_Tele*NO3/ (NO3+Kno3_Tele),0)	gN (gN)-1 d-1	*Teleaulax* potential nitrate transport; light dependent
T	RegN_	A	regNsda_Tele+UmT_Tele*BR_Tele	N/N/d	regeneration rate through basal respiration PLUS also N released due to SDA for *Teleaulax*
T	TGnh4_	A	Umax_Tele*NC_Tele*10	dl	*Teleaulax* transport:growth needs ratio for ammonium
T	TGno3_	A	Umax_Tele*NC_Tele*2	dl	*Teleaulax* transport:growth needs ratio for nitrate ; set as 0 if incapable of using nitrate
T	Vnh4_	A	MIN(uTP_Tele,PVnh4_Tele)	gN (gN)-1 d-1	*Teleaulax* potential usage of ammonium
T	Vno3_	A	IF(uTP_Tele>PVnh4_Tele, MIN((uTP_Tele-PVnh4_Tele), PVno3_Tele),0)	gN (gN)-1 d-1	*Teleaulax* potential usage of nitrate
T	uTP_	A	IF(RegN_Tele<Ndem_Tele, Ndem_Tele-RegN_Tele,0)	N/N/d	net incorporation of DIN with phototrophy after usage of internally regenerated NH4 for *Teleaulax*
T	alphau_	A	alpha_Chl_Tele*ChlC_Tele	(m2)* (µmol-1 photon)	Specific slope of PE curve of *Teleaulax*
T	Nu_	A	MIN(1, (RegN_Tele+PVnh4_Tele+PVno3_Tele)/PS_Tele)	dl	Nu status of phototrophic component of *Teleaulax*
T	PS_	A	PSqmax_Tele*(1-EXP(-alphau_Tele*avgPFD*24*60*60/ PSqmax_Tele))	N/N/d	gross PS for *Teleaulax*; uses averaged light over watercolumn NOT Smith integration
T	PSqmax_	A	maxGPS_Tele*Nu_Tele_alt	d-1	Maximum photosynthetic rate down-regulated by nutrient stress; *Teleaulax*

Continued on next page

Table A.1 continued from previous page

o	vn	vt	equations and values	unit	description
T	CR_	A	Enc_Tele_Meso*PR_Tel_Meso*opt_CR_Meso	Alg *Mesodinium*-1 d-1	potential capture of *Teleaulax* taking into account all factors, *Teleaulax* is not toxic
T	CRC_	A	CR_Tele*Ncell_Tele/Ncell_Meso	gN gN-1 d-1	Potential N-specific ingestion of *Teleaulax* by *Mesodinium*
T	ingN_	A	IF(CRC_Syn>thres_Syn, MIN(opmaxIng_Tele*(CRC_Syn-thres_Syn)/(CRC_Syn-thres_Syn+KI_Tele), CRC_Syn),0)	gN (gN)-1 d-1	Ingestion rate of prey-N by *Teleaulax*
T	KI_	A	opmaxIng_Tele/4	gN (gN)-1 d-1	satiation control constant for *Teleaulax*
T	lig_	A	IF(CRC_Tele=0,0,ingN_Meso*CRC_Tele/SCRC_Meso)	gN (gN)-1 d-1	ingestion rate of Alg by Prot
T	av_fratio_	A	SLIDINGAVERAGE(fratio_Tele,1,0)	dl	daily average of protist f-ratio
T	fratio_	A	IF(N_tot_Tele>0,Vno3_Tele/N_tot_Tele,0)	dl	f-ratio of Protist
T	N_tot_	A	IF(RegN_Tele<Ndem_Tele, RegN_Tele,Ndem_Tele)+Vnh4_Tele+Vno3_Tele	N/N/d	total nitrogen use of Protist
T	netPS_	A	Ndem_Tele-RegN_Tele	N/N/d	net photosynthesis of *Teleaulax*. Photosynthesis minus MR, SDA and BR. Essentially equal to uTP_Tele with the difference that it is not switched to 0, when it would become negative. For control purposes
T	nos_	A	10^9 *N_Teleaulax/Ncell_Tele	Prot cells (m3)-1	Cell abundance of *Teleaulax*
T	nosL_	A	nosML_Tele*1000	cells L-1	cell concentration of *Teleaulax*
T	nosML_	A	nos_Tele/10^6	Prot cells ml-1	Cell abundance of *Teleaulax*
T	thres_cell_	A	(10^6*thres_Tele)/Ncell_Tele	cells L-1	miniumum cells that can be ingested
T	u_	A	ingN_Tele+uTP_Tele-voidN_Tele-netRegN_Tele	gN (gN)-1 d-1	growth rate of *Teleaulax*

Continued on next page

Table A.1 continued from previous page

o	vn	vt	equations and values	unit	description
T	uhet_	A	u_Tele-uTP_Tele	gN (gN)-1 d-1	heterotrophic growth rate of the *Teleaulax*
T	UmT_	A	Umax_Tele*Q10^((T-RT)/10)	gN gN-1 d-1	Umax at current temperature; this is the maximum possible growth rate which may only be achieved growing mixotrophically
T	voidN_	A	ingN_Tele*(1-AEN_Tele)	gN (gN)-1 d-1	voiding rate of N by *Teleaulax*
T	Nu_Tele_alt	SV	0 + Nu_Tele_rate	dl	N-status of *Teleaulax* (averaged)
T	uAV_Tele_alt	SV	0 + U_Tele_alt	gN (gN)-1 d-1	
T	N_Teleaulax	SV	Inoc_Tele - death_Tele - DON_Tele - ingMeso - reg_Tele - void_Tele - wash_Tele + DONup_Tele + ing_Tele + upnh4_Tele + upno3_Tele + washin_Tele	mgN m-3	*Teleaulax* N-biomass
M	v_	C	0.00036	m s-1	speed of motility of *Mesodinium* (Jiang et al 2018); youtube (now)
M	NC_	C	0.265	gN gC-1	Redfield ratio for N:C (mole 16:105) for *Mesodinium* (Moeller et al. 2011)

Continued on next page

Table A.1 continued from previous page

o	vn	vt	equations and values	unit	description
M	percent_	C	1/100		proportion of nitrogen *Mesodinium* of total nutrient load
M	AEN_	C	0.6	dl	Assimilation efficiency for N entering from prey (food) ingestion; *Mesodinium*
M	BR_	C	0.1	dl	Scaler for basal respiration rate in *Mesodinium* for reference to maximum growth rate (on the basis that faster growing species have inherent higher BR rates)
M	deathCo_	C	10	dl	death coefficient
M	Umax_	C	0.52	N/N/d	*Mesodinium* maximum possible N-specific growth rate at neutral temperature (Yih et al. 2004)
M	ChlC_	C	0.055	gChl (gC)-1	Mass ratio content of chlorophyll:C in *Mesodinium*. No photoacclimation is assumed, so this is de facto the maximum content. (Rial et al. 2013, Gustafson et al. 2000)
M	critIR_	C	25	d	maximum period of time between ingestions of one *Teleaulax* cell per *Mesodinium* cell to enable maximum phototrophy
M	Knh4_	C	14	mgN m-3	*Mesodinium* half saturation constant for ammonium
M	Kno3_	C	7	mgN m-3	*Mesodinium* half saturation constant for nitrate
M	alpha_Chl_	C	5.05E-06	(m2 g-1 chl.a)* (gC µmol-1 photon)	Slope of Chl-specific PE curve (Johnson & Stoecker 2005); *Mesodinium*
M	opt_CR_	C	0.3	dl	proportion of prey of optimal characteristics captured by starved *Mesodinium*
M	thres_	C	7.55E-03	mgN m-3	Threshold for predation on *Mesodinium* (nitrogen worth 1 cell L-1)

Continued on next page

Table A.1 continued from previous page

o	vn	vt	equations and values	unit	description
M	tox_	C	0	dl	Toxicity factor for *Mesodinium*; 0 not toxic
M	r_	C	36/2	µm	radius of *Mesodinium* cell (Olenina et al. 2006; Montagnes et al. 2008)
M	relMaxPrey_	C	1/8	dl	maximum prey:*Mesodinium* size ratio
M	relMinPrey_	C	0.8/36	dl	minimum prey:*Mesodinium* size ratio
M	relOpPrey_	C	2.2/60	dl	optimal prey:*Mesodinium* size ratio
M	DON_leak_	A	SUM(Vnh4_Meso,Vno3_Meso)*PS_leakage+ (DON_up_Meso*SDA+BR_Meso*uTP_Meso)	gN (gN)-1 d-1	loss of *Mesodinium* nh4 is SDA of DON uptake and basal respiration of growth rate (specific dynamic action + basal respiration + PS leak; *Mesodinium*
M	DON_up_	A	MAX(1e-9, ((0.1*UmT_Meso)*lDON)/ (Knh4_Meso+lDON))*op_PIl_Meso	gN (gN)-1 d-1	*Mesodinium* potential usage of DON (Fasham et al. 1990), DON*0.1 is for using only 10% of DON, which is labile and usable DON will only be taken up, if *Mesodinium* is photosynthesising. According to Fasham, DON is supplying carbon for photosynthesis
M	Ccell_	A	a*(4/3*PI*(r_Meso)^3)^b	pgC cell-1	C content of *Mesodinium*
M	Enc__	A	(24*60*60)*PI* (r_Alg/1E6+r_Meso/1E6)^2* nos_Alg*(v_Alg^2+3*v_Meso^2+4*w^2)* ((v_Meso^2+w^2)^-0.5)*3^-1	Alg Prot-1 d-1	encounter rate of a cell of Alg by a cell of *Mesodinium*
M	Enc_Syn_	A	(24*60*60)*PI* (r_Syn/1E6+r_Meso/1E6)^2* nos_Syn*(v_Syn^2+3*v_Meso^2+4*w^2)* ((v_Meso^2+w^2)^-0.5)*3^-1	Alg Prot-1 d-1	encounter rate of a cell of *Synechococcus* by a cell of *Mesodinium*

Continued on next page

Table A.1 continued from previous page

o	vn	vt	equations and values	unit	description
M	Enc_Tele_	A	(24*60*60)*PI* (r_Tele/1E6+r_Meso/1E6)^2*nos_Tele* (v_Tele^2+3*v_Meso^2+4*w^2)* ((v_Meso^2+w^2)^-0.5)*3^-1	Alg Prot-1 d-1	encounter rate of a cell of *Teleaulax* by a cell of *Mesodinium*
M	Ncell_	A	Ccell_Meso*NC_Meso	pg N cell-1	N content per cell of *Mesodinium*
M	Inoc_	A	N_load*percent_Meso/100	µg N L-1	nitrogen initial inoculation of Meso
M	death_	A	IF(N_Mesodinium>1e-9, N_Mesodinium*(death_con+mort_Meso))	mgN m-3 d-1	Protist death rate for uZ, GNCM, SNCM when growth rate falls beneath a limit and a continous death rate
M	delay_PiI_	A	IF(Av_PiI_meso>0,1/decayT_Meso,0)	d-1	deterioration (loss of functionality) of opPiI assuming a linear relationship. There is a trap here because the linearity may be if Nu changes durng the decay event. *Mesodinium*
M	DON_	A	IF(N_Mesodinium>1e-9, N_Mesodinium*DON_leak_Meso)	gN (gN)-1 d-1	DON leak by *Mesodinium*
M	Donout_	A	SUM(death_Meso,void_Meso)	mgN m-3 d-1	DON leak from Meso
M	DONup_	A	IF(N_Mesodinium>1e-9, DON_up_Meso*N_Mesodinium)	mgN m-3 d-1	*Mesodinium* population growth rate supported by labile DON
M	ing__	A	IF(N_Alg>1e-9 AND N_Mesodinium>1e-9, N_Mesodinium*lig_Alg)	gN (gN)-1 d-1	Ingestion rate of Alg-N by *Mesodinium*
M	ing_Meso	A	IF(N_Mesodinium>1e-9, N_Mesodinium*ingN_Meso,0)	mgN m-3 d-1	*Mesodinium* population ingestion rate
M	ingMeso	A	IF(N_Teleaulax>1e-6 AND N_Mesodinium>1e-6, N_Mesodinium*lig_Tele,0)	gN (gN)-1 d-1	Ingestion rate of prey-N by *Teleaulax*
M	lig_Syn_	A	IF(CRC_Syn_Meso=0,0, ingN_Meso*CRC_Syn_Meso/SCRC_Meso)	gN (gN)-1 d-1	ingestion rate of Alg by Prot

Continued on next page

Table A.1 continued from previous page

o	vn	vt	equations and values	unit	description
M	Nu_Meso_rate	A	(Nu_Meso-Nu_Meso_alt)*10	dl	N-status of *Mesodinium* (averaged intermediate)
M	reg_	A	IF(N_Mesodinium>1e-9, N_Mesodinium*netRegN_Meso,0)	mgN m-3 d-1	*Mesodinium* population N-regeneration rate
M	U__alt	A	(u_Meso-uAV_Meso_alt)*10	gN (gN)-1 d-1	growth rate of *Mesodinium* (average intermediate)
M	U_PiI_	A	IF(Av_PiI_meso<PiI_Meso, (PiI_Meso-Av_PiI_meso)/TIMESTEP,0)	dl	input to operational PiI; this ensures that the minimum level of the operational value is always the current PiI; *Mesodinium*
M	upnh4_	A	IF(N_Mesodinium>1e-9, N_Mesodinium*(Vnh4_Meso),0)	mgN m-3 d-1	*Mesodinium* population growth rate supported by ammonium
M	upno3_	A	IF(N_Mesodinium>1e-9, N_Mesodinium*Vno3_Meso)	mgN m-3 d-1	*Mesodinium* population growth rate supported by nitrate
M	void_	A	IF(N_Mesodinium>1e-9, N_Mesodinium*voidN_Meso,0)	mgN m-3 d-1	*Mesodinium* population N-voiding rate
M	wash_	A	dil*N_Mesodinium	mgN m-3 d-1	Protist washout by dilution
M	wasin_	A	dil*(Inoc_Meso)*0.2*Sw_land_runoff	mgN m-3 d-1	*Mesodinium* washin by dilution
M	assN_	A	ingN_Meso*AEN_Meso	gN (gN)-1 d-1	Assimilation rate of prey-N into *Mesodinium*-N
M	DeathI_	A	IF(uAV_Meso_alt<0 AND uAV_Meso_alt>growth_min_Meso, (uAV_Meso_alt/growth_min_Meso)^deathCo_Meso, 0)	dl	normalised death index
M	growth_min_	A	-1*BR_Meso/2	dl	minimum growth rate of *Mesodinium*, where death is setting in at a moderate rate
M	maxGPS_	A	maxGU_Meso*pCritMax	gN (gN)-1 d-1	*Mesodinium* maximum N-specific growth rate as supported by phototrophy
M	maxGU_	A	UmT_Meso*(1+BR_Meso)	N/N/d	gross assimilation needed to support UmT_Meso

Continued on next page

Table A.1 continued from previous page

o	vn	vt	equations and values	unit	description
M	maxIAss_	A	maxGU_Meso-(maxGU_Meso*pCritMin)	N/N/d	maximum assimilation of ingested material, taking into account the maximum gross growth rate, and the critical proportion that must come via phototrophy (set by pCritMin) ; *Mesodinium*
M	mort_	A	IF(uAV_Meso_alt<growth_min_Meso, UmT_Meso, IF(uAV_Meso_alt>growth_min_Meso AND uAV_Meso_alt<0, DeathI_Meso*UmT_Meso,0))	N/N/d	death rate of *Mesodinium* when growth rate falls beneath a certain level
M	opmaxIAss_	A	MAX((UmT_Meso*BR_Meso), MIN(possU_Meso-PAss_Meso,maxIAss_Meso))	N/N/d	operational maximum possible assimilation of ingested material; this cannot exceed possU-grossPS, nor can it exceed maxgrossU/pCritmin. However, as a minimum level survival grazing is allowed; *Mesodinium*
M	opmaxIng_	A	opmaxIAss_Meso/(AEN_Meso*(1-SDA))	N/N/d	maximum possible Ingestion rate to satisfy the maximum possible assimilation rate, taking into account SDA and AE; *Mesodinium*
M	possU_	A	MIN((PAss_Meso+1e-6)/pCritMin,maxGU_Meso)	N/N/d	shortfall in N that could be covered by assimilation of ingested materials, taking into account any proportion of nutrition that must come via phototrophy (defined by pCritMin); inclusion of 1e-6 is to prevent a problem with PAss_Meso being 0
M	regNsda_	A	assN_Meso*SDA	gN (gN)-1 d-1	*Mesodinium* N-specific N-release rate; this amount may be regenerated, or potentially (for a mixotroph) re-assimilated
M	abco_	A	abco_Chl*opChlC_Meso/NC_Meso	m2 (mgN)-1	*Mesodinium*_N2 specific coefficient for light absorbance
M	attco_	A	N_Mesodinium*abco_Meso	m-1	Attenuation coefficient to *Mesodinium* N-biomass
M	cellprey_ cellpred_d_	A	lig_T_alt_Tel*(Ncell_Meso/Ncell_Tele)	cell *Teleaulax* cell *Mesodinium*-1 d-1	ingestion of algal cells per *Mesodinium* cells per day.

Continued on next page

Table A.1 continued from previous page

o	vn	vt	equations and values	unit	description
M	decayT_	A	critIR_Meso*Nu_Meso_alt	d	longetivity of phototrophy accounting for nutrient status (this is miply as a linear relationship; it could be sigmoidal, it could relate to UV etc.) (d); *Mesodinium*
M	ICrit_	A	1/critIR_Meso	cell cell -1 d-1	critical ingestion rate. Prey items per *Mesodinium* per day.
M	IInd_	A	(cellprey_cellpred_d_Meso/ICrit_Meso)	dl	ratio of cells eaten and cells *Mesodinium* needs to eat.
M	op_PiI_	A	IF(Av_PiI_meso>0, MAX(Av_PiI_meso, PiI_Meso),1e-12)	dl	operational photosynthetic ingestion index; this is done, so the NCM to have acquired a chloroplast in the past time; *Mesodinium*
M	opAlphaChl_	A	op_PiI_Meso*alpha_Chl_Meso	(m2 g-1 chl.a)* (gC µmol-1 photon)	Slope of Chl-specific PE curve dependent on frequency of prey ingestion by *Mesodinium*
M	opPSmax_	A	opPSmax_NCM_Meso	gN gN-1 d-1	operational PSmax, this maximum PS rate cannot go above maxGPS_Meso (absolute PSmax) of the protist. In case of the phytoplankton and the CM this value is fix and equal to maxGPS_Prot. In case of the GNCM and SNCM this value is flexible
M	opPSmax_ NCM_	A	op_PiI_Meso*maxGPS_Meso	gN gN-1 d-1	maximum photosynthetic rate dependent on amount of ingested chloroplasts by *Mesodinium*
M	PiI_	A	IF(cellprey_cellpred_d_Meso>ICrit_Meso, 1,IInd_Meso)	dl	Prey ingestion index of *Mesodinium*
M	opChlC_	A	op_PiI_Meso*ChlC_Meso	gChl (gC)-1	Chl:C ratio of *Mesodinium* ratioed to the relative maximum photosynthetic growth rate of the protist to the prey. For NCMs this value needs reconsideration!
M	Ndem_	A	PS_Meso*(1-MR)	N/N/d	N demand to satisfy concurrent photosynthesis corrected for MR costs; *Mesodinium*

Continued on next page

Table A.1 continued from previous page

o	vn	vt	equations and values	unit	description
M	netRegN_	A	IF(RegN_Meso>Ndem_Meso, RegN_Meso-Ndem_Meso,0)	N/N/d	net regeneration of N which occurs if internal regeneration of N exceeds the concurrent demands driven by incoming PS; *Mesodinium*
M	PAss_	A	PS_Meso*(1-MR)	N/N/d	net phototrophy, from gross phototrophy minus the cost of anabolism required for incorportion of DIN. This is set by MR, but in reality it is affected by the f-ratio as far more effort is required to reduce NO3 to NH4 within the cell. *Mesodinium*
M	PVnh4_	A	IF(NH4>(14*0.01), maxGPS_Meso*TGnh4_Tele*NH4/(NH4+Knh4_Tele),0)	gN (gN)-1 d-1	*Mesodinium* potential NH4 supply as transport PLUS the current internal regeneration of NH4. Limit is set to the limitation of NH4 detection. (Mol nitrogen, 14)
M	PVno3_	A	IF(NO3>(14*0.01), maxGPS_Meso*TGno3_Tele*NO3/(NO3+Kno3_Tele),0)	gN (gN)-1 d-1	*Mesodinium* potential nitrate transport; light dependent
M	RegN_	A	regNsda_Meso+UmT_Meso*BR_Meso	N/N/d	regeneration rate through basal respiration PLUS also N released due to SDA for *Mesodinium*
M	TGnh4_	A	Umax_Meso*NC_Meso*10	dl	*Mesodinium* transport:growth needs ratio for ammonium
M	TGno3_	A	Umax_Meso*NC_Meso*2	dl	*Mesodinium* transport:growth needs ratio for nitrate ; set as 0 if incapable of using nitrate
M	Vnh4_	A	MIN(uTP_Meso,PVnh4_Meso)	gN (gN)-1 d-1	*Mesodinium* potential usage of ammonium
M	Vno3_	A	IF(uTP_Meso>PVnh4_Meso, MIN((uTP_Meso-PVnh4_Meso),PVno3_Meso),0)	gN (gN)-1 d-1	*Mesodinium* potential usage of nitrate
M	uTP_	A	IF(RegN_Meso<Ndem_Meso, Ndem_Meso-RegN_Meso,0)	N/N/d	net incorporation of DIN with phototrophy after usage of internally regenerated NH4 for *Mesodinium*

Continued on next page

Table A.1 continued from previous page

o	vn	vt	equations and values	unit	description
M	alphau_	A	opAlphaChl_Meso*opChlC_Meso	(m2)* (µmol-1 photon)	Specific slope of PE curve of *Mesodinium*
M	Nu_	A	MIN(1, (RegN_Meso+PVnh4_Meso+PVno3_Meso)/PS_Meso)	dl	Nu status of phototrophic component of *Mesodinium*
M	PS_	A	PSqmax_Meso*(1-EXP(-alphau_Meso*avgPFD*24*60*60/ PSqmax_Meso))	N/N/d	gross PS for *Mesodinium*; uses averaged light over watercolumn NOT Smith integration
M	PSqmax_	A	opPSmax_Meso*Nu_Meso_alt	d-1	Maximum photosynthetic rate down-regulated by nutrient stress of *Mesodinium*
M	CR_	A	Enc_Meso_Dino*PR_Meso_Dino*opt_CR_Dino	*Mesodinium* *Dinophysis*-1 d-1	potential capture of Alg taking into account all factors, *Teleaulax* is not toxic
M	CR_Alg_	A	Enc_Alg_Meso*PR_Alg_Meso*palat_Alg*opt_CR_Meso	Alg Prot-1 d-1	potential capture of Alg taking into account all factors
M	CR_Syn_	A	Enc_Syn_Meso*PR_Syn_Meso*opt_CR_Meso*palat_syn	Alg *Mesodinium*-1 d-1	potential capture of *Synechococcus* by *Mesodinium* taking into account all factors
M	CRC_	A	CR_Meso*Ncell_Meso/Ncell_Dino	gN gN-1 d-1	Potential N-specific ingestion of *Mesodinium* by *Dinophysis*
M	CRC_Alg_	A	CR_Alg_Meso*Ncell_Alg/Ncell_Meso	gN gN-1 d-1	Potential N-specific ingestion of Alg by *Mesodinium*
M	CRC_Syn_	A	CR_Syn_Meso*Ncell_Syn/Ncell_Meso	gN gN-1 d-1	Potential N-specific ingestion of *Synechococcus* by *Mesodinium*
M	ingN_	A	IF(SCRC_Meso>SUM(thres_Alg,thres_Tele,thres_Syn), MIN(opmaxIng_Meso*(SCRC_Meso-thres_Alg-thres_Tele-thres_Syn)/ (SCRC_Meso-thres_Alg-thres_Tele-thres_Syn+KI_Meso), SCRC_Meso), 0)	gN (gN)-1 d-1	Ingestion rate of prey-N by *Mesodinium*
M	KI_	A	opmaxIng_Meso/4	gN (gN)-1 d-1	satiation control constant of *Mesodinium*

Continued on next page

Table A.1 continued from previous page

o	vn	vt	equations and values	unit	description
M	SCRC_	A	CRC_Tele+CRC_Syn_Meso+CRC_Alg_Meso	gN gN-1 d-1	sum of potential prey capture rates by *Mesodinium*
M	PR_Alg_	A	IF((relMaxPrey_Meso>rel_Alg_Meso AND rel_Alg_Meso>relMinPrey_meso), IF (rel_Alg_Meso<relOpPrey_Meso, (rel_Alg_Meso-relMinPrey_meso)/ (relOpPrey_Meso-relMinPrey_meso), (relMaxPrey_Meso-rel_Alg_Meso)/ (relMaxPrey_Meso-relOpPrey_Meso)),0)	dl	Prey handling index for Alg by *Mesodinium*
M	PR_Syn_	A	IF((relMaxPrey_Meso>rel_Syn_Meso AND rel_Syn_Meso>relMinPrey_meso), IF (rel_Syn_Meso<relOpPrey_Meso, (rel_Syn_Meso-relMinPrey_meso)/ (relOpPrey_Meso-relMinPrey_meso), (relMaxPrey_Meso-rel_Syn_Meso)/ (relMaxPrey_Meso-relOpPrey_Meso)),0)	dl	Prey handling index for *Synechococcus* by *Mesodinium*
M	PR_Tel_	A	IF((relMaxPrey_Meso>rel_Tele_Meso AND rel_Tele_Meso>relMinPrey_meso), IF (rel_Tele_Meso<relOpPrey_Meso, (rel_Tele_Meso-relMinPrey_meso)/ (relOpPrey_Meso-relMinPrey_meso), (relMaxPrey_Meso-rel_Tele_Meso)/ (relMaxPrey_Meso-relOpPrey_Meso)),0)	dl	Prey handling index for *Teleaulax* by *Mesodinium*
M	rel_Alg_	A	r_Alg/r_Meso	dl	prey:pred radius for Alg:*Mesodinium*
M	rel_Syn_	A	r_Syn/r_Meso	dl	prey:pred radius for Syn:*Mesodinium*
M	rel_Tele_	A	r_Tele/r_Meso	dl	prey:pred radius for *Teleaulax*:*Mesodinium*

Continued on next page

Table A.1 continued from previous page

o	vn	vt	equations and values	unit	description
M	av_fratio_	A	SLIDINGAVERAGE(fratio_Meso,1,0)	dl	daily average of protist f-ratio
M	fratio_	A	IF(N_tot_Meso>0,Vno3_Meso/N_tot_Meso,0)	dl	f-ratio of Protist
M	N_tot_	A	IF(RegN_Meso<Ndem_Meso, RegN_Meso,Ndem_Meso)+Vnh4_Meso+Vno3_Meso	N/N/d	total nitrogen use of Protist
M	netPS_	A	Ndem_Meso-RegN_Meso	N/N/d	net photosynthesis of *Mesodinium*. Photosynthesis minus MR, SDA and BR. Essentially equal to uTP_Meso with the difference that it is not switched to 0, when it would become negative. For control purposes
M	nos_	A	10^9 *N_Mesodinium/Ncell_Meso	Prot cells (m3)-1	Cell abundance of *Mesodinium*
M	nosL_	A	nosML_Meso*1000	cells L-1	cell concentration of *Mesodinium*
M	nosML_	A	nos_Meso/10^6	Prot cells ml-1	Cell abundance of *Mesodinium*
M	thres_cell_	A	(10^6*thres_Meso)/Ncell_Meso	cells L-1	miniumum cells that can be ingested
M	u_	A	ingN_Meso+uTP_Meso-voidN_Meso-netRegN_Meso	gN (gN)-1 d-1	growth rate of *Mesodinium*
M	uhet_	A	u_Meso-uTP_Meso	gN (gN)-1 d-1	heterotrophic growth rate of the *Mesodinium*
M	UmT_	A	Umax_Meso*Q10^((T-RT)/10)	gN gN-1 d-1	Umax at current temperature; this is the maximum possible growth rate which may only be achieved growing mixotrophically
M	voidN_	A	ingN_Meso*(1-AEN_Tele)	gN (gN)-1 d-1	voiding rate of N by *Mesodinium*

Continued on next page

Table A.1 continued from previous page

o	vn	vt	equations and values	unit	description
M	N_Mesodinium	SV	Inoc_Meso - death_Meso - DON_Meso - ingDino - reg_Meso - wash_Meso - void_Meso + DONup_Meso + ing_Meso + upnh4_Meso + upno3_Meso + washin_Meso	mgN m-3	*Mesodinium* N-biomass
M	Av_PiI_	SV	0 - delay_PiI_Meso + U_PiI_Meso		operational photosynthetic ingestion index –>for the *Mesodinium* to remember it has ingested a chloroplast before
M	Nu_Meso_alt	SV	0 + Nu_Meso_rate	dl	N-status of *Mesodinium* (averaged)
M	uAV_Meso_alt	SV	0 + U_Meso_alt	gN (gN)-1 d-1	
D	v_	C	1.70E-04	m s-1	speed of motility of *Dinophysis* (Jiang et al 2018)
D	NC_	C	0.125	gN gC-1	Redfield ratio for N:C (mole 16:105) for *Dinophysis* (Rao and Pan 1993)
D	percent_	C	0.5/100		proportion of nitrogen *Dinophysis* of total nutrient load (1:20 pred:prey (Hernández-Urcera et al. 2018))

Continued on next page

Table A.1 continued from previous page

o	vn	vt	equations and values	unit	description
D	AEN_	C	0.6	dl	Assimilation efficiency for N entering from prey (food) ingestion; *Dinophysis*
D	BR_	C	0.1	dl	Scaler for basal respiration rate in *Dinophysis* for reference to maximum growth rate (on the basis that faster growing species have inherent higher BR rates)
D	deathCo_	C	10	dl	death coefficient
D	Umax_	C	0.51	N/N/d	*Dinophysis* maximum possible N-specific growth rate at neutral temperature (Smith et al 2018, Kim et al. 2008) Riisgaard & Hansen 2009 Gentien et al. 1995
D	ChlC_	C	0.045	gChl (gC)-1	Mass ratio content of chlorophyll:C in *Dinophysis*. No photoacclimation is assumed, so this is de facto the maximum content. (Olenina et al. 2006, Hansen et al. 2016)
D	critIR_	C	5	d	maximum period of time between ingestions of one *Mesodinium* prey cell per *Dinophysis* cell to enable maximum phototrophy
D	Knh4_	C	14	mgN m-3	*Dinophysis* half saturation constant for ammonium
D	Kno3_	C	7	mgN m-3	*Dinophysis* half saturation constant for nitrate
D	alpha_Chl_	C	4.22E-06	(m2 g-1 chl.a)* (gC µmol-1 photon)	Slope of Chl-specific PE curve (Hansen et al. 2016); *Dinophysis*
D	opt_CR_	C	0.5	dl	proportion of prey of optimal characteristics captured by starved *Dinophysis*
D	tox_	C	0	dl	Toxicity factor for *Dinophysis*; 0 not toxic

Continued on next page

Table A.1 continued from previous page

o	vn	vt	equations and values	unit	description
D	r_	C	70/2	µm	radius of *Dinophysis* cell (Suzuki et al. 2009,Larsen and Moestrup 1992,Garcia-Cuetos et al. 2010;,Rodríguez et al. 2012,Bérard-Therriault et al. 1999)
D	relMaxPrey_	C	60/78	dl	maximum prey:*Dinophysis* size ratio
D	relMinPrey_	C	2/176	dl	minimum prey:*Dinophysis* size ratio
D	relOpPrey_	C	30/127	dl	optimal prey:*Dinophysis* size ratio
D	DON_leak_	A	Vnh4_Dino*PS_leakage+(DON_up_Dino*SDA + BR_Dino*uTP_Dino)	gN (gN)-1 d-1	loss of *Dinophysis* nh4 is SDA of DON uptake and basal respiration of growth rate (specific dynamic action + basal respiration + PS leak; *Dinophysis*
D	DON_up_	A	MAX(1e-9, ((0.1*UmT_Dino)*lDON)/ (Knh4_Dino+lDON))*op_Pil_Dino	gN (gN)-1 d-1	*Dinophysis* potential usage of DON (Fasham et al. 1990), DON*0.1 is for using only 10% of DON, which is labile and usable DON will only be taken up, if *Dinophysis* is photosynthesising. According to Fasham, DON is supplying carbon for photosynthesis
D	Ccell_	A	a*(4/3*PI*(r_Dino)^3)^b	pgC cell-1	C content of *Dinophysis*
D	Enc_Meso_	A	((24*60*6)*PI* (r_Dino/1E6+r_Meso/1E6)^2*nos_Meso* (v_Dino^2+3*v_Meso^2+4*w^2)*((v_Meso^2+w^2)^-0.5)* 3^-1+ (24*60*60)*PI* (r_Meso/1E6+r_Dino/1E6)^2*nos_Meso* (v_Meso^2+3*v_Dino^2+4*w^2)* ((v_Dino^2+w^2)^-0.5)*3^-1) /2	Alg Prot-1 d-1	encounter rate of a cell of *Mesodinium* by a cell of *Dinophysis*. If the prey is faster than the predator, the velocity for prey and predator are inverted.
D	Ncell_	A	Ccell_Dino*NC_Dino	pg N cell-1	N content per cell of *Dinophysis*
D	death_	A	IF(N_Dinophysis>1e-9, N_Dinophysis*(death_con+mort_Dino))	mgN m-3 d-1	*Dinophysis* death rate when growth rate falls beneath a limit and a continous death rate

Continued on next page

Table A.1 continued from previous page

o	vn	vt	equations and values	unit	description
D	delay_PiI_	A	IF(Av_PiI_Dino>0,1/decayT_Dino,0)	d-1	deterioration (loss of functionality) of opPiI assuming a linear relationship. There is a trap here because the linearity may be if Nu changes durng the decay event. *Dinophysis*
D	DON_	A	IF(N_Dinophysis>1e-9, N_Dinophysis*DON_leak_Dino,0)	gN (gN)-1 d-1	DON leak by *Dinophysis*
D	DONout_	A	SUM(death_Dino,void_Dino)	mgN m-3 d-1	DON leak from Dino
D	DONup_	A	IF(N_Dinophysis>1e-9,DON_up_Dino*N_Dinophysis)	mgN m-3 d-1	*Dinophysis* population growth rate supported by labile DON
D	ing	A	IF(N_Mesodinium>1e-9, ingN_Dino*N_Dinophysis,0)	gN (gN)-1 d-1	Ingestion rate of *Mesodinium*-N by *Dinophysis*
D	ing_	A	IF(N_Dinophysis>1e-9, N_Dinophysis*ingN_Dino,0)	mgN m-3 d-1	*Dinophysis* population ingestion rate
D	Nu_Dino_rate	A	(Nu_Dino-Nu_Dino_alt)*10	dl	N-status of *Dinophysis* (averaged intermediate)
D	reg_	A	IF(N_Dinophysis>1e-9, N_Dinophysis*netRegN_Dino,0)	mgN m-3 d-1	*Dinophysis* population N-regeneration rate
D	U_Dino_alt	A	(u_Dino-uAV_Dino_alt)*10	gN (gN)-1 d-1	growth rate of *Dinophysis* (average intermediate)
D	U_PiI_	A	IF(Av_PiI_Dino<PiI_Dino, (PiI_Dino-Av_PiI_Dino)/TIMESTEP,0)	dl	input to operational PiI; this ensures that the minimum level of the operational value is always the current PiI
D	upnh4_	A	IF(N_Dinophysis>1e-9, N_Dinophysis*(Vnh4_Dino),0)	mgN m-3 d-1	*Dinophysis* population growth rate supported by ammonium
D	void_	A	IF(N_Dinophysis>1e-9, N_Dinophysis*voidN_Dino,0)	mgN m-3 d-1	*Dinophysis* population N-voiding rate
D	wash_	A	dil*N_Dinophysis	mgN m-3 d-1	*Dinophysis* washout by dilution
D	washin_	A	dil*(Inoc_Dino)*0.2*Sw_land_runoff	mgN m-3 d-1	*Dinophysis* washin by dilution
D	assN_	A	ingN_Dino*AEN_Meso	gN (gN)-1 d-1	Assimilation rate of prey-N into *Dinophysis*-N

Continued on next page

Table A.1 continued from previous page

o	vn	vt	equations and values	unit	description
D	DeathI_	A	IF(uAV_Dino_alt<0 AND uAV_Dino_alt>growth_min_Dino, (uAV_Dino_alt/growth_min_Dino)^deathCo_Dino, 0)	dl	normalised death index, *Dinophysis*
D	growth_min_	A	-1*BR_Dino/2	dl	minimum growth rate of *Dinophysis*, where death is setting in at a moderate rate
D	maxGPS_	A	maxGU_Dino*pCritMax	gN (gN)-1 d-1	*Dinophysis* maximum N-specific growth rate as supported by phototrophy
D	maxGU_	A	UmT_Dino*(1+BR_Dino)	N/N/d	gross assimilation needed to support UmT_Dino
D	maxIAss_	A	maxGU_Dino-(maxGU_Dino*pCritMin)	N/N/d	maximum assimilation of ingested material, taking into account the maximum gross growth rate, and the critical proportion that must come via phototrophy (set by pCritMin) ; *Dinophysis*
D	mort_	A	IF(uAV_Dino_alt<growth_min_Dino,UmT_Dino, IF(uAV_Dino_alt>growth_min_Dino AND uAV_Dino_alt<0, DeathI_Dino*UmT_Dino,0))	N/N/d	death rate of *Dinophysis* when growth rate falls beneath a certain level
D	opmaxIAss_	A	MAX((UmT_Dino*BR_Dino),MIN(possU_Dino-PAss_Dino,maxIAss_Dino))	N/N/d	operational maximum possible assimilation of ingested material; this cannot exceed possU-grossPS, nor can it exceed maxgrossU/pCritmin. However, as a minimum level survival grazing is allowed; *Dinophysis*
D	opmaxIng_	A	opmaxIAss_Dino/(AEN_Meso*(1-SDA))	N/N/d	maximum possible Ingestion rate to satisfy the maximum possible assimilation rate, taking into account SDA and AE; *Dinophysis*
D	possU_	A	MIN((PAss_Dino+1e-6)/pCritMin,maxGU_Dino)	N/N/d	shortfall in N that could be covered by assimilation of ingested materials, taking into account any proportion of nutrition that must come via phototrophy (defined by pCritMin); inclusion of 1e-6 is to prevent a problem with PAss_Dino being 0

Continued on next page

Table A.1 continued from previous page

o	vn	vt	equations and values	unit	description
D	regNsda_	A	assN_Dino*SDA	gN (gN)-1 d-1	*Dinophysis* N-specific N-release rate; this amount may be regenerated, or potentially (for a mixotroph) re-assimilated
D	abco_	A	abco_Chl*opChlC_Dino/NC_Dino	m2 (mgN)-1	Phytoplankton-N2 specific coefficient for light absorbance
D	attco_	A	N_Dinophysis*abco_Dino	m-1	Attenuation coefficient to phytoplankton N-biomass
D	Inoc_	A	N_load*percent_Dino/100	µg N L-1	nitrogen initial inoculation of Dino (8 cells L-1)
D	cellprey_ cellpred_d_	A	lig_T_alt_Dino*(Ncell_Dino/Ncell_Meso)	cell Alg cell Prot-1 d-1	ingestion of *Mesodinium* cells per *Dinophysis* cells per day.
D	decayT_	A	critIR_Dino*Nu_Dino_alt	d	longetivity of phototrophy accounting for nutrient status (this is miply as a linear relationship; it could be sigmoidal, it could relate to UV etc.) (d); *Dinophysis*
D	ICrit_	A	1/critIR_Dino	cell cell -1 d-1	critical ingestion rate. *Mesodinium* cells per *Dinophysis* per day.
D	IInd_	A	(cellprey_cellpred_d_Dino/ICrit_Dino)	dl	ratio of cells eaten and cells *Dinophysis* needs to eat.
D	op_PiI_	A	IF(Av_PiI_Dino>0, MAX(Av_PiI_Dino, PiI_Dino),1e-12)	dl	operational photosynthetic ingestion index; this is done, so *Dinophysis* to have acquired a chloroplast in the past time
D	opAlphaChl_	A	op_PiI_Dino*alpha_Chl_Dino	(m2 g-1 chl.a)* (gC µmol-1 photon)	Slope of Chl-specific PE curve dependent on frequency of prey ingestion; *Dinophysis*
D	opPSmax_	A	opPSmax_NCM_Dino	gN gN-1 d-1	operational PSmax, this maximum PS rate cannot go above maxGPS_Dino (absolute PSmax) of the protist. In case of the phytoplankton and the CM this value is fix and equal to maxGPS_Dino. In case of the GNCM and SNCM this value is flexible

Continued on next page

Table A.1 continued from previous page

o	vn	vt	equations and values	unit	description
D	opPSmax_ NCM_	A	op_PiI_Dino*maxGPS_Dino	gN gN-1 d-1	maximum photosynthetic rate dependent on amount of ingested chloroplasts; *Dinophysis*
D	PiI_	A	IF(cellprey_cellpred_d_Dino>ICrit_Dino, 1,IInd_Dino)	dl	Prey ingestion index
D	opChlC_	A	op_PiI_Dino*ChlC_Dino	gChl (gC)-1	Chl:C ratio of *Dinophysis* ratioed to the relative maximum photosynthetic growth rate of the protist to the prey. For NCMs this value needs reconsideration!
D	Ndem_	A	PS_Dino*(1-MR)	N/N/d	N demand to satisfy concurrent photosynthesis corrected for MR costs; *Dinophysis*
D	netRegN_	A	IF(RegN_Dino>Ndem_Dino, RegN_Dino-Ndem_Dino,0)	N/N/d	net regeneration of N which occurs if internal regeneration of N exceeds the concurrent demands driven by incoming PS
D	PAss_	A	PS_Dino*(1-MR)	N/N/d	net phototrophy, from gross phototrophy minus the cost of anabolism required for incorportion of DIN. This is set by MR, but in reality it is affected by the f-ratio as far more effort is required to reduce NO3 to NH4 within the cell. *Dinophysis*
D	PVnh4_	A	IF(NH4>(14*0.01), maxGPS_Dino*TGnh4_Tele*NH4/ (NH4+Knh4_Tele),0)	gN (gN)-1 d-1	*Dinophysis* potential NH4 supply as transport PLUS the current internal regeneration of NH4. Limit is set to the limitation of NH4 detection. (Mol nitrogen, 14)
D	RegN_	A	regNsda_Dino+UmT_Dino*BR_Dino	N/N/d	regeneration rate through basal respiration PLUS also N released due to SDA for *Dinophysis*
D	TGnh4_	A	Umax_Dino*NC_Dino*8	dl	*Dinophysis* transport:growth needs ratio for ammonium
D	TGno3_	A	Umax_Dino*NC_Dino*2	dl	*Dinophysis* transport:growth needs ratio for nitrate ; set as 0 if incapable of using nitrate
D	Vnh4_	A	MIN(uTP_Dino,PVnh4_Dino)	gN (gN)-1 d-1	*Dinophysis* potential usage of ammonium

Continued on next page

Table A.1 continued from previous page

o	vn	vt	equations and values	unit	description
D	uTP_	A	IF(RegN_Dino<Ndem_Dino, Ndem_Dino-RegN_Dino,0)	N/N/d	net incorporation of DIN with phototrophy after usage of internally regenerated NH4 for *Dinophysis*
D	alphau_	A	opAlphaChl_Dino*opChlC_Dino	(m2)* (µmol-1 photon)	Specific slope of PE curve of *Dinophysis*
D	Nu_	A	MIN(1, (RegN_Dino+PVnh4_Dino)/PS_Dino)	dl	Nu status of phototrophic component of *Dinophysis*
D	PS_	A	PSqmax_Dino*(1-EXP(-alphau_Dino*avgPFD*24*60*60/ PSqmax_Dino))	N/N/d	gross PS for *Dinophysis*; uses averaged light over watercolumn NOT Smith integration
D	PSqmax_	A	opPSmax_Dino*Nu_Dino_alt	d-1	Maximum photosynthetic rate down-regulated by nutrient stress of *Dinophysis*
D	ingN_	A	IF(CRC_Meso>thres_Meso, MIN(opmaxIng_Dino*(CRC_Meso-thres_Alg)/ (CRC_Meso-thres_Meso+KI_Dino), CRC_Meso), 0)	gN (gN)-1 d-1	Ingestion rate of prey-N
D	KI_	A	opmaxIng_Dino/4	gN (gN)-1 d-1	satiation control constant
D	PR_Alg_	A	IF((relMaxPrey_Dino>rel_Alg_Dino AND rel_Alg_Dino>relMinPrey_Dino), IF (rel_Alg_Dino<relOpPrey_Dino, (rel_Alg_Dino-relMinPrey_Dino)/ (relOpPrey_Dino-relMinPrey_Dino), (relMaxPrey_Dino-rel_Alg_Dino)/ (relMaxPrey_Dino-relOpPrey_Dino)),0)	dl	Prey handling index for Alg by *Dinophysis*

Continued on next page

Table A.1 continued from previous page

o	vn	vt	equations and values	unit	description
D	PR_Meso_	A	IF((relMaxPrey_Dino>rel_Meso_Dino AND rel_Meso_Dino>relMinPrey_Dino), IF (rel_Meso_Dino<relOpPrey_Dino, (rel_Meso_Dino-relMinPrey_Dino)/ (relOpPrey_Dino-relMinPrey_Dino), (relMaxPrey_Dino-rel_Meso_Dino)/ (relMaxPrey_Dino-relOpPrey_Dino)),0)	dl	Prey handling index for *Mesodinium* by *Dinophysis*
D	rel_Alg_	A	r_Alg/r_Dino	dl	prey:pred radius for Alg:*Dinophysis*
D	rel_Meso_	A	r_Meso/r_Dino	dl	prey:pred radius for *Mesodinium*:*Dinophysis*
D	netPS_	A	Ndem_Dino-RegN_Dino	N/N/d	net photosynthesis of *Dinophysis*. Photosynthesis minus MR, SDA and BR. Essentially equal to uTP_Dino with the difference that it is not switched to 0, when it would become negative. For control purposes
D	nos_	A	10^9 *N_Dinophysis/Ncell_Dino	*Dinophysis* cells (m3)-1	Cell abundance of *Dinophysis* (10^6 = pg to ug; 10^3 = liter to m^3 –>10^9)
D	nosL_	A	nosML_Dino*1000	cells L-1	cell concentration of *Dinophysis*
D	nosML_	A	nos_Dino/10^6	*Dinophysis* cells ml-1	Cell abundance of *Dinophysis*
D	u_	A	ingN_Dino+uTP_Dino-voidN_Dino-netRegN_Dino	gN (gN)-1 d-1	growth rate of *Dinophysis*
D	uhet_	A	u_Dino-uTP_Dino	gN (gN)-1 d-1	heterotrophic growth rate of the *Dinophysis*
D	UmT_	A	Umax_Dino*Q10^((T-RT)/10)	gN gN-1 d-1	Umax at current temperature; this is the maximum possible growth rate which may only be achieved growing mixotrophically
D	voidN_	A	ingN_Dino*(1-AEN_Dino)	gN (gN)-1 d-1	voiding rate of N

Continued on next page

Table A.1 continued from previous page

o	vn	vt	equations and values	unit	description
D	N_Dinophysis	SV	Inoc_Dino - death_Dino - DON_Dino - reg_Dino - void_Dino - wash_Dino + DONup_Dino + ing_Dino + upnh4_Dino + washin_Dino	mgN m-3	*Dinophysis* N-biomass
D	Av_PiI_	SV	0 - delay_PiI_Dino+ U_PiI_Dino		operational photosynthetic ingestion index –>for *Dinophysis* to remember it has ingested a chloroplast before
D	Nu_Dino_alt	SV	0 + Nu_Dino_rate	dl	N-status of *Dinophysis* (averaged)
D	lig_T_alt_	SV	0 + ligMD	gN (gN)-1 d-1	ingestion rate by Dino intermediate
D	uAV_Dino_alt	SV	0 + U_Dino_alg	gN (gN)-1 d-1	
	DON_ex	C	3	mgN m-3	nitrogen initial inoculation of DON
	DON_labile	C	0.1	dl	percent of total DON that is transformed into labile DON (DFAA)
	Sw_DON_decay	C	0.3*0	dl	decay rate of labile DON
	Sw_land_runoff	C	0	dl	switch for nutrient runoff (land); when dil is switched on, only nutrients (from land) will be washed in and no organisms
	PS_leakage	C	0.1	dl	percentage of photosynthesis that is leaked out of the cell

Continued on next page

Table A.1 continued from previous page

o	vn	vt	equations and values	unit	description
	a	C	0.216	dl	Parameter for derivation of C-cell content for protist of a given volume
	b	C	0.939	d	l Parameter for derivation of C-cell content for protist of a given volume
	w	C	0	m s-1	root-mean-squared turbulence (ca. 0 to 0.003)
	dil	C	0	d-1	dilution rate
	LD	C	0.7	dl	proportion of time as lights-on
	MLD	C	5	m	Water (optical) depth
	N_load	C	280	µg N L-1	Total nitrogen in the system
	percent_NH4	C	10/100		proportion of nitrogen NH4 of total nutrient load
	percent_NO3	C	0.87	%	proportion of NO3 of total nitrogen load
	PFD	C	5	µmol photon m-2 s-1	Surface irradiance (set here as a constant)
	pCritMax	C	1	dl	maximum proportion of ProtUmax achievable using phototrophy alone
	pCritMin	C	0.1	dl	proportion of total resource required from phototrophy; this allows control of mixotrophy where the organism MUST procure a proportion of its C via phototrophic biochemistry
	SDA	C	0.3	gN (gN)-1	Specific dynamic action (anabolic respiration cost for assimilating N)
	abco_Chl	C	0.02	m2 (mg Chl)-1	Light absorbance coefficient for chlorophyll

Continued on next page

Table A.1 continued from previous page

o	vn	vt	equations and values	unit	description
	attco_W	C	0.05	m-1	Absorbance coefficient for growth medium (water)
	death_con	C	0.05	dl	continous death percentage of the entire population
	MR	C	0.2	N/N/d	anabolic respiration cost for assimilated DIN
	RT	C	15	deg C	reference temperature for UmRT (temperature in experiment)
	T	C	15	deg C	temperature
	UmRT	C	0.7	d-1	maximum growth rate using NH4-N at reference T
	Q10	C	1.8	dl	Q10 for UmRT
	DON_leak	A	SUM(Vnh4_Syn,Vno3_Syn)* PS_leakage+DON_up*SDA+BR_Syn*uTP_Syn	gN (gN)-1 d-1	loss of bacterial nh4 is SDA of DON uptake and basal respiration of growth rate (specific dynamic action + basal respiration + PS leak; *Synechoccus*
	DON_up	A	MAX(1e-9,((0.1*UmT_Syn)*lDON)/ (Knh4_Syn+lDON))	gN (gN)-1 d-1	Syn potential usage of DON (Fasham et al. 1990), DON*0.1 is for using only 10% of DON, which is labile and usable DON will only be taken up, if *Synechococcus* is photosynthesising. According to Fasham, DON is supplying carbon for photosynthesis
	external_NH4	A	percent_NH4*N_load	µg N L-1	nitrogen initial inoculation of NH4
	external_NO3	A	percent_NO3*N_load	µg N L-1	nitrogen initial inoculation of NO3
	t0_NH4	A	N_load*percent_NH4	µg N L-1	NH4 initial nutrient load
	t0_NO3	A	percent_NO3*N_load	µg N L-1	NO3 initial nutrient load

Continued on next page

Table A.1 continued from previous page

o	vn	vt	equations and values	unit	description
	AP	A	SUM(upnh4_Alg,upnh4_Syn,upnh4_Tele,upno3_Alg, upno3_Syn,upno3_Tele,upnh4_Dino, upnh4_Meso,upno3_Meso)*MLD	mmol N m-2 d-1	depth integrated areal primary production
	DONout	A	SUM(DONout_Syn,DONout_Alg, DON_Tele,DON_Meso,DON_Dino)	mgN m-3 d-1	DON leak from all organisms
	DONup	A	SUM(DON_Syn,DON_Alg, DONup_Tele,DONup_Meso,DONup_Dino)	mgN m-3 d-1	all organisms growth rate supported by labile DON
	lDON_decomp	A	lDON*Sw_DON_decay	mgN m-3 d-1	degradation rate of lDON by bacteria into NH4
	ligMD	A	(ingN_Dino-lig_T_alt_Dino)*10	gC (gC)-1 d-1	ingestion rate of Meso by Dino in carbon
	ligTM	A	(lig_Tele-lig_T_alt_Tel)*10	gC (gC)-1 d-1	ingestion rate of Tele by Meso in carbon
	slDON_decomp	A	slDON*Sw_DON_decay	mgN m-3 d-1	degradation rate of slDON by bacteria into NH4
	wash_lDON	A	dil*(DON_ex-lDON)	mgN m-3 d-1	lDON washin vs washout by dilution
	wash_nh4	A	dil*(external_NH4-NH4)	mgN m-3 d-1	Ammonium washin vs washout by dilution
	wash_no3	A	dil*(external_NO3-NO3)	mgN m-3 d-1	Nitrate washin vs washout by dilution
	wash_slDON	A	dil*(DON_ex-slDON)	mgN m-3 d-1	slDON washin vs washout by dilution
	avgPFD	A	Light_surf/att_tot*(1-EXP(-att_tot))	µmol photon m-2 s-1	light switch for specific amount of light, when light is on for distinct period of time (averaged over depth)
	Light_surf	A	IF(FRAC(TIME)<LD,PFD,0)	µmol photon m-2 s-1	light swich for specific amount of light, when light is on for distinct period of time
	Light_surface	A	IF(FRAC(TIME)<LD,PFD,0)	µmol photon m-2 s-1	light swich for specific amount of light, when light is on for distinct period of time

Continued on next page

Table A.1 continued from previous page

o	vn	vt	equations and values	unit	description
	att_tot	A	MAX(MLD*(attco_W+attco_Alg+ attco_Syn+attco_Tele+attco_Meso+ attco_Dino),1e-12)	dl	Total light attenuation
	exatt	A	EXP(-att_tot)	dl	negative exponent of total light attenuation
	sysN	A	NO3+NH4+N_Alg+N_Teleaulax+Synechococcus+ N_Mesodinium+N_Dinophysis+slDON+lDON	mgN m-3	System N-balance
	lDON	SV	0 - DONup - lDON_decomp + DONout + wash_lDON	mgN m-3	labile dissolved organic nitrogen (DON)
	slDON	SV	1 - slDON_decomp + death_Alg + death_Syn + Donout_Meso + DONout_Tele + wash_slDON	mgN m-3	semi-labile and lablie DON
	NH4	SV	t0_NH4 - upnh4_Syn - upnh4_Alg - upnh4_Tele - upnh4_Meso - upnh4_Dino + lDON_decomp+ slDON_decomp+ reg_Dino+ reg_Meso+ reg_Tele+ wash_nh4	mgN m-3	Ammonium-N

Continued on next page

Table A.1 continued from previous page

o	vn	vt	equations and values	unit	description
	NO3	SV	t0_NO3 - upno3_Syn - upno3_Alg - upno3_Tele - upno3_Meso + wash_no3	mgN m-3	Nitrate-N
	lig_T_alt_Tel	SV	0 + ligTM	gN (gN)-1 d-1	ingestion rate of *Teleaulax* (intermediate)
	cum_prod	SV	0 + cum_prod	mmolN m-2	cummulative primary production

Appendix B

Supplementary Material for the CNP *Teleaulax* model - model equations

TABLE B.1: Equations of the "Perfect Beast" Model (Flynn and Mitra, 2009) with the mixoplankton submodel configured as the constitutive mixoplankton *T. amphioxeia* after tuning the model to experimental data of the cryptophyte grown in three different nutrient conditions. Listed are the variable or constant namea, their equation or assigned value (definition) and the description of their function. vt = variable type (C = constant, A = auxiliary, SV = state variable). The equations are sorted by the organism they describe.

organism	name	vt	equations and values	documentation and unit
alga	*aAAsyn*	C	1.5	amino acid synthesis cost (C/N)
alga	*aAKt*	C	14*1	Algal half saturation constant for NH4 transport (ugN/L)
alga	*aalpha*	C	5.00E-06	Algal Chl-specific initial slope to PI curve, giving gC fixed per gChl.a per photon (m2g-1 chl.a)(gC umol-1 photon),
alga	*aApref*	C	2	Algal relative preference for NH4 usage; dl
alga	*abeta*	C	0.05	Algal power for controling uptake of non-limiting nutrient; dl
alga	*aBR*	C	0.05	phytoplankton basal respiration rate; dl
alga	*aChlabs*	C	0.06	Algal maximum possible ChlC; dl
alga	*aDOCpc*	C	0.1	% of Cfix released as DOC by phytoplankton; dl
alga	*aKQN*	C	10	Algal dimensionless quota constant for N; dl
alga	*aKQP*	C	0.1	Algal dimensionless quota constant for P; dl
alga	*aKxi*	C	0.1	Algal K for control of nutrient uptake; dl
alga	*aM*	C	3	Algal scalar for controlling photoacclimation (dl)
alga	*aMetMult*	C	3	Algal metabolic cost mutliplier to achieve required GGE for dinos; dl
alga	*aNCabs*	C	0.25	Algal absolute maximum N:C (gN/gC)
alga	*aNCmax*	C	0.25	Algal max N:C; gN g-1C

Continued on next page

Table B.1 continued from previous page

organism	name	vt	equations and values	documentation and unit
alga	*aNCmin*	C	0.06	Algal minimum NC (gN/gC)
alga	*aNKt*	C	14*1	Algal half saturation constant for NO3 transport (ugN/L)
alga	*aNpref*	C	1	Algal relative preference for NO3 usage; dl
alga	*aPCabs*	C	0.04	Algal absolute maximum P:C (gP/gC)
alga	*aPCmax*	C	0.02	Algal maximum P:C quota that affects growth (gP/gC)
alga	*aPCmin*	C	0.005247	Algal minimum PC (gP/gC)
alga	*aPKu*	C	31	Algal half saturation constant for DIP uptake (ugP/L)
alga	*aQh*	C	4	Algal control h for nutrient uptake; dl
alga	*aUmax*	C	0.7	Algal maximum rate of photosynthesis-driven growth; d-1
alga	*ESD_A*	C	3	ESD of phytoplankton; um
alga	*initaC*	C	1.00E-21	Algal initial carbon biomass (ugC/L)
alga	*tox_A*	C	0	toxicity factor for phytoplankton; 0 = non toxic dl
alga	*aalpha_OP*	A	IF(PFT=2, aalpha, 0)	Algal Chl-specific initial slope to PI curve, giving gC fixed per gChl.a per photon (m2g-1 chl.a)(gC umol-1 photon),
alga	*aAV*	A	IF((aUmpN<aAVP), 1, 0)*aUmpN+IF((aUmpN>=aAVP), 1, 0)*aAVP	Algal NH4 uptake (N/C/d)
alga	*aAVP*	A	IF((NH4>0), 1, 0)*aUmpN*aApref* NH4/(NH4+aAKt)	Algal potential relative NH4 transport; dl
alga	*aBRop*	A	aUmax*aBR*1.01* ((NCabs-aNC)/(NCabs-aNCmin))/ ((NCabs-aNC)/(NCabs-aNCmin)+0.01)* IF((aNC<NCabs), 1, 0)	Algal basal respiration rate, including term to halt respiration at high NC (gC/gC/d)
alga	*aChlC*	A	aChl/aC	Phytoplankton Chla:C (gChl/gC)

Continued on next page

Table B.1 continued from previous page

organism	name	vt	equations and values	documentation and unit
alga	*aChldeg*	A	aChlC*((1-aNCu)*aCu)	Phytoplankton change in ChlC with degradation with C growth (g Chl g-1C d-1)
alga	*aChlloss*	A	aChldeg*aC	loss of phytoplankton chlorophyll through degradation mgChl/m3/d
alga	*aChlsyn*	A	daChlC*aC	phytoplankton chlorophyll synthesis mgChl/m3/d
alga	*aCu*	A	aPS-aRphot-aBRop	Algal growth rate (d-1)
alga	*aDINup*	A	aupN*aC	Algal total DIN uptake ugN/L/d = mgN/m3/d
alga	*aDIPup*	A	aupP*aC	Algal total DIP uptake ugP/L/d = mgP/m3/d
alga	*aDOCout*	A	aC*aPS*aDOCpc	Algal contribution to DOC (ugC/L/d)
alga	*afrat*	A	aNV/(aNV+aAV+1e-12)	Algal f-ratio; dl
alga	*agro*	A	aC*aCu	algal population growth (ugC/L/d)
alga	*aICout*	A	aC*(aBRop+aRphot)	Algal DIC output (ugC/L/d)
alga	*aICup*	A	aC*aPS	Algal DIC uptake; mgC/m3/d
alga	*aIPup*	A	aC*aupP	Algal P uptake; mgP/m3/d
alga	*aN check*	A	aC*aNC	real conc of prey N (ugN/L)
alga	*aNC*	A	aN/aC	Algal N:C (gN/gC)
alga	*aNCu*	A	IF((aNC<=aNCmax), 1, 0)*IF((aNC>=aNCmin), 1, 0)* (1+aKQN)*(aNC-aNCmin)/((aNC-aNCmin)+aKQN* (aNCmax-aNCmin))+IF((aNC>aNCmax), 1, 0)	Algal normailised N/C quota description; dl
alga	*aNgraz*	A	mIgN_A	grazing of algal N biomass by mixoplankton mgN/m3/d

Continued on next page

Table B.1 continued from previous page

organism	name	vt	equations and values	documentation and unit
alga	*aNH4u*	A	aupN*(1-afrat)	Algal NH4 usage (N/C/d)
alga	*aNH4up*	A	aC*aNH4u	Algal NH4 uptake (ugN/L/d)
alga	*aNO3u*	A	aupN*afrat	Algal NO3 usage (N/C/d)
alga	*aNO3up*	A	aC*aNO3u	Algal NO3 uptake (ugN/L/d)
alga	*aNPCu*	A	MIN(1, MIN(aNCu, aPCu))	Algal threshold selection of phototrophic growth control (by N or P status dl)
alga	*aNV*	A	IF((aAVP<aUmpN), 1, 0)*(IF((aAVP+aNVP<aUmpN), 1, 0)*aNVP+IF((aAVP+aNVP>=aUmpN), 1, 0)*(aUmpN-aAVP))	Algal NO3 uptake (N/C/d)
alga	*aNVP*	A	IF((NO3>0), 1, 0)*aUmpN*aNpref* NO3/(NO3+aNKt)	Algal potential relative NO3 transport; dl
alga	*aP check*	A	aC*aPC	Algal biomass P (ugP/L)
alga	*aPC*	A	aP/aC	Algal P:C (gP/gC)
alga	*aPCu*	A	(1+aKQP)*(aPC-aPCmin)/((aPC-aPCmin)+aKQP* (aPCmax-aPCmin))*IF((aPCmin<aPC), 1, 0)* IF((aPC<aPCmax), 1, 0)+IF((aPC>=aPCmax), 1, 0)	Algal normailised P:C quota description (dl)
alga	*aPgraz*	A	mIgP_A	Grazing of algal P by mixoplankton mgP/m3/d
alga	*aPqm*	A	(aUmax+aBRop+aNCmax*aUmax* (aredco+aAAsyn*aMetMult))*aNPCu+1e-6	Algal potential maximum photosynthesis rate (gC g-1C d-1) was (Um+basres+NCm*Um*(redco+1.5))* MIN(NCu,PCu)+1e-6
alga	*aPS*	A	aPqm*(LN(aPyt+SQRT(1+aPyt^2))- LN(aPyt*exat+SQRT(1+(aPyt*exat)^2)))/attenuation	Algal depth integrated photosynthesis at a given instant in time taking into account mixing depth and attenuations; N/N/d
alga	*aPSrel*	A	MIN(1, aPS/aPqm)	Algal rate of photosynthesis relative to max (dl)

Continued on next page

Table B.1 continued from previous page

organism	name	vt	equations and values	documentation and unit
alga	*aPyt*	A	(aalpha*aChlC*PFD*24*60*60)/aPqm	Algal photosynthesis according to the Smith equation; dl
alga	*aRphot*	A	aredco*aupN*afrat+aupN*aAAsyn*aMetMult	Algal phototophic driven respiration (gC/gC/d)
alga	*aUmpN*	A	aUmax*aNCmax	Total Algal N uptake (N/C/d)
alga	*aupN*	A	(aAV+aNV)*(IF((aNCu>aNPCu), 1, 0)*IF((aNC<aNCabs), 1, 0)* aNPCu^abeta+IF((aNCu=aNPCu), 1, 0))* IF((aNC<aNCabs-0.002), 1, 0)*(1+aKxi^aQh)*(1-aNC/aNCabs)^aQh/ ((1-aNC/aNCabs)^aQh+aKxi^aQh)	Algal total DIN uptake (gN/gC/d)
alga	*aupP*	A	IF((DIP>0), 1, 0)*IF((aPC<aPCabs), 1, 0)*aUmax*5* aPCmax*(IF((aPCu>aNPCu), 1, 0)*aNPCu^abeta+IF((aPCu=aNPCu), 1, 0))*DIP/(DIP+aPKu)*(1+aQh^aKxi)* (1-aPC/aPCabs)^aQh/((1-aPC/aPCabs)^aQh+aKxi^aQh)	Algal DIP uptake (gP/gC/d)
alga	*Ccell_A*	A	a*(4/3*PI*(r_A)^3)^b	C content of phytoplankton cell pgC/cell
alga	*CR_A*	A	Encd_AM*PR_A*Palat_A*optimal_CR	potential capture of phytoplankton prey by mixoplankton taking into accoutn all factors (i.e., palatability, allometry, encounter rate) phytoplankton cells/mixoplankton cell/d
alga	*CRC_A*	A	CR_A*Ccell_A/Ccell_M	potential C specific ingestion of phytoplankton by mixoplankton gC/gC/d
alga	*daChlC*	A	IF((aChlC<aChlabs), 1, 0)*aChlabs*aNPCu*aM*aUmax* (1-MIN(1, aPS/aPqm))^0.5*(1+0.05)* (1-aChlC/aChlabs)/(1-aChlC/aChlabs+0.05)	Phytoplankton change in ChlC with synthesis with C growth (g Chl g-1C d-1)
alga	*nos_A*	A	1e9*aC/Ccell_A	numeric cell abundance of phytoplankton Phy cells/m3
alga	*Palat_A*	A	(aNCu+1e-6)^tox_A	palatability index for phytoplankton dl

Continued on next page

Table B.1 continued from previous page

organism	name	vt	equations and values	documentation and unit
alga	*PR_A*	A	IF((relMaxPrey>rel_A AND rel_A>relMinPrey), IF(rel_A<relOpPrey, (rel_A-relMinPrey)/(relOpPrey-relMinPrey), (relMaxPrey-rel_A)/(relMaxPrey-relOpPrey)), 0)	Prey handling index for phytoplankton by mixoplankton, taking into account the prey:pred relative size dl
alga	*r_A*	A	ESD_A/2	phytoplankton radius; um
alga	*rel_A*	A	r_A/r_M	prey:pred for phytoplankton dl
alga	*v_A*	A	1e-6*(38.542*(ESD_A^0.5424))	motility of phytoplankton; m/s
alga	*waChl*	A	DIL*aChl	dilution rate of chlorophyll; mgChl/m3
alga	*waN*	A	DIL*aN	dilution rate of phytoplankton nitrogen; mgN/m3
alga	*waP*	A	DIL*aP	dilution rate of phytoplankton phosphorus; mgP/m3
alga	*wSC*	A	DIL*aC	Algal wash in/out (ugC/L/d)
alga	*aC*	SV	initaC -aCgraz +agro -wSC	Phytoplankton (prey) C; ugC/L = mgC/m3
alga	*aChl*	SV	aC*aChlabs -aChlgraz -aChlloss +aChlsyn -waChl	chlorophyll content of phytoplankton mgChl/m3
alga	*aN*	SV	aNCmax*initaC +aDINup -aNgraz -waN	phytoplankton N biomass mgN/m3

Continued on next page

Table B.1 continued from previous page

organism	name	vt	equations and values	documentation and unit
alga	*aP*	SV	initaC*aPCmax +aDIPup -aPgraz -waP	algal P biomass ugP/L = mgP/m3
bacteria	*bBNC*	C	0.12	Bacterial N:C (g/g)
bacteria	*bBPC*	C	0.045	Bacterial P:C (g/g)
bacteria	*bcM*	C	2	Bacterial cost multiplier to alter the respiration rate of the cell; dl
bacteria	*bINrs*	C	1.46	Bacterial Respiratory cost for the assimilation of ammonium; gC respired per gDIN incorporated (E.coli data, assuming N is as NH4 and C is as sugars). (gC/gN)
bacteria	*bKcN*	C	14	Bacterial K for cDOM_N (ugN/L)
bacteria	*bKcOMC*	C	24	Bacterial K for cDOM-C (ugC/L)
bacteria	*bKcP*	C	0.31	Bacterial K for cDOM-P (ugP/L)
bacteria	*bKN*	C	1.4	Bacterial K for DIN (ugN/L)
bacteria	*bKOC*	C	12	Bacterial half saturation for DOC-C (ugC/L)
bacteria	*bKP*	C	0.31	Bacterial K for DIP (ugP/L)
bacteria	*bKsOMC*	C	12	half saturation for sDOM-C (ugC/L)
bacteria	*bmNC*	C	0.5	Bacterial max N:C for usage (gN/gC)
bacteria	*bmPC*	C	0.05	Bacterial max P:C for usage (gP/gC)

Continued on next page

Table B.1 continued from previous page

organism	name	vt	equations and values	documentation and unit
bacteria	*bONrs*	C	0.857	Bacterial respiratory cost for the assimilation of amino acids; gC respired per gDON assimilated, assumes DON is as amino acids BUT that C is as sugars. It also assumes that the full range of amino; dl acids are available. (gC/gN)
bacteria	*brbasC*	C	0.05	Bacterial basal respiration when just C is limiting (gC/gC/d)
bacteria	*brbasN*	C	0.1	Bacterial basal respiration term when N is limiting (gC/gC/d)
bacteria	*brbasP*	C	0.2	Bacterial basal respiration term when P is limiting (gC/gC/d)
bacteria	*brelcCPref*	C	0.25	relative preference of cDOMC by bacteria; dl
bacteria	*brelcXpref*	C	1	Bacterial relative C preference (dl)
bacteria	*brelpref*	C	1	Bacterial relative preference of DOMX over DIX; must >=1; if preference is for DIX then this index must be pointed to DIX (dl)
bacteria	*brelsCpref*	C	1	Bacterial relative preference of DOM-C over DOC; must >=1; if preference is for DOC then this index must be pointed to DOC (dl)
bacteria	*bUm*	C	0.501	Bacterial maximum net growth rate (gC/gC/d)
bacteria	*ESD_B*	C	0.45	ESD of bacteria; um
bacteria	*initbC*	C	1.00E-21	Bacterial initial biomass; mgC/m3 = ugC/L
bacteria	*NCm*	C	0.3	maximum mass ratio of N:C which could be attained in the organic form, (gN/gC)
bacteria	*PCm*	C	0.03	maximum mass ratio of P:C which could be attained in the organic form (gP/gC)
bacteria	*bBN*	A	BC*bBNC	Bacterial N (ugN/L)

Continued on next page

Table B.1 continued from previous page

organism	name	vt	equations and values	documentation and unit
bacteria	*bBP*	A	BC*bBPC	Bacterial P (ugP/L)
bacteria	*bBR*	A	bRbas*bUm*(1-brelU)	Bacterial basal respiration (gC/gC/d)
bacteria	*bbrelN*	A	(btotNV/btotCV)/bBNC	Bacterial relative N use (actual N uptake / actual C uptake)/N/C (dl)
bacteria	*bbrelP*	A	(btotPV/btotCV)/bBPC	Bacterial relative P use (actual P uptake / actual C uptake)/P/C (dl)
bacteria	*bC_wash*	A	DIL*BC	Bacterial washout (ugC/L/d)
bacteria	*bcOMCup*	A	BC*bcOMu	Bacterial DOM-C uptake (ugC/L/d)
bacteria	*bcOMCV*	A	brelcCPref*cDOMC/(cDOMC+bKcOMC)	Bacterial cDOM-C availability; quotient for uptake of C from cDOM, with preference scalar (dl)
bacteria	*bcOMNup*	A	BC*bcONu	Bacterial uptake of cDOM-N (ugN/L/d)
bacteria	*bcOMNV*	A	IF((cDOMN>0), 1, 0)*cDOMN/(cDOMN+bKcN)*brelcXpref	Bacterial cDOM-N availability (dl)
bacteria	*bcOMPup*	A	BC*bcOPu	Bacterial uptake of cDOM-P (ugP/L/d)
bacteria	*bcOMPv*	A	IF(cDOMP>0, cDOMP/(cDOMP+bKcP)*brelcXpref)	Bacterial cDOM-P availability (dl)
bacteria	*bcOMu*	A	bgroCu-bOCuse-bsOMu	DOM-C from combined DOM (C/C/d)
bacteria	*bcONC*	A	IF(cDOMN>0.001, cDOMN/(cDOMC+1e-200))	semilabile DOM N:C use (N/C)
bacteria	*bConcON*	A	IF((bcONC>bmNC), 1, 0)*IF((cDOMN>0), 1, 0)*bcONC/bmNC*2	Bacterial use of cDOM-N (ugN/L/d)
bacteria	*bConcOP*	A	IF((bcOPC>bmPC), 1, 0)*IF((cDOMP>0), 1, 0)*bcOPC/bmPC*2	Bacterial use of cDOM-P (ugP/L/d)
bacteria	*bConsON*	A	IF((bsONC>bmNC), 1, 0)*IF((sDOMN>0), 1, 0)*bsONC/bmNC*2	Bacterial use of sDOM-N (ugN/L/d)
bacteria	*bConsOP*	A	IF((bsOPC>bmPC), 1, 0)*IF((sDOMP>0), 1, 0)*bsOPC/bmPC*2	Bacterial use of sDOM-P (ugP/L/d)

Continued on next page

Table B.1 continued from previous page

organism	name	vt	equations and values	documentation and unit
bacteria	*bcONu*	A	bgroNu-bINu-bsONu	potential contribution to N needs from cDOM-N (N/C/d)
bacteria	*bcOPC*	A	IF(cDOMP>0.001, cDOMP/(cDOMC+1e-200))	refractory DOM P:C (gP/gC)
bacteria	*bcOPu*	A	bgroPu-bIPu-bsOPu	potential contribtion to P needs from cDOM-P (P/C/d)
bacteria	*bCRes*	A	bmCres+bBR	respiration of C from bacteria associated with basal and metabolic respiration (ugC/L/d)
bacteria	*bCu*	A	bOCuse+bsOMu+bcOMu-bCRes	net growth rate (gC/gC/d)
bacteria	*bCup*	A	BC*(bOCuse+bsOMu+bcOMu)	total gross intake of C to bacteria (ugC/L/d)
bacteria	*bDINup*	A	bINu*BC*IF((NH4>0), 1, 0)	Bacterial NH4 uptake (ugN/L/d)
bacteria	*bDIPup*	A	bIPu*BC*IF((DIP>0), 1, 0)	Bacterial uptake of DIP (ugP/L/d)
bacteria	*bDIPV*	A	IF(DIP>0, DIP/(DIP+bKP))	Bacterial DIP availability (dl)
bacteria	*bDOCup*	A	BC*bOCuse	Bacterial uptake of DOC-C (ugC/L/d)
bacteria	*bgroCu*	A	MIN(bbrelN, bbrelP, 1)*btotCV	total need for C by bacteria (gC/gC/d)
bacteria	*bgroNu*	A	bgroCu/(1/bBNC+bNrsyn)	total need for N by bacteria (gN/gC/d)
bacteria	*bgroPu*	A	bgroNu*bBPC/bBNC	total need for P by bacteria (gP/gC/d)
bacteria	*bICout*	A	BC*bCRes	Bacterial DIC output (ugC/L/d)
bacteria	*bINu*	A	bgroNu*bINV/(bINV+bsOMNV+bcOMNV)	Bacterial DIN use (N/C/d)
bacteria	*bINV*	A	NH4/(NH4+bKN)*IF((NH4>0), 1, 0)	Bacterial NH4 availability (dl)
bacteria	*bIPu*	A	bgroPu*bDIPV/(bDIPV+bsOMPV+bcOMPv)	Bacterial DIP use (P/C/d)

Continued on next page

Table B.1 continued from previous page

organism	name	vt	equations and values	documentation and unit
bacteria	*bmCres*	A	((bsONu*bONrs+bINu*bINrs)+bcONu*bONrs)*bcM	bacterial metabolic respiration cost; ugC/L/d
bacteria	*bNrsyn*	A	bcM*(bINrs*bINV+bONrs*(bsOMNV+bcOMNV))/ (bINV+bsOMNV+bcOMNV)	Bacterial cost of N-assimilation; dl
bacteria	*bOCuse*	A	bgroCu*bOCV/(bOCV+bsOMCV+bcOMCV)	Bacterial use of DOC (gC/gC/d)
bacteria	*bOCV*	A	IF((DOC>0), 1, 0)*DOC/(DOC+bKOC)	quotient for uptake of DOC (dl)
bacteria	*bRbas*	A	brbasC+MAX((1-bbrelN)*(brbasN-brbasC)* IF((bbrelN<=1), 1, 0), (1-bbrelP)*(brbasP-brbasC)* IF((bbrelP<=1), 1, 0))	Basal respiration rate control; contains a switch to set basal respiration depending on whether N or P is more limiting (gC/gC/d)
bacteria	*bregN*	A	bBR*BC*bBNC+bConsON+bConcON	Bacterial regulation of N use (ugN/L/d)
bacteria	*bregP*	A	bBR*BC*bBPC+bConsOP+bConcOP	Bacterial regulation of P use (ugP/L/d)
bacteria	*brelU*	A	bgroCu/bVm	Bacterial relative growth rate (dl)
bacteria	*bsOMCup*	A	BC*bsOMu	uptake of sDOM-C into bacteria (ugC/L/d)
bacteria	*bsOMCV*	A	brelsCpref*sDOMC/(sDOMC+bKsOMC)* IF((sDOMC>0), 1, 0)	Bacterial sDOM-C availability; quotient for uptake of C from sDOM, with preference scalar (dl)
bacteria	*bsOMNup*	A	BC*bsONu	Bacterial uptake of sDOM-N (ugN/L/d)
bacteria	*bsOMNV*	A	IF((sDOMN>0), 1, 0)*sDOMN/(sDOMN+bKN)*brelpref	Bacterial sDOM-N availability (dl)
bacteria	*bsOMPup*	A	BC*bsOPu	Bacterial sDOP usage (ugP/L/d)
bacteria	*bsOMPV*	A	IF(sDOMP>0, sDOMP/(sDOMP+bKP)*brelpref)	Bacterial sDOM-P availability (dl)
bacteria	*bsOMu*	A	bgroCu*bsOMCV/(bOCV+bsOMCV+bcOMCV)	use of C from semi-labile DOM; balance of C need comes from DOM (gC/gC/d)

Continued on next page

Table B.1 continued from previous page

organism	name	vt	equations and values	documentation and unit
bacteria	*bsONC*	A	sDOMN/sDOMC*IF((sDOMN>0), 1, 0)	semilabile DOM N:C (gN/gC)
bacteria	*bsONu*	A	bgroNu*bsOMNV/(bINV+bsOMNV+bcOMNV)	Bacterial sDOM-N use (N/C/d)
bacteria	*bsOPC*	A	sDOMP/sDOMC*IF((sDOMP>0), 1, 0)	semilabile DOM P:C (gP/gC)
bacteria	*bsOPu*	A	bgroPu*bsOMPV/(bDIPV+bsOMPV+bcOMPv)	Bacterial sDOM-P use (P/C/d)
bacteria	*btotCV*	A	MIN(bVm, bVm*(bOCV+bsOMCV+bcOMCV))	actual rate of C uptake (gC/gC/d)
bacteria	*btotNV*	A	bBNC*bVm*MIN(bINV+bsOMNV+bcOMNV, 1)	Bacterial total N usage (gN/gC/d)
bacteria	*btotPV*	A	bBPC*bVm*MIN(bDIPV+bsOMPV+bcOMPv, 1)	Bacterial total P usage (gP/gC/d)
bacteria	*bVm*	A	bUm+bcM*bUm*bONrs*bBNC	Gross growth rate (gC/gC/d)
bacteria	*Ccell_B*	A	a*(4/3*PI*(r_B)^3)^b	C content of bacterial cell pgC/cell
bacteria	*CR_B*	A	Encd_BM*PR_B*optimal_CR	potential capture of bacterial prey by mixoplankton taking into account all factors (i.e., allometry, encounter rate) bacterial cells/mixoplankton cell/d
bacteria	*CRC_B*	A	CR_B*Ccell_B/Ccell_M	potential C-specific ingestion of bacteria by mixoplankton gC/gC/d
bacteria	*DINr*	A	resN+(mVONtr-mVONt)	Mixoplankton regeneration rate of N as NH4 (gN/gC/d)
bacteria	*DIPr*	A	resP+(mVOPtr-mVOPt)	Mixoplankton regeneration rate of P as DIP (gP/gC/d)
bacteria	*hetCup*	A	mCas_OP-Rhet	heterotrophic assimilation of C (gC/gC/d)
bacteria	*hetNup*	A	'mNas OP'-(resN+nh4reas)	heterotrophic assimilation of N by mixoplankton (gN/gC/d)
bacteria	*hetPup*	A	mPas_OP-(resP+Preas)	heterotrophic assimilation of P by mixoplankton (gP/gC/d)
bacteria	*HGGE*	A	(mCas_OP-Rhet)/'lgCA OP'	hetero GGE; dl

Continued on next page

Table B.1 continued from previous page

organism	name	vt	equations and values	documentation and unit
bacteria	*mICout*	A	mC*(mRTot+mBRi)	Mixoplankton DIC output (ugC/L/d) (ugC/L/d)
bacteria	*mICup*	A	mC*mPS	Mixoplankton DIC uptake (ugC/L/d)
bacteria	*mIPup*	A	mC*mIPu_OP	Mixoplankton P uptake (ugP/L/d)
bacteria	*mNH4u*	A	mupN_OP*(1-mfrat)	Mixoplankton NH4 transport (gN/gC/d)
bacteria	*mNH4up*	A	mC*mNH4u	Mixoplankton NH4 uptake (ugN/L/d)
bacteria	*mNO3u*	A	(mupN_OP*mfrat)	NO3 transport (gN/gC/d)
bacteria	*mNO3up*	A	mC*mNO3u	Mixoplankton NO3 uptake (ugN/L/d)
bacteria	*mregN*	A	DINr*mC	Mixotroph N release (ugN/L/d)
bacteria	*mregP*	A	DIPr*mC	Mixoplankton total P release (ugP/L/d)
bacteria	*mVOCt*	A	mDgC-mCas_OP-(mBRi+100e-102)	Mixoplankton loss of C as POC (gC/gC/d)
bacteria	*mVONL*	A	mVONt*mC+mFNdeath+mNdeath	Mixoplankton loss of N as PON (ugN/L/d)
bacteria	*mVONt*	A	(IF(((mVONtr/mVOCt)>NCm), 1, 0)*mVOCt*NCm)+ (IF(((mVONtr/mVOCt)<=NCm), 1, 0)*mVONtr)+1e-9	Mixoplankton rate of removal of excess nitrogen to maintain N:C constant (N/C/d)
bacteria	*mVONtr*	A	mDgC*mfFNC-mCas_OP*mNCm	Mixoplankton rate of N voiding as balance of that ingested versus that required to maintain mixotroph N:C (N/C/d)
bacteria	*mVOPt*	A	(IF(((mVOPtr/mVOCt)>PCm), 1, 0)*mVOCt*PCm)+ (IF(((mVOPtr/mVOCt)<=PCm), 1, 0)*mVOPtr)+1e-9	Mixoplankton rate of removal of excess P to maintain the predator P:C constant (P/C/d)
bacteria	*mVOPtr*	A	mDgC*mfFPC-mCas_OP*mPCm	Mixoplankton rate of P voiding as balance of that ingested versus that required to maintain P:C (P/C/d)

Continued on next page

Table B.1 continued from previous page

organism	name	vt	equations and values	documentation and unit
bacteria	*nh4reas*	A	Rhet*mNCm*(1-RegN)	Mixoplankton NH4 re-assimilated (gN/gC/d)
bacteria	*nos_B*	A	1e9*BC/Ccell_B	numeric abundance of bacterial cells bacterial cells/m3
bacteria	*Npcreas*	A	nh4reas/photNup*100	Mixoplankton % total N assimilated that is obtained by re-assimilation; %
bacteria	*PGGE*	A	(mPS-Rphot)/mPS	Mixoplankton photo GGE; dl
bacteria	*photCup*	A	mPS-Rphot	Mixoplankton net photosynthesis (gC/gC/d)
bacteria	*photNup*	A	mupN_OP+nh4reas	Mixoplankton total phototrophic N assimilation (N/C/d)
bacteria	*photPup*	A	mIPu_OP+Preas	Mixoplankton total phototrophic P assimilation (P/C/d)
bacteria	*Ppcreas*	A	Preas/photPup*100	Mixoplankton % total P assimilated that is obtained by re-assimilation; %
bacteria	*PR_B*	A	IF((relMaxPrey>rel_B AND rel_B>relMinPrey), IF(rel_B<relOpPrey, (rel_B-relMinPrey)/ (relOpPrey-relMinPrey), (relMaxPrey-rel_B)/(relMaxPrey-relOpPrey)), 0)	prey handling index for bacteria by mixoplankton, taking into account the prey:pred relative size; dl
bacteria	*Preas*	A	Rhet*mPCm*(1-RegP)	Mixoplankton P re-assimilated (gP/gC/d)
bacteria	*r_B*	A	ESD_B/2	bacteria radius; um
bacteria	*rel_B*	A	r_B/r_M	prey:pred for bacteria dl
bacteria	*sDOMCout*	A	DIL*(sDOMC-initsDOMC)+bsOMCup	DOMC in/out and bacterial usage (ugC/L/d)
bacteria	*sDOMNout*	A	DIL*(sDOMN-initsDOMN)+bConsON+bsOMNup	DOM-N in/out and bacterial usage (ugN/L/d)
bacteria	*sDOMPout*	A	DIL*(sDOMP-initsDOMP)+bConsOP+bsOMPup	DOM-P in/out abnd bacterial usage (ugP/L/d)

Continued on next page

Table B.1 continued from previous page

organism	name	vt	equations and values	documentation and unit
bacteria	*tf_rat*	A	mNO3u/(hetNup+mNH4u+mNO3u)	total f-ratio, taking into account heterotrophic N-assimilation; dl
bacteria	*v_B*	A	1e-6*(38.542*(ESD_B^0.5424))	motility of bacteria; m/s
bacteria	*VOCL*	A	mVOCt*mC+mCdeath+mFCdeath	Mixoplankton rate of removal of excess carbon to maintain the Mixoplankton X:C constant (ugC/L/d)
bacteria	*BC*	SV	initbC -bC_wash +bCup -bICout -mIgC_B	bacterial carbon biomass; ugC/L = mgC/m3
external	*a*	C	0.216	Parameter for derivation of Ccell content for protist of a given volume; dl
external	*aredco*	C	1.71	C respired to support nitrate reduction through to intracellular ammonium (gC/gN)
external	*b*	C	0.939	Parameter for derivation of Ccell content for protist of a given volume; dl
external	*ChlAtt*	C	0.02	attentuation of light by Chl (m2/mgChl) note that ugChl/L = mgChl/m3 Chl abs in red light Kirk 75; 10.94 m2/gChl; Fasham et al 06 used 20
external	*initDIC*	C	25000	Initial DIC (ugC/L)
external	*initDIP*	C	55.4	Initial DIP (ugP/L)
external	*initDOC*	C	12	Initial DOC (ugC/L)
external	*initNH4*	C	14*1	Initial NH4 (ugN/L)

Continued on next page

Table B.1 continued from previous page

organism	name	vt	equations and values	documentation and unit
external	*initNO3*	C	438.3	Initial NO3 (ugN/L)
external	*initsDOMC*	C	12*1	Initial semi-labile DOM-C (ugC/L)
external	*initsDOMN*	C	14*0.1	Initial semi-labile DOM-N (ugN/L)
external	*initsDOMP*	C	31*0.01	Initial semi-labile DOM-P (ugP/L)
external	*LD*	C	16/24	fraction of day illuminated; dl
external	*mix_depth*	C	0.2	mixed layer depth; set at 1e-12 to disregard (m)
external	*PAR*	C	350	Surface PAR (umol photon/m2/s)
external	*w*	C	0	root-mean-squared turbulence m/2 values between 0 and 0.003; m s-1
external	*water_atten*	C	0.05	attenuation of light by water (m-1)
external	*attenuation*	A	mix_depth*(water_atten+TChl*ChlAtt)	attenuation of light by water and by Chl; dl
external	*DICin*	A	aICout+mICout+bICout	Changes in DIC due to algal, mixotroph and bacterial consumptions (ugC/L/d)
external	*DICuse*	A	(aICup+mICup+aDOCout+mDOCout)	DIC use by algae and mixotrophs; note there is an additional part that goes to contribute to DOC production; (ugN/L/d)
external	*DIPin*	A	mregP+bregP	regenerative input of DIP (ugP/L/d)
external	*DIPuse*	A	aIPup+mIPup+bDIPup	DIP usage (ugP/L/d)
external	*DOCin*	A	mDOCout+aDOCout	DOC contributions from algal and mixotroph C-fixation (ugC/L/d)
external	*DOCout*	A	DIL*(DOC-initDOC)+bDOCup	Changes in DOC by washin/out and bacterial consumption (ugC/L/d)

Continued on next page

Table B.1 continued from previous page

organism	name	vt	equations and values	documentation and unit
external	*exat*	A	EXP(-attenuation)	exponent of attenuation dl [mathematical intermediate]; dl
external	*LDcycle*	A	IF((FRAC(TIME)<LD), 1, 0)	light dark cycle; dl
external	*NH4in*	A	mregN+bregN	Regeneration of NH4 from mixotroph and bacteria (ugN/L/d)
external	*NH4use*	A	aNH4up+mNH4up+bDINup	NH4 usage by algae, bac and mixotroph (ugN/L/d)
external	*NO3use*	A	mNO3up+aNO3up	NO3 usage by algae and mixotroph (ugN/L/d)
external	*PFD*	A	PAR*LDcycle	Available surface PAR; Ámol photon m-2 s-1
external	*sysC*	A	DIC+aC+mC+mFC+BC+DOC+sDOMC	system C (ugC/L)
external	*sysN*	A	NH4+NO3+mN+mFN+sDOMN+aN+bBN	system N (ugN/L)
external	*sysP*	A	DIP+aP+mP+mFP+bBP+sDOMP	system P (ugP/L)
external	*TChl*	A	mC*(mChlC+mFChlC)+aC*aChlC	total Chl (ugChl/L)
external	*wDIC*	A	DIL*(DIC-initDIC)	DIC wash in/out (ugC/L/d)
external	*wDIP*	A	DIL*(DIP-initDIP)	DIP wash in/out (ugP/L/d)
external	*wNH4*	A	DIL*(NH4-initNH4)	NH4 wash in/out (ugN/L/d)
external	*wNO3*	A	DIL*(NO3-initNO3)	NO3 wash in/out (ugN/L/d)
external	*DIC*	SV	initDIC +DICin -DICuse -wDIC	Dissolved Inorganic Carbon; ugC/L = mgC/m3

Continued on next page

Table B.1 continued from previous page

organism	name	vt	equations and values	documentation and unit
external	*DIP*	SV	initDIP +DIPin -DIPuse -wDIP	dissolved inorganic phosphorus; mgP/m3
external	*DOC*	SV	initDOC +DOCin -DOCout	Disoolved Organic Carbon (i.e., with NO N or P), 12 is 1uM; ugC/L = mgC/m3
external	*NH4*	SV	initNH4 +NH4in -NH4use -wNH4	ammonia; ugN/L = mgN/m3
external	*NO3*	SV	initNO3 -NO3use -wNO3	nitrate; ugN/L = mgN/m3
external	*sDOMC*	SV	initsDOMC -sDOMCout +VOCL	semi-labile dissolved organic material as carbon; ugC/L = mgC/m3
external	*sDOMN*	SV	initsDOMN +mVONL -sDOMNout	semi-labile dissolved organic material as nitrogen; ugN/L = mgN/m3
external	*sDOMP*	SV	initsDOMP +mVOPL -sDOMPout	semi-labile dissolved organic matter as phosphorus; ugP/L = mgP/m3
mixoplankton	*AEmax*	C	0.8	Mixoplankton maximum value of AE; this cannot attain 1, dl

Continued on next page

Table B.1 continued from previous page

organism	name	vt	equations and values	documentation and unit
mixoplankton	*AEmin*	C	0.2	Mixoplankton minimum AE when confronted with excess ingestion; dl
mixoplankton	*avgT*	C	0.5	averaging time; d
mixoplankton	*death_R*	C	0.05	Mixoplankton specific mortality rate; gC/gC/d
mixoplankton	*DIL*	C	0.05*0	wash in/out (dilution) rate (d-1)
mixoplankton	*Enc_crit*	C	20	number of days that a NCM can survive without needing fresh prey to conduct phototrophy days; d
mixoplankton	*ESD_M*	C	5	ESD of *Teleaulax*, um
mixoplankton	*FCabs*	C	0.2	Mixoplankton maximum possible digestive vacuole size (gC/gC)
mixoplankton	*FCmin*	C	0	Mixoplankton minimum digestive vacuole size; this need not be zero (gC/gC)
mixoplankton	*halfLife*	C	10	half life of chloroplast machinery days; d
mixoplankton	*Hasm*	C	4	Mixoplankton Hill constant for digestion rate (dl)
mixoplankton	*Heq*	C	4	Mixoplankton AE control Hill function dl
mixoplankton	*Hhet*	C	20	Mixoplankton Hill for derepression of digestive vacuole size (dl)
mixoplankton	*Hlng*	C	4	Mixoplankton H for feedback of ingestion from how replete gut is dl
mixoplankton	*Hpbal*	C	4	Mixoplankton H for Pbal control (dl)
mixoplankton	*Hpd*	C	10	Mixoplankton control of digestion dl

Continued on next page

Table B.1 continued from previous page

organism	name	vt	equations and values	documentation and unit
mixoplankton	*HRC*	C	4	Mixoplankton Hill function for control of X regeneration vs re-assimilation
mixoplankton	*Hv*	C	9	Hill constant for description of mixoplankton motility associated with satiation; dl
mixoplankton	*initmC*	C	112.1	Mixoplankton initial carbon biomass; mgC/m3 = ugC/L
mixoplankton	*Kasm*	C	0.25	Mixoplankton half saturation for digestion rate (dl)
mixoplankton	*Kec*	C	10	Mixoplankton half saturation constant for AE_FQ, to compute AE; 10 gives maximum; 1e-6 to switch off; dl
mixoplankton	*Keq*	C	1.00E-06	Mixoplankton half saturation constant for AE control standard value is 0.4; set at 1e-6 to remove this link; dl
mixoplankton	*Khet*	C	1	Mixoplankton K for control of switching on predation as relPS declines; dl
mixoplankton	*KIng*	C	0.64	Mixoplankton half saturation constant for control of ingestion based on satiation dl
mixoplankton	*Kpbal*	C	0.1	Mixoplankton K for controlling pbal (dl)
mixoplankton	*Kpd*	C	1	Mixoplankton control of digestion dl
mixoplankton	*KQP*	C	0.1	Mixoplankton dimensionless quota constant for P; dl
mixoplankton	*KRC*	C	1	Mixoplankton K for control of X regeneration vs re-assimilation; regeneration becomes increasingly likely as X:C tends to XCabs
mixoplankton	*Kv*	C	0.3	half saturation constant for description of mixoplankton motility associated with satiation; dl

Continued on next page

Table B.1 continued from previous page

organism	name	vt	equations and values	documentation and unit
mixoplankton	*mAAsyn*	C	1.5	amino acid synthesis cost (C/N)
mixoplankton	*mAKt*	C	14*1	Mixoplankton half saturation constant for NH4 transport ugN/L
mixoplankton	*malpha*	C	5.00E-06	Chl-specific initial slope to PI curve, giving gC fixed per gChl.a per photon (m2g-1 chl.a)(gC umol-1 photon) This is relevant for CM, SNCM and phytoplankton
mixoplankton	*mApref*	C	2	Mixoplankton relative preference for NH4 usage dl
mixoplankton	*mbeta*	C	0.05	Mixoplankton power for controling uptake of non-limiting nutrient dl
mixoplankton	*mBR*	C	0.05	mixoplankton basal respiration dl
mixoplankton	*mChlCabs*	C	0.006	Mixoplankton maximum possible constitutive Chl:C ratio; Chl:C
mixoplankton	*mDOCpc*	C	0.1	Mixoplankton % of Cfix released (dl)
mixoplankton	*MetMult*	C	3	Mixoplankton metabolic cost mutliplier to achieve required GGE for dinos; dl
mixoplankton	*mKQN*	C	10	Mixoplankton dimensionless quota constant for N; dl
mixoplankton	*mKxi*	C	0.1	Mixoplankton K for control of nutrient uptake dl
mixoplankton	*mM*	C	3	Mixoplankton scalar for controlling photoacclimation (dl)
mixoplankton	*mMR*	C	0.3	Mixoplankton respiration cost associated with metabolic functions (gC/gC)
mixoplankton	*mNCm*	C	0.2	Mixoplankton maximum N:C that affects phototrophic growth (gN/gC)
mixoplankton	*mNCo*	C	0.05	minimum mixoplankton N:C (gN/gC)

Continued on next page

Table B.1 continued from previous page

organism	name	vt	equations and values	documentation and unit
mixoplankton	*mNKt*	C	14*1	Mixoplankton half saturation constant for NO3 transport (ugN/L)
mixoplankton	*mNpref*	C	1	Mixoplankton relative preference for NO3 usage dl
mixoplankton	*mPCm*	C	0.02	Mixoplankton maximum P:C quota that affects growth (gP/gC)
mixoplankton	*mPCo*	C	0.005	Mixoplankton minimum P:C quota (gP/gC)
mixoplankton	*mPKu*	C	31	Mixoplankton half saturation constant for DIP uptake (ugP/L)
mixoplankton	*mQh*	C	4	Mixoplankton control h for nutrient uptake dl
mixoplankton	*mUm*	C	0.7	Mixoplankton maximum growth rate growing under heterotrophic nutrition (C/C/d)
mixoplankton	*mUphot*	C	0.35*2.55	Mixoplankton maximum rate of photosynthesis-driven growth gC/gC/d
mixoplankton	*NCabs*	C	0.25	absolute maximum possible organic N:C (gN/gC)
mixoplankton	*optimal_CR*	C	0.2	proportion of prey of optimal characteristics captured by starved mixoplankton dl
mixoplankton	*Pause_T*	C	10	time (d) between pauses, or enter a specific time to pause for debugging
mixoplankton	*Pbalcrit*	C	0.1	Mixoplankton minimum required contribution of photo Cfix to total C for growth (quotient; dl) when model run as protozooplankton, the value of this should be 0 this value needs to be changed for mixoplankton, depending on functional types and species
mixoplankton	*PCabs*	C	0.04	Mixoplankton absolute maximum P:C (gP/gC)
mixoplankton	*PFT*	C	4	switch to choose protist functional type; dl

Continued on next page

Table B.1 continued from previous page

organism	name	vt	equations and values	documentation and unit
mixoplankton	*PLNupcon*	C	0.9	PLN uptake rate control as % of growth rate; i.e., 0.9 means that PLN uptake is 90% of Urel dl
mixoplankton	*redco*	C	1.71	C respired to support nitrate reduction through to intracellular ammonium (gC/gN)
mixoplankton	*relMaxPrey*	C	0.3	maximum prey:pred dl
mixoplankton	*relMinPrey*	C	0.025	minimum prey:pred dl
mixoplankton	*relOpPrey*	C	0.2	Optimal prey:pred dl
mixoplankton	*SMix*	C	1	Mixoplankton switch for substitiutional 0; additive 1 For example, for most CM dinos this should be 1 based on work by Hae Jin Jeong; dl
mixoplankton	*Spd*	C	0	Switch to relate mixoplankton C demand to digestion; 0 if C-fixation does not affect digestion; 1 otherwise This should be 0 for *Teleaulax*; eats very little and probably only for phosphorous; dl
mixoplankton	*Stype*	C	1	Switch for controlling expression of the trait for grazing by mixoplankton in response to C, N or P MFT status; 1 for growth, 2 for N status, 3 for P status, 4 for N and P status; dl
mixoplankton	*SVol*	C	0	Mixoplankton volume sharing 0 if no volume sharing; dl
mixoplankton	*v_Mmin*	C	5.55E-05	minimum motility rate of *Teleaulax*; m/s Meunier et al. (2013)
mixoplankton	*aCgraz*	A	mIgC_A	feeding on algae by mixoplankton mgC/m3/d = ugC/L/d
mixoplankton	*aChlgraz*	A	mIgChl	ingestion of prey cholorophyll by predator ugC/L/d
mixoplankton	*aCuin*	A	mCu	intermediate in averaging calculations; d-1
mixoplankton	*aCuout*	A	DELAYPPL(aCuin[1], 1, 0)	intermediate in averaging calculations; d-1

Continued on next page

Table B.1 continued from previous page

organism	name	vt	equations and values	documentation and unit
mixoplankton	*AEqual*	A	AEmin+(AEmax-AEmin)*(1+Kec)*MINup/(MINup+Kec)	efficiency parameter for assimilation/digestion, RH function linked to prey QUALITY giving a value between 0 & 1 (i.e. quotient). AE can never reach 1; dl
mixoplankton	*AEquan*	A	IF(Keq>10e-6, (AEmin+(AEmax-AEmin)*(1+Keq^Heq)* (1-Urel)^Heq/((1-Urel)^Heq+Keq^Heq)), IF(Keq=1e-6, AEmax))	AE changing in response to changes in relative growth rate; decreases with increases growth rate; i.e. linked to QUANTITY. Turn this off by setting KecQ=1e-6; dl
mixoplankton	*AgC*	A	mCas_OP*mC	rate of incorporation of C into mixoplankton biomass (ugC/L/d)
mixoplankton	*AgN*	A	'mNas OP'*mC	assimilation of nitrogen into mixoplankton biomass ugN/L/d
mixoplankton	*AgP*	A	mPas_OP*mC	assimilation of phosphorus into mixoplankton biomass ugP/L/d
mixoplankton	*aPqmM*	A	(aUmax+aBR+aNCmax*aUmax* (aredco+aAAsyn*aMetMult))+1e-6	Mixoplankton kleptochloroplastic maximum possible Pmax for prey (gC/gC/d) .. assumes that on ingestion the nutrient status within the kleptochloroplasts is enhanced to maximum
mixoplankton	*avgmPS*	A	PSint/avgT	Mixotroph average C-fixation (C/C/d)
mixoplankton	*Ccell_M*	A	a*(4/3*PI*(r_M)^3)^b	C content of Mixoplankton cell pgC/cell
mixoplankton	*Cfix*	A	Cfix_OP*mC	C fixed into mixoplankton biomass by constitutive and klepto Chl (ugC/L/d)
mixoplankton	*Cfix_OP*	A	IF(PFT=2 OR PFT=3 OR PFT=4 ORPFT=5, mPS)	C fixed into mixoplankton biomass by constitutive and klepto Chl (ugC/L/d)
mixoplankton	*ChlCm*	A	mChlCabs_OP-IF((SVol=1), 1, 0)*((mFCC/(1+mFCC))/12)	Bacterial total N usage maximum Chl:C (gChl/gC); the value of 12 is C:Chl for the volume of photosystems
mixoplankton	*ChlCSyn_OP*	A	IF(PFT=3, ChlCSynmax*Pcon, (IF (PFT=4 OR PFT=5, ChlCSynmax)))	Mixoplankton change in ChlC with synthesis with C growth (g Chl g-1C d-1)

Continued on next page

Table B.1 continued from previous page

organism	name	vt	equations and values	documentation and unit
mixoplankton	*ChlCSynmax*	A	IF((mChlC<ChlCm), 1, 0)*ChlCm*mNPCu*mM*mUphot* ((1-MIN(1, Cin/mPqm))^0.5)*(1+0.05)* (1-mChlC/ChlCm)/(1-mChlC/ChlCm+0.05)	Mixoplankton change in ChlC with synthesis with C growth (g Chl g-1C d-1)
mixoplankton	*Cin*	A	mPS+(mCas_OP*IF((SMix=0), 1, 0))	Mixoplankton total C input to control the demand for Chl; if MixSwitch=0 then this is substitutional, with C from ingestion compensating for a shortfall in C-fixation. If MixSwitch=1 then only the contribution by Cfix is considered (C/C/d)
mixoplankton	*CMPS*	A	mPqm*(LN(MPyt+SQRT(1+MPyt^2))-LN(MPyt*exat+SQRT(1+(MPyt*exat)^2)))/ attenuation	Mixoplankton depth integrated photosynthesis using constitutive Chl at a given instant in time taking into account mixing depth and attenuations; dl
mixoplankton	*CpreyNC*	A	(CRC_A*aNC+CRC_B*bBNC)/(CRC_A+CRC_B)	captured prey N:C ratio; gN/gC
mixoplankton	*CpreyPC*	A	(CRC_A*aPC+CRC_B*bBPC)/(CRC_A+CRC_B)	captured prey P:C ratio; gP/gC
mixoplankton	*Cresp*	A	mC*mRTot	rate of loss of C through respiration from mixoplankton community (ugC/L/d)
mixoplankton	*delta*	A	MIN(1, Encd_AM/EncCrit_avg)	factor for modifying the parameters for photosynthesis for NCM as a function of availability of special prey dl
mixoplankton	*delta up*	A	IF(PFT=3, delta*((PLNmax-PLN)/TIMESTEP))	rate of uptake of plastids to ensure functioning of acquired phototrophy related photosynthesis mg DNA/m3/d
mixoplankton	*dFChlC*	A	mFChlC*PLN_decay	Mixoplankton decrease in gut ChlC due to degradation Chl/C/d
mixoplankton	*EncCrit_avg*	A	1/Enc_crit	Average population critical encounter rate prey/pred/day
mixoplankton	*Encd_AM*	A	(24*60*60)*IF(v_M>v_A, (PI*(r_A/1e6+r_M/1E6)^2*nos_A* (v_A^2+3*v_M^2+4*w^2)* (v_M^2+w^2)^(-0.5)*3^-1), (PI*(r_M/1e6+r_A/1E6)^2*nos_A* (v_M^2+3*v_A^2+4*w^2)* (v_A^2+w^2)^(-0.5)*3^-1))	Encounter rate of a cell of phytoplankton cell by a mixoplankton cell per day prey cells/mixoplankton cell/d

Continued on next page

Table B.1 continued from previous page

organism	name	vt	equations and values	documentation and unit
mixoplankton	*Encd_BM*	A	(24*60*60)* IF(v_M>v_B, (PI*(r_B/1e6+r_M/1E6)^2*nos_B* (v_B^2+3*v_M^2+4*w^2)*(v_M^2+w^2)^(-0.5)*3^-1), (PI*(r_M/1e6+r_B/1E6)^2*nos_B* (v_M^2+3*v_B^2+4*w^2)* (v_B^2+w^2)^(-0.5)*3^-1))	encounter rate of a cell of bacteria by a cell of mixoplankton bacteria/mixoplankton/d
mixoplankton	*FCmax*	A	IF((SMix=0), 1, 0)*(FCmin+(1-(1+Khet^Hhet)* Urel^Hhet/(Urel^Hhet+Khet^Hhet))* (FCabs-FCmin)) +IF((SMix=1), 1, 0)*FCabs	Mixoplankton maximum operational gut size, developed in response to C,N,P stress; PbalCon ensures that a minimum level of photo Cfix occurs
mixoplankton	*FCrel*	A	mFCC/FCabs*IF((mFCC>0), 1, 0)	Mixoplankton size of FC relative to the maximum possible FCabs; this is used to determine the availability of material in the digestive vacuole for digestion (dl)
mixoplankton	*FCrelV*	A	MIN(1, mFCC/FCmax*IF((mFCC>0), 1, 0))	Mixoplankton relative capacity of gut - this is used to halt ingestion as the gut fills; this value changes as FCmax varies as a function of C,N,P stress (dl)
mixoplankton	*FCuse*	A	mDgC/mFCC	Mixoplankton specific rate of gut consumption (d-1)
mixoplankton	*GNCMPS*	A	(aPqmM*mNPCu)* (LN(GNCMPyt+ SQRT(1+GNCMPyt^2))- LN(GNCMPyt*exat+ SQRT(1+(GNCMPyt*exat)^2)))/attenuation	Mixoplankton depth integrated photosynthesis using klepto-Chl at a given instant in time taking into account mixing depth and attenuations [only applicable for GNCM]; d-1
mixoplankton	*GNCMPyt*	A	(aalpha_OP*mFChlC*PFD*24*60*60)/(aPqmM*mNPCu)	Mixoplankton klepto-photosynthesis according to the Smith equation dl [this is relevant only for the GNCM]; dl
mixoplankton	*IgCA OP*	A	IF(PFT=5, 0, CRC_A*'mFC fb')	Mixoplankton C-specific ingestion rate, (g prey C / g mixo C /d)
mixoplankton	*IgCB OP*	A	IF(PFT=5, 0, CRC_B*'mFC fb')	Mixoplankton C-specific ingestion rate, (g prey C / g mixo C /d)
mixoplankton	*IgFChlC OP*	A	IF(PFT=5, 0, CRC_A*aChlC*'mFC fb')	Mixoplankton ingestion of prey Chl (g SChl / g mC / d) = (g SChl/ g SC) * (g SC / g mC / d)

Continued on next page

Table B.1 continued from previous page

organism	name	vt	equations and values	documentation and unit
mixoplankton	*lgNA OP*	A	IF(PFT=5, 0, CRC_A*aNC*'mFC fb')	Ingestion of phytoplankton prey N into mixoplankton feeding vacuole gN/gC/d
mixoplankton	*lgNB OP*	A	IF(PFT=5, 0, CRC_B*bBNC*'mFC fb')	Ingestion of bacterial prey N into mixoplankton feeding vacuole gN/gC/d
mixoplankton	*lgPA_OP*	A	IF(PFT=5, 0, CRC_A*aPC*'mFC fb')	Ingestion of prey P into mixoplankton; P/C/d
mixoplankton	*lgPB OP*	A	IF(PFT=5, 0, CRC_B*bBPC*'mFC fb')	Ingestion of prey P into mixoplankton; P/C/d
mixoplankton	*mAE*	A	MIN(AEqual, AEquan)	Actual AE as the minimum of quality and quantity linked AE; dl
mixoplankton	*malpha_OP*	A	IF(PFT=3, (Pcon*malpha), IF(PFT=4 OR PFT=5, malpha), 0)	operational malpha for different protist FT Chl-specific initial slope to PI curve, giving gC fixed per gChl.a per photon (m2g-1 chl.a)(gC umol-1 photon) This is relevant for CM, SNCM and phytoplankton
mixoplankton	*mAV*	A	IF((UmpN<mAVP), 1, 0)*UmpN+IF((UmpN>=mAVP), 1, 0)*mAVP	Mixoplankton actual NH4 uptake; (ugN/L/d)
mixoplankton	*mAVP*	A	IF((NH4>0.01), 1, 0)*UmpN*mApref*NH4/(NH4+mAKt)	Mixoplankton potential relative NH4 transport; dl
mixoplankton	*mBalRes*	A	IF((Pbal>Pbalcrit), 1, 0)*(Pbal-Pbalcrit)/(1-Pbalcrit)	Mixoplankton photo vs hetero balance; Pbal varies between 0 and 1 as Cfix supports Cu; critPbal defines the critical value of Pbal. BalRes returns a value of 0 (Pbal is less than sufficient to allow digestion) to 1 (allow maximum digestion as sufficient Cfix is happening). If critPbal=0 then digestion is always allowed. (dl)
mixoplankton	*mBRb*	A	mBRop-mBRi	basal resp from predator body, this occurs when XSC cannot support BR (gC/gC/d)
mixoplankton	*mBRi*	A	IF((mBRop<=XSC), 1, 0)*mBRop+IF((mBRop>XSC), 1, 0)*XSC	support of BR using XSC (gC/gC/d)
mixoplankton	*mBRop*	A	mUm*mBR*1.01*((NCabs-mNC)/(NCabs-mNCo))/ ((NCabs-mNC)/(NCabs-mNCo)+0.01)*IF((mNC<NCabs), 1, 0)	basal respiration rate, including term to halt respiration at high NC (gC/gC/d)

Continued on next page

Table B.1 continued from previous page

organism	name	vt	equations and values	documentation and unit
mixoplankton	*mCas*	A	AE_op*mDgC	Mixoplankton assimilation rate of carbon (gC/gC/d)
mixoplankton	*mCas_OP*	A	IF(PFT=1 OR PFT=2 OR PFT=3 OR PFT=4, mCas)	Mixoplankton assimilation rate of carbon (gC/gC/d)
mixoplankton	*mCdeath*	A	mCdeath_OP*mC	loss due to death in the absence of food ugN/L/d this is appilcable for GNCM, SNCM and protozooplankton
mixoplankton	*mCdeath_OP*	A	mdeath	rate of loss due to death in the absence of prey (gC/gC/d)
mixoplankton	*mChlC*	A	mChl/mC	gChl/gC protist (body) Chl:C ratio
mixoplankton	*mChlCabs_OP*	A	IF(PFT=3, (Pcon*mChlCabs), IF(PFT=4 OR PFT=5, mChlCabs), 0)	Mixoplankton maximum possible constitiutive ChlC; dl
mixoplankton	*mChldeath*	A	mC*mChldeath_OP	loss due to death ugChl/L/d
mixoplankton	*mChldeath_OP*	A	mCdeath_OP*mChlC	rate of loss due to death in the absence of prey (gP/gC/d)
mixoplankton	*mChldeg*	A	mChlC*(((1-mNPCu)*mUphot)+IF(mChlC>mChlCabs_OP, 1, 0))	Mixoplankton change in ChlC with degradation with C growth (g Chl g-1C d-1)
mixoplankton	*mChlloss*	A	mChldeg*mC	rate of loss of chlorophyll through degradation ugChl/L/d
mixoplankton	*mChlsyn*	A	ChlCSyn_OP*mC	rate of chlorophyll synthesis gChl/L/d
mixoplankton	*mCu*	A	(mCas_OP+mPS)-mRTot	Mixoplankton net C-growth (gC/gC/d)
mixoplankton	*mCu_op*	A	((Cfix+AgC)-Cresp)/mC	emergent mixoplankton growth rate; gC/gC/d
mixoplankton	*mdeath*	A	IF(mNC>0.8*NCabs AND avgCu<0, death_R, 0)+(1-mNPCu)*death_R	mixoplankton mortality (gC/gC/d)
mixoplankton	*mDgC*	A	1.1*(IF((mFCC>10e-201), 1, 0)*PbalCon*mIm*PD* (1+Kasm^Hasm)*FCrel^Hasm/(FCrel^Hasm+Kasm^Hasm))	digestion of material held in the gut, as a sigmoidal function of gut contents relative to the value of GCrelA (gC/gC/d)

Continued on next page

Table B.1 continued from previous page

organism	name	vt	equations and values	documentation and unit
mixoplankton	*mDINup*	A	mupN_OP*mC	uptake of DIN by mixoplankton to support photosynthesis ugN/L
mixoplankton	*mDIPup*	A	mIPu_OP*mC	uptake of DIP by mixoplankton to support photosynthesis ugP/L
mixoplankton	*mDOCout*	A	mDOCpc*mPS*mC	Mixoplankton DOC release ugC/L/d
mixoplankton	*mFC fb*	A	(1+KIng^HIng)*(1-FCrelV)^HIng/ ((1-FCrelV)^HIng+KIng^HIng)	feedback from feeding vacuole fullness dl
mixoplankton	*mFCC*	A	mFC/mC	Mixoplankton gut contents relative to body biomass (gC/gC)
mixoplankton	*mFCdeath*	A	mC*mFCdeath_OP	loss due to death ugC/L/d
mixoplankton	*mFCdeath_OP*	A	mCdeath_OP*mFCC	rate of loss due to death in the absence of prey (gC/gC/d)
mixoplankton	*mFChlC*	A	mFChl/mC	prey Chl within mixoplankton (i.e. as kleptochloroplast) g Chl / g mixo biomass
mixoplankton	*mFChldeath*	A	mC*mFChldeath_OP	loss due to death ugChl/L/d
mixoplankton	*mFChldeath_OP*	A	mCdeath_OP*mFChlC	rate of loss due to death in the absence of prey (gChl/gC/d)
mixoplankton	*mFChlup*	A	dFChlC*mC	Mixoplankton decrease in gut ChlC due to digestion Chl/L/d
mixoplankton	*mFCup*	A	mDgC*mC	rate of consumption of carbon from the mixoplankton digestive vacuole; ugC/L/d
mixoplankton	*mfFNC*	A	mFNC/mFCC	NC of material in the feeding vacuole (gN in F : gC in mixo) / (gC in F : gC in mixo)
mixoplankton	*mfFPC*	A	mFPC/mFCC	PC of material in the feeding vacuole (gP in F : gC in mixo) / (gC in F : gC in mixo)
mixoplankton	*mFNC*	A	mFN/mC	Mixoplankton gut N contents relative to body C biomass (gN of gut /gC of body)

Continued on next page

Table B.1 continued from previous page

organism	name	vt	equations and values	documentation and unit
mixoplankton	*mFNdeath*	A	mC*mFNdeath_OP	loss due to death ugN/L/d
mixoplankton	*mFNdeath_OP*	A	mCdeath_OP*mFNC	rate of loss due to death in the absence of prey (gN/gC/d)
mixoplankton	*mFNup*	A	FCuse*mFNC*mC	rate of consumption of nitrogen from the mixoplankton digestive vacuole ugN/L/d
mixoplankton	*mFPC*	A	mFP/mC	P in mixoplankton DV compared to C in mixoplankton body (gP/gC)
mixoplankton	*mFPdeath*	A	mC*mFPdeath_OP	loss due to death ugP/L/d
mixoplankton	*mFPdeath_OP*	A	mCdeath_OP*mFPC	rate of loss due to death in the absence of prey (gP/gC/d)
mixoplankton	*mFPup*	A	FCuse*mFPC*mC	rate of consumption of nitrogen from the mixoplankton digestive vacuole ugP/L/d
mixoplankton	*mfrat*	A	mNV/(mNV+mAV+1e-12)	Mixoplankton f-ratio; dl
mixoplankton	*mIgC_A*	A	mC*'IgCA OP'	ingestion rate of phytoplankton into mixoplankton digestive vacuole ugC/L/d
mixoplankton	*mIgC_B*	A	'IgCB OP'*mC	ingestion rate of bacteria into mixoplankton feeding vacuole ugC/L/d
mixoplankton	*mIgChl*	A	'IgFChlC OP'*mC	uptake of prey chlorophyll by mixoplankton mmoles Chl/m3/d
mixoplankton	*mIgN_A*	A	'IgNA OP'*mC	N prey uptake into mixoplankton digestive vacuole ugN/L/d
mixoplankton	*mIgN_B*	A	'IgNB OP'*mC	N prey uptake into mixoplankton digestive vacuole ugN/L/d
mixoplankton	*mIgP_A*	A	IgPA_OP*mC	P prey uptake into mixoplankton digestive vacuole ugP/L/D
mixoplankton	*mIgP_B*	A	'IgPB OP'*mC	P prey uptake into mixoplankton digestive vacuole ugP/L/D

Continued on next page

Table B.1 continued from previous page

organism	name	vt	equations and values	documentation and unit
mixoplankton	*mIm*	A	((mUm+mBRop)/(1-mMR))*1/(MAX(AE_op, 0.1))	Mixoplankton ingestion rate required to support Um with the current food quality AE_FQ (gC/gC/d) WAS (mUm+BRop)/(mAE*(1-mMR))
mixoplankton	*MINup*	A	MIN(RelNC, RelPC, 1)	minimal threshold control to select the release of nitrogen and/or phosphorus for differences in the values of SXC and ZXC, ratio (dl)
mixoplankton	*mIPu*	A	IF((DIP>0.01), 1, 0)*IF((mPC<PCabs), 1, 0)*mUphot*5*mPCm*(IF((mPCu>mNPCu), 1, 0)* mNPCu^mbeta+IF((mPCu=mNPCu), 1, 0))*DIP/(DIP+mPKu)* (1+mQh^mKxi)*(1-mPC/PCabs)^mQh/ ((1-mPC/PCabs)^mQh+mKxi^mQh)	Mixoplankton DIP uptake (gP/gC/d)
mixoplankton	*mIPu_OP*	A	IF(PFT=3 OR PFT=4 OR PFT=5, mIPu)	Mixoplankton DIP uptake (gP/gC/d)
mixoplankton	*mNas*	A	mCas_OP*mNCm*IF((mCas_OP>0), 1, 0)	incorporation of N for growth of mixoplankton (gN/gC/d)
mixoplankton	*mNas OP*	A	IF(PFT=1 OR PFT=2 OR PFT=3 OR PFT=4, mNas)	incorporation of N for growth of mixoplankton (gN/gC/d)
mixoplankton	*mNC*	A	mN/mC	Mixoplankton body N:C (gN/gC)
mixoplankton	*mNCu*	A	IF((mNC<=mNCm), 1, 0)*IF((mNC>=mNCo), 1, 0)*(1+mKQN)* (mNC-mNCo)/((mNC-mNCo)+mKQN* (mNCm-mNCo))+IF((mNC>mNCm), 1, 0)	normalised function describing the nitrogen status of the mixoplankton cellular biomass relative to the carbon; i.e., normailised N/C quota description dl
mixoplankton	*mNdeath*	A	mNdeath_OP*mC	mixoplankton death ugN/L/d
mixoplankton	*mNdeath_OP*	A	mCdeath_OP*mNC	rate of loss due to death in the absence of prey (gN/gC/d)
mixoplankton	*mNPCu*	A	MIN(1, MIN(mNCu, mPCu))	Leibig function describing the minimum of the nitrogen and phosphorus cellular status of the mixoplankton as a quotient. Thus, value of 1 = very happy; value of 0 = very sad dl

Continued on next page

Table B.1 continued from previous page

organism	name	vt	equations and values	documentation and unit
mixoplankton	*mNrep*	A	IF((mNC>mNCm), 1, 0)*(1-(NCabs-mNC)/(NCabs-mNCm))	Mixoplankton repressor of regenerated N reassimilation; decreases as NC approaches NCabs (dl)
mixoplankton	*mNresp*	A	resN*mC	loss of N from mixoplankton through respiration ugN/L/d
mixoplankton	*mNV*	A	IF((mAVP<UmpN), 1, 0)*(IF((mAVP+mNVP<UmpN), 1, 0)* mNVP+IF((mAVP+mNVP>=UmpN), 1, 0)*(UmpN-mAVP))	Mixoplankton NO3 transport as proportion of total; (ugN/L/d)
mixoplankton	*mNVP*	A	IF((NO3>0.01), 1, 0)*UmpN*mNpref*NO3/(NO3+mNKt)	Mixoplankton potential relative NO3 transport gN/gC/d
mixoplankton	*mPas*	A	mCas_OP*mPCm*IF((mCas_OP>0), 1, 0)	incorporation of P for growth of mixoplankton (gP/gC/d)
mixoplankton	*mPas_OP*	A	IF(PFT=1 OR PFT=2 OR PFT=3 OR PFT=4, mPas)	incorporation of P for growth of mixoplankton (gP/gC/d)
mixoplankton	*mPC*	A	mP/mC	Mixoplankton body P:C (gP/gC)
mixoplankton	*mPCu*	A	(1+KQP)*(mPC-mPCo)/((mPC-mPCo)+KQP* (mPCm-mPCo))*IF((mPCo<mPC), 1, 0)* IF((mPC<mPCm), 1, 0)+IF((mPC>=mPCm), 1, 0)	normalised function describing the phosphorus status of the mixoplankton cellular biomass relative to the carbon; normailised P:C quota description (dl)
mixoplankton	*mPdeath*	A	mPdeath_OP*mC	mixoplankton loss; ugP/L/d
mixoplankton	*mPdeath_OP*	A	mCdeath_OP*mPC	rate of loss due to death in the absence of prey (gP/gC/d)
mixoplankton	*mPqm*	A	(mUphot+mBRop+mNCm*mUphot* (redco+mAAsyn*MetMult))*mNPCu+1e-6	constitutive mixoplankton potential maximum photosynthesis rate (gC g-1C d-1) was (Um+basres+NCm*Um* (redco+1.5))* MIN(NCu,PCu)+1e-6
mixoplankton	*mPrep*	A	IF((mPC>mPCm), 1, 0)*(1-(PCabs-mPC)/(PCabs-mPCm))	Mixoplankton repressor of regenerated P reassimilation; decreases as PC approaches PCabs (dl)
mixoplankton	*mPresp*	A	mC*resP	loss of P from mixoplankton through respiration ugP/L/d
mixoplankton	*mPS*	A	CMPS+GNCMPS	Mixoplankton total gross C-fix, including constitutive + klepto (C/C/d)

Continued on next page

Table B.1 continued from previous page

organism	name	vt	equations and values	documentation and unit
mixoplankton	*MPyt*	A	(malpha_OP*mChlC*PFD*24*60*60)/mPqm	Mixoplankton photosynthesis according to the Smith equation for CM and SNCM; dl
mixoplankton	*mRTot*	A	Rhet+Rphot	Mixoplankton total respiration rate (gC/gC/d)
mixoplankton	*mupN*	A	(mAV+mNV)*(IF((mNCu>mNPCu), 1, 0)*IF((mNC<NCabs), 1, 0)* mNPCu^mbeta+IF((mNCu=mNPCu), 1, 0))* IF((mNC<NCabs-0.002), 1, 0)*(1+mKxi^mQh)* (1-mNC/NCabs)^mQh/((1-mNC/NCabs)^mQh + mKxi^mQh)	Mixoplankton rate of total DIN uptake (gN/gC/d)
mixoplankton	*mupN_OP*	A	IF(PFT=3 OR PFT=4 OR PFT=5, mupN)	Mixoplankton rate of total DIN uptake (gN/gC/d)
mixoplankton	*mVOPL*	A	mVOPt*mC+mFPdeath+mPdeath	Mixoplankton loss of P as voided organics (ugP/L/d)
mixoplankton	*nos_M*	A	10^9*TmC/Ccell_M	numeric cell abundance of mixoplankton mixoplankton cells/m3
mixoplankton	*Pause Control*	A	PAUSEIF(FRAC(TIME/Pause_T)=0)	control to pause time; d
mixoplankton	*Pbal*	A	IF((avgCas>0), 1, 0)*(MIN(1, mPS/(avgCas+1e-24)))	Mixoplankton balance of total Cfix (inc that from prey Chl) to growth rate - note that because of circularity this not linked to gross C input .... gross Cfix to net Cintake; returns a value of 0 if TPS contributes 0% to growth rate, and upto 1 as TPS increases contribution to Cu
mixoplankton	*PbalCon*	A	(1+Kpbal^Hpbal)*mBalRes^Hpbal/ (mBalRes^Hpbal+Kpbal^Hpbal)* IF((Pbalcrit>0), 1, 0)+IF((Pbalcrit=0), 1, 0)	Mixoplankton controler of ingestion from material in gut by the relative rate of photosynthesis. As soon as Pbal>critPbal this value rises rapidly to 1 to allow digestion to occur. Dl
mixoplankton	*Pcon*	A	MIN(1, PLN/PLNmax)	factor for modifying the parameters for photosynthesis for NCM as a function of availability of special prey; this maintains a value of 1 for at least the period defined by Enc_crit after the value of Enc_f falls below 1; dl

Continued on next page

Table B.1 continued from previous page

organism	name	vt	equations and values	documentation and unit
mixoplankton	*PD*	A	1-Spd*((1+Kpd^Hpd)*PSrel^Hpd/(PSrel^Hpd+Kpd^Hpd))	Mixoplankton control on digestion by C fixation (i.e., PSrel); if switch is enabled then digestion of captured prey is linked to relPS - if sufficient C is flowing from PS then decrease digestion dl
mixoplankton	*PLN_decay*	A	LN(2)/(IF(PFT=2, 0.5, halfLife))	PLN decay rate per day; d-1
mixoplankton	*PLN_degrade*	A	PLN_decay*PLN	degradation of PLN mg DNA/m3/d
mixoplankton	*PLN_up*	A	PLN*PLN_uprate	uptake of "new" material from plastids to run acquired phototrophy mg DNA/m3/d
mixoplankton	*PLN_uprate*	A	IF(PFT=3, PLNupcon*Urel, 0)	N specific PLN uptake rate gN/gN/d
mixoplankton	*PLNmax*	A	0.05*mN	maximum value for PLN indexed to mN biomass mgN/m3/d
mixoplankton	*preyNgut*	A	mFC*mfFNC	preyN in mixoplankton feeding vacuole (ugN/L)
mixoplankton	*preyPgut*	A	mFC*mfFPC	Mixoplankton preyP in gut (ugP/L)
mixoplankton	*prodRat*	A	mPS/mRTot	Mixoplankton production:respiration ratio; dl
mixoplankton	*PSrel*	A	MIN(1, mPS/mPqm)	Mixoplankton relative rate of photosynthesis (dl)
mixoplankton	*r_M*	A	ESD_M/2	mixoplankton radius; um
mixoplankton	*Rate_1*	A	mCas_OP	intermediate for calculating average Cas; dl
mixoplankton	*Rate_2*	A	DELAYPPL(Rate_1[1], 1, 0)	intermediate for calculating average Cas; dl
mixoplankton	*Rate_31*	A	DELAYPPL(Rate_32[1], 1, 0)	intermediate in averaging calculations
mixoplankton	*Rate_32*	A	'lgCA OP'	intermediate in averaging calculations
mixoplankton	*Rate_33*	A	mDgC	intermediate in averaging calculations

Continued on next page

Table B.1 continued from previous page

organism	name	vt	equations and values	documentation and unit
mixoplankton	*Rate_34*	A	DELAYPPL(Rate_33[1], 1, 0)	intermediate in averaging calculations
mixoplankton	*Rate_35*	A	mAE	intermediate in averaging calculations
mixoplankton	*Rate_36*	A	DELAYPPL(Rate_35[1], 1, 0)	intermediate in averaging calculations
mixoplankton	*Rate_37*	A	mPS	intermediate in averaging calculations
mixoplankton	*Rate_38*	A	DELAYPPL(Rate_37[1], avgT, 0)	intermediate in averaging calculations
mixoplankton	*RegN*	A	(1+KRC^HRC)*mNrep^HRC/(1e-12+(mNrep^HRC+KRC^HRC))	Mixoplankton control of N regeneration (dl) 1e-12 included within the denominator to prevent a mathematical error generated by division by zero
mixoplankton	*RegP*	A	(1+KRC^HRC)*mPrep^HRC/(1e-12+(mPrep^HRC+KRC^HRC))	Mixoplankton control of P regeneration (dl)
mixoplankton	*RelNC*	A	CpreyNC/mNCm	Mixoplankton relative prey N to predator N (dl)
mixoplankton	*RelPC*	A	CpreyPC/mPCm	Mixoplankton relative prey P to predator P (dl)
mixoplankton	*relU_M*	A	avgCu/(mUm+mUphot)	relative growth rate of mixoplankton dl
mixoplankton	*resN*	A	Rhet*mNCm*RegN	Mixoplankton stoichiometric-linked N respiration with hetertrophic respiration, assuming that the base N:C of core biological material accords with NCm (gN/gC/d)
mixoplankton	*resP*	A	mPCm*Rhet*RegP	Mixoplankton stoichiometric-linked P respiration with heterotrophic respiration, assuming that the base P:C of core biological material accords with PCm (gP/gC/d)
mixoplankton	*Rhet*	A	mBRb+mCas_OP*mMR	respiration rate from heterotrophic processes (gC/gC/d)
mixoplankton	*Rphot*	A	redco*mupN_OP*mfrat+(mupN_OP+nh4reas)* mAAsyn*MetMult	Mixoplankton phototrophic driven respiration (gC/gC/d)

Continued on next page

Table B.1 continued from previous page

organism	name	vt	equations and values	documentation and unit
mixoplankton	*TmC*	A	mC+mFC	Mixoplankton total POC , body + gut (ugC/L)
mixoplankton	*TmN*	A	mN+preyNgut	Mixoplankton total PON (ugN/L)
mixoplankton	*TmP*	A	mP+preyPgut	Mixoplankton total POP (ugP/L)
mixoplankton	*UmpN*	A	mUphot*mNCm	Mixoplankton maximum N-source uptake potential gN/gC/d
mixoplankton	*Urel*	A	IF((Stype=1), 1, 0)*MIN(1, avgCu/mUm) + IF((Stype=2), 1, 0)*mNCu +IF((Stype=3), 1, 0)* mPCu +IF((Stype=4), 1, 0)*MIN(mNCu, mPCu)	Mixoplankton relative growth rate associated with physiological status. dl
mixoplankton	*v_M*	A	v_Mmax+0*(v_Mmin+(v_Mmax-v_Mmin)* (1-((relU_M^Hv/(relU_M^Hv+Kv^Hv))*(1+Kv^Hv))))	mixoplankton motility related to satiation computed as a function of the ratio of emergent growth rate and maximum growth rate; m/s
mixoplankton	*v_Mmax*	A	(10^-6)*(38.542*(ESD_M^0.5424))	maximum velocity of mixoplankton, m/s
mixoplankton	*wmC*	A	mC*DIL	Mixoplankton C wash out (ugC/L/d)
mixoplankton	*wmChl*	A	mChl*DIL	mixoplankton chlorophyll wash out ugChl/L/d
mixoplankton	*wmFC*	A	DIL*mFC	dilution rate of carbon from mixoplankton feeding vacuole; mgC/m3
mixoplankton	*wmFChl*	A	DIL*mFChl	dilution rate of chlorophyll from mixoplankton feeding vacuole; mgChl/m3
mixoplankton	*wmFN*	A	DIL*mFN	dilution rate of nitrogen from mixoplankton feeding vacuole; mgN/m3
mixoplankton	*wmFP*	A	DIL*mFP	dilution rate of phosphorus from mixoplankton feeding vacuole; mgP/m3
mixoplankton	*wmN*	A	mN*DIL	dilution of mN ugN/L/d
mixoplankton	*wmP*	A	DIL*mP	dilution loss of mP ugP/L/d

Continued on next page

Table B.1 continued from previous page

organism	name	vt	equations and values	documentation and unit
mixoplankton	*wPLN*	A	PLN*DIL	PLN wash out mg DNA/m3/d
mixoplankton	*XSC*	A	AEqual*mDgC*(1-MINup)	Mixoplankton supply of C (from sugars etc.) for support of respiration but not used for protoplasmic purposes (C/C/d)
mixoplankton	*avgAE*	SV	0 +Rate_35 -FILLINZEROES(Rate_36)	average mixoplankton AE; dl
mixoplankton	*avgCas*	SV	1E-24 +Rate_1 -FILLINZEROES(Rate_2)	state variable for the history of carbon assimilation by mixoplankton; gC/gC/d
mixoplankton	*avgCu*	SV	0 +aCuin -FILLINZEROES(aCuout)	day average net mixoplankton growth rate; (d-1)
mixoplankton	*avgDgC*	SV	0 +Rate_33 -FILLINZEROES(Rate_34)	Average digestion of material held in the mixoplankton feeding vacuole, as a sigmoidal function of gut contents relative to the value of GCrelA; gC/gC/d
mixoplankton	*avgIgC*	SV	0 -FILLINZEROES(Rate_31) +Rate_32	average mixoplankton ingestion rate; gC/gC/d
mixoplankton	*mC*	SV	initmC +AgC +Cfix -Cresp -mCdeath -wmC	mixoplankton body biomass carbon; ugC/L = mgC/m3

Continued on next page

Table B.1 continued from previous page

organism	name	vt	equations and values	documentation and unit
mixoplankton	*mChl*	SV	mC*(mChlCabs_OP/3) -mChldeath -mChlloss +mChlsyn -wmChl	chlorophyll in constitutive mixoplankton ugChl/L/d = mgChl/m3/d
mixoplankton	*mFC*	SV	0.1e-11 -mFCdeath -mFCup +mIgC_A +mIgC_B -wmFC	carbon in mixoplankton feeding vacuole mgC/m3 = ugC/L
mixoplankton	*mFChl*	SV	0.1e-11 -mFChldeath -mFChlup +mIgChl -wmFChl	prey Chl within mixoplankton feeding vacuole (i.e., as kleptochloroplast) ugChl/ L/d
mixoplankton	*mFN*	SV	0.1e-11 -mFNdeath -mFNup +mIgN_A +mIgN_B -wmFN	prey nitrogen within mixoplankton feeding vacuole; ugN/L/d; mgN/m3

Continued on next page

Table B.1 continued from previous page

organism	name	vt	equations and values	documentation and unit
mixoplankton	*mFP*	SV	0.1e-11 -mFPdeath -mFPup +mIgP_A +mIgP_B -wmFP	prey phosphorus within mixoplankton feeding vacuole; ugP/L/d; mgP/m3
mixoplankton	*mN*	SV	initmC*mNCm +AgN +mDINup -mNdeath -mNresp -wmN	mixoplankton N biomass ugN/L = mgN/m3
mixoplankton	*mP*	SV	initmC*mPCm +AgP +mDIPup -mPdeath -mPresp -wmP	mixoplankton P biomass ugP/L = mgP/m3
mixoplankton	*PLN*	SV	0.0001 +'delta up' -PLN_degrade +PLN_up -wPLN	acquired phototrophy related plastid control mg DNA /m3
mixoplankton	*PSint*	SV	0 +Rate_37 -FILLINZEROES(Rate_38)	intermediate in average of mixo PS